Università degli Studi di Padova
Centro interdipartimentale “Centro Ricerche Fusione”

Universidade de Lisboa
Instituto Superior Técnico (IST)

JOINT RESEARCH DOCTORATE IN FUSION SCIENCE AND ENGINEERING
Cycle XXVIII

Thermo-mechanical analyses and design of components for fusion devices

Coordinator: Prof. Paolo Bettini

Supervisors: Prof. Piergiorgio Sonato
Dr. Mauro Dalla Palma

Candidate: Nisarg Patel

Padova, January 2016

ABSTRACT

RFX-mod has proven its potentiality by achieving important experimental results in both reverse field pinch and tokamak configurations, so providing its contribution to fusion research program. Further challenges will be explored with the machine upgrade named RFX-mod2 under detailed design. This thesis presents the mechanical design modifications of the torus assembly and the verifications undertaken through thermo-mechanical simulations.

Custom solutions for the vacuum boundary of the RFX-mod2 are proposed considering compatibility with the as-built experiment and with the upgrade concept mechanically consisting of the old vacuum vessel removal. The solutions are developed considering the above constraints and the technological feasibility.

Mechanical design of Toroidal Support Structure (TSS) is carried out to make it vacuum tight. The vacuum boundary is designed at the toroidal assembly joints by developing different sealing solutions compatible with the stringent requirements of the present components: ceramic-metal brazed rings at the two poloidal joints, fully welded plate at the external equatorial joint, and Thin Resistive Plate at the internal equatorial joint. A simplified experimental mock-up is proposed to qualify the technological feasibility of sealing solutions; furthermore, relevant technical specifications are prepared for the procurement.

Design calculations are developed for passive stabilizing shell modifications considering requirements to provide structural support to first wall tiles and withstand thermal loads. New rings supporting the stabilizing shell on TSS are designed by series of finite element simulations to select proper material, number of rings and support geometry considering applied loads.

Load specifications for the components of RFX-mod2 are prepared considering different operating conditions and combinations of thermal, structural and electromagnetic loads to be applied to finite element simulations of the machine. The component design is supported by thermo-mechanical analyses undertaken by developing 3D models in ANSYS environment and results are verified against the ITER structural design criteria for in-vessel components and ASME pressure vessel design rules. As reported in this thesis, the preliminary mechanical design of the vacuum boundary and in-vacuum components of RFX-mod2 machine has been completed and verifications carried out resulted satisfied demonstrating the validity of the proposed solutions.

RIASSUNTO

RFX-mod ha dimostrato le sue potenzialità avendo conseguito importanti risultati sperimentali nelle configurazioni reverse field pinch e tokamak, pertanto contribuendo al programma di ricerca sulla fusione. Nuove sfide saranno esplorate con la macchina modificata e denominata RFX-mod2, attualmente in fase di progetto. Questa tesi presenta le modifiche del progetto meccanico dell'assieme toroidale e le verifiche condotte mediante simulazioni termo-meccaniche.

Soluzioni speciali vengono proposte per il confinamento del vuoto di RFX-mod2 considerando la compatibilità con la macchina costruita e con il concetto di modifica costituita meccanicamente dalla rimozione della camera da vuoto. Le soluzioni sono state sviluppate in considerazione dei suddetti vincoli e della fattibilità tecnologica.

Il progetto meccanico della struttura toroidale di supporto è stato svolto per renderla a tenuta di vuoto. La barriera da vuoto è stata progettata alle giunzioni della struttura toroidale sviluppando diverse soluzioni di tenuta compatibili con i stringenti requisiti dei componenti attuali: anelli ceramico-metallo brasati ai giunti poloidali, un piatto saldato al giunto equatoriale esterno, una lamiera resistiva al giunto equatoriale interno. Un simulacro sperimentale è stato proposto per qualificare la fattibilità tecnologica delle soluzioni di tenuta; inoltre, sono state preparate le relative specifiche tecniche per la fornitura.

I calcoli progettuali sono stati sviluppati per il guscio di stabilizzazione passiva considerando i requisiti di fornire supporto strutturale alle tegole della prima parete e di sopportare i carichi termici. Nuovi anelli di supporto del guscio di stabilizzazione sulla struttura toroidale sono stati progettati mediante una serie di simulazioni agli elementi finiti per selezionare il materiale, il loro numero e la geometria di supporto considerando i carichi applicati.

Le specifiche di carico per i componenti di RFX-mod2 sono state preparate valutando diverse condizioni d'esercizio e combinazioni di carichi termici, strutturali ed elettromagnetici per essere applicate alle simulazioni agli elementi finiti della macchina. Il progetto dei componenti è stato avvalorato da analisi termo-meccaniche condotte sviluppando modelli tridimensionali in ambiente ANSYS ed i risultati sono stati verificati applicando i codici per la progettazione dei recipienti a pressione ASME e dei componenti in vuoto di ITER. Come descritto nella tesi, è stato completato il progetto meccanico preliminare della barriera vuoto e dei componenti in vuoto della macchina RFX-mod2 e le verifiche condotte risultano soddisfatte ed hanno dimostrato la validità delle soluzioni proposte.

ACKNOWLEDGEMENT

I would like to extend thanks to all persons who so generously contributed to the work presented in this thesis.

I am especially grateful to my supervisors Prof. Piergerogio Sonato and Dr. Mauro Dalla Palma for sharing their knowledge and extending their significant support and cooperation. I am also grateful to Dr. Simone Peruzzo for providing support and valuable time.

I am thankful to my colleagues in Consorzio RFX, particularly the “Ingegneria del Plasma” group. I would like to thank everybody who have helped and encouraged me during these three years. I am hugely appreciative to them.

The blessings of God, my respective parents and my family members make the way for completion of my work and given me continuous encouragement, my heartfelt thanks to them. I would like to express my special thanks to my brother-in-law Mr. N. RaviPragash for his throughout guidance. Finally and most importantly, I would like to thank my wife for her constant support.

Nisarg Patel

TABLE OF CONTENTS

ABSTRACT…… i

RIASSUNTO……..iii

ACKNOLEDGEMENT…… v

CHAPTER 1 INTRODUCTION.....1

1.1 Thermonuclear fusion 1

1.1.1 Magnetic Confinement Fusion (MCF): 1

1.2 The Reversed Field Pinch magnetic configuration 4

1.3 The RFX experiment.....6

1.4 Mechanical systems of RFX-mod.....7

1.4.1 First Wall tiles.....8

1.4.2 Vacuum Vessel 10

1.4.3 Passive stabilizing shell 12

1.4.4 Toroidal Support Structure (TSS).....13

1.5 Assembly sequence of RFX-mod.....18

CHAPTER 2 RFX-mod2: AN UPGRADE OF RFX-mod MACHINE 19

2.1 The requirements of modifications 20

2.2 List of major mechanical modifications.....21

2.3 Modifications of Toroidal Support Structure (TSS) 23

2.3.1 Requirements and constraints 23

2.3.2 Vacuum sealing solutions at TSS cuts.....23

2.3.3 Closing of other openings on TSS 36

2.3.4 TSS rails.....39

2.4 Modification of passive stabilizing shell.....41

2.5 Design of supporting rings 42

2.6 Assembly and integration.....42

CHAPTER 3 TECHNOLOGICAL FEASIBILITY.....45

3.1 Technological feasibility of proposed solutions 45

3.2 Technical specification of prototype.....46

3.2.1 Identification of requirements.....47

3.2.2 Tests to be performed:.....47
3.2.3 Services.....47
3.2.4 Hardware.....48
3.2.5 Fabrication and assembly steps.....50
CHAPTER 4 LOAD SPECIFICATIONS.....53
4.1 Description of loads on RFX-mod experiment.....53
4.1.1 Mechanical Load Path in RFX-mod.....53
4.1.2 Operating conditions of RFX-mod experiment.....54
4.1.3 Types of loads on RFX-mod experiment.....55
4.2 Description of loads on RFX-mod2.....60
4.2.1 Mechanical Load Path in RFX-mod2.....60
4.2.2 Operation Scenarios of RFX-mod2.....60
4.2.3 Types of loads on RFX-mod2.....64
4.2.4 Load combination and criteria for the verification of RFX-mod2 components 66
4.2.5 Design criteria for verification.....68
CHAPTER 5 THERMAL ANALYSIS.....74
5.1 Model-A (5° sector of shell and FW tiles).....75
5.1.1 Description of model-A.....75
5.1.2 Simulation of normal plasma operation.....77
5.2 Model-B (30° sector of toroidal assembly).....80
5.2.1 Description of model B.....80
5.2.2 Common Boundary conditions for analyses.....82
5.2.3 Simulation of baking and glow discharge cleaning condition.....83
5.2.4 Simulation of normal RFP operation.....86
5.2.5 Simulation of Wall mode locking.....89
5.3 Conclusion.....93
CHAPTER 6 THERMO-MECHANICAL ANALYSIS AND VERIFICATION OF THE PASSIVE STABILIZING SHELL ASSEMBLY.....94
6.1 Study of the interfaces between stabilizing shell and TSS.....94
6.1.1 Design conditions and parameters.....94

6.2 Selection of ring material and number 98
6.3 Development of the interface of rings with shell and TSS 104
6.3.1 Concept 2.1: Supporting rings with 1 top stud and 2 bottom sliding studs . 106
6.3.2 Concept 2.2: Supporting rings with 1 top stud and 2 bottom sliding studs with full shell 108
6.3.3 Concept 2.3: Supporting rings with only 2 bottom sliding studs - Full shell 110
6.3.4 Concept 2.4: Supporting rings with radial sliding support and full shell 112
6.4 Thermo-mechanical verifications of the stabilizing shell assembly 115
6.4.1 Description of model 115
6.4.2 General boundary conditions for the model 116
6.4.3 Simulation of normal RFP operation 117
6.4.4 Simulation of fast termination of plasma 120
6.4.5 Simulation of wall mode locking 121
6.4.6 Simulation of fault case of electromagnetic event 124
6.4.7 Modal analysis for Seismic event 127
6.5 Conclusion 129
CHAPTER 7 **THERMO-MECHANICAL ANALYSIS AND VERIFICATION OF THE TOROIDAL SUPPORT STRUCTURE** 130
7.1 Thermo-mechanical verifications of Toroidal support structure 131
7.1.1 Model description 131
7.1.2 Common Boundary conditions 133
7.1.3 Simulation of baking and GDC operation 137
7.1.4 Simulation of normal RFP operation 140
7.1.5 Simulation of fast termination of plasma 143
7.1.6 Simulation of wall mode locking 144
7.1.7 Simulation of fault case of electromagnetic event 145
7.1.8 Buckling analysis of TSS 148
7.2 Mechanical verification of Thin Resistive Plate 149
7.3 Conclusion 152
CHAPTER 8 CONCLUSION AND FUTURE WORK 154

Appendix A: Material properties……158

Bibliography……..162

CHAPTER 1 INTRODUCTION

1.1 Thermonuclear fusion

Energy is essential for today's society and it is an uncertain issue in long run. Taking into consideration world population growth, energy needs may arise extremely. The renewable energies can be a substitute, but they are not expected to be able to satisfy the total demand even if they will contribute much more in the future. The most foreseen alternative is fusion process which is the foremost source of energy in universe. Thermonuclear fusion is the process occurs naturally at the core of the sun and stars. Gravity plays an important role for confinement of fusion process in sun and stars. In fusion reaction, two light atomic nuclei of hydrogen fuse together in the presence of high temperature and pressure to form heavier nuclei of helium as shown in Figure 1. During the reaction an enormous amount of energy is released. Fusion has some key features which make it an attractive option in a future energy blend: the fusion process is inherently safe; waste which will not be a burden for future generations; no emission of greenhouse gases; and the capacity for large scale energy production.

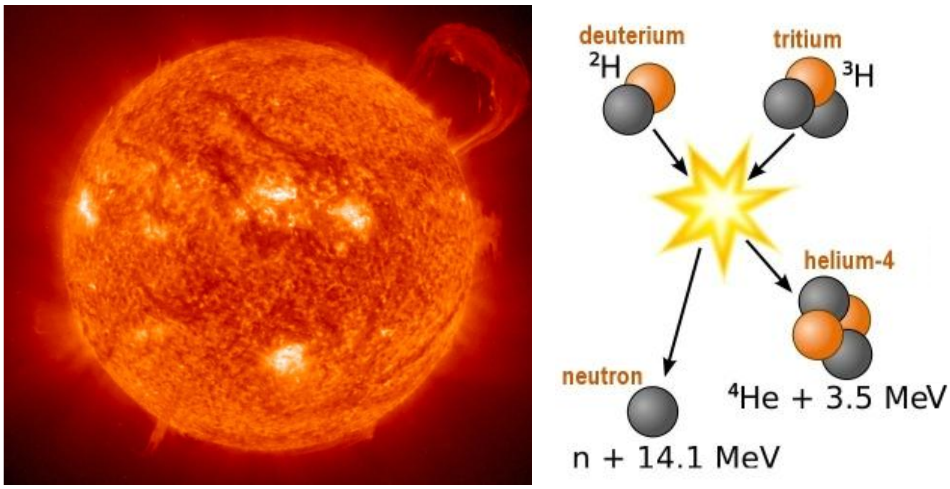

Figure 1: The Sun and the fusion process

With the growing energy demands, fusion energy proves to be a very competent and promising option and hence synergic efforts are underway to achieve viable controlled fusion reaction. There are two basic different methods to recreate the required conditions of temperature and pressure for the thermonuclear fusion reactions to happen: Magnetic Confinement Fusion (MCF) and Inertial Confinement Fusion (ICF).

1.1.1 Magnetic Confinement Fusion (MCF):

The magnetically confined thermonuclear fusion works on the fact that current can easily flow in plasma and plasma particles (nuclei and electrons) can be confined through magnetic field inside their vacuum chamber. The interaction between plasma current and magnetic field gives rise to the confining force. Since early research in the field of fusion process, several machines with several different magnetic configurations have been built

and tested. The most successful configuration is based on toroidal geometry, which is free from the problem of losses at the ends.

Presently there are three main toroidal MCF configurations are in use: the Tokamak, the Stellarator and the Reversed Field Pinch (RFP) magnetic configuration. All of them share the toroidal concept but the magnetic configuration is rather different. The magnetic field is always arranged in order to obtain helical field lines whose goal is to provide plasma equilibrium and stability of confined particles, but they are varies on how configuration obtained.

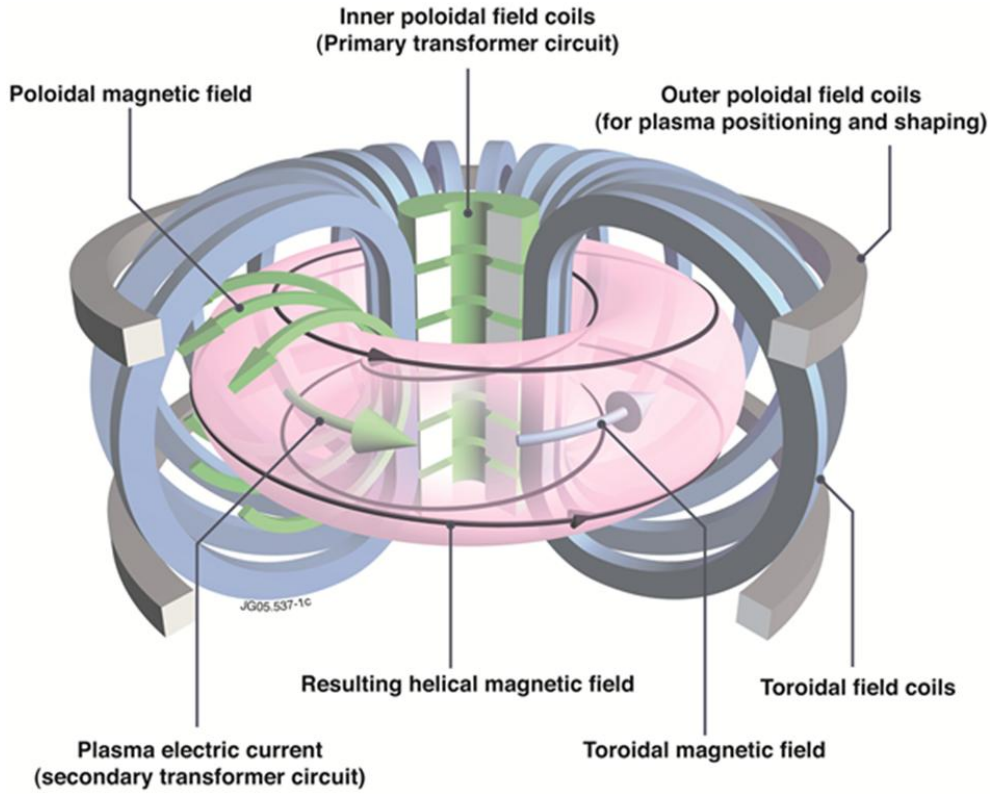

Figure 2: Schematic view of Tokamak configuration

In the Tokamak, toroidal field is produced by a series of coils uniformly distributed around the plasma torus, and the poloidal field component is produced by electric current flowing through the plasma. It is an axisymmetric configuration. The plasma current is usually induced by transformer action and plasma heating is provided by plasma current as shown in Figure 2. Tokamak is the most-researched configuration for producing controlled thermonuclear fusion power.

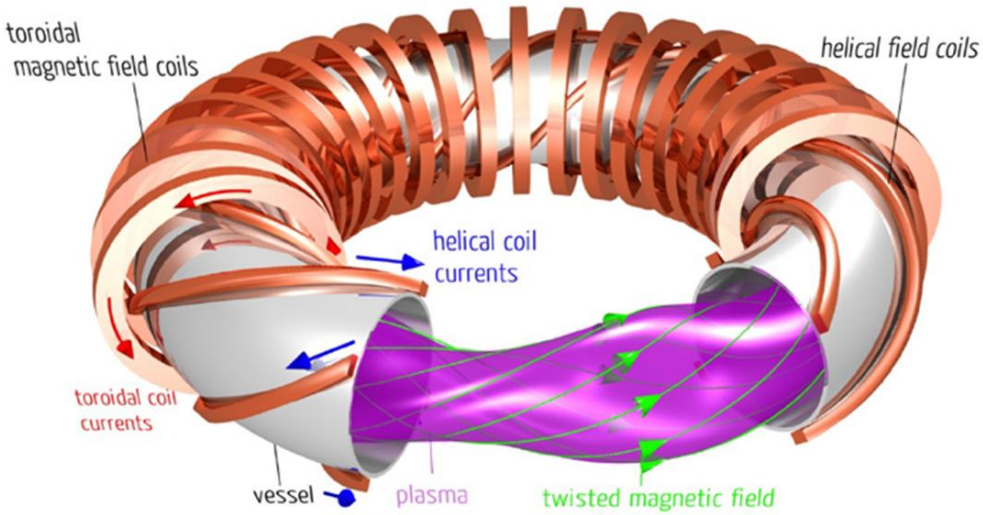

Figure 3: Schematic view of Stellarator configuration

In the Stellarator, the magnetic field configuration is produced only by a series of coils surrounding plasma, which may themselves be helical in shape. No net current is induced in the plasma. This naturally allows for operations in steady state, but on the other hand this configuration requires the design and building of coils with complex, non-planar shapes. In the absence of plasma current, heating depends upon non-ohmic methods.

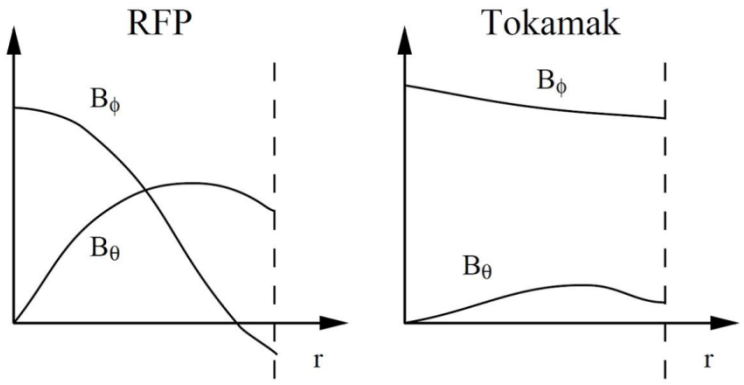

Figure 4: Schematic of RFP and Tokamak configurations magnetic field

The Reversed Field Pinch (RFP) configuration is similar like Tokamak, the toroidal and poloidal components of magnetic field are produced same as in a tokamak. The major difference in RFP is higher current flowing through the plasma and the direction of the toroidal field at edge of the plasma is reversed as shown in Figure 4. In contrast to the tokamak, magnetic field lines in a RFP are almost poloidal, therefore the RFP is near to a curved Z-pinch [1].

Today the research in the field of magnetically confined thermonuclear fusion is carried out at Universities, Laboratories and Research Centres all around the world. The research reported in this document has been carried out at Consorzio RFX in Padova, where a RFP machine is present, namely the Reversed-Field eXperiment (RFX-mod).

1.2 The Reversed Field Pinch magnetic configuration

The Reversed Field Pinch (RFP) magnetic configuration is an axisymmetric system like tokamak. Vacuum vessel is surrounded by a set of toroidal field coils and central solenoid provides the necessary loop voltage for discharge and to drive a current in the plasma inside the vessel. Most of the magnetic field is created by the currents flowing in the plasma. External coils provide small edge toroidal field whose sign is reversed with respect to the central one as shown in Figure 5 and hence it is called RFP configuration.

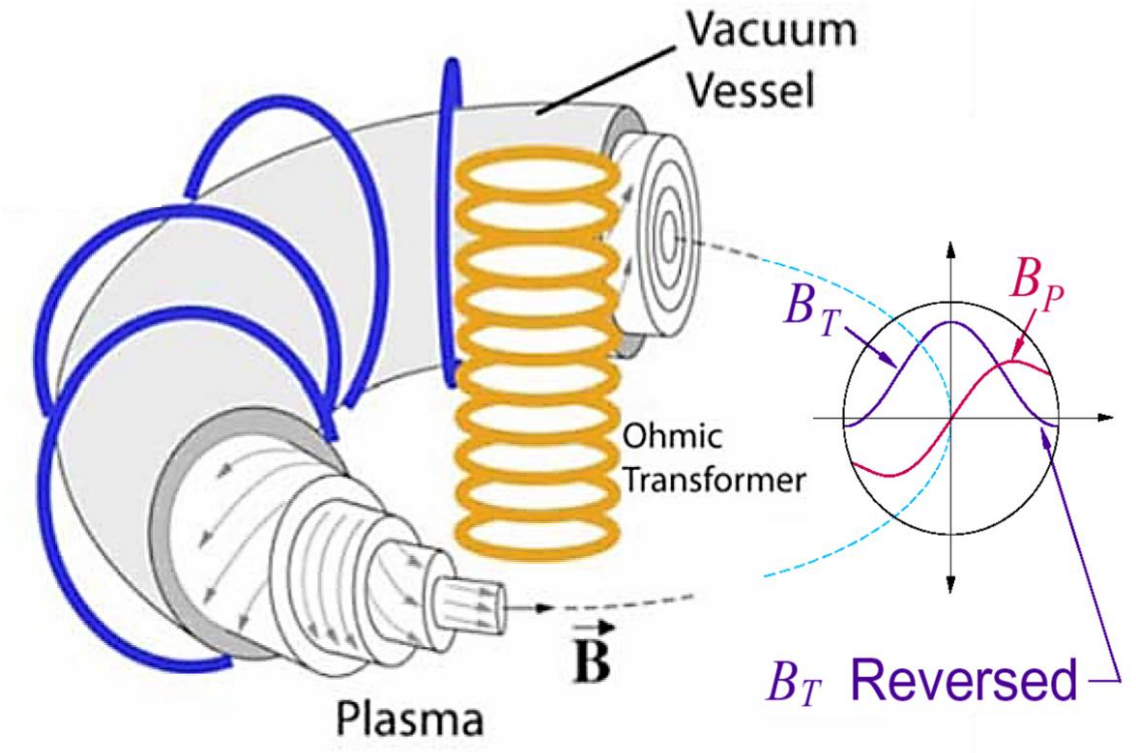

Figure 5: The Reversed Field Pinch magnetic configuration

The RFP configuration has several advantages over other configurations as described below:

- Depend on ohmic heating only
- High engineering beta
- Use of normal coils (rather than superconducting)
- High mass power density
- Efficient maintenance/disassembly
- Possibly free choice of aspect ratio

In RFP plasma current is an order of magnitude larger comparing with tokamak. For the same plasma resistivity in both configurations, ohmic heating is two orders of magnitude larger in RFP [1]. Therefore a RFP should be able to reach thermonuclear temperatures without any additional heating.

The magnetic configuration produces most of its magnetic field by helical currents flowing into the plasma. Since TF coils has to produce only a weak reversed toroidal field at the

edge, there is no need for superconducting coils in RFP and allows choice for normal conductors. This also lowers the requirements on the thickness of their neutron shielding, and on the growth of the radial build up. The coils are also subjected to lower forces than in a tokamak or a stellarator, which decreases the mechanical constraints [1]. The strong self-organization mechanism characterizes the RFP configuration disruption-free because it corresponds to a full magnetohydrodynamics (MHD) relaxation of the magnetic field.

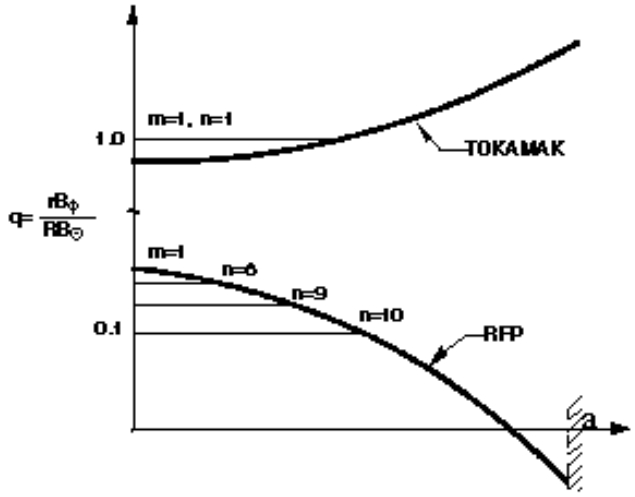

Figure 6: Safety factors comparison of RFP and Tokamak

Typically RFP is a low (q < 1) safety factor configuration, along the minor radius starting from centre safety factor profile is typically decreasing and negative at the edge as shown in Figure 6. RFP is therefore an intrinsically unstable configuration. In the RFP the edge radial magnetic field needs to be controlled either by a thick shell or preferably by feedback controlled saddle coils [2]. This is important to avoid resistive wall modes which are unstable and to improve plasma confinement.

Presently the largest RFP is the RFX-mod device (R = 2 m, a = 0.459 m, maximum current 2 MA) in Padua (Italy). Other present machines are MST (R= 1.5 m, a = 0.5 m, nominal current 0.6 MA) in Madison (USA), EXTRAP T2R (R = 1.24 m, a = 0.18 m, nominal current 300 kA) in Stockholm (Sweden), RELAX (R = 0.51 m, a = 0.25 m, nominal current 80 kA) in Kyoto (Japan), and KTX (R = 1.4 m, a = 0.4 m, nominal current 1 MA) in Hefei (China).

1.3 The RFX experiment

Reversed Field eXperiment (RFX) is a toroidal device designed and built in Padova for experiments on magnetically confined and ohmically heated plasmas in the reversed field pinch (RFP) configuration. Figure 7 shows Arial view of machine hall. RFX is the biggest machine in the RFP configuration, with major radius of 2 m and minor radius of 0.459 m and the highest plasma current up to 2 MA [3].

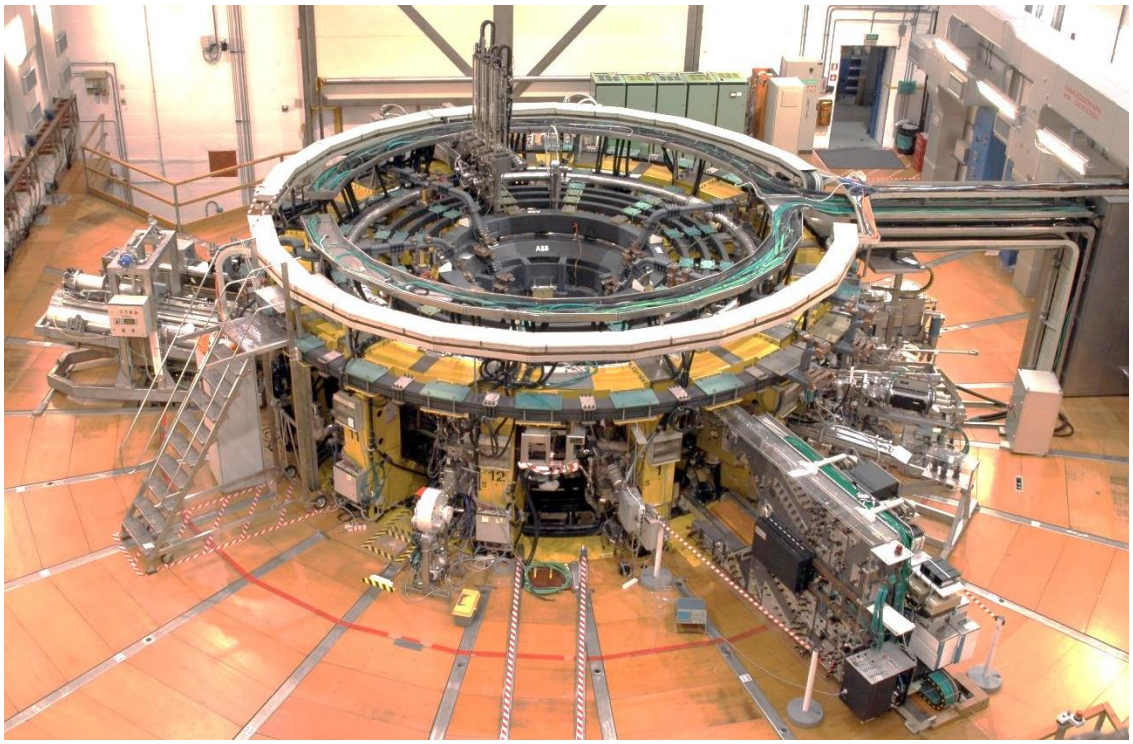

Figure 7: Ariel view of RFX-mod machine

RFX is started the operations in 1992 until 1999. After a fire in the former RFX device in December 1999 which destroyed the significant part of power supplies, it was renewed and upgraded as RFX-mod during the period 2000-2004 [4]. The plasma operations started again in 2004. The main parameters of the RFX-mod machine are listed in Table 1.

Table 1 Main parameters of RFX-mod machine

Major radius, R	[m]	2.0
Minor radius, a	[m]	0.459
Maximum plasma current, Ip	[MA]	2.0
Maximum applied toroidal field, B	[T]	0.7

The machine is able to produce toroidal magnetic field 0.7 T (at the beginning of the plasma pulse) and 0.44 T reversed field at the wall (during the plasma current flat-top). The plasma operation pulse length is 0.5 s. The machine can be operated as low field Tokamak also.

In RFX-mod, the original 65 mm thick stabilizing shell of RFX (which had a magnetic field penetration time constant shell = 500 ms) was replaced with a 3 mm copper shell, whose time constant for penetration of vertical magnetic field (≈50 ms) is ≈10 times shorter than pulse duration [5]. Important features of RFX-mod are a set of 192 independently driven saddle coils [6] aimed at actively controlling the local radial perturbations at the edge, new design of the first wall tiles and passive stabilizing shell.

The aim of machine modification is to improve the performances of the machine by [4]:

- Increasing the first wall power handling capability
- Improving the vacuum vessel wall protection [7]
- Enlarging the plasma breakdown operational window
- Improving the axisymmetric equilibrium control by a reduction of the vertical field penetration time constant with a new passive shell
- Minimising the poloidal and toroidal gap field error

1.4 Mechanical systems of RFX-mod

The machine assembly of RFX-mod is similar as typical RFP system as shown in Figure 8, consisting of First Wall (FW) tiles, a vacuum vessel, a passive stabilizing shell, Toroidal Support Structure (TSS) and magnet system. Magnet system is formed by Ohmic Heating (OH) coils for generating essential flux swing, Field Shaping (FS) coils for plasma shaping and positioning, Toroidal Field (TF) coils for toroidal magnetic field and Saddle coils for the active control of MHD instabilities using for radial magnetic field system.

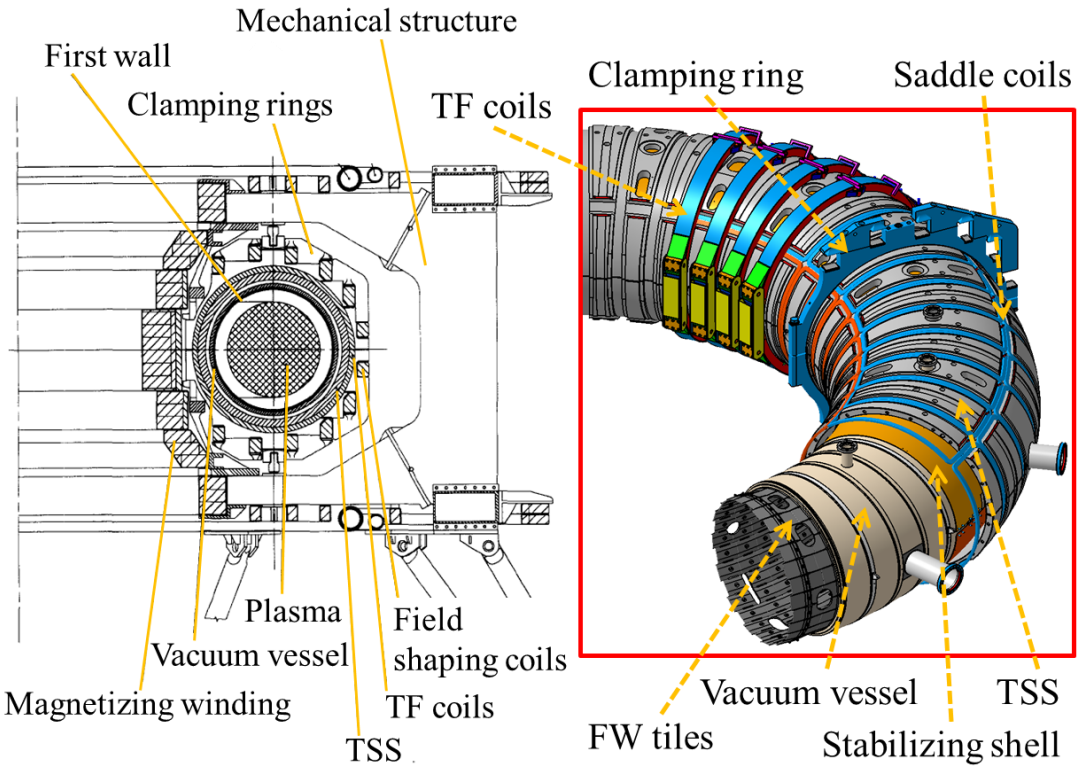

Figure 8: Sectional view and Isometric view of RFX-mod mechanical structure

The vertical cross-section of the torus in Figure 8 schematically shows the relative positioning of first wall, vacuum vessel, passive stabilizing shell, TSS, clamping rings and different magnet systems.

RFX-mod assembly is shown in Figure 8, the vacuum vessel is a sandwich structure made of INCONEL 625. The plasma-facing surface of the vessel is fully covered by 2016 graphite tiles [8], acting like armour against heat fluxes coming from the plasma. The passive stabilizing shell is made up of 3 mm thick copper plate. The passive stabilizing shell is installed on outer surface of vacuum vessel for stabilization against magnetohydrodynamic (MHD) modes. Vacuum vessel is supported on Toroidal Support Structure by 48 radial clamps. The TSS is a made-up of stainless steel (AISI304L) having grooves on its external surface. Main requirement of TSS is to support all surrounding systems. TSS is divided into four parts by its toroidal and poloidal cuts. The top and bottom TSS is preloaded together by 24 clamping rings and left and right TSS are joined together by insulated bolted connections. Clamping Rings also provide support to FS coils. The TSS and OH coils are supported by C-shaped mechanical structure at 12 toroidal toroidal locations.

1.4.1 First Wall tiles

The vacuum vessel (R=1995 mm, a=475 mm) is completely covered by 2016 First Wall (FW) tiles (72 toroidal arrays of 28 poloidal tiles) made of polycrystalline graphite tiles as shown in Figure 10. Graphite was selected due to its low atomic number Z and for its capability to withstand high power loads. FW tiles are supported on 72 stiffening rings of VV by means of bayonet keys. The internal radius of FW tile envelope surface is 0.459 m. The dimensions of the tiles are ~102 mm in the poloidal direction and 130–210 mm along the toroidal direction.

The original first wall tiles were replaced in RFX-mod machine to obtain better protection against local plasma-wall interaction. The shape of the tiles was redesigned to improve plasma-wall interaction by reducing the heat flux peaking on leading edge and to achieve more uniform power distribution [9]. The tiles are also designed to give housing for a number of sensors to be installed behind the tiles, inside the vacuum vessel [7]. The tiles are installed using central bayonet key and Belleville washers as shown in Figure 9. The tiles are having rib at its back side to provide proper vertical alignment inside VV stiffening ring groove. The maximum thickness of the tile is equal to 18 mm in the central rib area of the tile. This thickness allows the housing of the tile fixing keys and ensures sufficient mechanical strength. The ends of tiles have thickness up to 9 mm which provide space for sensors to be installed back side of tiles and vacuum vessel.

Severe mechanical and thermal loads are affecting to FW tiles due to localized plasma wall interactions. During a full-power pulse with plasma current I = 2MA, 20 MJ of thermal

power deposits on the first wall. The electrodynamic forces are acting on the tiles due to eddy currents and halo currents [10] flowing through tiles to VV.

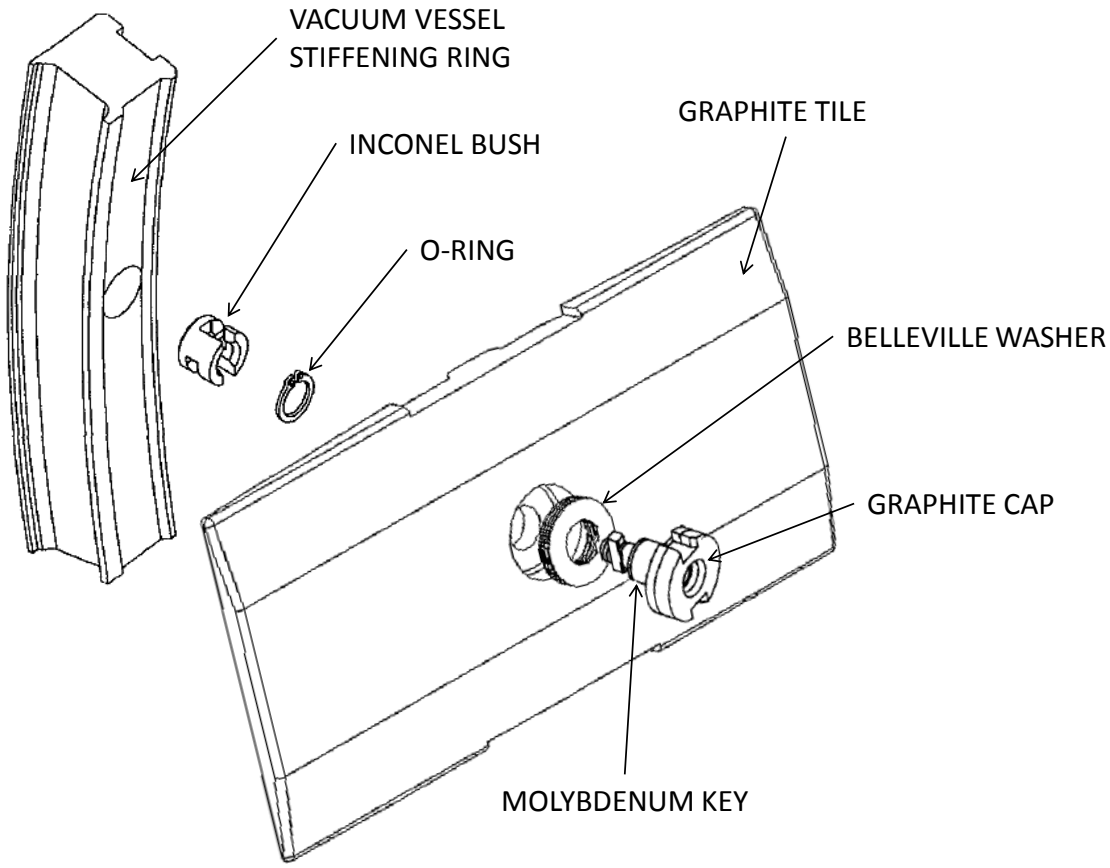

Figure 9: First Wall tile with supporting system

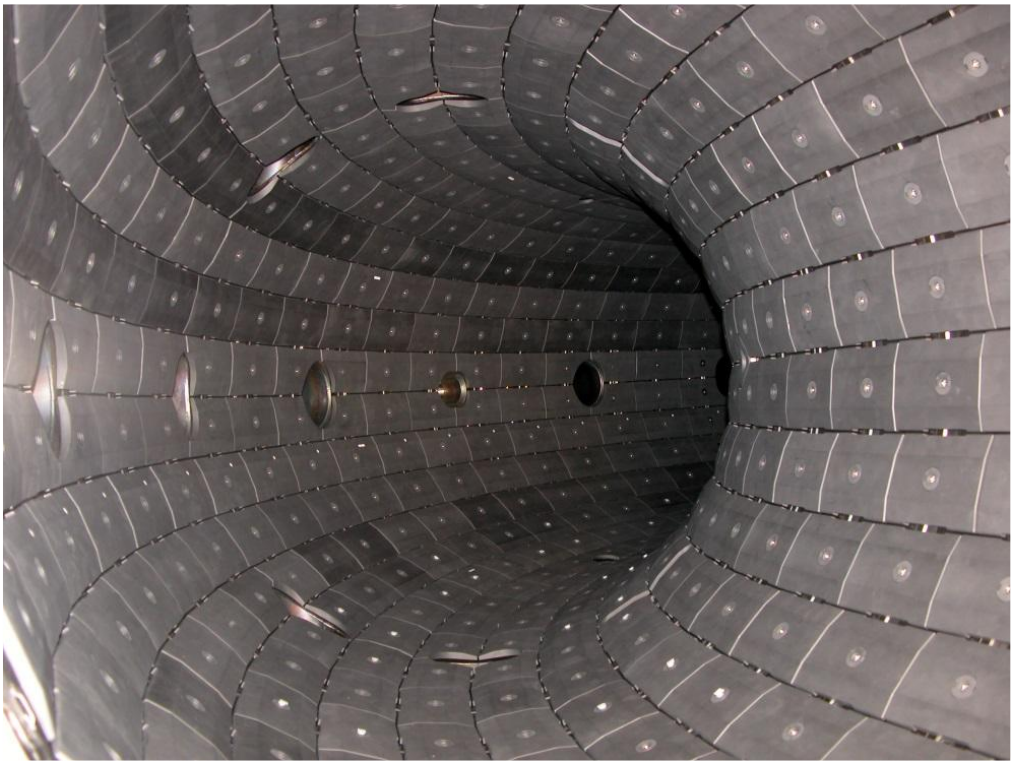

Figure 10: FW tiles installed in RFX-mod

1.4.2 Vacuum Vessel

The vacuum vessel is fully welded double wall rigid structure. It is composed of 72 wedge-shaped stiffening rings, consisting sandwich structure in between each ring. The sandwich structure has double wall with a 2 mm thick inner wall and a 1 mm thick outer wall, a 0.5 mm corrugated sheet welded to the inner and the outer walls as shown in Figure 11. The space between inner and outer walls is used either for cooling purpose or creating secondary vacuum boundary.

The VV have 12 equatorial ports of 150 mm diameter for vacuum pumping and two vertical ports for access to the interspace. Another 12 equatorial ports and other vertical ports are in use for plasma diagnostics, gas injection, glow discharge cleaning (GDC) and in-vessel inspection. The 360° assembly of VV is shown in Figure 12 with port arrangements. The larger ports are not directly welded to the thin walls; a 30 mm thick plate locally replaces the sandwich structure to obtain a stiffer support and to reinforce the port edge against plasma erosion as shown in Figure 11 [8]. The stiffening ring is having 28 equispaced holes to support the FW tiles and provides the required stiffness.

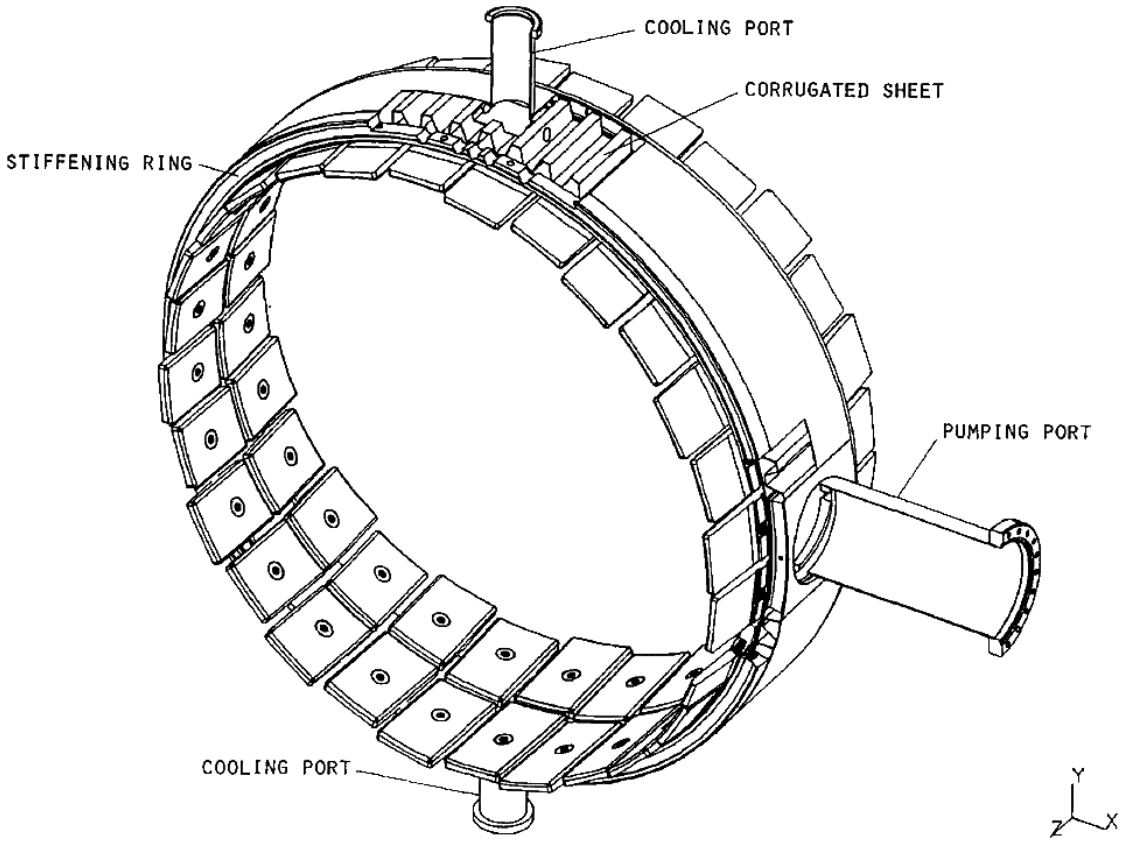

Figure 11: Detailed view of 5° wedge element of vacuum vessel

The VV is supported on TSS by 48 connecting rods, equally spaced around inner and outer equatorial circumstances. The connecting rods are thermally and electrically insulated by ceramic glass inserts. The connecting rods allow only radial thermal expansion of VV, while constrain any other movement. Table 2 shows major parameters of VV.

Table 2 Vacuum vessel main characteristics [8]

Material		Inconel 625
Major radius (ambient temperature)	mm	1995
Major radius (350°C)	mm	2003
Inner minor radius excluding tiles (ambient temperature)	mm	475
Overall thickness	mm	30
Evacuated volume	m^3	9
Mass	kg	4000
Toroidal resistance	mΩ	1.1
Transverse field diffusion time constant	ms	1.0
Toroidal field diffusion time constant	ms	2.1

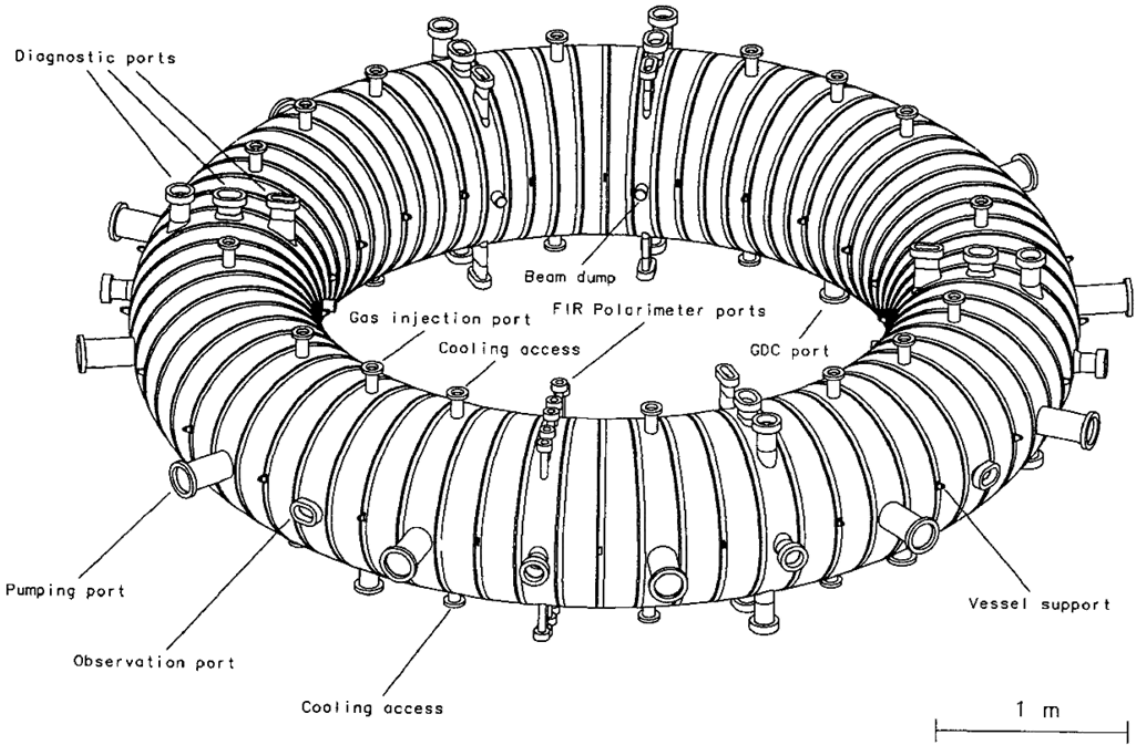

Figure 12: The vacuum vessel assembly

The VV was carefully designed considering its requirements and applicable loading conditions. The non-magnetic alloys Inconel 625 material is selected for VV considering its high electrical resistivity and good mechanical properties. The toroidal loop resistance of the vacuum vessel is 1.1 mΩ. It should be maintained UHV (10^{-9} mbar) conditions and withstand atmospheric pressure. The VV is designed for atmospheric pressure, first wall forces and the first wall weight and electrodynamic loads. The static FE analysis performed considering above mentioned forces. The dynamic analysis of the vessel was performed to calculate the fundamental frequencies of the structure along with the modal shapes and then the dynamic response to the transient loads [8]. The symmetry of the structure minimizes vertical and horizontal electromagnetic forces and high stiffness of reduces further support requirements. The VV is designed for baking temperature of 350° C as per RFX operating requirement, but in RFX-mod the baking temperature reduced to 180°C considering limit of newly designed passive stabilizing shell [4].

1.4.3 Passive stabilizing shell

In RFX-mod, VV is closely surrounded by a passive stabilizing shell to give plasma stabilization against magnetohydrodynamic (MHD) modes. It is made up 3 mm thick copper plate which is divided into four segments. Each segment will extend approximately 180° in the poloidal direction and 190° in the toroidal direction, to create an insulated overlapping joint for a 20° toroidal sector as shown in Figure 13 [11]. Main parameters of passive stabilizing shell are given in Table 3

Table 3 Main parameters of passive stabilizing shell

Material		UNS C10200
Major radius	mm	1995
Inner minor radius	mm	511.5
Thickness	mm	3
Vertical field penetration time constant	ms	50

The original 65 mm thick aluminium stabilizing shell (time constant of 500 ms) of RFX is replaced by 3 mm thin copper stabilizing shell (time constant of 50 ms) in RFX-mod machine considering magnetic fluctuations on short timescales. This new passive stabilizing shell contributes in the stabilization of the plasma MHD modes during the first 40/50 ms of each pulse. The copper is selected to minimise the overall radial dimension of the new shell.

The stabilizing shell is assembled on the external surface of VV in order to minimize the distance from the plasma edge. Presently the distance between shell and plasma edge is 54 mm. The stabilizing shell is retained its position over VV by means of 95 clamping bands, each clamping band is preloaded by means of two screws located on the inner and outer equatorial plane. The electrical and thermal insulation between the vacuum vessel and the shell is realized by 6.5 mm thick insulating spacers, located in correspondence with the band positions. The insulation is having a maximum temperature rating of 220 °C. The spacers allow the location of various diagnostic sensors such as pick-up coils, radial coils, rogowski coils and thermocouples.

The penetration of the electric and magnetic fields into the plasma region is ensured by the insulation of two of the four gaps of the shell (one poloidal and one toroidal). The external equatorial joint is short circuited by means of a series of copper plates which are fixed to both halves of the shell as shown in Figure 13. Insulation is provided between both halves by maintaining air gap of 20 mm at internal equatorial gap. The poloidal insulated joint is obtained by the insertion of a 2 mm thick PTFE sheet between the overlapping sectors of the shell. The second poloidal joint is short circuited by welding [4].

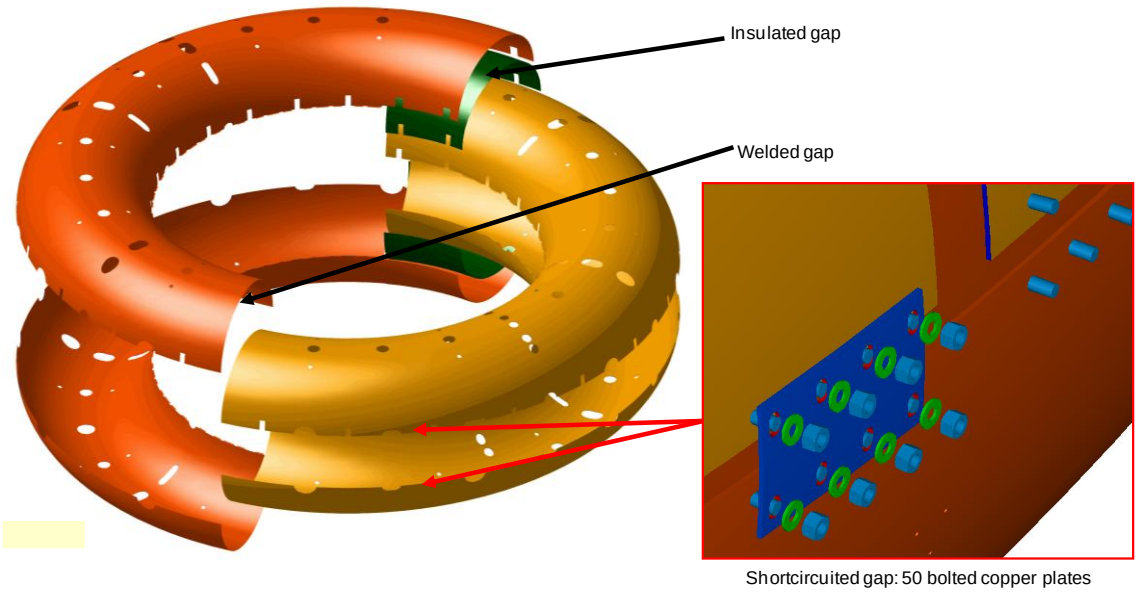

Figure 13: Passive stabilizing Shell

Thermal analysis carried out to verify the behaviour of new stabilizing shell under baking and pulse operating condition. Figure 14 shows average temperature gain by stabilizing shell, which is always 40° C lower than vacuum vessel and compensate the difference of thermal expansion [11]. Structural verification is also carried out by static and dynamic FE analyses to identify stress distribution in the shell and in the clamping bands for nominal and fault conditions and results found well below the yield strength of the material [4] [11].

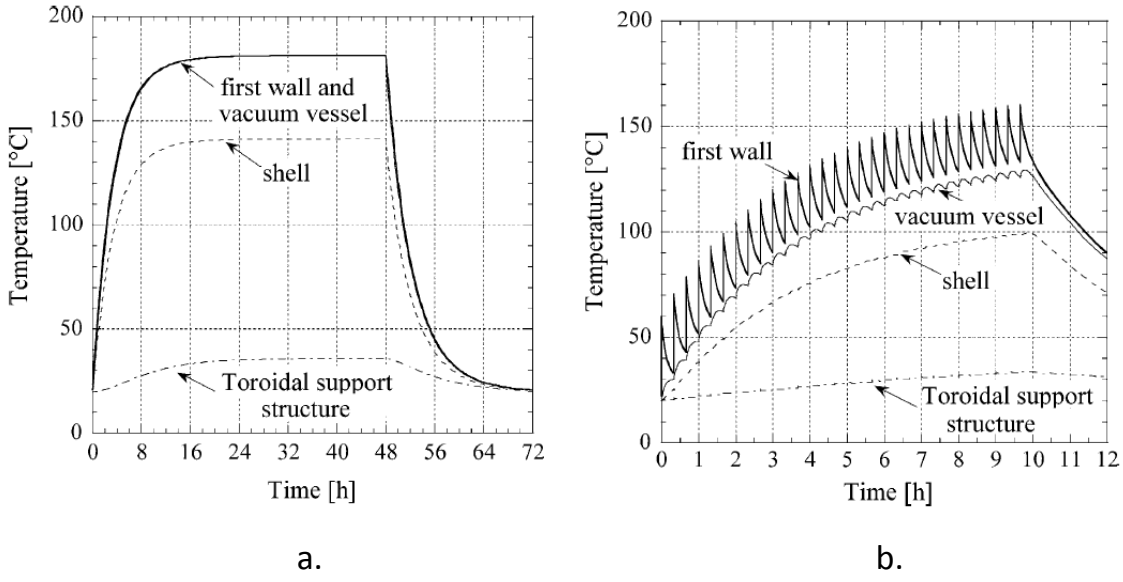

Figure 14: Average temperatures of the components during (a.) Baking and wall conditionings and (b.) an experimental session [11]

1.4.4 Toroidal Support Structure (TSS)

The original 65 mm thick aluminium stabilizing shell of RFX experiment was intend for plasma stabilization against MHD and to provide structural support to VV and surrounding system. In RFX-mod, new Toroidal Support Structure was designed and developed for structural support requirement. Main parameters of TSS are given in Table 4.

Table 4 Main parameters of Toroidal Support Structure

Material		AISI 304L
Major radius	mm	2000
Inner minor radius	mm	553
Outer minor radius	mm	600
Wall thickness	mm	47
Minimum wall thickness at groove	mm	20

The TSS is a stainless steel (AISI304L) toroidal shell having a maximum thickness of 47 mm and minimum thickness of 20 mm as shown in Figure 15. Its major radius is 2 m and the outer minor radius is 0.6 m. The TSS is providing support to the saddle coils, the Toroidal Field (TF) coils, the field shaping coils at its external surface and the vacuum vessel assembly at its internal side [11]. The 48 radial supports for VV are provided at its internal surface as shown in Figure 15.

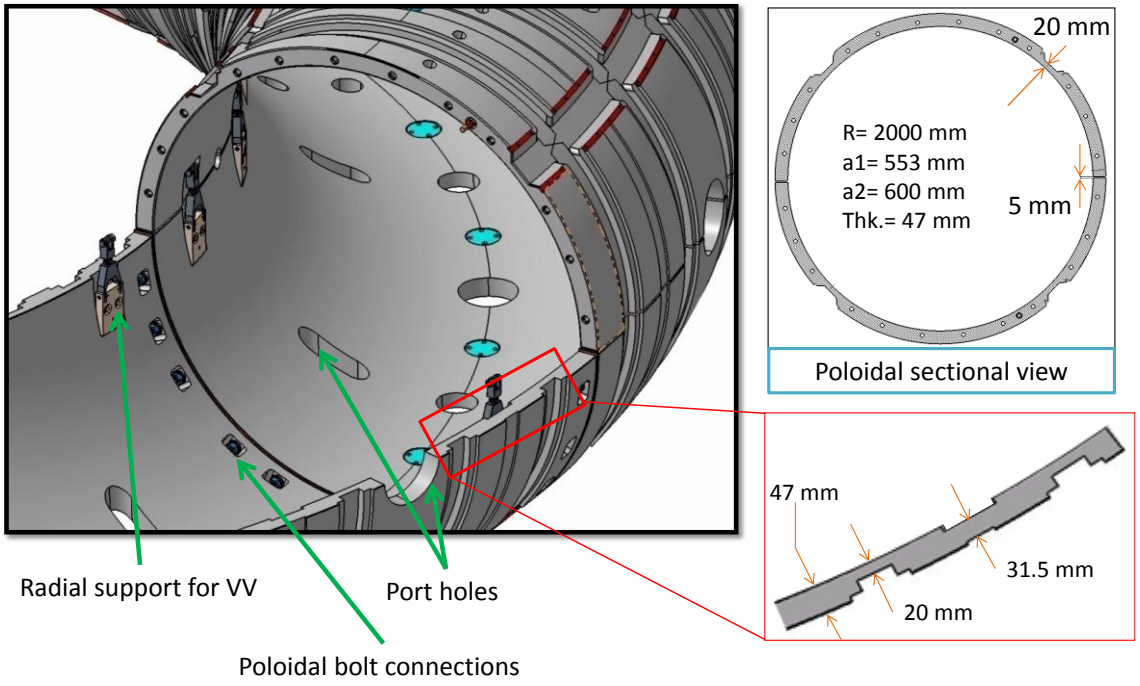

Figure 15: Details of TSS

On external surface of the TSS, poloidal and toroidal grooves are machined to accommodate the 192 saddle coils, the 48 toroidal field coils and 24 clamping rings as shown in Figure 15. The minimum thickness of 20 mm is in correspondence with the grooves for the saddle coils.

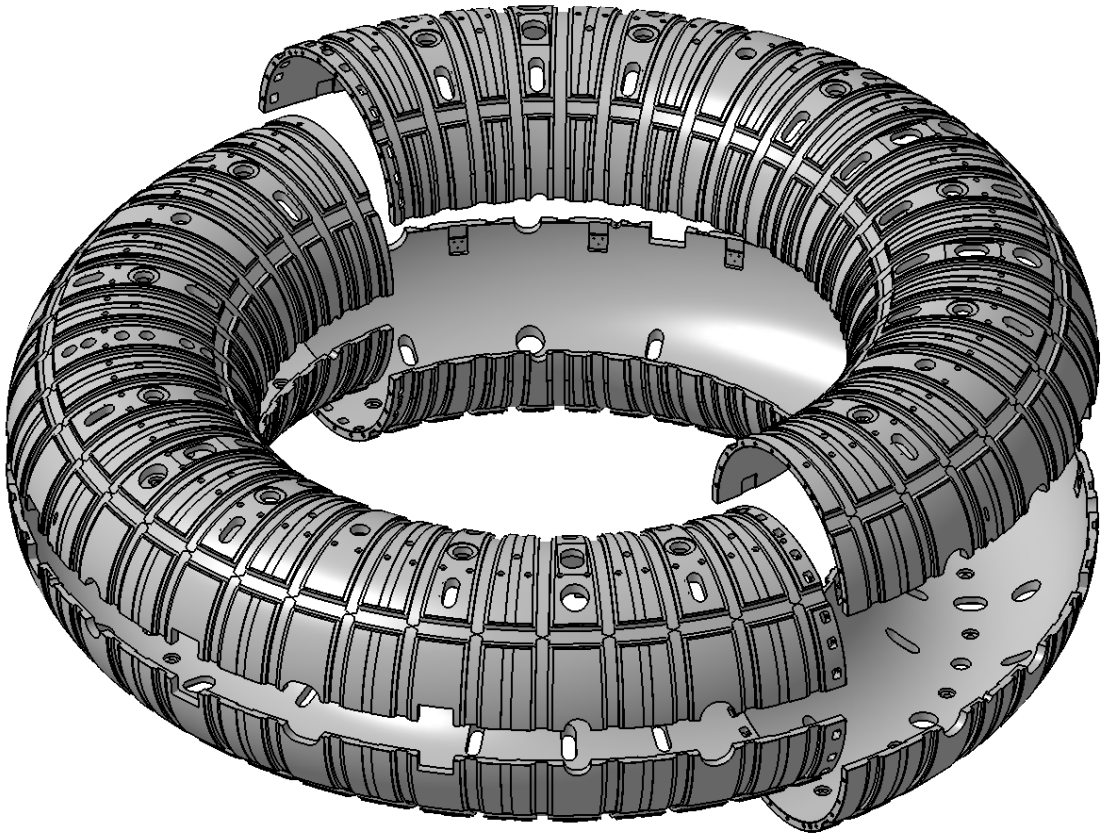

Figure 16: Toroidal Support Structure (TSS)

For electrical and assembly reasons, the TSS is made in four parts, each extending for 180° both in the toroidal and poloidal directions as shown in Figure 16. There is 5 mm gap between all four parts which are used to ensure penetration of electric and magnetic field to plasma region. The external equatorial joint is electrically insulated with a 5 mm thick epoxy glass sheet. The internal equatorial joint is short-circuited by inserting silver plated copper elements.

The two bolted poloidal joints are electrically insulated by means of a 5 mm epoxy glass layer, heat-shrinkable tubing of the bolt shanks and epoxy glass washers (see Figure 15). 24 bolts of size M16 (12 upper and 12 lower) were screwed on the corresponding epoxy glass bush of M27 at each poloidal joint [12]. Bolt connections are accommodated within TSS wall thickness and cuts (24x2) are provided in TSS for bolt tightening as shown in Figure 15 and Figure 17. The epoxy fibreglass-G11 (EP GC 203) bush and bolted joint was verified by FE analysis and experimental tests. Preload of 70 kN (torque of 150 Nm) was considered with non-axisymmetric electrodynamic loads and a quite good uniformity of the contact pressure at the interface. The average pressure in the contact area is about 11 MPa and no detachments were found between the surfaces of the joint [12]. The poloidal gaps of the TSS may be subjected to a maximum voltage up to 1.5 kV during the experimental operations [11].

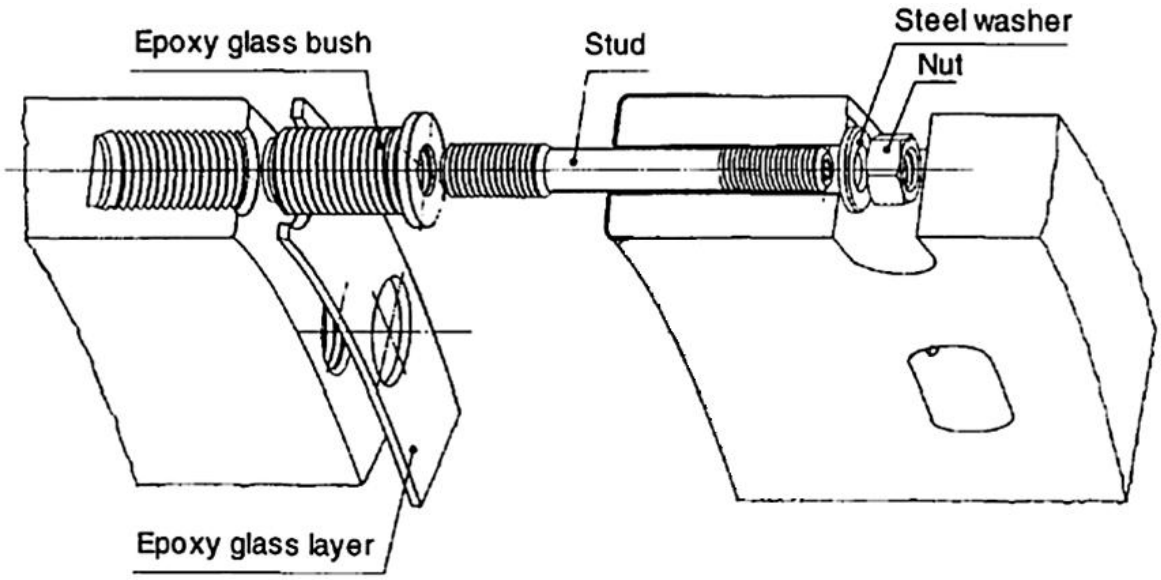

Figure 17: Exploded view of poloidal bolting connection of TSS

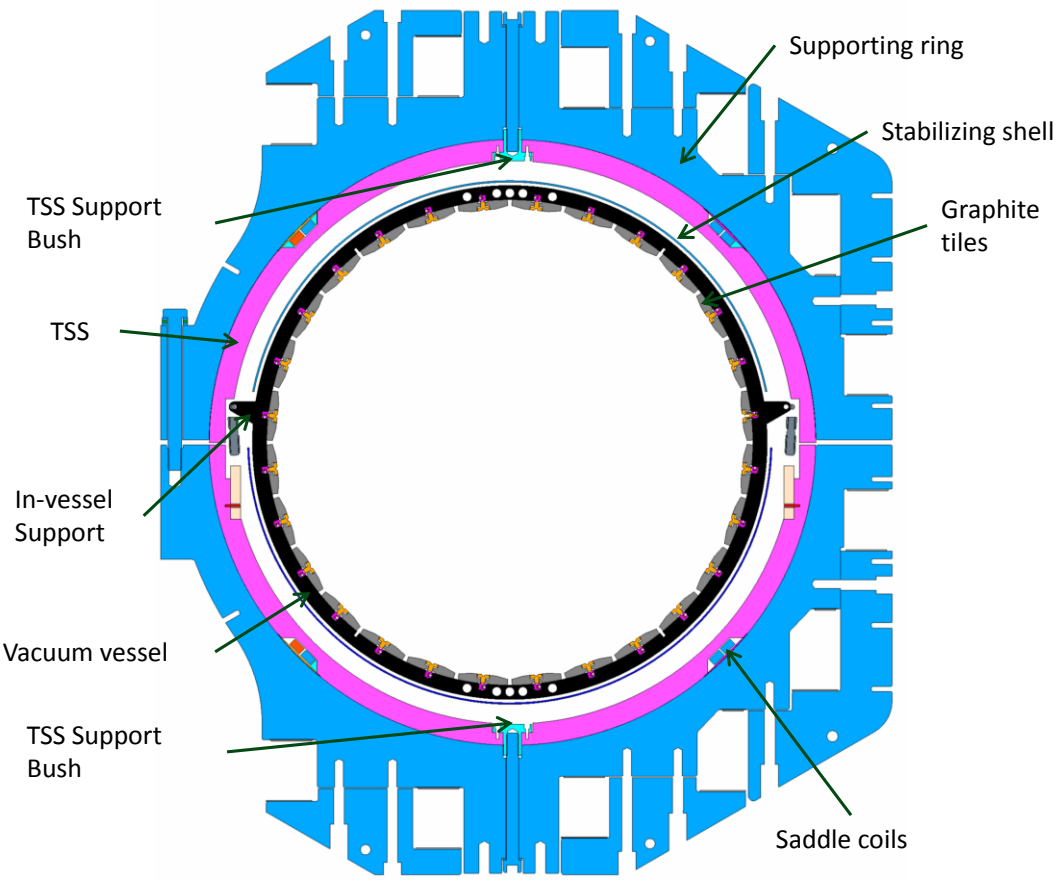

Figure 18: Poloidal sectional view of TSS assembly

The upper and the lower halves are preloaded together by 24 clamping rings with total 15 MN preload applied to TSS [11]. TSS is supported through 48 TSS bushes on its top (24) and bottom (24) corresponding to location of clamping rings (see Figure 15 and Figure 18). Out of total 24 clamping rings, only 12 clamping rings (alternatively) are supported through mechanical structure.

There are total 153 openings provided in TSS for different port access (22 external equatorial ports, 9 internal equatorial ports, and 122 vertical ports) as shown in Figure 15.

The TSS design was verified by static FE analyses considering the clamping preload and electrodynamic loads imparted by each component during the pulse. The maximum Von Mises stresses (~ 85 MPa) were located in correspondence with the clamping rings at the intersection with the toroidal grooves (see Figure 19). The dominant contribution is coming from the preload of the clamping rings and the toroidal coils [11].

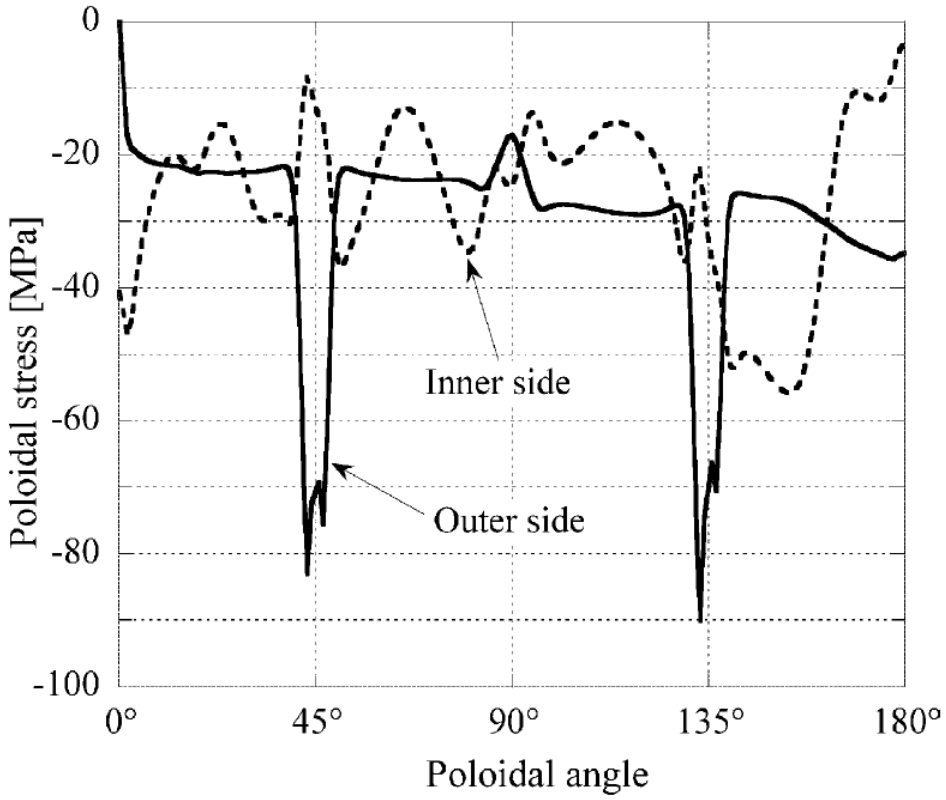

Figure 19: Poloidal stress (SY) in the TSS at clamping rings location [11]

1.5 Assembly sequence of RFX-mod

Followings are the common steps performed for the assembly of toroidal components:

1. Lower TSS joined at poloidal cut by bolted joint and coupled with lower parts of 24 clamping rings
2. Vacuum vessel sub assembly is prepared
   a. FW tiles installed on its internal surface
   b. Sensors and cable routing prepared
   c. Stabilizing shell installed on its external side by means of 95 clamping bands
3. VV sub-assembly install in side lower TSS by radial supports (refer Figure 20)
4. Upper TSS is joined at poloidal cut by bolted joint and coupled with upper parts of 24 clamping rings
5. Toroidal assembly completed by closing Upper and lower TSS at toroidal cut by clamping rings connections

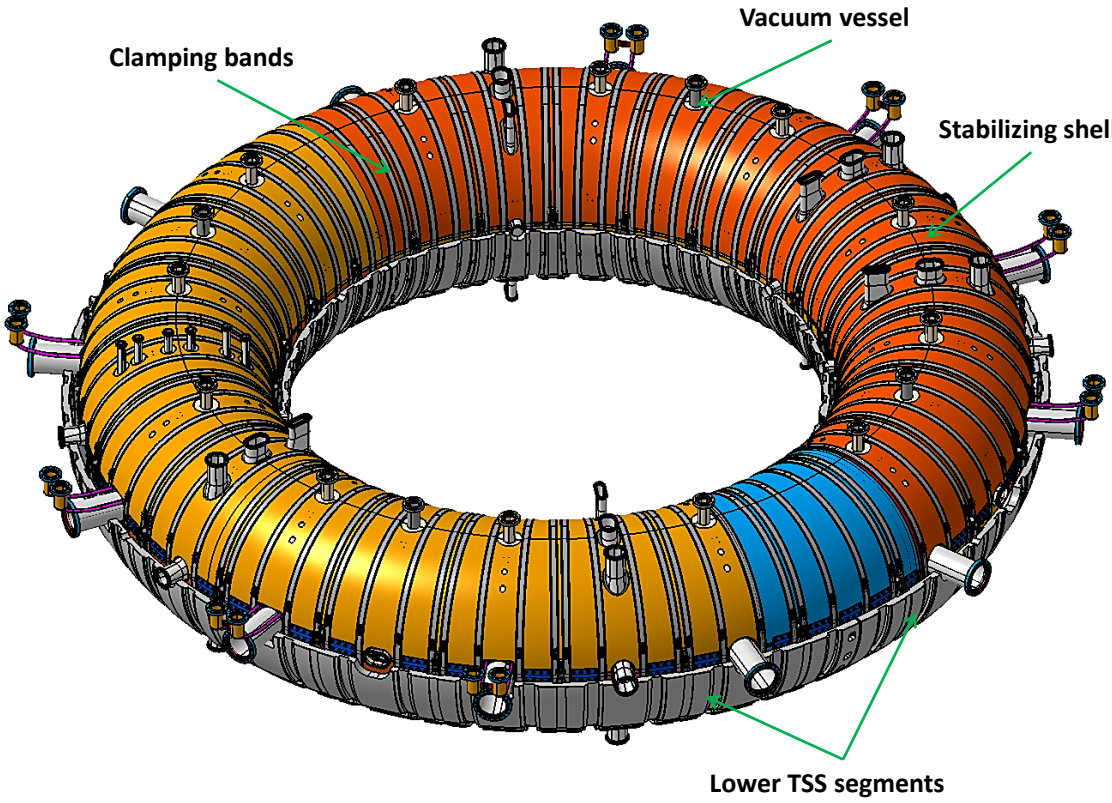

Figure 20: Toroidal assembly of RFX-mod

CHAPTER 2 RFX-mod2: AN UPGRADE OF RFX-mod MACHINE

After first modification in the machine, RFX-mod [4] is in operation since 2004 and providing its contribution to fusion research program. RFX-mod has proved its potentiality with its achievements combined with other RFP experiments. The RFX-mod experimental campaign has presented range of results advancing the understanding of the RFP as a fusion concept. The RFX-mod major contribution is in field of Theory and modelling, Active control of MHD instabilities, Transport studies and Turbulence studies [13]. RFX-mod above 1 MA plasma current illustrates that spontaneously plasma self-organizes in a single-axis helical state, with an internal transport barrier. It has also contributed to basic physics issues like dynamo effect and magnetic reconnection. It is developing active control algorithms of MHD instabilities assessing the effect of the magnetic boundary on TM rotation. RFX-mod is advancing in cross-configuration studies of MHD, density limit, ITBs, turbulence and Resonant Magnetic Perturbation (RMP). The determined experimental activity was accompanied by theory program and international collaborations.

Full exploitation of RFX-mod sought upgrade of machine to provide more scientific contribution to the development of the international Tokamak and Stellarator program. The general motivations [13] for the possibility of improving the RFX-mod device are as follows:

- Advance the RFP physics as a fusion concept; a RFP fusion reactor has the potential advantage of the concentration of the magnetic field within the plasma, with small applied toroidal field and large plasma current density; in principle, there is no need of additional heating required and no disruptions
- Extend the RFX-mod capability of exploring several critical issues for Fusion Science, offering the opportunity of a transversal view with respect to the magnetic confinement. Such issues include three-dimensional physics, MHD stability control, high density limit and turbulence physics, impurity behaviour, plasma-wall interaction in presence of transient high power loads, transport barriers, 3D non-linear MHD modelling and disruption mitigation studies
- Strengthen the study of basic plasma physics issues and their links with other fields, for example self-organisation, dynamo mechanism, magnetic reconnection and turbulence.

The proposed main areas of modifications for the RFX-mod device are:

A. Improvement of the magnetic front-end
   - A.1 Removal of conductive Inconel vacuum vessel to eliminate the braking torque induced by the vacuum vessel to the plasma rotation
   - A.2 Reduction of plasma-Cu shell distance to minimize the radial field at the plasma edge
   - A.3 Improvement of time and spatial resolution of magnetic sensors
B. Mitigation of the effects of plasma-wall interaction

B.1 Change of first wall material and wall conditioning techniques to minimize the hydrogenic species recycling during the pulse and at the same time maintaining the capability of high power load sustainment; this will improve the density control and extend the operational scenarios both in RFP and Tokamak configuration

C. Re-arrangement of equatorial accesses

C.1 For application of heating system (few hundreds kW of neutral beam and/or ECRH) to favour the L-H transition in Tokamak configuration

C.2 To increasing the flexibility of diagnostic interfaces

The requirement of modifications A.1 and A.2 is discussed in detailed below in section 2.1, which are intended for research work described in this thesis.

2.1 The requirements of modifications

Conventional RFP plasma is surrounded by a closefitting, thick, conducting shell whose inductor/resistor (L/R) time is much longer than the duration of the discharge. Such a shell is necessary in order to stabilize external kink modes which would otherwise rapidly destroy the plasma [14]. In the presence of thick shell, the dominant MHD modes (m=1 tearing modes) are resonant in the plasma core. The core tearing modes are responsible for the dynamo action which maintains the field reversal, and therefore, generally known as dynamo modes.

In RFX-mod during the plasma start-up phase the dynamo modes form a toroidally localized phase-lock to the shell and remains locked (non-rotating) throughout the duration of the discharge. The stationary phase-lock significantly degrade the overall plasma confinement and also gives rise to a toroidally localized, stationary ‘‘hot spot’’ on the plasma facing surface. If the plasma current is made sufficiently large, this ‘‘hot spot’’ overheats the facing surface, leading to the influx of impurities into the plasma, and the eventual termination of the discharge. Indeed, the maximum achievable plasma current in RFX is limited by this effect [15]. The presence of a resistive shell close to the plasma has been indicated as a possible cause of the wall-locking of the MHD modes observed in RFX-mod also at very low values of the plasma current (>70-80kA) [16]. However, feedback control system can keep dynamo tearing modes into slow rotation virtually for any amplitude, as demonstrated in RFX-mod [17]. A close-fitting shell is required to minimize the radial field at the plasma edge and related geometrical distortion. In the present RFX-mod layout the stabilizing shell is relatively loose-fitting due to the presence of the 3 cm thick Inconel vacuum vessel facing the plasma [17].

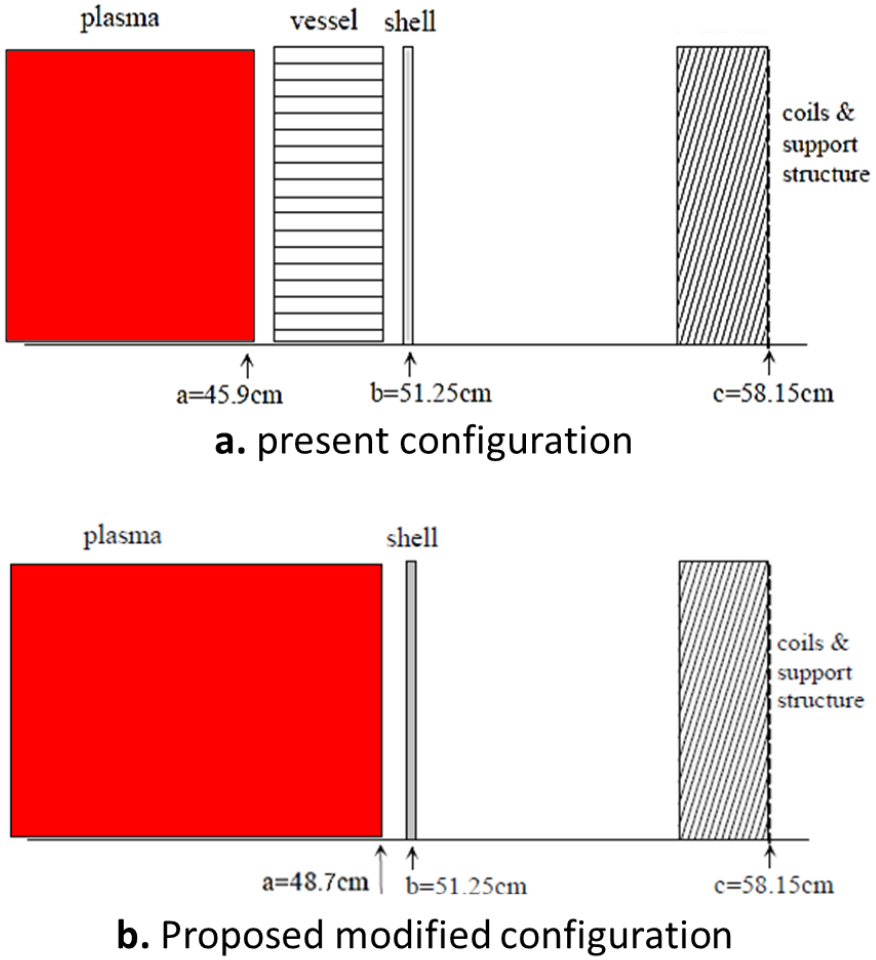

Figure 21: sketch of the structures surrounding the plasma

The present configuration of the RFX-mod boundary is sketched in Figure 21(a.). It includes plasma (minor radius a = 459 mm) surrounded by 30 mm thick vacuum vessel. The 3 mm passive stabilizing shell is placed (radius b=512.5 mm) outside of VV and a Toroidal Support Structure (radius c=581.5 mm) supporting the control coils.

In order to optimize the plasma-shell proximity, different configurations were evaluated. The analysis carried out using RFXlocking+Sidebands code to possible configurations. Calculations are described in detail in the internal note [17]. The main result of the analysis is that the most convenient solution is the configuration with the hypothesis of removing present vacuum vessel and to make toroidal support structure vacuum tight. The new configuration with proposed modification is shown in Figure 21(b.).

2.2 List of major mechanical modifications

The research work in present thesis is mainly concentrated on the modifications, which proposes to remove vacuum vessel and bring plasma close to passive stabilizing shell.

The new mechanical modification proposed to improve passive MHD control by bringing passive stabilizing shell as near as possible to the plasma (reduced plasma-shell distance) and to improve plasma wall lock mode scenario by minimizing braking torque on plasma

through the elimination of vacuum vessel. This would allow enlarging the plasma section and bringing its boundary closer to the passive stabilizing shell, which is maintained at same position and shielded by a new first wall.

Major mechanical modifications considered are listed below;

1. Remove vacuum vessel and make Toroidal Support Structure (TSS) vacuum tight
    a. Design vacuum sealing of TSS at toroidal and poloidal cuts
    b. Design of port integration and closing of other openings
2. Supports FW tiles on passive stabilizing shell
3. Design of passive stabilizing shell modifications
4. New support system for passive stabilizing shell

New assembly procedure and sensor cable routing

2.3 Modifications of Toroidal Support Structure (TSS)

Toroidal Support Structure was evaluated for design of vacuum sealing and makes it compatible to use as new vacuum vessel.

2.3.1 Requirements and constraints

By removing the vacuum vessel, the TSS has to comply with the following requirements:

- Vacuum tightness;
- Electrical insulation at two poloidal cuts and at least one toroidal cut;
- Support the stabilising shell and the FW tiles.

Features at the present TSS have to be considered for the foreseen modifications; the main TSS constraints are:

- The thickness of the sealing surface is varying from 20 mm to 47 mm due to grooves machined on its external surface to accommodate the 192 saddle coils, the 48 toroidal field coils, and 24 clamping rings;
- Non-planar sealing surface due to port holes at external toroidal cut;
- Toroidal and poloidal sealing surfaces crosses each other;
- Only 5 mm gap is available between surfaces to accommodate sealing and electrical insulation;
- No feasibility of flange connection (Only connection options are, clamping rings for toroidal cuts, present bolted connection at poloidal cuts).

2.3.2 Vacuum sealing solutions at TSS cuts

Different vacuum sealing technique were studied and evaluated to design seals for TSS cuts considering above stringent conditions. The main goal of sealing design study is to provide leak free seal and required electrical insulation.

2.3.2.1 Survey of sealing techniques

There are wide ranges of commercially available seal choices. For any vacuum chambers there are two broad categories for static sealing joints: permanent joints and demountable joints.

Permanent sealing options are realized through welding, brazing or soldering and gluing (epoxy resin). Demountable sealing options are realized through flanged connection with elastomer or metal seals.

- **Demountable Seals**

  The demountable seals are most common for vacuum chambers with flanged joint, flange to flange connections with sealing material in between. The flanges might be sealed by a clamp ring, a set of clamps or by bolts. The opposite sides of a seal are

compressed between the walls or gland which create zero clearance within and provides an effective seal. Typical sealing material and configurations are explained below:

- ✓ **Elastomers**

  Most common choice of elastomer gasket is an O-ring in groove and sometimes flat gasket used form of seals for static seal design. They are economical and easy to use. O-rings seals can perform effectively over a wide range of pressures. Performance of O-ring seal depends on wide range of operating conditions. O-ring seal design includes the basic parameters like sealing mechanism, section of O-ring size, material selection, calculating gland dimensions, preload, temperature and operational environment effects. O-rings typically fail in their applications because of the combined adverse effects of several environmental factors. For vacuum applications the permeability of the material is an important parameter while material selection. Back-up rings are used to save the O-ring from excessive deformation.

  For optimum sealing performance, correct O-ring selection is the direct result of a number of design considerations. These considerations include: size, squeeze, stretch, chemical compatibility, and the ability to resist pressure, temperature, and friction. Figure 22 shows the general parameters for O-ring selection and gland design.

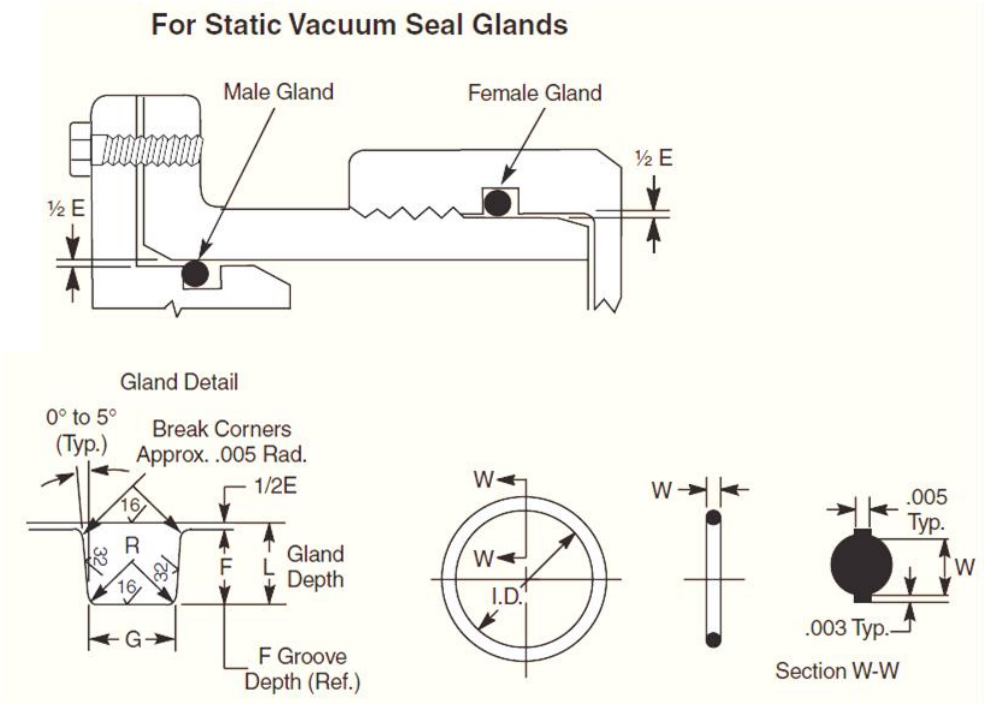

Figure 22: Parameters for O-ring selection and gland design [18]

- ✓ **Metallic seals**

  Metal seals are normally used in vacuum applications when higher vacuum levels (10^{-8} torr) are desired. Common metal seals include the knife-edge (refer Figure 23) (Conflat™), wire seal and Helicoflex™ seal. Solid metal gaskets require very

smooth, plain surface finishes and high clamping forces. Metal gaskets combinations with soft fillers such as double jacketed and spiral-wound can tolerate greater surface roughness and will seat with lesser compressive forces. Most common materials for metallic seals are copper, aluminium and indium.

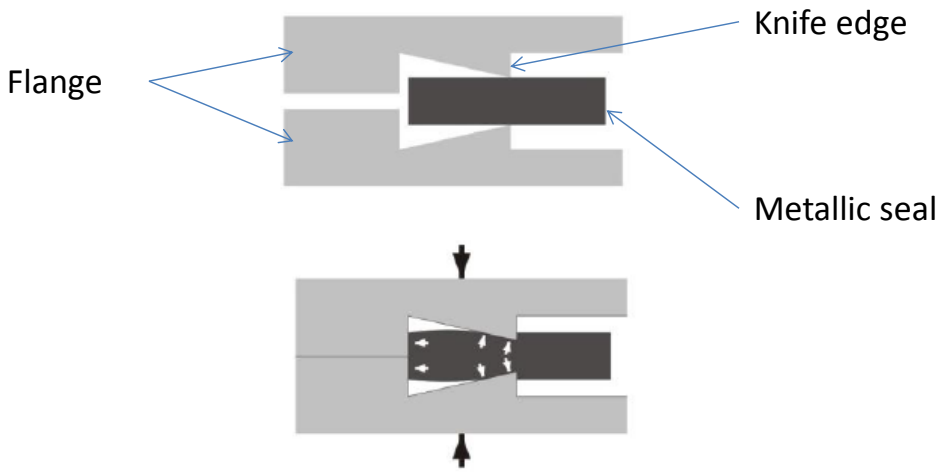

Figure 23: Metallic seal

- **Permanent Seals**

Permanent seals in vacuum technology are achieved by welding, brazing or fusing. In recent years, vacuum-resistant adhesives have also come into use to join components. The selected technology must be appropriately designed for the major requirements with respect to mechanical strength, temperature and alternating thermal loads, as well as the required tightness. Material combinations such as metal-to-metal, glass-to-glass, glass-to-metal, metal-to-ceramic and glass-to-ceramic are being used more frequently in vacuum technology. Metals are most often joined by means of welding and brazing. Non-detachable joints between metal and glass are produced by fusing.

- ✓ **Welding**

In vacuum equipment, components of plain and stainless steel are usually welded together for vessels and joints. To ensure that the welds that are produced are vacuum-tight, it is necessary to use proper materials that are free of cracks and voids, and whose surfaces are smooth and free of grease. Welds should be made on the vacuum side of the pressure boundary whenever possible to avoid vacuum-side gaps and cracking. When not possible they should be full penetration welds. If necessary an additional atmosphere-side weld can be performed to increase mechanical stability. In this connection, it is important that this supplemental weld not be continuous in order to allow leak detection.

- ✓ **Brazing**

Brazing is a process used to join two or more metals and/or materials together. Brazing is a joining process wherein metals are bonded together using a filler metal with a melting temperature greater than 450 °C, but lower than the melting temperature of the base metal. Filler metals are generally alloys of silver (Ag),

aluminium (Al), gold (Au), copper (Cu), cobalt (Co) or nickel (Ni). The liquid filler metal is drawn into the gap between the joining surfaces by capillary action. The brazing process is performed under vacuum or in clean inert gas atmosphere to obtain oxide-free, high-strength joints. Brazing is by far the most widely used joining process when mechanically reliable vacuum tight joints are required to operate at relatively high temperatures.

Brazing has been extensively investigated and employed for metal/ceramic joining. Brazing allows low-cost large-scale joining of intricate geometries and is not necessarily restricted to flat surfaces.

- ✓ **Diffusion Bonding**

In diffusion bonding, two interfaces can be joined at an elevated temperature (about 50% - 90% of the absolute melting point of the parent material) using an applied pressure for a time period. Diffusion bonding is causing atoms from each part to diffuse across and create joint. Materials join together without melting. The temperature of bonding is usually lower than the fusion temperature but high enough to cause sufficient diffusion at the bonding interface. It can bond different and materials combinations.

The major parameters of the process are surface finish, bonding temperature, pressure and time. Figure 24 shows the mechanism of diffusion bonding.

It produces high quality joints so that neither metallurgical discontinuities nor porosity exist across the interface. With properly controlled process variables, the joint would have strength and ductility equivalent to those of the parent material. Good dimensional tolerances for the products can be attained.

The process is slow due to diffusion needs time to take place. The process needs to be carried out either in vacuum or in controlled atmosphere. Depending upon the materials being joined, a thin layer of interlayer is often introduced at the joining interface.

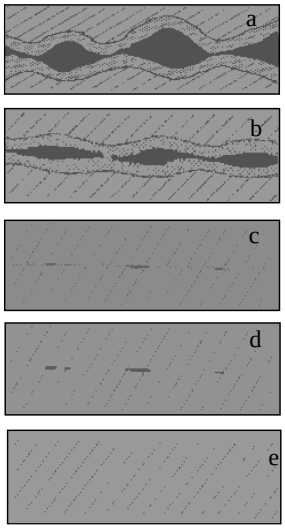

a) Initial 'point' contact

b) Yielding and creep leading to reduced voids

c) Final yielding and creep (some voids left)

d) Continued vacancy diffusion, leaving few small voids

e) Bonding is complete

Figure 24: Diffusion bonding mechanism [19]

2.3.2.2 Madison Symmetric Torus: A case study

The vacuum vessel of the Madison Symmetric Torus (MST) is 5 cm thick aluminium shell and serves as both the primary toroidal field winding of the machine and as a stabilizing, close conducting shell. Besides diagnostic portholes, the vacuum vessel has two functional cuts that allow magnetic flux to enter and leave the MST. The design of the MST requires both poloidal and toroidal voltage gaps [20]. These cuts provide breaks to conductive shell of the vacuum vessel and work as vacuum seal. The vacuum seal and the interior of the gap are protected from the plasma by a ceramic tile. This simple system has worked well for both the poloidal and toroidal gaps even if gaps cross are a potentially troublesome region calling as "triple joint" [21].

The vessel cuts are vacuum sealed and electrically insulated both toroidally and poloidally with flat Viton gasket joined at the triple joints and vulcanised at room temperature. The viton gasket will be cut and assembled from commercially available sheet stock. The gasket will be compressed by array of insulated bolts, allowing sufficient uniform pressure to assure a seal. . The engineering team used this technique also in the original octupole, levitated octupole and Tokapole II machines. A special method for adjusting local squeezing pressure is well needed to be incorporated into the seal design, they were confident that such a seal can be reliable made [21].

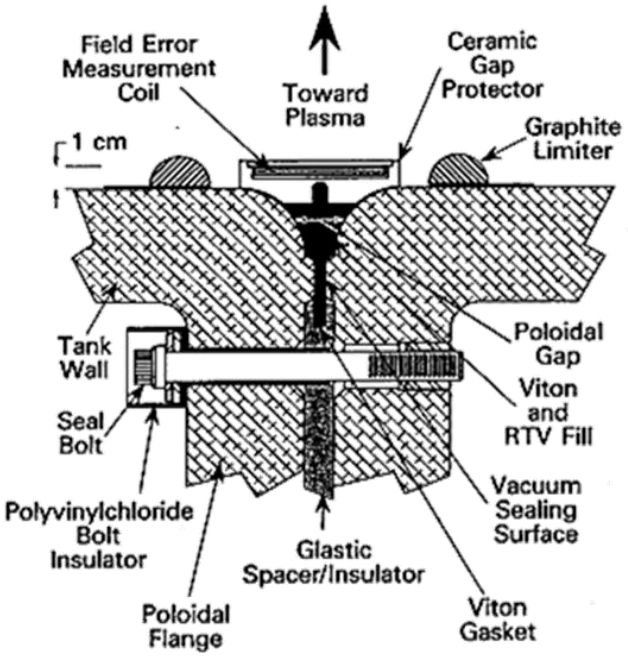

Figure 25: Gap protection, insulation and vacuum sealing of MST [20]

MST was considered as a very close case study to requirements of RFX-mod2 sealing design. But same vacuum sealing technique cannot be used in RFX-mod2 due to some stringent constraint like varying wall thickness and no space to accommodate flange uniformly pressuring the seal.

2.3.2.3 Summary and selection of sealing techniques for RFX-mod2

A summary of the investigated solutions is proposed in the following in order to select the proper techniques to be implemented in RFX-mod2.

Table 5 Summary of vacuum sealing techniques assessment

Sr. #	Solution	Remarks	Status
1	O-ring / Gasket	Not possible to provide bolted flange connections for uniform pressure Life of elastomeric material is not high Difficult to design crossing	Dropped
3	Glued Insulation	Mainly used for vacuum leaks Good for small size components	Dropped
4	Weld seal	Can be consider at one of the equatorial cut Good at external equatorial cut due to port holes	Considered
5	Diffusion bond	Good for insulated vacuum seal Need very high temp. for steel-ceramic joints Required control atmosphere Not easy for big size components	Dropped
6	Brazing solution	Required control atmosphere Ceramic-ceramic joint is difficult Not easy for big size components	Dropped
7	Resistive plate weld	Not full insulation	considered
8	Braze-weld solution		considered

Assessment of different sealing solutions and combination (O-ring solution, gasket solution, Weld solution, Resistive plate weld solution, Braze-weld solution) carried out for the vacuum sealing at TSS cuts. It is not feasible to use commercially available sealing solutions considering stringent constraints at each cut. Table 5 shows different solutions evaluated for vacuum sealing.

Considering explained stringent constraints and requirements in section 2.3.1, different technological solutions designed for the TSS cut are (see Figure 26):

- fully welded solution at the external equatorial cut;
- welding of a thin resistive plate (TRP) at the internal equatorial cut;
- Welding of ceramic-metal brazed rings at the two poloidal cuts.

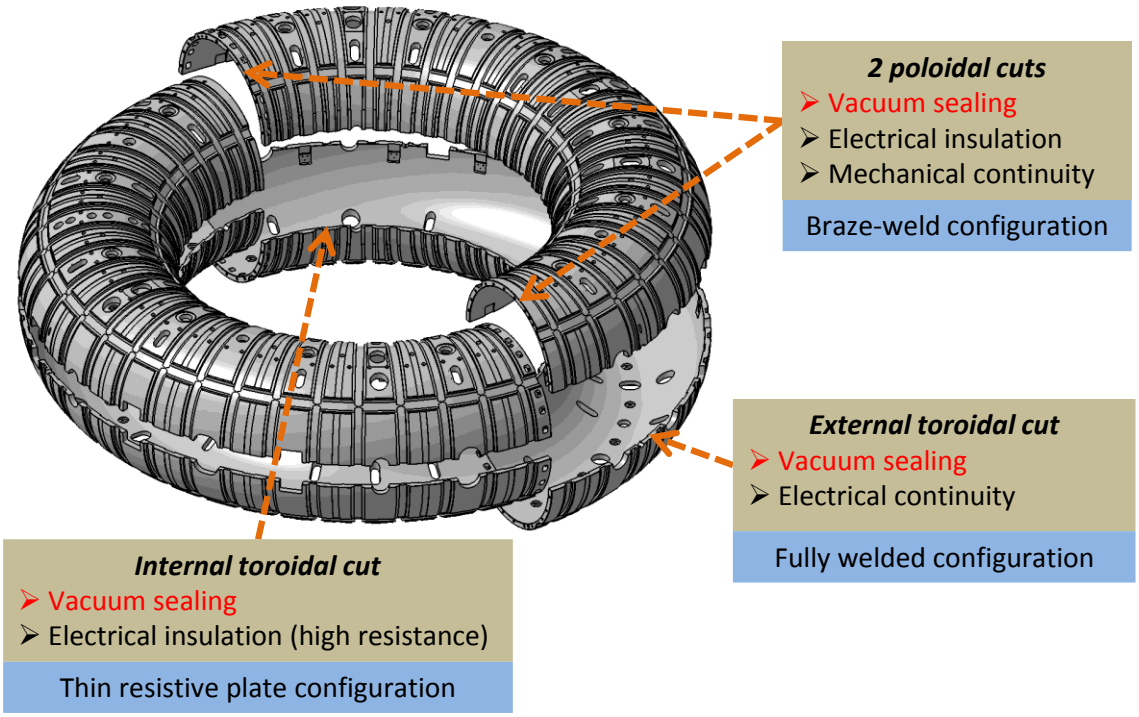

Figure 26: Vacuum sealing configuration of TSS

2.3.2.4 Vacuum sealing solution at external toroidal cut

The external toroidal cut of TSS is the most demanding in terms of vacuum sealing design, as the sealing surface is non-planar due to available port access on the cut as shown in Figure 27. Fully welded configuration is the most suitable solution for sealing at this cut. As there is 5 mm gap between top and bottom TSS in present configuration, it will be maintained by providing spacer. A 5 mm thick spacer of same material as TSS (AISI 304L) will be welded to top and bottom TSS as shown in Figure 28.

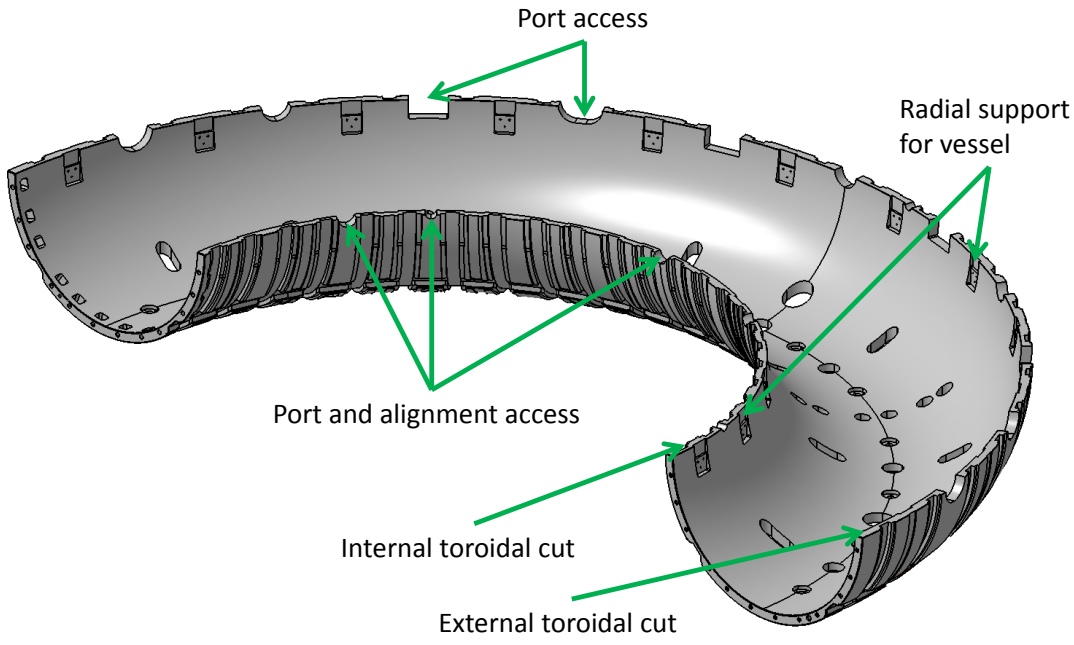

Figure 27: Present configuration of external and internal toroidal cut

The vacuum tightness will be provided by lip weld at inner edge (plasma facing) of spacer-TSS joint to avoid trapped air between surfaces. Weld lips will be prepared by machining on TSS and spacer at inner edges. Firstly spacer and port extension (see Figure 29) will be welded on bottom TSS and then top TSS will close the TSS assembly. The mechanical stiffness will be conformed reasonably by intermittent structural weld at the ex-vacuum side. The same welding solution will be realised to integrate diagnostic and pumping port-holes on the TSS as shown in Figure 29.

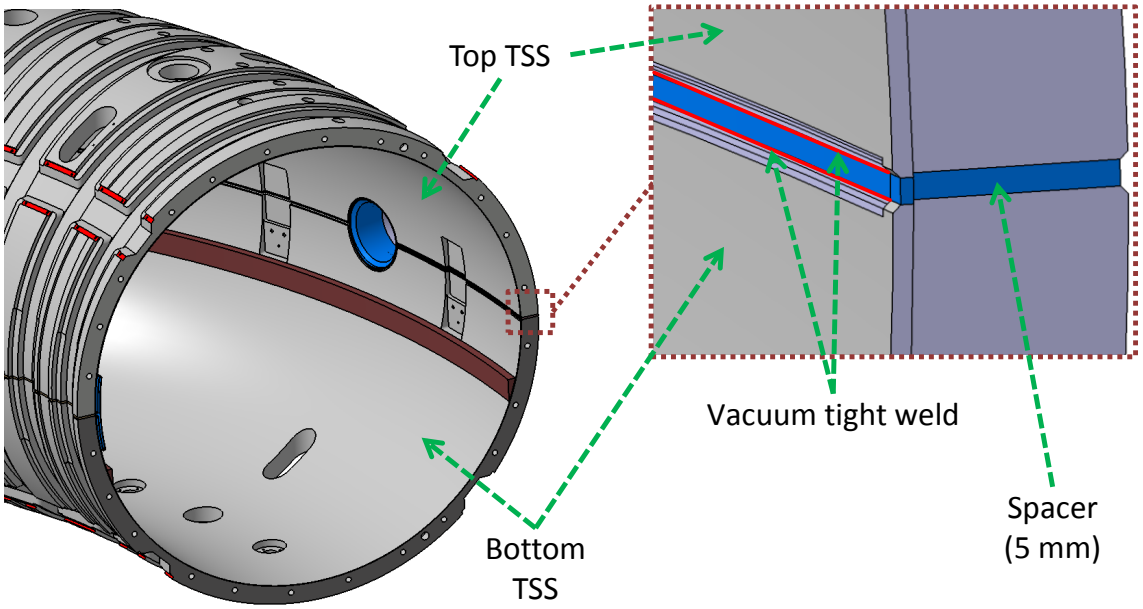

Figure 28: Fully welded sealing at external toroidal cut

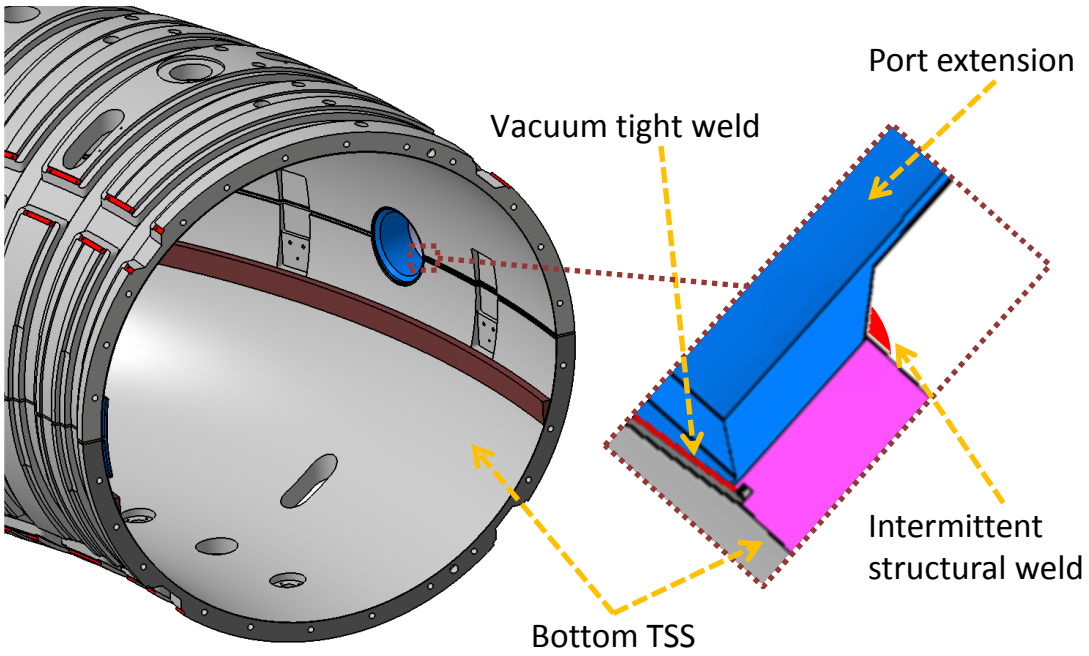

Figure 29: Port extension attachment at external toroidal cut

The proposed vacuum sealing configuration will provide electrical continuity at external toroidal cut for RFX-mod2, which is opposite compared with the present RFX-mod configuration.

2.3.2.5 Vacuum sealing solution at Internal toroidal cut

At internal toroidal cut, now it is necessary to provide vacuum sealing and electrical insulation. In the present configuration on internal toroidal cut the diagnostic and alignment access is available which makes the sealing surface non-planar as shown in Figure 27. The present diagnostic and alignment features at this cut will be removed and plane surface will be prepared for sealing.

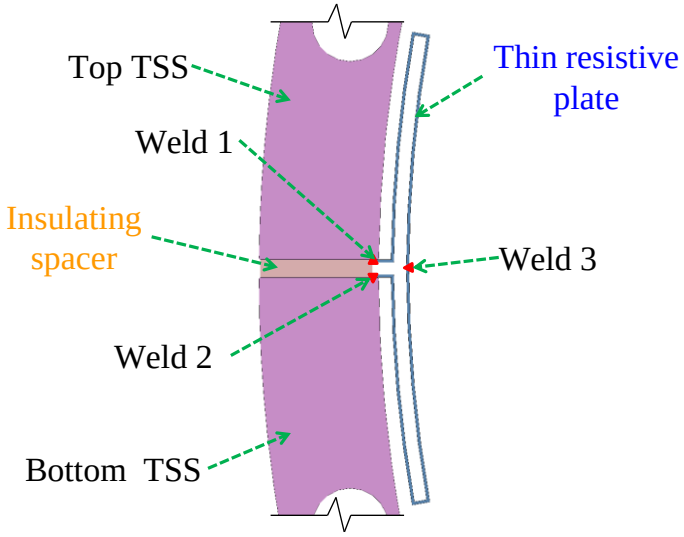

Figure 30: Sectional view of resistive plate vacuum sealing and weld sequence

Many different vacuum sealing configurations were proposed and discussed for this cut, finally novel approach of welding of Thin Resistive Plate (TRP) is proposed for vacuum sealing at internal toroidal cut. The TRP is a long plate, welded to top and bottom TSS at its end, produce vacuum sealing and high resistive path instead full electrical insulation. The TRP is made of two U-shaped plates, welded separately to top and bottom TSS respectively and then sealing will be closed by welding at plasma side as shown in Figure 30. TRP will be prepared with 1 mm thick metallic plate. Total poloidal length of TRP is 400 mm as shown in Figure 31 and TRP will be developed along the 180° toroidal direction of the TSS.

At both end of each TRP, the closing plate will close the end of shaped resistive plate as shown in Figure 31. Radial width of resistive plate is 12 mm which will easily accommodate in available space of 38 mm between TSS and stabilizing shell.

INCONEL® 625 (UNS N06625) [22] is selected material TRP. INCONEL has high resistivity (1.3•10-6 Ω•m) and excellent weldability which makes it best suited material for the TRP. Inconel 625 is Ni-Cr based superalloy. INCONEL is used for its high-temperature strength, mechanical properties, excellent fabricability (including joining), and outstanding corrosion resistance. Its high strength enables it to be used for thinner-walled vessels. It has wide service temperature window, ranging from cryogenic to 980°C [22].

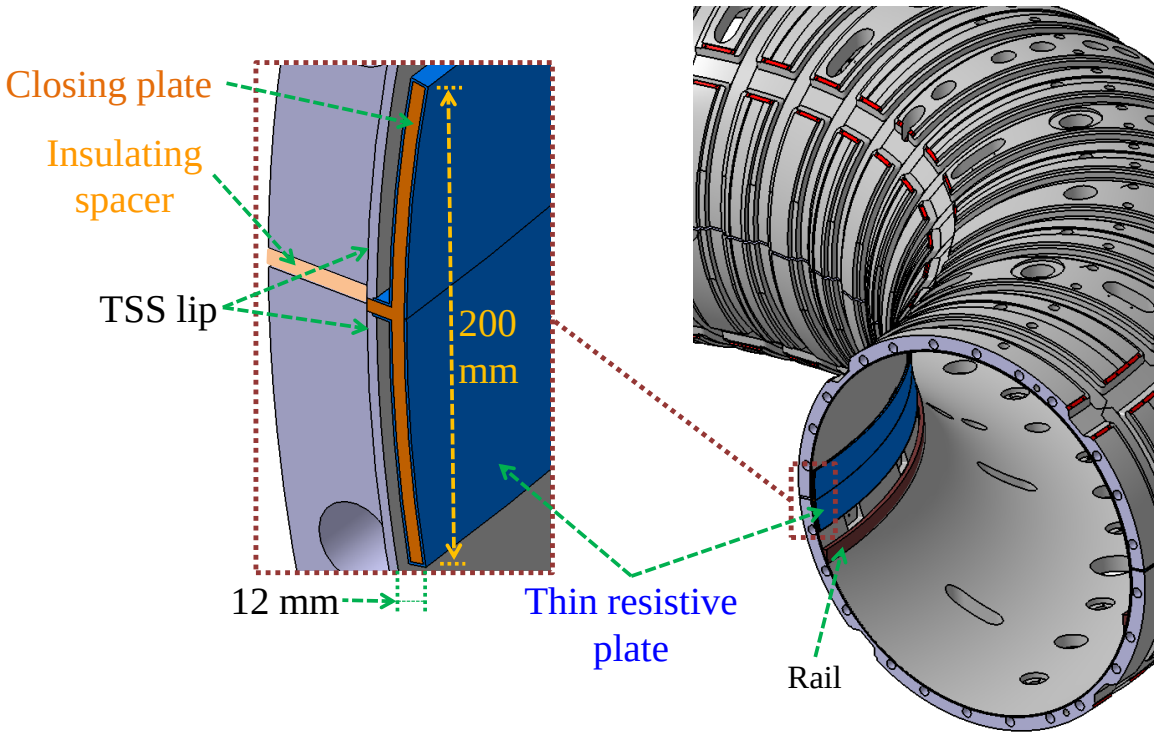

Figure 31: Thin resistive plate sealing at the internal equatorial cut

A 5 mm thick Fibreglass Reinforced Plastic (FRP) plate will be placed between top and bottom TSS to provide electrical insulation. This vacuum sealing solution produce two different electric path; one is TRP and other shortest path is through closing plate. Resistance of second path is very high compared to the resistance of TRP (R1 < R2), which makes the solution viable. Basic resistance calculation for TRP is carried out as shown below,

Electrical resistance,

$$\boldsymbol{R = \rho \frac{L}{A}} \qquad \textbf{2-1}$$

Electrical resistance of TRP,

$$\boldsymbol{R1 = \rho \frac{0.4}{2\pi r * th} = \rho \frac{0.4}{2\pi * 1.5 * 0.001} = 42.4 * \rho = 55.12\ \mu\Omega} \qquad \textbf{2-2}$$

Electrical resistance of closing plate,

$$\boldsymbol{R2 = \rho \frac{0.005}{0.007 * 0.001} = 714.3 * \rho = 929\ \mu\Omega} \qquad \textbf{2-3}$$

Total electrical resistance,

$$\boldsymbol{\frac{1}{R} = \frac{1}{R1} + \frac{1}{R2}} \qquad \textbf{2-4}$$

$$\boldsymbol{R = 52.1\ \mu\Omega}$$

The total poloidal resistance provided by TRP is 50 μΩ, which is compatible with the inductor-resistor circuit requirement: the TRP resistance shall be in the range 50μΩ ± 30% to proper damp oscillations of electrical currents as the TRP shall be coupled with the given circuit including power supplies.

The TRP has to withstand the 1 bar pressure difference between the air side and vacuum side. Local reinforcements were investigated to preserve the radial width of the TRP. Structural verification has been done using FE analysis and details are given in section 7.2.

2.3.2.6 Vacuum sealing solution at poloidal cut

At two poloidal cuts it is required to provide vacuum sealing and electrical insulation. The proposed sealing solution is ceramic-metal brazed rings, in which two metallic rings are brazed on each side of the ceramic ring to prepare weld lips as shown in Figure 32. The prepared lips will be welded to TSS on both sides of ring assembly by positioning the welding torch from outside of TSS through its periphery. The ceramic ring is having dimension of OD 1112 mm, ID 994 mm and thickness 15 mm. The metallic rings are 1 mm thick plate with s-shaped section as shown in Figure 32 to produce weld lips. Dimensions of metallic rings are OD 1110 mm, ID 998 mm and 3 mm wide. Total width of ring assembly is 21 mm (see Figure 32).

Kovar® alloy (UNS K94610) is selected for metallic rings as its thermal expansion coefficient is close to that one of polycrystalline Alumina [23].

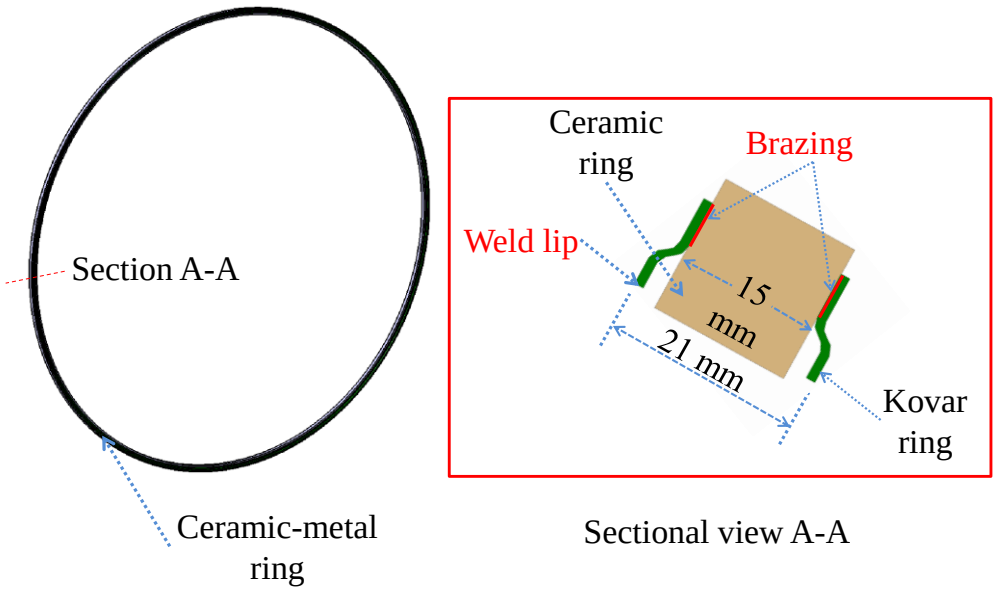

Figure 32: Ceramic-metal ring assembly and sectional view

The present available gap in RFX-mod machine between TSS at poloidal cut is 5 mm. It is required to increase gap at this cut to accommodate ceramic-metal ring and TSS weld lips. TSS segments will be machined for 13 mm on each side in order to realise the total required gap of 31 mm (5+21+5) as shown in Figure 33. Furthermore, lips for welding at the both ends of the TSS will be prepared (see Figure 33). The bolted connection will take place from external side after welding at poloidal joint.

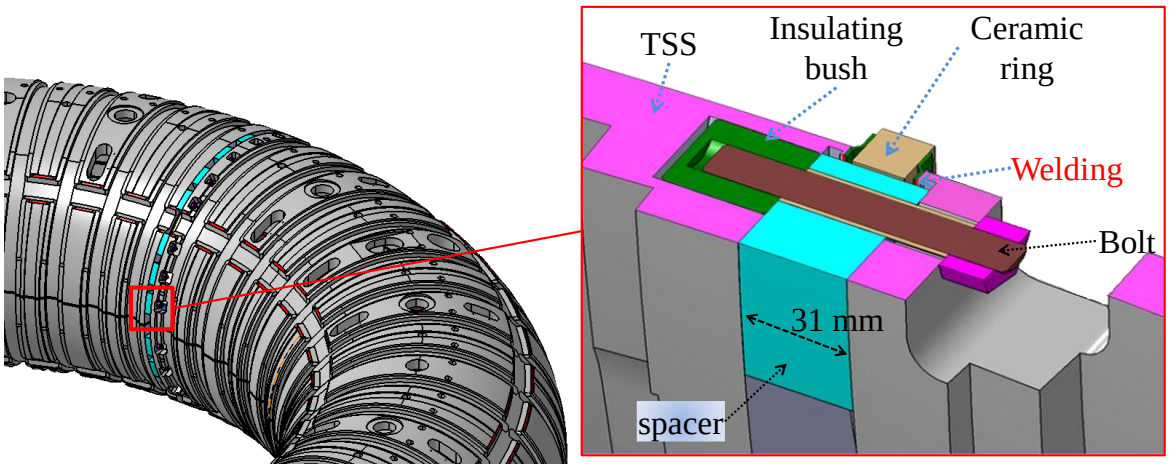

Figure 33: Isometric sectional view of bolted joint at poloidal cut

The vacuum tightness will be prepared by welding of TSS weld lips ring assembly weld lips on its both sides by positioning the welding torch from outside of TSS through its periphery. Micro-welding torches can provide precision welding performance on thin-materials and limited-access joints. Short torch bodies allow pen-like control on even the most complex applications and welding application using extremely thin base metals. The following processes have been applied with success to Micro-welding; resistance, flash, arc (TIG, MIG and plasma) and laser. The miniature 80-degree TIG torch head is only 5/8-inch long and 3/8 inch in diameter, allowing it to be maneuverer in even in the tightest of spaces [24]. Also laser welding is useful process for higher working distance (up to 50 cm) between tool and work piece.

2.3.2.7 Mechanical continuity at poloidal joint

Toroidal mechanical continuity at poloidal joints will be provided by the present bolted connections of RFX-mod machine [12] with slight modifications shown on Figure 33. The poloidal gap will be increased by 13 mm on both side of TSS at each poloidal joint. Ceramic spacers of 31 mm thickness will be placed between TSS at poloidal joint, which will transmit the toroidal forces and realise electrical insulation. The ceramic spacers are divided in 12 pieces considering the assembly to be finished from external side. The ceramic-metal ring will not take any mechanical load and perform only as vacuum sealing at poloidal cut. The bolting access cut on TSS will be increased on its toroidal width to provide sufficient space for bolting assembly from external side.

Total 24 bolts of size M16 screwed on the corresponding fibreglass-G11 (EP GC 203) bushes of M27 at each poloidal joint [12]. The material of TSS and the insulating bush will be cut by 13 mm due to machining of TSS at poloidal section, new length of bush will become 27 mm after 13 mm reduction. Mechanical verifications has been carried out to evaluate the feasibility of the modification using calculation [25] [26]as below,

Tensile stress area,

$$A_t = 0.7854\ (D - \frac{0.9743}{n})^2 \qquad \textbf{2-5}$$

Length of thread engagement,

$$L_e = \frac{2 \times A_t}{K_n max \times \pi \times \left(\frac{1}{2} + 0.57735 \times n \times (E_s min - K_n max)\right)} \qquad \textbf{2-6}$$

Shear area of the external thread (bolt),

$$A_s = \pi \times n \times L_e \times K_n max \left(\frac{1}{2n} + 0.57735 \times (E_s min - K_n max)\right) \qquad \textbf{2-7}$$

Shear area of the internal thread (hole),

$$A_n = \pi \times n \times L_e \times D_s min \left(\frac{1}{2n} + 0.57735 \times (D_s min - E_n max)\right) \qquad \textbf{2-8}$$

Thread engagement factor,

$$J = \frac{A_s \times Tensile\ strength\ of\ external\ thread\ material\ (bolt)}{A_n \times Tensile\ strength\ of\ internal\ thread\ material\ (hole)} \qquad \textbf{2-9}$$

Following data of insulating bush (M27) and bolt (M16) have been used for calculations.

Table 6 Thread data for bush and bolt of poloidal joints

Parameters	Abr.	Unit	Bush	Bolt
Basic Major Diameter	D	mm	27	16
Pitch	p	mm	3	2
Thread per inch	n=1/p		0.33	0.50
maximum minor diameter of internal thread	$K_n$max	mm	24.3	14.2
minimum pitch diameter of external thread	$E_s$min	mm	25	14.5
maximum pitch diameter of internal thread	$E_n$max	mm	25.3	14.9
minimum major diameter of external thread	$D_s$min	mm	27	15.7
Tensile Strength, Ultimate (SS304L)	Ts	MPa	310	477

Followings are outcomes of calculations for above equations (2-5 to 2-9),

Table 7 Results of thread engagement calculations

Parameters	Abr.	Unit	Bush	Bolt
Tensile-stress area	A_t	mm^2	455	155
Length of thread engagement	Le	mm	18.6	11.9
Shear area of the external thread (bolt)	As	mm^2	911	310
Shear area of the internal thread (hole)	An	mm^2	1279	423
Thread engagement factor	J		0.46	1.13
New length of thread engagement	Q	mm	-NA-	13.4

The calculations carried out to check required length of engagement between TSS-Insulation bush and Insulating bush-Bolt. In the case of Insulating bush-Bolt connection, the Female thread material strength is lower. So, length of engagement (Le) is increased by thread engagement factor (J) to prevent the female thread stripping. Above results shows that new required length of engagement between TSS and insulating bush is 18.55 mm and between insulating bush and bolt is 13.42, which is satisfied with the reduced length of insulating bush of 27 mm.

2.3.3 Closing of other openings on TSS

There are different other openings existing on TSS (see Figure 34) which needs to close or integrate for vacuum tightness of TSS. These openings need to close before providing vacuum sealing on TSS cuts. List of other openings are as follows,

i. TSS support openings (24 x 2)
ii. Bolt connection opening at poloidal cuts (24 x 2)
iii. Port openings (153)

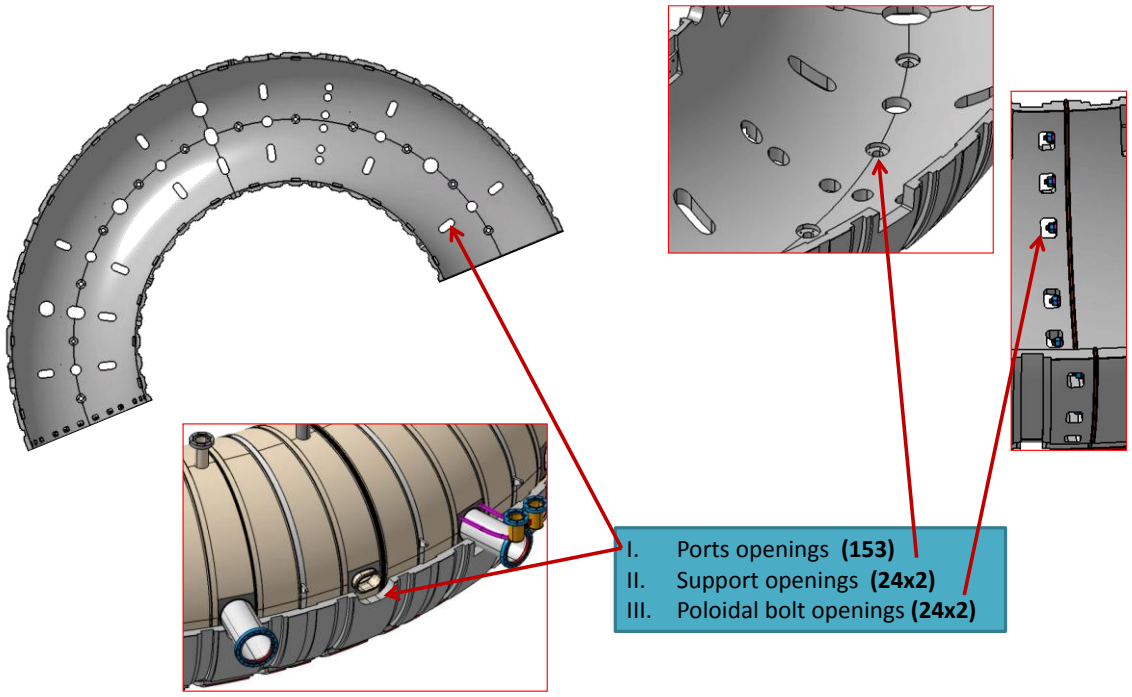

Figure 34: Different openings on TSS

The TSS is fixed to clamping ring through support bushes (see Figure 35). There are 24 supports bushes on top TSS and 24 supports bushes on bottom TSS. Bushes are evenly distributed at every 15° toroidally. These support openings will be sealed by welding a metallic disc of diameter 90 mm and 1 mm thickness at each support opening. The material of the weld plate will be AISI 304L, similar as TSS. The welding will be carried out at internal surface after fixing bushes to TSS as shown in Figure 35.

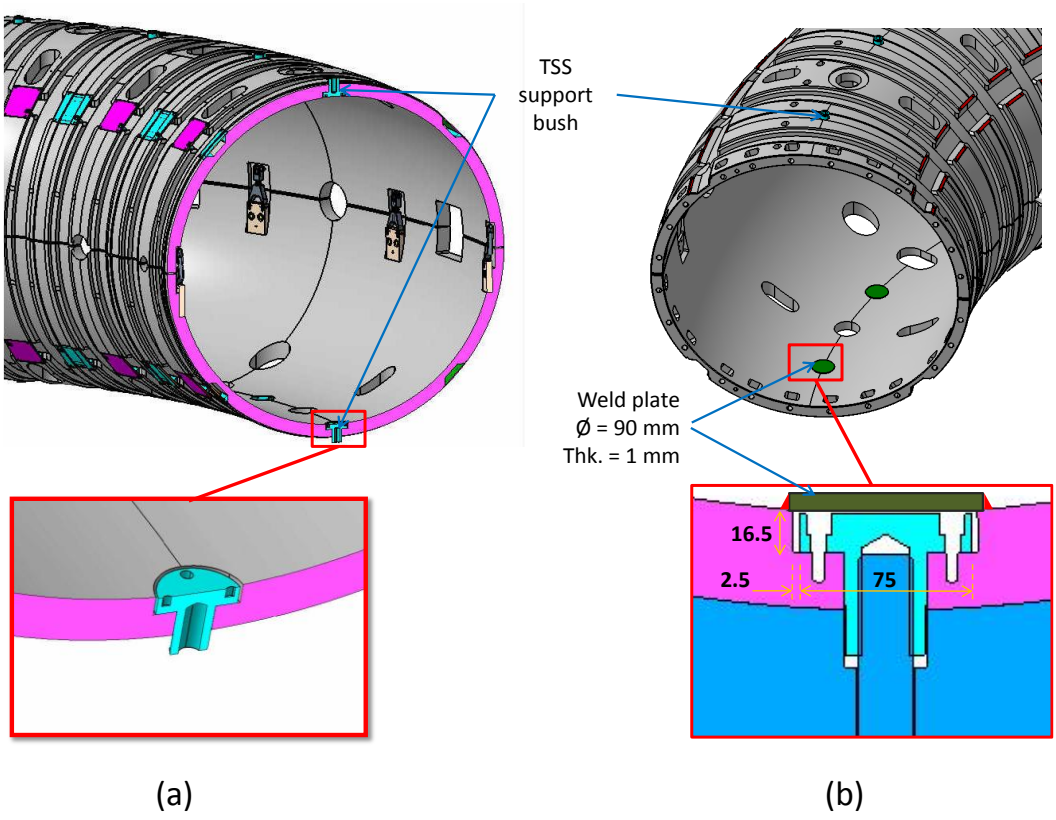

Figure 35 TSS support opening (a) support bush on TSS (b) closing of support openings

The present In-wall bolted joint at poloidal cut will be used in RFX-mod2. There are 24 rectangular holes (54 x 43 mm) poloidally distributed for the access of bolting connection (see Figure 36 (a)). For each TSS segment, openings for poloidal bolt joint will be closed at internal surface of TSS by welding of 1 mm thick cylindrical sheet of AISI 304L as shown in Figure 36 (b). There is possibility to seals each individual holes by separate sealing plates for the sake of easiness.

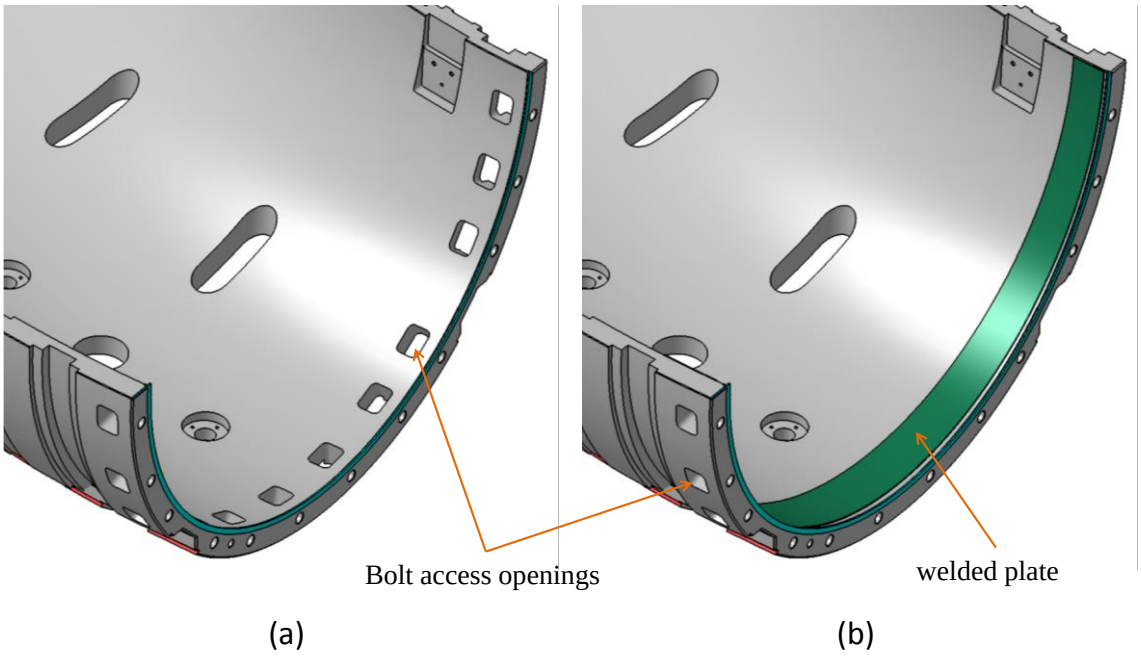

Figure 36: (a) Bolt access openings at poloidal joint and its (b) closing solution

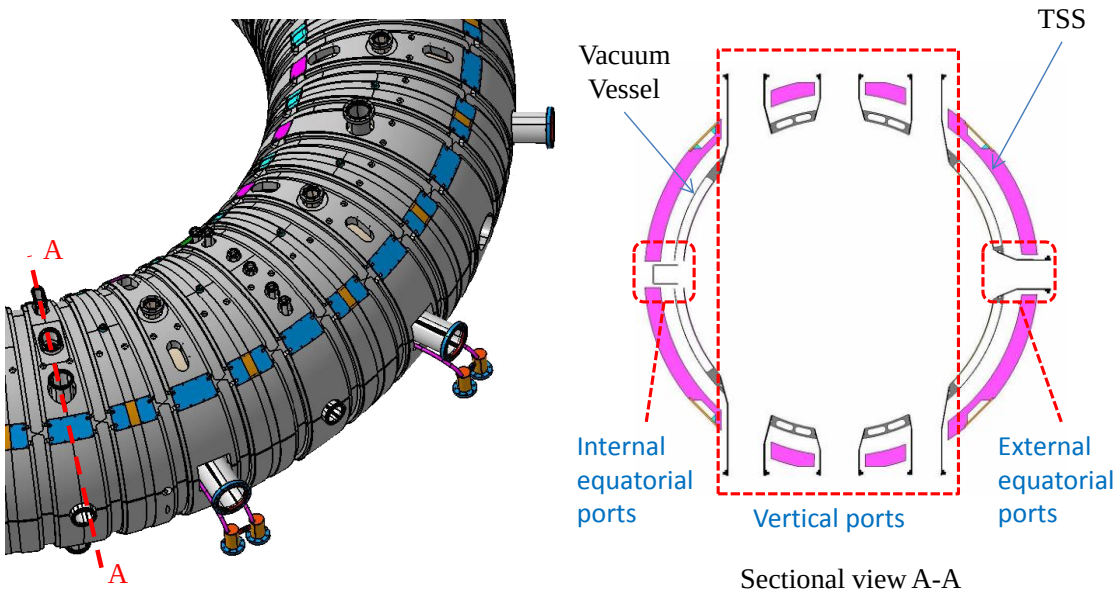

Figure 37: Types of port access on TSS

There are different ports openings are available on TSS for pumping and diagnostics including cable routing. There are total 153 port holes on TSS at following listed location (refer Figure 37),

- External equatorial ports = 22
- Internal equatorial ports = 9
- Vertical ports = 122

As per the shape of vacuum vessel ports, the TSS port holes have different cross sectional shape like Square, Oval, and Circle (see Figure 37). Port holes are bigger in size than original ports on vacuum vessel, this arise the requirement of port extension between original ports and TSS port holes. The gaps between ports and TSS port holes are mainly 10 to 15 mm.

Internal equatorial ports (9) will be closed and provide flat surface to accommodate the TRP sealing at internal equatorial cut. Vertical ports (122) and external equatorial ports (22) will be integrated to TSS. Ports will maintain its present position and size. Ports will be integrated to TSS through port extension as shown in Figure 38. Port extension will be joined to TSS internal surface by lip seal weld and structural stability will be provided through intermittent structural weld at external side. Below Figure 38 shows port integration scheme at external equatorial cut.

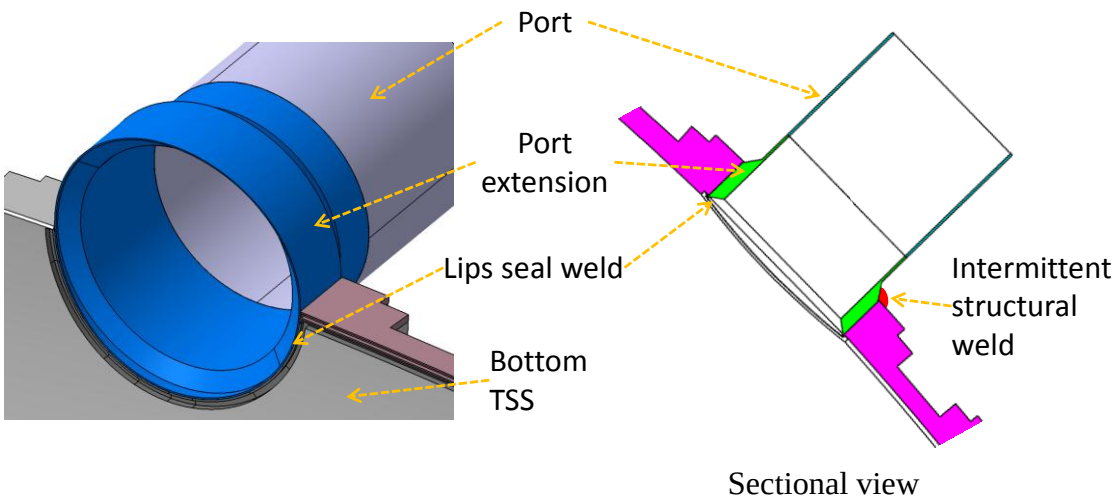

Figure 38: Port integration scheme at external equatorial cut

2.3.4 TSS rails

As the present vacuum vessel will be removed in RFX-mod2, so new supporting rings (refer section 2.5) are designed to support passive stabilizing shell inside TSS. The supporting rings will be supported through rails inside TSS. The rails are designed to install on internal surface of bottom TSS segments to provide support to stabilizing shell and ease of assembly insertion. These rails will be installed 150 mm below equatorial plane as shown in Figure 39.

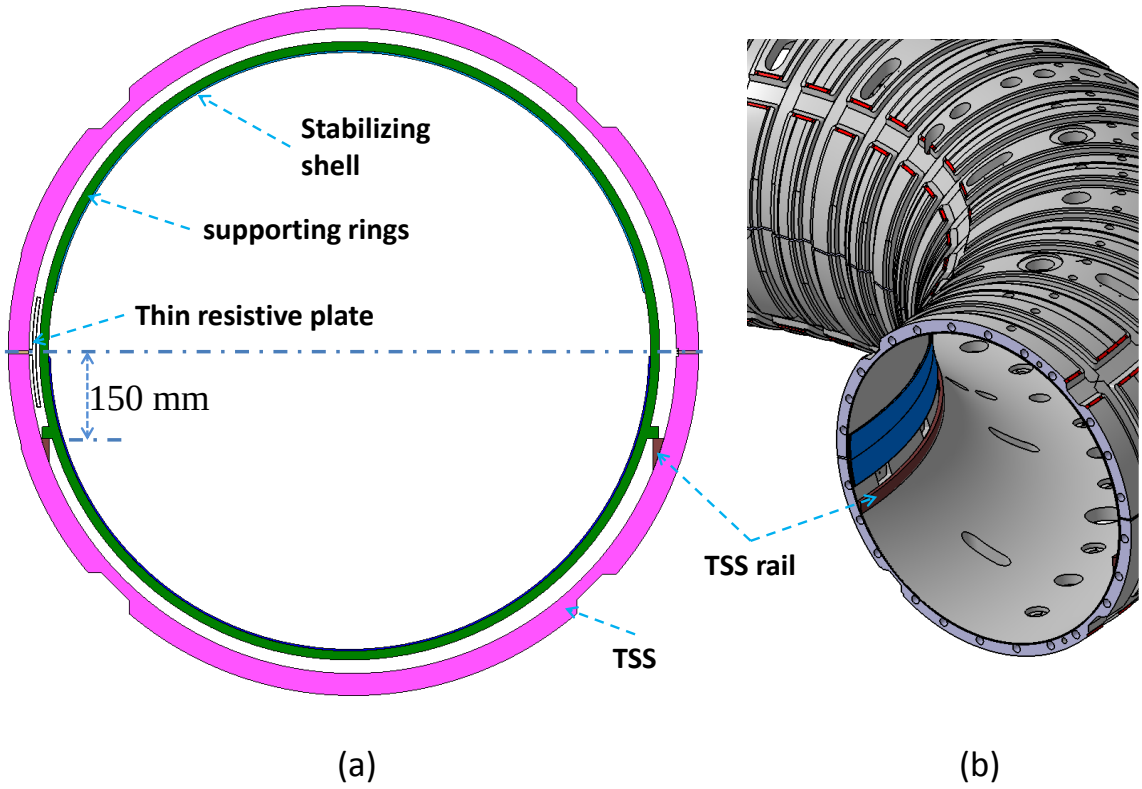

Figure 39: TSS rails (a) Poloidal sectional view (b) Isometric view

The major modifications of TSS can be summarized as shown in Table 8. Structural behaviour of TSS considering the modifications is verified using Thermo-mechanical analyses. Details of thermal analyses are given in 0 and details of structural analyses are given in CHAPTER 7.

Table 8 Summary of TSS modifications

Sr. #	TSS Modification	Quantity	Modification
1	Internal equatorial ports	9	To be closed
2	External equatorial ports	22	To be integrated
3	Vertical Ports	122	To be integrated
4	TSS support openings	48	To be sealed from inner side
5	Poloidal bolt openings	48	To be sealed from inner side
6	Rail for shell support	2	To be installed
7	External toroidal cut	1	Fully welded vacuum seal
8	Internal toroidal cut	1	Thin resistive plate weld seal
9	Poloidal cuts	2	Ceramic-metal ring Weld-braze sealing

2.4 Modification of passive stabilizing shell

In RFX-mod2, the stabilizing shell has to perform as structural component in addition to previous requirement of passive stabilization of plasma MHD. The stabilizing shell has to provide support to FW tiles and withstand thermal and structural loads.

The stabilizing shell will maintain its geometrical position with major radius of 1995 mm and inner minor radius of 511.5 mm. First wall tiles will be mounted on its internal surface, hence plasma minor radius will increase and become a= 487 mm.

The stabilizing shell is a toroidal shell with 3 mm thickness, made up of oxygen free copper (UNS C10200). The present (in RFX-mod) overlapping of 20° sector of the stabilizing shell [4] will be removed considering new assembly procedure as explained in the section 2.6. It will have four segments; each segment is extending to 180º in toroidal and poloidal direction similar as TSS.

At the toroidal cut the upper and lower shells have gap of 20 mm. The upper and lower shells will be bolted together by series of plates. Considering magnetic field penetration, the shell joint configurations at inner and outer equatorial joint are reversed with respect to TSS joint configuration. The inner equatorial joint will be short circuited by means of copper plates and the outer toroidal joint will be insulated by means of epoxy glass plates as shown in Figure 40.

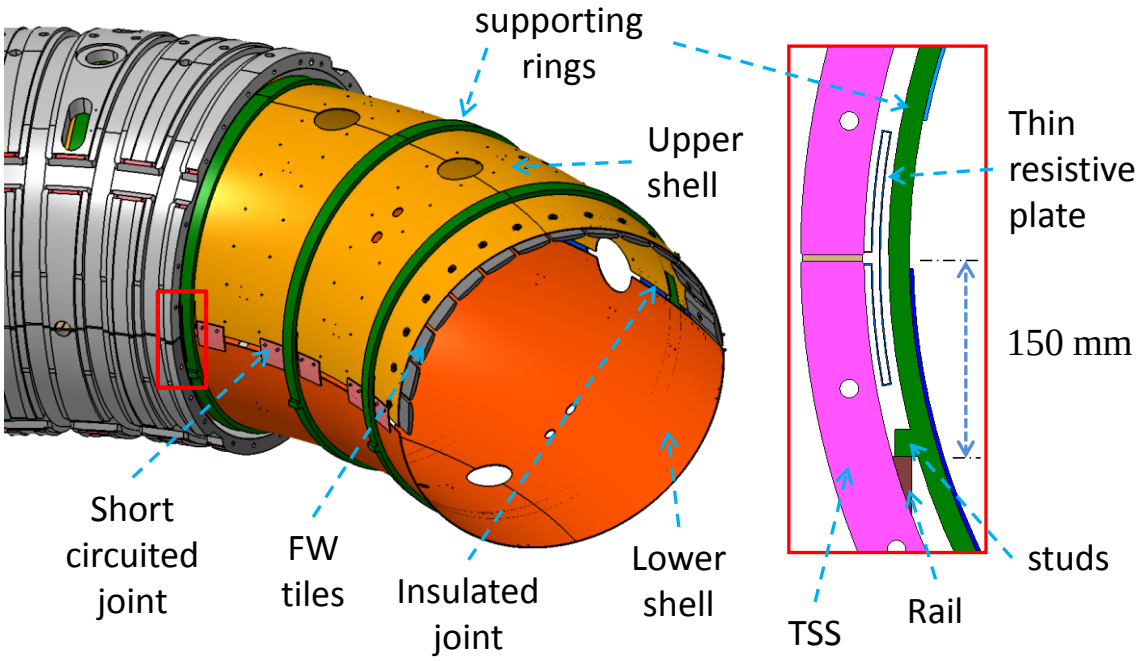

Figure 40: Stabilizing shell and supporting ring assembly

The design modifications of stabilizing shell is verified using Thermo-mechanical analyses. Details of thermal analyses are given in 0 and details of structural analyses are given in CHAPTER 6.

2.5 Design of supporting rings

New supporting rings are designed to support the stabilizing shell on TSS and to maintain the circular shape. Total 24 supporting rings are evenly positioned along the toroidal direction. Bolted connection is considered to fix the stabilizing shell inside supporting rings.

The supporting ring is designed by series of FE simulations to select proper material, number of rings and support geometry considering loads from stabilizing shell. The major design parameter is the thermal expansion of stabilizing shell under baking load condition. The results are described in CHAPTER 6. The supporting rings are designed to allow free thermal expansion of stabilizing shell, which is maximum 7 mm at most distant radial point. There is no net vertical force acting in the stabilizing shell assembly.

The supporting rings are supported on TSS rail through radial studs. Each supporting ring is having two radial sliding studs at inner equatorial side and external equatorial side. The studs are located 150 mm below equatorial plane in order to accommodate the TRP as shown in Figure 40. Length of sliding edge of support stud is 12.5 mm. The supporting ring is having inner radius of 514.5 mm, radial thickness of 15 mm and toroidal width of 70 mm, which left 23 mm of gap between supporting rings and TSS internal surface.

TORLON® 5030 material is selected to realise the supporting rings considering its high glass transition temperature, vacuum compatibility, mechanical strength and its thermal expansion coefficient very close to that one of the stabilising shell made of OFC [27].

Torlon® 5030 is a 30% glass-fiber reinforced grade of polyamide-imide (PAI) resin [27]. It offers high strength and modulus and exceptional creep resistance. It has thermal expansion characteristics similar to aluminum and therefore excellent dimensional stability.

The mechanical properties (refer A.3) of Torlon® 5030 resin makes it a candidate for metal replacement in high temperature, high stress applications. In addition, it offers outstanding electrical properties, which makes it ideal for high performance parts such as connectors, switches and relays. Torlon has the highest strength and stiffness of any thermoplastic up to 275°C. It has outstanding resistance to wear, creep and chemicals.

2.6 Assembly and integration

The new assembly sequence for RFX-mod2 machine proposed considering above defined modifications as shown in Figure 41. This design requires a special assembly procedure as follows:

1. Separate sub-assemblies will be prepared for right and left TSS segments (Top on bottom)
   a. Integrate port and seal different openings of TSS at each segment
   b. Welding of rails for shell insertion

c. Vacuum sealing of external toroidal cut by welding of spacer to top and bottom TSS
d. Vacuum sealing of internal toroidal cut by welding of resistive plate to top and bottom TSS

2. Separate sub-assemblies will be prepared for right and left stabilizing shell
(Top on bottom)
   a. Joining of upper and lower half of stabilizing shell
   b. Bolting of stabilizing shell to supporting rings
   c. Fixing of sensor and cable routing
   d. Installation of FW tiles
3. The sub-assembly of stabilizing shell and supporting rings are inserted inside the TSS sub-assembly through sliding of supporting ring on TSS rails
4. Prepare assembly of ceramic-metal brazed rings
5. Closing of poloidal cut
(Right and left)
   a. Vacuum sealing of TSS sub-assemblies at poloidal cut by placing ceramic-metal brazed rings and
   b. Bolting at poloidal joint of TSS sub-assemblies

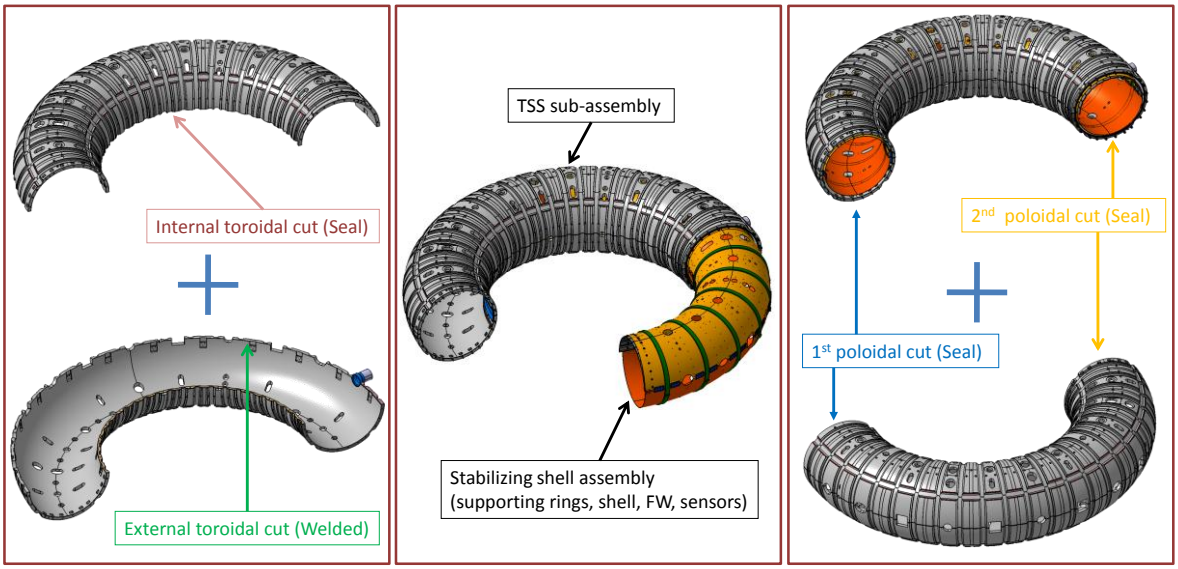

1. ***Separate sub-assemblies will be prepared for right and left TSS segments***
2. ***Insertion of stabilizing shell assembly on TSS rails***
3. ***Both poloidal cuts will be sealed***

Figure 41: Assembly sequence for RFX-mod2 machine

CHAPTER 3 TECHNOLOGICAL FEASIBILITY

3.1 Technological feasibility of proposed solutions

In view of complexity and transition of sealing at poloidal-toroidal crossing, the anticipated solutions of welded and brazed joints needs be qualified by testing prototype.

The proposed sealing solution at poloidal cut is ceramic-metal brazed rings. Such large ceramic rings (refer Figure 32), having outer diameter of 0.6 m and brazed to metal plates at its both side is a technological challenge [28].

High purity engineering alumina [29] is considered as ceramic material in the present reference design and Kovar® alloy (UNS K94610) [30] is selected for metallic rings to braze to ceramic. Kovar® alloy is nickel alloy (29% Ni, 17% Co, 0.3% Mn, 0.2% Si and balance Fe), low expansions alloy whose chemical composition is controlled within narrow limits to assure precise uniform thermal expansion properties, very ductile and able to absorb the stresses. Kovar and alumina ceramic have similar expansion curves [28] [31]. The expansion characteristics of Kovar match both Pyrex glasses and alumina ceramics, making it one of the most popular of the controlled expansion alloys for hermetic sealing applications. Kovar is produced to ensure good properties for machining and deep drawing, and is a porosity free product [30]. kovar alloy has good welding and forming capability. Kovar is used in applications such as vacuum tubes, microwave tubes, transistors, diodes, hybrid packages, and other kinds of scientific instruments. Below Table 9 shows main properties of kovar alloy;

Table 9 Kovar Alloy Properties

Density	kg/m^3	8360
Melting Point	°C	1449
Electrical Resistivity	μΩ-cm	49
Thermal Conductivity	W/m-K	17.3
Specific Heat	J/(kg*K)	460
Thermal Expansion(25°C to 450°F)	μm/m°C	5.3
Tensile Strength	MPa	517
Yield Strength	MPa	345
Modulus of Elasticity	MPa	138000
Poisson's Ratio		0.317

Kovar can be joined to ceramic by active brazing process [32]. Active brazing technique can be used for joining of the ceramic-metal ring assembly and silver-copper based filler metal can be used for the process. High-purity silver-copper eutectic filler material for vacuum bonding (Cusil™); nominal composition by weight is 72% Ag, 28% Cu (both within ±1%) and its liquidus and solidus temperature is 780 °C. Active brazing is an effective method for joining, because the addition of filler metals can effectively improve

the wettability of ceramic [33]. It requires clean vacuum oven to avoid oxidations and consequent joint degradation.

This brazed joint of Kovar ring with ceramic ring is required to assess its mechanical strength under high temperature, because at the end this assembly has to be weled with TSS to provide vacuum sealing.

Proposed sealing concept and assembly steps must be qualified by fabrication of mock-up for its critical requirements. A simplified mock-up on cylindrical pipe is proposed and details are given in following subsection.

3.2 Technical specification of prototype

The design solutions need to show technological feasibility for its critical requirements. Proposed sealing concept and assembly steps must be qualified by fabrication of mock-up. A simplified mock-up on cylindrical pipe is proposed for the same as shown in Figure 42and technical specifications are prepared.

This section presents the technical specification for prototype of TSS sealing solutions. The ultimate goal of the prototype is to verify proposed braze-weld solution at poloidal joint. In view of complexity and transition of sealing at poloidal-toroidal crossing, the proposed solutions of welded and brazed joints needs be qualified by testing prototype. The proposed prototype is considered for all major fabrication steps from machining, welding, and brazing to assembly which required for seal the TSS cuts.

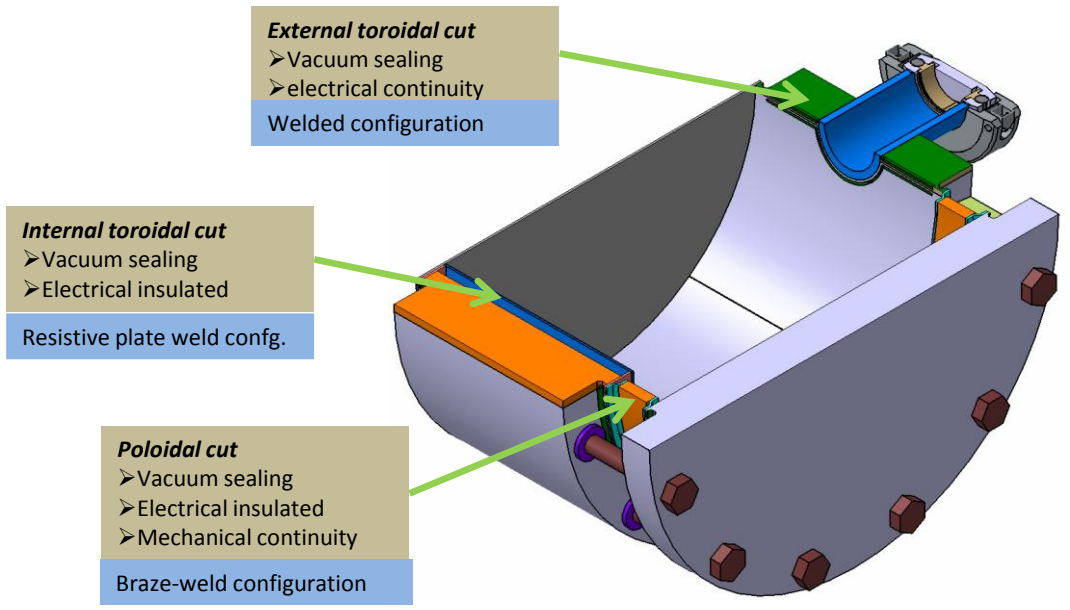

Figure 42: Sealing details of prototype

The proposed prototype will be performed on small size pipe (DN 200) section and it is not identical to RFX-mod2, certainly the dimension of the ring and the brazing on such a big diameter ring cannot be developed for the mock up due to cost of this R&D. Anyhow, it could allow the identification of the best procedures, geometries and materials to be used for sealing of RFX-mod2 experiment.

Tests required and presented in this document are considered the minimum possible to fulfil the goal of the ongoing task; anyway, some different tests could be carried out in addition of those foreseen to perform different desired measurement.

3.2.1 Identification of requirements

Proposed sealing solution should be verified by performing fabrication and assembly sequences on prototype. Following parameters can be studied on prototype,

1. Machining sequences and parameters to produce weld lip
2. Formation of thin resistive plate (TRP)
3. Ceramic-metal brazing
    a. same materials used: brazing alloy, ceramic, and metal sheet (Kovar)
    b. residual stresses due to different thermal expansion
    c. same path for the capillary gap filled by the brazing alloy (15 mm)
4. Availability of space for welding at poloidal gap
5. Welding temperature effect on brazing
6. Sequence of welding mainly at transition from toroidal to poloidal
7. Bolt joining at poloidal cut and its mechanical continuity
8. Electrical: Toroidal voltage holding and Poloidal resistance

3.2.2 Tests to be performed:

A. Ultrasonic detection of welded joint
B. Electrical tests:
    a) Electrical resistance
    b) Dielectric strength
C. Vacuum leak test
D. mechanical
    a) Static mechanical test: bolt preload of 80 KN and normal tensile force
    b) Fatigue test: Static load + cyclic load

3.2.3 Services

The following activities should be included in the supply,

i. Manufacturing process plan and Qualification plan
ii. Test to be done
    a) Visual inspections and dimensional verifications
    b) Ultrasonic test of weld and brazed joints
    c) Leak test
    d) Electrical voltage holding test
    e) Mechanical test of bolted joint
iii. Documents to be submitted
    a) Material certificates
    b) Final drawings

iv. Inspection and quality records with witness during tests

v. Brazing and Welding Procedure Specifications (WPS) supported by welds and welders qualification reports

3.2.4 Hardware

Figure 43 shows sectional view of prototype assembly. It shows all the components and respective position in assembly. Mock-up will be performed on pipe of OD 219 mm and length is 170 mm. The list of the main components and parts to be procured and prepared in accordance with the requirements is shown in Table 10. The final manufacturing prototype should be delivered to Consorzio RFX. The fabrication steps to be followed for assembly are detailed in Section 3.2.5.

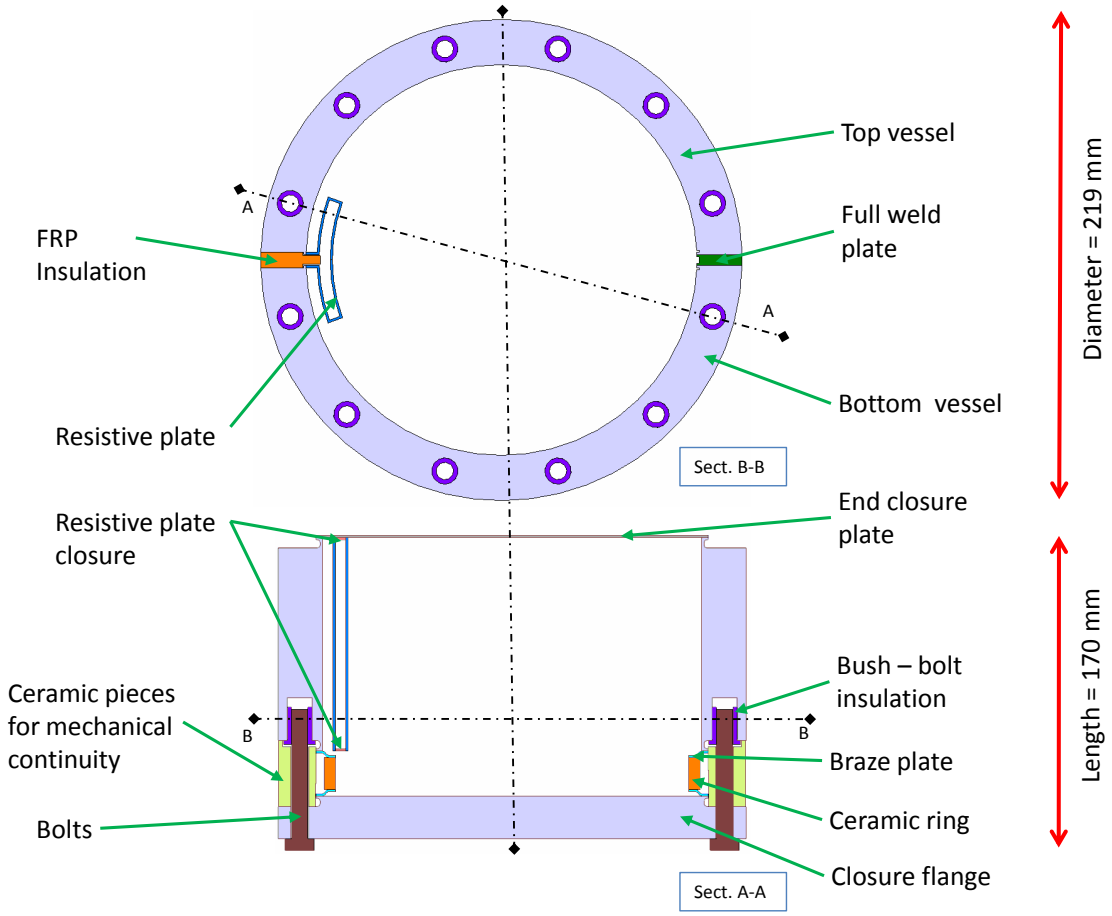

Figure 43: Sectional views of prototype

Table 10 Bill of material for prototype

Sr. #	Assembly	Description	Material	QTY.
1	A	Top vessel (Half cylinder of DN200 pipe, L=100 mm)	SS304L	1
2		Bottom vessel (Half cylinder of DN200 pipe, L=100 mm)	SS304L	1
3		Full weld plate (thk.=5 mm)	SS304L	2
4		FRP insulation (thk.=5 mm)	FRP	1
5		Thin resistive plate	Inconel625	2
6		Closure plate	Inconel625	2
7		Port (DN25 pipe, L=40 mm)	SS304L	1
8		KF flange (DN25)	SS304L	1
9		KF blank flange (DN25)	SS304L	1
10		KF Centering Rings (DN25)	SS304L	1
11		KF clamp (DN25)	SS304L	1
12	B	Ceramic ring	Alumina	1
13		Braze plate	kovar	2
14	C	End flanges	SS304L	2
15	D1.0	Insulator Bush (M12-M8)	Fiberglass G11	12
16	D1.1	Bolt M8	SS	24
17	D1.2	Ceramic spacer	Alumina	6
18	E	Support structure	SS304L	

3.2.5 Fabrication and assembly steps

The major purpose of the prototype is to verify fabrication (Welding, brazing) vacuum sealing component. Therefore supplier should follow general assembly sequence as describe below,

- Assembly A:
  a) On right cut of bottom vessel part, the full weld plates and port should be welded and on left cut side one of the TRP should be welded
  b) The other TRP should be welded on top vessel separately
  c) Then top and bottom vessel can be joining by welding at right cut and on left side lips of resistive plates.

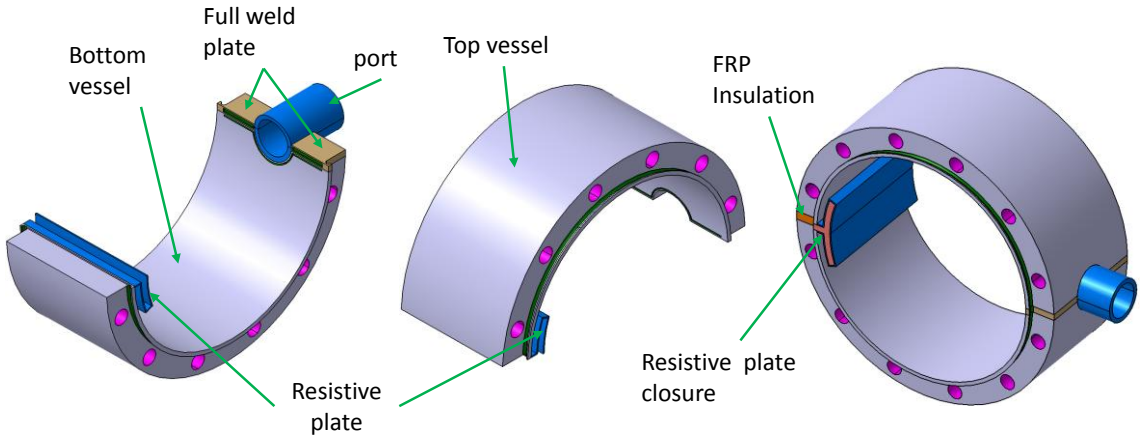

Figure 44: Assembly A: Sealing of top and bottom vessel at right and left cut

- Assembly B:
  a) Both braze plate should be brazed on each side of ceramic ring

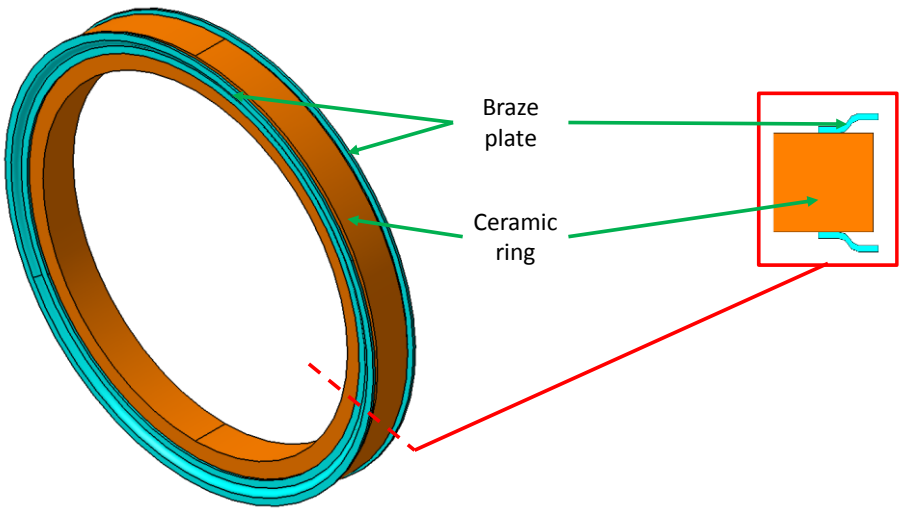

Figure 45: Assembly B: ceramic ring and braze plates

- Closing of rear end of Assembly A
  b) One of the end flange should be welded and bolted to rear end of assembly A

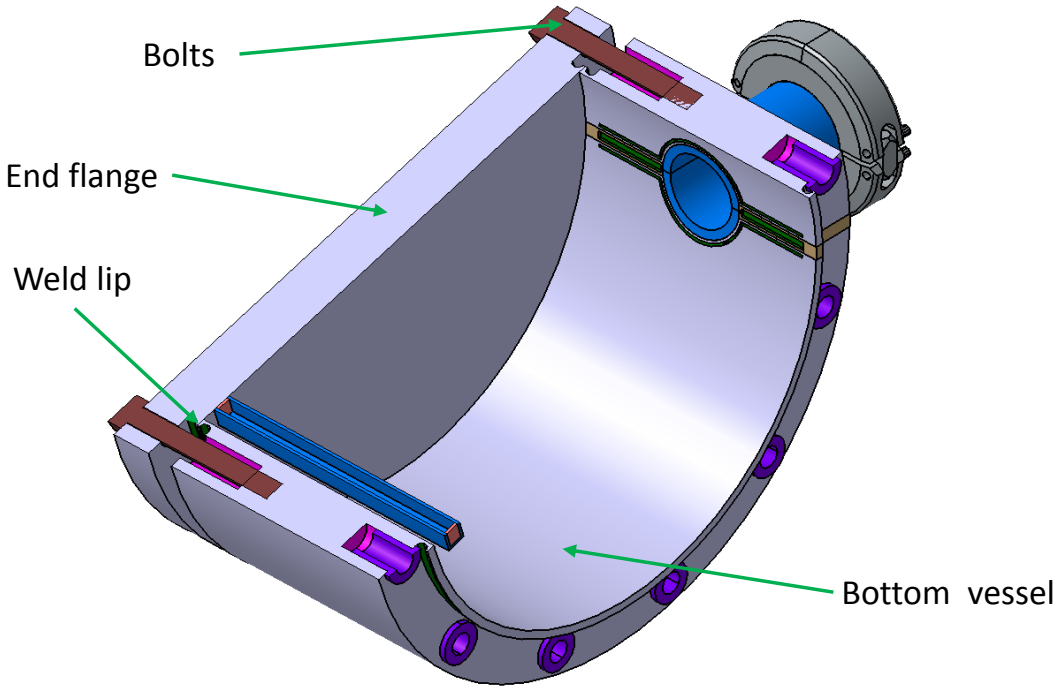

Figure 46: Closing of assembly A at rear end with end flange

- Poloidal joint
  a) Poloidal sealing will be carried out by welding braze plate of Assembly B to Assembly A and end flange
  b) Insert insulated bushes in assembly A
  c) Mechanical continuity will be done by providing ceramic spacer between end flange and assembly A and bolted joint will take place

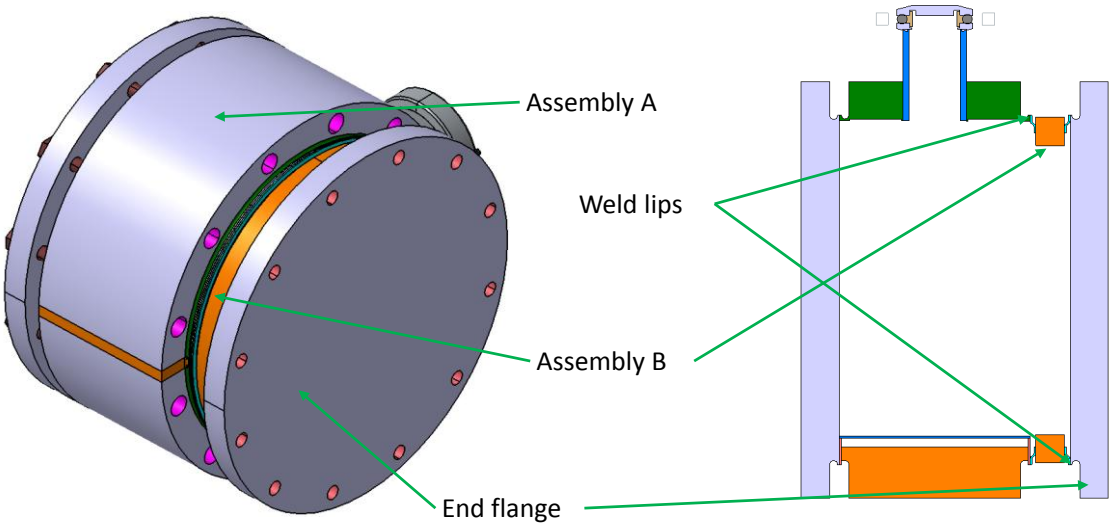

Figure 47: Poloidal joint of prototype

CHAPTER 4 LOAD SPECIFICATIONS

This chapter describes applicable loads and load combinations on RFX-mod2 mechanical components for its verification. The designed components must withstand many individual and combined loading conditions during both normal and off-normal scenarios. In order to verify the structural behaviour of designed mechanical assembly of RFX-mod2, mechanical loads were collected from published articles for RFX-mod components. The section 1 describes the loads and conditions obtained during the operation of the RFX-mod machine. The section 4.2 describes loads and conditions for RFX-mod2 with appropriate assumptions.

4.1 Description of loads on RFX-mod experiment

Main components of RFX-mod assembly are explained in chapter 2. In the following subsections the mechanical load path of the RFX-mod experiment is developed to be compared with that one of the modified machine RFX-mod2. The operating conditions and types of loads are analysed considering well known machine properties and experimental data to make assumptions for unknown loading conditions of RFX-mod2. The load case combinations for components of RFX-mod were not developed within this section as mechanical analyses and verifications of RFX-mod were only undertaken for few cases to check past assumptions and new developed finite element models.

4.1.1 Mechanical Load Path in RFX-mod

In order to better describe the mechanical loads from a system point of view it is worth briefly describing the general layout of the main component supports. The general arrangement of interfaces of the machine components has been developed.

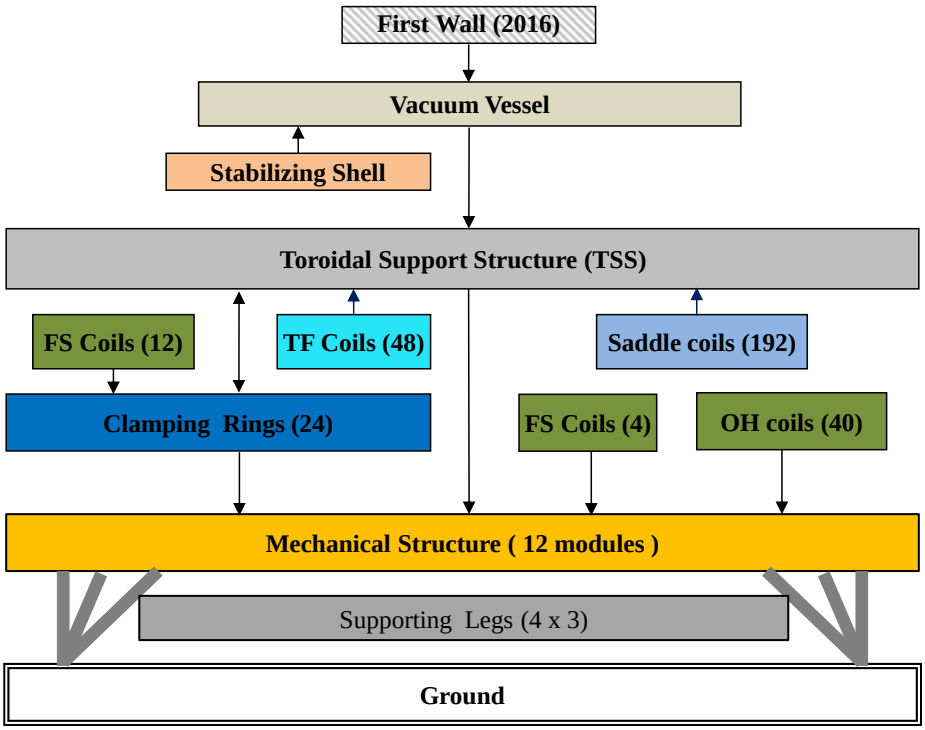

Figure 48: General layout of supports in RFX-mod

As shown in Figure 48, the complete RFX-mod assembly is supported 4 m above the floor level by 12 supporting legs rigidly fixed to the torus hall floor. The mechanical structure supported by legs consists of 12 C-shaped frames, each made of a vertical column and two horizontal arms. Column and arms of the C-frames have box cross-sections. All the OH magnetizing coils are supported on this mechanical structure. TSS and clamping ring assembly is supported by top and bottom ends of c-shaped mechanical structure. PF coils are supported by supporting rings. The TSS is also supporting the toroidal field coils, the saddle coils and the vacuum vessel. The 2016 first wall tiles and passive stabilizing shell are supported by vacuum vessel.

4.1.2 Operating conditions of RFX-mod experiment

Main operating conditions of the machine were considered in order to identify loads to be applied on the machine for verification of the design. Testing conditions were not considered separately as their loads were already included in pulsed condition. During and after manufacturing the following tests were carried out:

1. Leak tests were made by realising the same conditions of operation;
2. Pressure testing was not applied;
3. Thermal heating was not applied;
4. Handling and assembling during installation and maintenance were realised without applying loads different from those realised in operating conditions.

Baking and pulse operation the main operating conditions are described in the following.

4.1.2.1 Baking and Glow Discharge Cleaning

The FW tiles are entirely made of polycrystalline graphite. As graphite is good absorber of hydrogen and makes plasma density control extremely difficult, the baking and dc glow discharge cleaning (GDC) are required to reduce impurities residing on the graphite wall. During baking and GDC, the maximum achievable temperature is 170 °C to be kept constant for the whole sequence of several hours.

4.1.2.2 Pulse operation

RFX-mod machine can be operated in both configurations as a reversed-field pinch (RFP) and as a low current TOKAMAK. When operated as a RFP, RFX-mod achieves maximum plasma current of 2 MA with toroidal magnetic field up to 0.7 T and electron temperature up to 1.5 keV [13]. RFX-mod is not equipped with limiters or divertors, so that the plasma is in direct contact with the whole surface of the first wall, fully covered by graphite tiles. During normal plasma operation the full plasma heat load is deposited on FW tiles. The pulse duration is of 0.5 s in RFP configuration and there is 20 min of stand-by time between pulses. During normal plasma operations the magnetic field is active, which exerts electromagnetic loads on surrounding structures. During stand-by time between plasma

pulses there is no load acting on FW, VV and all other components, except gravity and preloads.

As a circular ohmic Tokamak, the machine operates with magnetic field up to 0.55 T and plasma current up to 0.2 MA [13]. This operating condition will produce fewer loads on components compared with RFP configuration. The Figure 49 shows maximum achievable plasma currents in both operating conditions.

All load specifications are described here considering RFP configuration as highest loading condition.

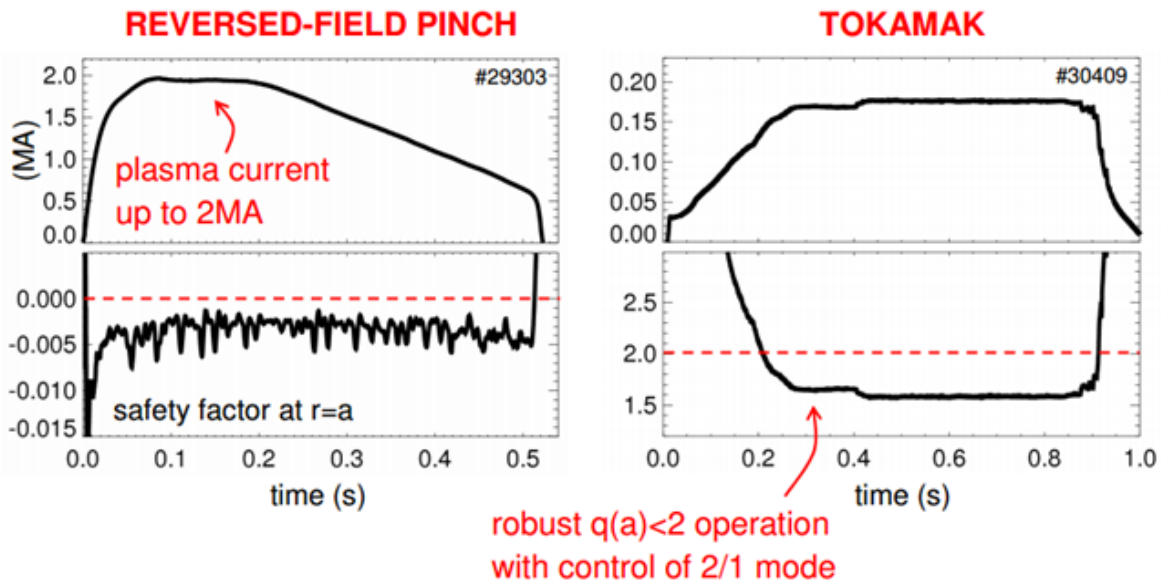

Figure 49: RFX-mod operation scenarios [34]

4.1.3 Types of loads on RFX-mod experiment

During normal plasma pulse operation, the different loads acting on the RFX-mod components are dead weights, external pressure, thermal gradient, and dynamic electromagnetic loads.

The mechanical loads acting on the assembly can be divided into four categories [35]:

- *Inertial loads:* Dead weight, Seismic events
- *Pressure loads:* These loads are induced by vacuum pressure
- *Thermal loads:* These are caused by temperature gradients inside the VV structure caused due to plasma interaction and during baking operation.
- *Electromagnetic (EM) loads:* These loads are normally a strong design driver and act upon nearly all conductive structures during transient events (e.g. plasma disruptions, VDEs, and magnet current fast discharge).

Among these loads, EM loads and thermal loads are the principal contributors for RFX components design. The components must withstand many individual and combined loading conditions during both normal and off-normal operations. Loads applied on RFX-mod were collected from data published in old articles [11] [7] [36] [37] [12] [4].

Table 11 List summarizing the single load cases

Ref.#	Load case	Load type	Characteristic loads
4.1.3.1	Dead weight	Static	Weight of components
4.1.3.2	Preload	Static	Total 15 MN on TSS
4.1.3.3.1	Thermal Loads (Baking)	Static	170 °C up to 100 hrs
4.1.3.3.2	Thermal Loads (Pulsed Operation)	Transient	20 MJ applied to the first wall for Pulse of 0.3 s after every 20 min for 10 h during a day
4.1.3.3.3	Thermal Loads (Localized)	Transient	10 times high energy experts on FW tiles sector compared to normal heat load
4.1.3.4	Electromagnetic loads	Dynamic	Evaluated for 3 different scenarios

4.1.3.1 Dead weight

All masses supported by the Toroidal Supporting Structure (TSS) were considered for simulations [11].

4.1.3.2 Preload

Two different types of preload applied on TSS:

First preload pressure is coming from clamping rings. Two halves (Top and Bottom) of TSS are preloaded together by means of 24 clamping rings; this load is well described in section 4.2.3.3 because of its application on RFX-mod2.

Second preload pressure is coming from TF coil belts. TF coils are pressed on surface of TSS by means of belts, which exerts pressure of 3MPa on surfaces which supports.

4.1.3.3 Thermal Loads

Thermal loads are applied on the First wall, vacuum vessel and other structure mainly during baking and normal pulsed plasma operation. Evolution of the entire components connected with Vacuum vessel for thermal loading conditions are essential during the experimental sessions to identify mechanical behaviour. Thermal loads for different conditions are as described below.

4.1.3.3.1 Baking operation

The plasma configuration of RFX-mod causes strong plasma wall interactions (PWI) and thermal power deposition on the wall that can locally reach values of the order of tens MW/m^2 [38]. To control plasma density and PWI, the wall conditioning processes like Glow Discharge Cleaning (GDC) and baking need to be carried out.

The maximum baking temperature goes up to 170 °C using approximately 28 kW heating power [11] for operating cycle from ~ 70 to 100 hrs. The baking on the RFX-mod vessel is performed through an eddy current system at 50 Hz that induces a toroidal current in the vessel. The poloidal distribution of the eddy currents introduces a poloidal distribution of the temperature on the vessel with a maximum temperature that attains 200°C on the inner side of the vessel. Hence baking can be considered as a steady state thermal load.

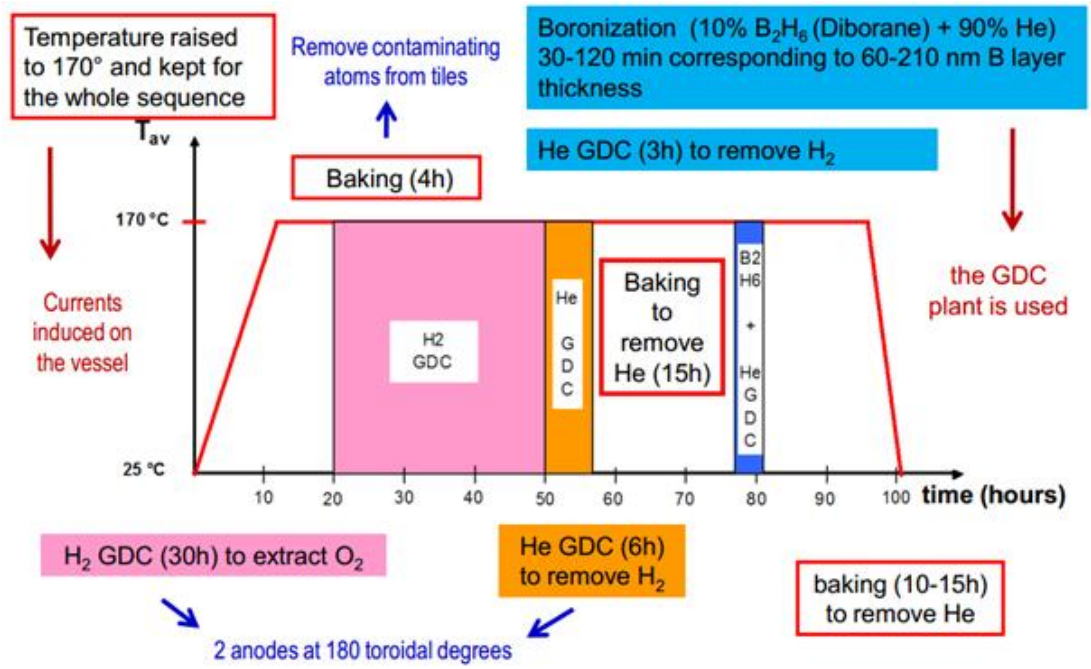

Figure 50: Glow discharge cleaning and baking operation of RFX-mod [36]

The RFX-mod Glow Discharge Cleaning (GDC) system consists of two electrodes at ±180° toroidally that can be inserted up to the centre of the vessel by manipulators. Each electrode is fed by DC power supply (1.5A @1 kV).

Following are described the general steps for wall conditioning techniques [39]:

- Temperature raised to 170°C and kept for the whole sequence
- Baking (4h) for outgassing pressure stabilization
- H_2 GDC (30-40h) to extract O_2, N_2 (CH_4 also formed and removed)
- He GDC (6-10h) to remove H_2
- Baking to favourite the removal of He (15h)
- Boronization (B_2H_6 10% - He 90%)

4.1.3.3.2 Design thermal loads for RFP pulsed operation

Heat loads on the graphite first wall were evaluated during past analyses [8] [11] considering the following design parameters at full performance (2 MA of plasma current):

- Total energy: 20 MJ
- Design pulse duration: 0.3 s
- Average power: 67 MW
- Average power density: 1.8 MW/m^2 spread on 38.1 m2 total first wall area.

The above scenario produces consistent data corresponding to average values to be used for the design of the RFX-mod2 simulations to analyse and verify the new design solutions.

$$Heat\ flux = \frac{Energy\ (MJ)}{Time\ (s) * Area(m^2)} = \frac{20}{0.3 * 38.1} = 1.8\ MW/m^2 \qquad \textbf{4-1}$$

4.1.3.3.3 Localised thermal loads

In RFX-mod, plasma rotation can lock with specific toroidal location due to MHD modes. This gives localized hot spot on plasma facing surface. RFX-mod experiment data shows that during plasma-wall locking incident the total 67 MW power is deposited on a small portion of the first wall at the mode locking position resulting in an increased power densities ~10 times the average power density: 18 MW/m^2.

4.1.3.4 Electromagnetic loads

In a fusion experiment, changing of magnetic fields is closely coupled to the electrically conducting metal structure. The impact of eddy-current effects produced in conducting structures needs to be evaluated in design. The axisymmetric electromagnetic forces acting on the vacuum vessel, shell, and TSS have been calculated by means of a 2D code and non-axisymmetric EM loads have been calculated by means of 3D finite element analyses [4].

Magnetic field from different coil systems and plasma current can produce the following forces in structural components of RFX-mod machine:

4.1.3.4.1 Axisymmetric electromagnetic load

The axisymmetric electromagnetic (EM) load inputs are received from electrodynamic analyses. The electromagnetic loads have been evaluated by means of a 2D numerical code based on an integral formulation of electromagnetic equations [40] [37]. The loads are considered for different scenarios as mentioned below:

- normal plasma operation with reference shot at 2 MA (# 29262)
- shot with plasma current of 2 MA and with fast termination (# 29283).
  The fast termination is supposed to occur during the flat-top phase. The plasma current decays from its nominal steady state value of 2 MA with a quasi linear ramp down of 250 ms duration: on the basis of the RFX experimental data base this assumption is still rather conservative and it produces the highest stresses on the passive structures [37] [12].
- shot without plasma current.
  This is the case of fault condition occurring in the control system, in which coil systems are discharged without detection of plasma current.

The transient electromagnetic (EM) load inputs are received from 2D electrodynamic analysis [41] in terms of each 10° poloidal angle between 0 and 180°. Looking at the

variation of force with time, the time instance of maximum load conditions are identified for each scenario as listed in the following Table 12.

Table 12 Summary of electromagnetic load input time selection

Scenarios	Time for Cu-shell	Time for TSS & FSW
normal plasma operation with 2 MA	0.0481 s	0.0256 s
plasma current of 2 MA and with fast termination	0.163 s	0.1635 s
pulse without plasma current	0.0521 s	0.0281 s

The identified maximum forces are applied to the passive stabilizing shell, TSS and FSW for static structural simulation. Following aassumptions are taken to apply loads on structural model:

- EM forces will be different at each poloidal angle, but identical along the toroidal angle:
  $F_{\Theta 1\phi 1} = F_{\Theta 1\phi 2}$, $F_{\Theta 1\phi 1} \neq F_{\Theta 2\phi 1}$
- Loads are defined for poloidal angles between 0 and 180°, so symmetry w.r.t. the equatorial plane is assumed
  - TSS: Same radial direction and opposite tangential direction when mirroring the loads wrt equatorial plane
  - FSW: Same horizontal direction and opposite vertical directionwhen mirroring the loads wrt equatorial plane
- Total force is calculated considering 10° of the poloidal angle multiplied for the overall toroidal length
  - Total force will be multiplied by (30°/360°) as only 30˚ sector is considered for structural analysis
- FSW forces are divided by number of clamping rings (24) an applied to structural model.

4.1.3.4.2 Non-Axisymmetric electromagnetic load

The non-axisymmetric EM loads have been calculated by means of 3D finite element analyses. The maximum EM loads are localised in the proximity of the overlapped gap of stabilizing shell and tends to push up on one side and down on the other, depending on the direction of the toroidal field. The non-axisymmetric loads acting on the TSS and on the vessel are negligible [4].

4.2 Description of loads on RFX-mod2

As detailed in CHAPTER 2, the major modification of RFX-mod machine consists of the removal of the vacuum vessel with development of new supporting elements at the interfaces from the first wall to the TSS through passive shell. Similar to RFX-mod, structural loads are considered for the RFX-mod2 configuration identifying load combinations to be applied for the analyses and verifications of the new machine. The changes considered in loads and operating conditions for RFX-mod2 are described in the following subsections.

4.2.1 Mechanical Load Path in RFX-mod2

The general arrangement of interfaces of the RFX-mod2 machine components is shown in Figure 51. The mechanical load path of the modified machine can be compared with the RFX-mod (see Figure 48). The major supporting structure is maintained the same for RFX-mod and main changes are,

- Toroidal Support Structure (TSS) will realise also the new vacuum vessel
- The 2016 first wall tiles will be supported by the passive stabilizing shell that is supported on TSS through 24 supporting rings.

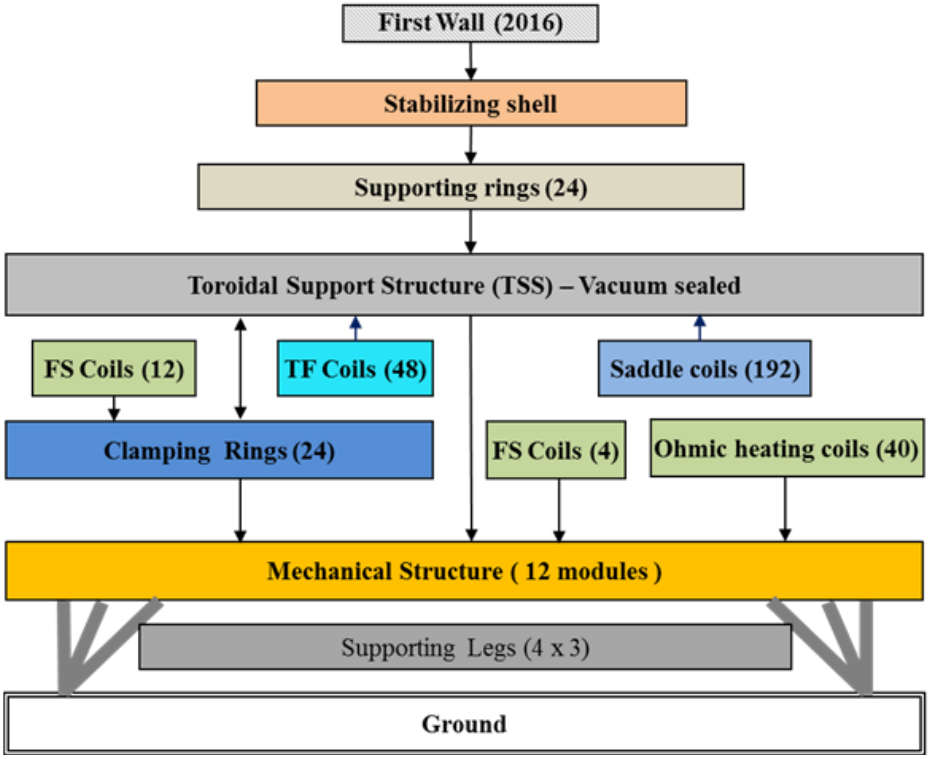

Figure 51: General layout of supports in RFX-mod2

4.2.2 Operation Scenarios of RFX-mod2

The following operating conditions are considered in order to identify loads to be applied on the machine for the verification of the design:

1. Baking and wall conditioning
2. Pulse operation

3. Seismic events
4. Testing conditions
5. Handling and assembling during installation

Baking, pulse operation, and seismic events are described in the following. For testing conditions, handling and assembling additional loads on the whole assembly are not produced with respect to the pulse operation, so they are considered implicitly verified.

4.2.2.1 Baking and Glow Discharge Cleaning

The baking and GDC in RFX-mod2 machine will be done at 170 °C, same temperature as RFX-mod. The design of the new baking system for RFX-mod2 is going on considering also solutions studied in the past [13]. One of two following methods will be used to bake the first wall:

- Pulse Discharge Cleaning system:

  The Pulse Discharge Cleaning can also provide an effective baking of the first wall in absence of the vacuum vessel. The PDC pulse has been produced for the effective power transferred to the plasma and from plasma to the first wall surface, half of the power is directly transferred from the plasma to the first wall whereas the other half is ohmically transferred to the passive stabilizing shell. On the base of available results as shown in Figure 52, the evaluation of the PDC pulse duration and of duty cycle is in progress, which is necessary to transfer up to 30 kW power to the first wall.

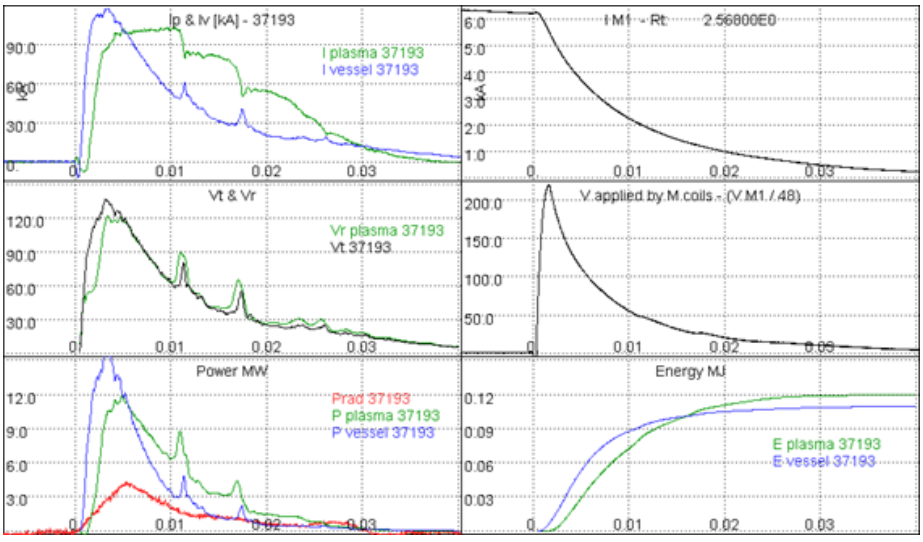

Figure 52: PDC pulse reproduced in RFX-mod [13]

- Eddy current system:

  As available for RFX-mod vacuum vessel [4], the baking of FW tiles can be performed by inducing toroidal eddy currents in the passive stabilizing shell. The poloidal distribution of the eddy currents introduces a poloidal distribution of the

temperature on the shell. This system requires short circuiting the passive stabilising shell at the poloidal cuts.

The Glow Discharge Cleaning (GDC) system for RFX-mod2 will be the same as available in RFX-mod with some improvements: the number of electrodes will be increased in order to attain a more uniform and effective cleaning of the wall. The proposal is to have 12 electrodes installed at new ports gained in the TSS which were dedicated to the cooling of the vessel in RFX-mod.

4.2.2.2 Pulse operation for RFX-mod2

The normal plasma operation will be similar to the RFX-mod operation scenario described in section 4.1.2.2 with experimental measurements. The input parameters for further design assessment are considered same as RFX-mod pulsed plasma operation scenario.

4.2.2.3 Seismic events

The seismic load consists of an oscillatory movement of the earth's surface due to an earthquake. The ground acceleration can be both in the horizontal and in the vertical direction and typically has a spectral content which leads to some level of support reaction load amplification.

In many cases seismic event is the most demanding loading condition, in particular for the supports and interface structures which must be sized for high strength, and often also for high stiffness.

The seismic analysis can be performed in the following steps [42]:

1. Linear static structural response with static loads
2. Modal analysis to determine natural frequencies
3. Structural response applying response spectrum (dynamic loads)

Seismic event severity, amplitude and repetitions depend on the geographical location of machine. In Italy the seismic design and verification of the buildings shall be made applying the "Nuove Norme Tecniche per le Costruzioni" D.M. 14/01/2008 (NTC) [43] and the "Circolare 02/02/2009 N. 617 Istruzioni per l'applicazione delle Nuove Norme Tecniche per le Costruzioni" [44] (these documents are written in Italian language). NTC is in agreement with the international standard and in particular with the EUROCODE and the European standard EN. NTC, similarly to EUROCODE 8 [45], requires the verification of buildings and equipment's at the limit states.

The RFX experiment is located in the industrial area of Padua city, Italy. The Italian Civil Protection Department has classified the italian territory based on past earthquakes' intensity and frequency and on the application of special regulations of buildings in areas. In the four main classes of seismic zone given, Padua is classified as "Zone 4 – Very low risk zone" [46].

Four limit states are grouped in two categories as shows in th following Table 13.

Table 13 Limit states for the seismic verification [NTC, eurocodice 8]

SLE – "Stati Limite di Esercizio" (Serviceability Limit states)	SLO	Fully Operational Limit State
	SLD	Damage Limit State
SLU – "Stati Limite Ultimi" (Ultimate Limit states)	SLV	Life Safety Limit State
	SLC	Collapse Prevention Limit State

On the basis of the site parameters, the return periods corresponding to SLD and SLV limit states are:

- SLD 50 years;
- SLV 475 years.

The ground acceleration spectra shown in Figure 53 and Figure 54 have to be considered respectively for SLD and SLV Limit States.

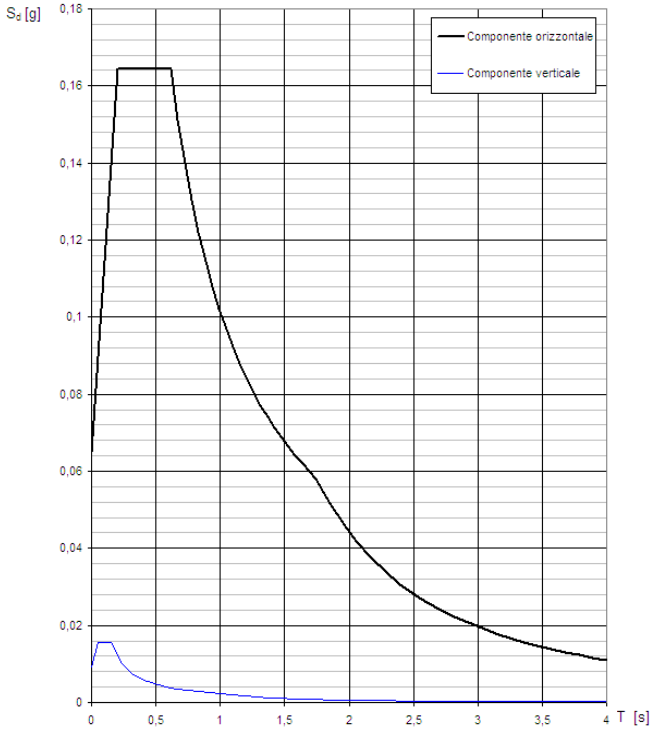

Figure 53: Horizontal and vertical ground acceleration elastic spectra at 5% of the critical damping for SLD limit state

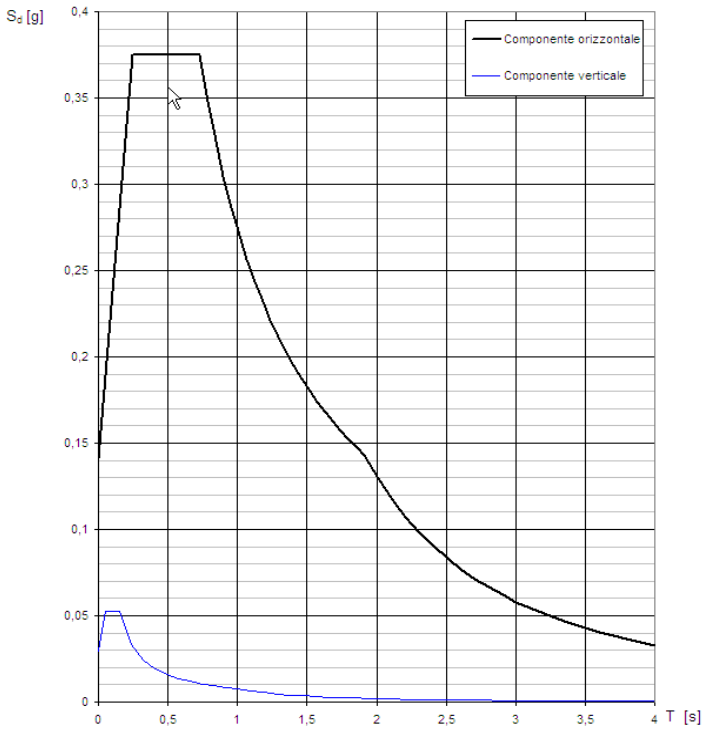

Figure 54: Horizontal and vertical ground acceleration elastic spectra at 5% of the critical damping for SLV limit state

Some values are taken from Figure 53 and Figure 54 above: accelerations higher than 0.15 g correspond to times within the range 0.2÷0.7 s and to frequencies of 1.5÷5 Hz for SLD limit state; accelerations higher than 0.3 g correspond to times within the range 0.2÷1 s and to frequencies of 1÷5 Hz for SLV limit state. So, the order of magnitude of the maximum frequencies is 10 Hz for not negligible accelerations to be considered for verifications.

Seismic verifications will not be performed for RFX-mod2 components, as there is not any modification of major supporting structure of machine. Only evaluations about the natural frequencies of components are discussed.

4.2.3 Types of loads on RFX-mod2

The loads to be applied for conceptual design and analysis of RFX-mod2 mechanical components can be taken comparable to loads for RFX-mod components as described in section 4.1.3. Following changes are considered for RFX-mod2 components design:

- External pressure will be applied on TSS
- The heat transfer path from first wall to vacuum vessel is changed and should be analysed
- The stabilizing shell will operate as structural element as it will provide support to FW tiles
- There is no overlapping sector in stabilizing shell
- Non-axisymmetric electromagnetic loads will be evaluated only for vertical insulated gaps of the TSS and stabilizing shell
- Supporting rings and its rail are required to stiffen and support the passive shell

4.2.3.1 Dead weights

Gravity loads occur due to masses that are accelerated by gravity. All masses to be considered for structural analysis are listed in Table 14 [47]. To reduce the computational burden, the components weight can be applied as point load or as distributed forces over corresponding surface. These masses correspond to the full (360°) toroidal structure.

Table 14 Masses of different component for gravity load case

	Components	Vol.	Density	Mass	Force
		m^3	kg/m^3	kg	N
In TSS components	FW (ALL)	0.3	2000	686	6730
	Shell	0.1	8940	1162	11400
Saddle	Saddle	0.2	8940	1520	14910
TF & connections	TF	1.2	8940	10701	104980
	Belt	0.3	7900	2677	26264
	Cable conn.	0.2	8940	1717	16839
PF coils	F3	0.1	8940	894	8770
	F4	0.1	8940	1073	10524
	F5	0.1	8940	1252	12278
	F6	0.2	8940	1699	16663
	F7	0.2	8940	1877	18417
	F8	0.2	8940	1609	15786

4.2.3.2 External pressure

The modified TSS has to provide UHV barrier for plasma operations. Hence it will be subjected to the atmospheric pressure of 10^5 N/m^2 at its external surface.

4.2.3.3 Preload

As described in section 2, two halves (Top and Bottom) of TSS are preloaded together by means of 24 clamping rings located with 15° step along the toroidal angle. This arrangement applies compressive forces on TSS with total 15 MN of preload on TSS [11]. The required force is applied by bolted connection on each ring. There is M27 single bolt connection at internal side and two M24 bolt connection at external side of each clamping ring. The actual applied torque is 1050 N*mm and 350 N*mm for M27 bolt and M24 bolt respectively.

Also the preload coming from TF coil belts is applicable. TF coils are pressed on surface of TSS by means of belts, which exerts pressure of 3MPa on surfaces which supports.

The TSS is supported to its top and bottom by mechanical structure through stack of disc spring and its total stiffness is 11600 N/mm [48]. This arrangement realises independent deformation of the toroidal assembly with respect to the supporting structure as the only interactions occur through the springs.

4.2.4 Load combination and criteria for the verification of RFX-mod2 components

All components must withstand many individual and combined loading conditions during both normal and off-normal operation scenarios. The component design should be evaluated for test, service and fault conditions as per design standards to provide a high degree of integrity. The ASME design rules are being used across the component design to establish event combinations and to classify them.

4.2.4.1 Description of Loading Categories and Criteria Levels

The approach specified in ASME Boiler and Pressure Vessel Code [49] and ITER Structural Design Criteria (In-vessel components) [50] was followed for component design. The design condition, the service levels and its correlation to the damage limit (normal, upset, emergency and faulted) and test loadings are defined in ASME NC for components class 2 that are not part of the reactor coolant pressure boundary. It is required that all loadings to be applied on components are already defined based on different operating conditions. Service levels are aimed at preventing a specific degree of damage to the component.

- Service Level A: Normal

  These are loadings arising from system startup, operation in the design power range, hot standby, and system shutdown.

  All structures, systems, and components are functional.

- Service Level B: Upset

  The events that cause Service Level B loadings include transients which result from any single operator error or control malfunction, transients caused by a fault in a system component requiring its isolation from the system, and transients due to loss of load or power. These events include any abnormal incidents not resulting in a forced outage.

  Cause negligible damage, all structures, systems, and components are functional. Anticipated maintenance and minor adjustment might be required.

- Service Level C: Emergency

  These are deviations from Service Level A loadings that have a low probability of occurrence and would require shutdown for correction of the loadings or repair of damage in the system. The total number of postulated occurrences for such events may not exceed 25.

It may cause significant local distortion. May need to inspect, call for repair or replacement of faulty components.

- Service Level D: Faulted

  These are the combinations of loadings associated with extremely low probability, namely, postulated events whose consequences are such that the integrity and operability of the nuclear energy system may be impaired to the extent that only consideration of public health and safety are involved.

  It may cause large general distortion and investment loss. Repair may not be considered economic. Minimum safety functions shall be maintained.

- Testing condition: Test
  These are pressure loadings that occur during hydrostatic tests, pneumatic tests, and leak tests. Other types of tests are classified as Service Level A or B loading. If any elevated temperature tests are specified as Test Loadings for a component, then these loadings shall be considered as part of Service Level B loadings.

As per ITER SDC-IC standard, all possible events experienced during the life of the machine have been classified into several categories listed in the following based on their probability of occurrence,

- Category I: Operational
- Category II: Likely
- Category III: Unlikely
- Category IV: Extremely Unlikely
- Category V: Testing

The Table 15 shows the design criteria for corresponding Loading Categories with respect to its service Levels.

Table 15 Design Criteria for Loading Categories and service Levels

Loading Event Category		Service Level	Damage Limit
I	Operational	A	Normal
II	Likely	A	Upset
III	Unlikely	C	Emergency
IV	Extremely unlikely	D	Faulted
V	Testing	Test	Test

It can be noted that the service level A is applied to upset damage limit instead of level B as explained above for the ASME code. This change is introduced in ITER SDC-IC because transient loadings classified as upset limit are likely to occur and need to be verified with high margin given for service level A.

4.2.5 Design criteria for verification

Thermo-mechanical FE calculations have been carried out to verify design modification of the RFX-mod components in compliance with ASME rules for Design-by-Analysis (DBA). The nonlinear thermo-mechanical analyses have been carried out implementing contact conditions and elastic behaviour of the materials. The DBA procedure is intended to guard against possible failure modes of components by performing detailed stress analysis of them.

The ITER structural design criteria for In-vessel Components are selected as the reference standard for structural verification since they are applicable to any vacuum vessel and in-vessel component. Furthermore, they consider many design rules including local fracture due to exhaustion of ductility and fast fracture which are not applied for the verifications in the following sections. This assumption is made as the ductility and the toughness of the materials are not reduced by irradiation and so the relaxation of locally high peak stress will occur without cracking in the RFX-mod2 components.

The basic stress limits are based on allowable stress (Sm) of material that is calculate as minimum from 2/3 of yield strength (Sy) or 1/3 of the ultimate tensile strength (Su) for all metallic materials except bolts.

The total elastic stress computed through FE analysis is decomposed in different categories of stress: General Primary Membrane (Pm), Local primary membrane (P_L), Primary bending stress (P_b), Secondary stress (Q) and Peak stress (F).

Design rules for service levels A and C are provided in the following, but not for level D corresponding to faulty damage limit because extremely unlikely loads are not simulated.

Design rules for service level A:

General Primary Membrane: $Pm \leq Sm\ (T_m, \Phi t_m)$

Local Primary Membrane: $P_L \leq \min [1.5 \cdot Sm\ (T_m, \Phi t_m), Sy\ (T_m, \Phi t_m)]$

Primary Membrane + Bending: $(P_L + P_b) \leq K_{eff} \cdot Sm\ (T_m, \Phi t_m)$

Primary + Secondary: $(Pm + P_b + Q) \leq Se\ (T_m, \Phi t_m)$

Design rules for service level C:

General Primary Membrane: $Pm \leq 1.2 \cdot Sm\ (T_m, \Phi t_m)$

Local Primary Membrane: $P_L \leq \min [1.5 \cdot 1.2 \cdot Sm\ (T_m, \Phi t_m), Sy\ (T_m, \Phi t_m)]$

Primary Membrane + Bending: $(P_L + P_b) \leq K_{eff} \cdot 1.2\ Sm\ (T_m, \Phi t_m)$

Primary + Secondary: $(Pm + P_b + Q) \leq 1.2\ Se\ (T_m, \Phi t_m)$

Where, Sm = allowable stress

Sy = minimum tensile yield strength

Keff = an effective bending shape factor (1.5 for RFX-mod2 components)

Se = allowable stress intensity

T_m = thickness-averaged temperature

Φt_m = thickness-averaged neutron fluence

The stress intensities are evaluated as von-Mises equivalent stresses produced by the post-processor of the FE code. Only the last three design rules (P_L, P_L+P_b, $Pm+P_b+Q$) will be applied in the following sections to carry out the design verifications, as the finite element code will produce local stresses for the simulated actual geometry; indeed, the CAD model implemented for simulations is very detailed and stress contours at gross sections are not evaluated.

4.2.5.1 Load case combination and component verification

The design conditions include pressure, temperature, electromagnetic and mechanical loadings; these conditions are selected as the basis for the design as described in section 4.1.3. Loading categories and service conditions cover those normal operating conditions, expected transients, and hypothesized accident conditions expected to occur during operation. This categorization is chosen to accommodate design criteria for safety importance components as well as in order to obtain a well-balanced design.

Table 16 reports the list of the load case combinations, load category and the Service Limit Levels considered for the component design. Load cases presented are combined considering the simultaneously application onto the machine during the operating scenarios given in section 4.1.2.

Table 17 reports the list for component verification. The load combination is applied onto each component for the thermal and mechanical verification according to ASME Boiler and Pressure Vessel Code Section VIII div.2 and according to SDC-IC. Some load combinations presented in Table 16 are not investigated with finite element analyses because they are not considered demanding and significant for the preliminary design of the machine at this time.

Table 16 Load case combinations for RFX-mod2

Load combination No.		Condition or event	Load category	Damage limit	ASME criteria	Loads								Remarks
						Inertial		Pre.	Thermal			Electromagnetics		
						Gravity	Seismic	Vacuum	Baking	Power density	Localized	Axisymmetric	Non-axisymmetric	
1. Test / Commissioning loading	1.1	Installation / Maintenance	V	Test	Test	●								Not considered separately as it is covered in pulsed normal RFP operation
	1.2	Vacuum leak test	V	Test	Test	●		●						Not considered separately as it is covered in pulsed normal RFP operation
2. Operational loadings	2.1	Baking and GDC	I	Normal	A	●		●	●					
	2.2	Normal RFP operation	I	Normal	A	●		●		●		●		
3. Likely loadings	3.1	Plasma fast termination	II	Upset	B	●		●		●		●	●	Two analysis performed considering different Electromagnetic loads
	3.2	Wall Mode Locking (PWI)	II	Upset	B	●		●			●	●		
4. Unlikely loadings	4.1	Fault condition - Emag	III	Emergency	C	●		●		●		●		
	3.3	Seismic event - 1	III	Emergency	C	●	SL-1	●		●		●		
5. Extremely unlikely loadings	5.1	Seismic event - 2	IV	Faulted	D	●	SL-2	●		●		●		

Table 17 Component verification table for RFX-mod2

Load combination No.		Condition or event	Stabilizing shell and Supporting rings*			Toroidal Support Structure**			Vacuum Sealing boundaries**	Remarks
			T	M	D	T	M	B	M	
1. Test / Commissioning loading	1.1	Installation / Maintenance								
	1.2	Vacuum leak test							W+P	Considered for TRP seal
2. Operational loadings	2.1	Baking and GDC	B	W		B	W+P			
	2.2	Normal RFP operation	U	$W+E_1$		U	$W+P+E_1$			
3. Likely loadings	3.1	Plasma fast termination	U	$W+E_2$		U	$W+P+E_2$			
	3.2	Wall Mode Locking	L	$W+E_1$		L	$W+P+E_1$			
4. Unlikely loadings	4.1	Fault condition - Emag		$W+E_3$			$W+P+E_3$	B		
	4.2	Seismic event - 1			D					
5. Extremely unlikely loadings	5.1	Seismic event - 2								

T=Thermal verification, M=Monotonic-type verification, B=Buckling verification, D=Modal analysis

* Mechanical analyses and verifications of these components are detailed in section 6

** Mechanical analyses and verifications of these components are detailed in section 7

Table 18 Key to codes used in the component verification table

Loads	Symbol	Description	Value
Thermal	**B**	Uniform temperature applied on FW	170 °C
	U	Uniform power density applied on FW	1.8 MW/m^2
	L	Plasma energy applied on a reduced part of FW during the pulse	18 MW/m^2
Structural	**W**	Weight	section 4.2.3.1
	P	Pressure and preloads	section 4.2.3.2 section 4.2.3.3
Electromagnetic	**E1**	Axisymmetric forces loading the machine during the pulse	section 4.1.3.4.1
	E2	Axisymmetric forces due to plasma fast termination	section 4.1.3.4.1
	E3	Axisymmetric forces loading the machine without plasma	section 4.1.3.4.1
	E4	Non-axisymmetric loading at the poloidal gap	section 4.1.3.4.2

CHAPTER 5 THERMAL ANALYSIS

Preliminary FE thermal analyses have been carried out for different loading conditions to evaluate temperature distributions in different components of modified torus assembly. Thermal analyses consider the changed heat transfer path due to design modifications. Considering thermal calculations, major change is FW tiles will be installed onto passive stabilizing shell and the passive stabilizing shell supported on Toroidal support Structure (TSS) by means of 24 supporting rings. Two different FE models were developed for analysis:

- Model-A was prepared for preliminary analyses, which include 5° sector of stabilizing shell and one poloidal array of 28 FW tiles. The model also includes washers for tile installation and positioning.
- Model-B includes a simplified 30° sector of FW tiles attached on stabilizing shell, supporting rings and toroidal support structure. Details of this model are discussed in following sections.

Model-A includes very fine mesh details with total number of elements 140544 for only 5° sector, so it is too demanding extend such geometry to a larger angle. The main advantage of this model is to simulate the heat flow from the first wall tiles to the stabilizing shell considering the actual geometry of the mechanical joint.

Model-B is useful to simulate a larger angle (28281 elements for 30°) including two rings supporting the passive stabilising shell onto the Toridal Support Structure (TSS) rail. This model-B can also be used to simulate non-uniform thermal loads applied onto first wall tiles, e.g. for plasma wall-locking.

Considered loading conditions are taken from Table 17;

1. Test / Commissioning loading: Thermal loads are not applied during this load combination
2. Operational loadings:
   - 2.1 Glow Discharge Cleaning and Baking: models B is used to this purpose, see sections 5.2.3
   - 2.2 Normal RFP operation: models A and B are used to this purpose, see sections 5.1.2 and 5.2.4
3. Likely loadings:
   - 3.1 Plasma fast termination: Thermal analyses are not developed for this load combination as they are similar to normal RFP operation
   - 3.2 Wall Mode Locking: model B is used for this analysis, see section 5.2.5

Analyses regarding points 2.1, 2.2, 3.2 are described in the following.

5.1 Model-A (5° sector of shell and FW tiles)

A preliminary analysis has been carried out to check the temperature distribution in stabilizing shell. As for RFX-mod2 the stabilizing shell will support the first wall carrying the total thermal load, the expected thermal deformation will be higher, so analyses are carried out to use for further design improvement.

5.1.1 Description of model-A

The model contains 5 degree sector of stabilizing shell, which accommodate 1 poloidal array of tiles (28 tiles) as shown in Figure 55. The model is prepared and meshed in ANSYS. Dimensional details of assembly are as below in Figure 56

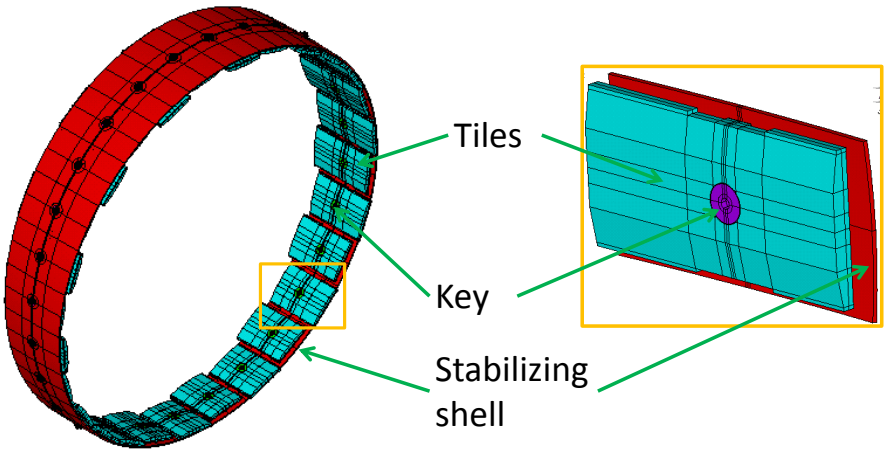

Figure 55 Assembly of 5° sector of stabilizing shell and FW tiles

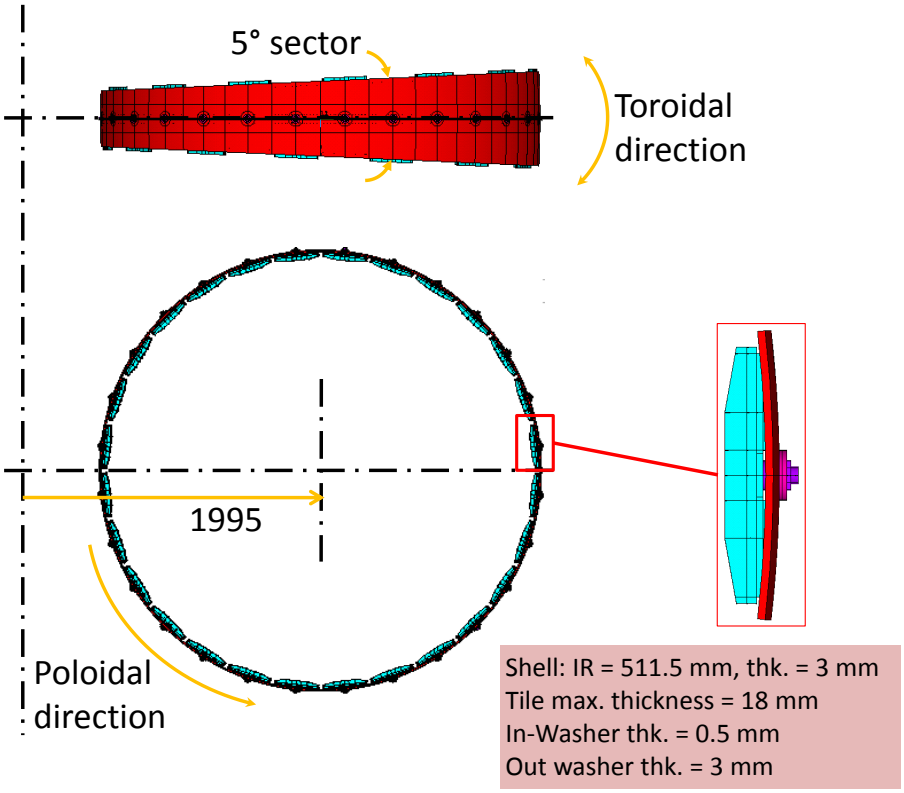

Figure 56 Dimensional details of assembly

Assembly consist tile attached to shell through key and supported through washer at back of shell. There is also a washer between shell and tile. Each tile is supported on shell by Inconel key. There is washer between shell and Tile which has groove in it to fix rotation of tile. For the simplicity of modelling the groove is not included in model. There is also out shell washer which provide flat surface to support key on it. Figure 57 shows section details.

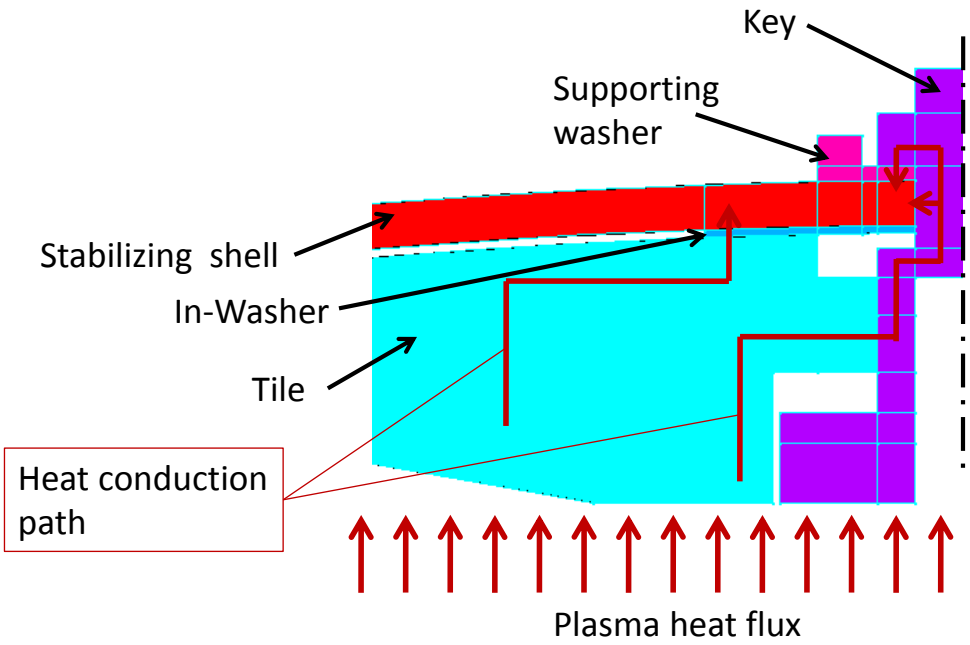

Figure 57 shows sectional view of single tile assembly and thermal conduction path

The following assumptions and simplifications are applied in the model,

1. Fillets and chamfers on tile are removed
2. Thickness of tile is considered uniform 12.5 mm (originally it is varying from 12.5 to 9.5)
3. In_washer (Between tile and shell) considered flat as alignment thickness of washer will not affect thermal simulation results
4. Belleville washers between tile and key are not developed
5. Stabilizing shell is model in top and bottom part but joints are considered in terms of partly nodal connection

The model is meshed in ANSYS14.5 using Solid278 element. To obtain good hex mesh model is divided in numbers of volumes. The entire model is mostly meshed with hex elements. Tetrahedral elements are used to mesh In-shell washer and backside rib of tile. Support of shell is made by Link33 elements. Figure 58 shows mesh generated on model. Number of elements = 140544, Number of nodes = 146936

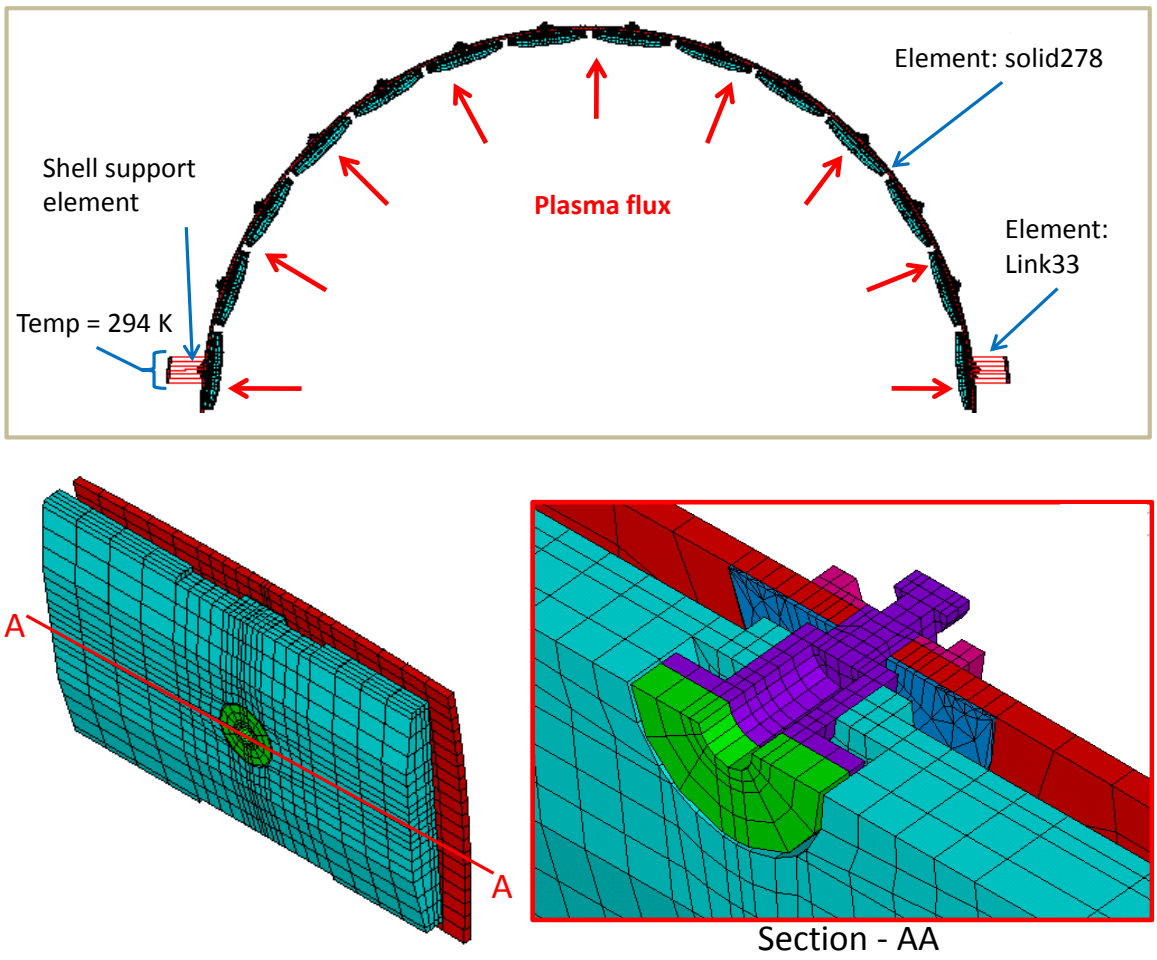

Figure 58: FE model of assembly and boundary condition

5.1.2 Simulation of normal plasma operation

5.1.2.1 Boundary condition for thermal transient analysis

For the transient thermal analysis of assembly, following conditions applied,

1. The machine at the beginning of the pulse operation will have a uniform room temperature equal to 294 K (21 °C)
2. This thermal load is applied for **30 Pulses** with **20 min** of pause between two consecutive pulses and with thermal conduction among the parts of the machine and natural convection with the air of the environment; about 30 pulses will be operated during Total **10 Hrs** of operation considered per day. The heat flux of 1.8 MW/m^2 is applied to FW tile plasma facing surface for each pulse.
3. the boundary condition at the supporting elements of the first wall is simplified by applying constant temperature of 301 K (28 °C) at end nodes of support as shown in Figure 58
4. Thermal radiation between tiles and stabilizing shell was not simulated in this model as its contribution results to be negligible with respect to conduction

5.1.2.2 Results of thermal transient analysis

The results of transient thermal analysis in terms of temperature distribution are shown in Figure 59. The graph in Figure 60 shows temperature distribution at different nodes on shell with respect to time.

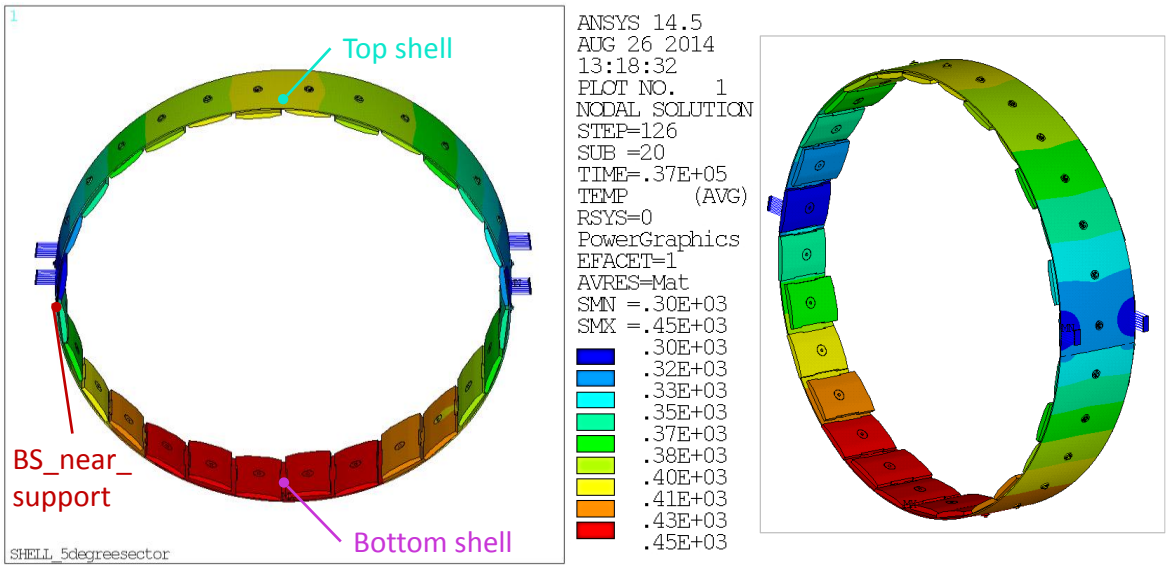

Figure 59: Temperature contour in shell (Max. temp. = 450 K)

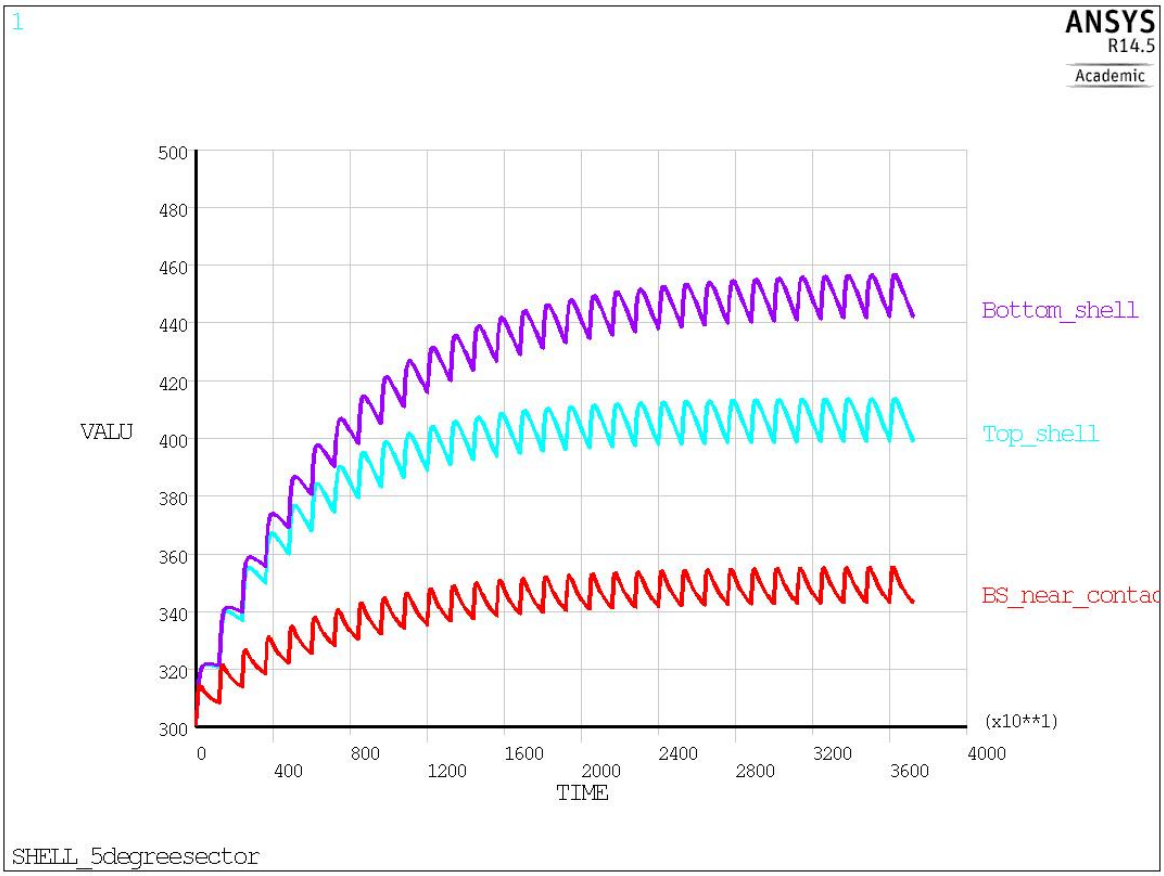

Figure 60: Temperature distribution in shell w.r.t time

Above results shows difference in temperature distribution within top and bottom shell that is due to fact that consideration of shell supporting elements which are slightly above equatorial plane. The constant temperature of 301 K (28 °C) is applied to the end nodes of contact elements.

So, maximum temp in top shell is 460 K (180 °C) at farthest distance from support. Shell near to support shows maximum temperature of 355 K (83 °C).

As bottom shell is partially connected to top shell, it attains maximum temperature of 460 K (180 °C) after operation of 30 pulses.

The main outcome of this analysis states that, thermal conduction between tiles and stabilizing shell is very good and shell attains same temperature of tiles, which eliminate the possibility of radiation calculation between tiles and stabilizing shell.

Considering maximum temperature of 473 K in the shell, copper (UNS C10200) maximum yield strength reduced to 55 MPa. Further model is used for preliminary static structural analysis for initial verification of stabilizing shell under FW tiles weight.

5.2 Model-B (30° sector of toroidal assembly)

5.2.1 Description of model B

A simplified model is prepared to carry out transient thermal analysis of the assembly for different thermal loads expected during experimental session. The model contains 30 degree sector of FW tiles (Array of 28 x 6 tiles), keys, stabilizing shell, supporting rings, rails and TSS as shown in Figure 61. The FW tiles are installed on stabilizing shell by means of keys, stabilizing shell is attached with supporting rings and supporting rings are supported on TSS rails.

Followings are assumptions and simplifications made in modelling,

1. The keys are modeled as cylindrical connection between tiles and stabilizing shell
2. Thickness of tile is considered uniform 11 mm (originally it is varying from 12.5 to 9.5)
3. Toroidal gap between top and bottom Stabilizing shell is not considered

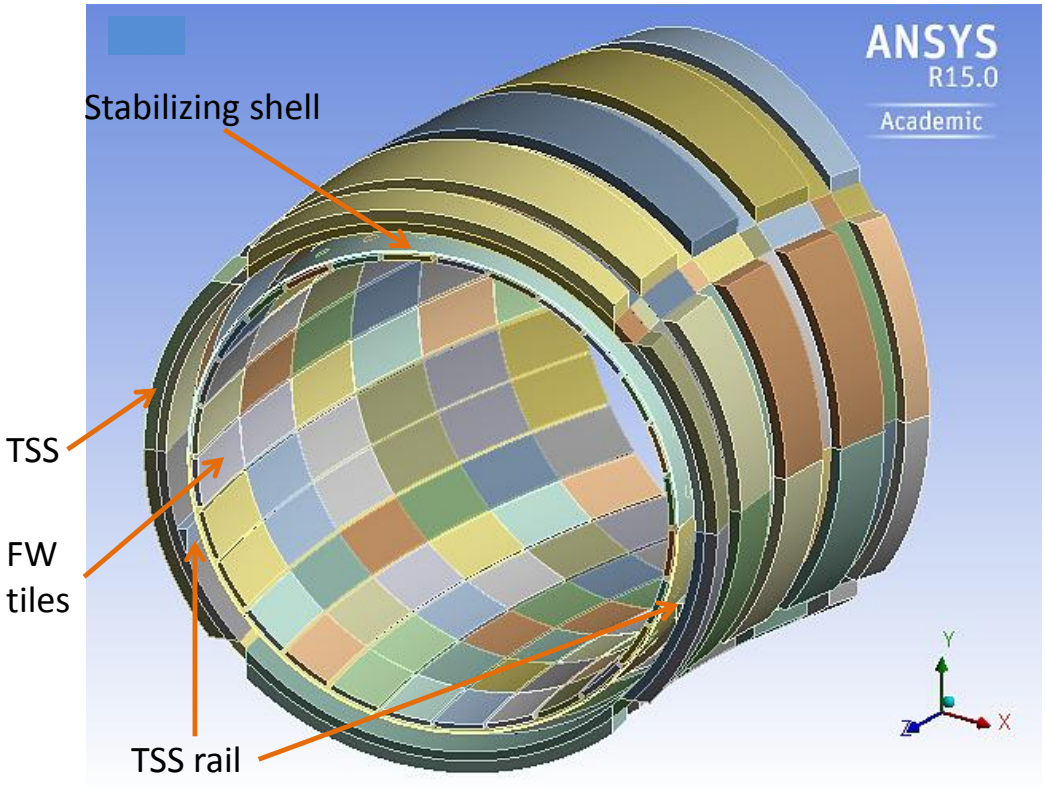

Figure 61: Geometrical model of 30 degree sector

Perfect thermal contact conditions were applied between components as shown in Figure 62. Bonded contacts are applied between all the mating components, except frictional contact condition (frictional coefficient = 0.2) applied between supporting rings and TSS rails (see Figure 63).

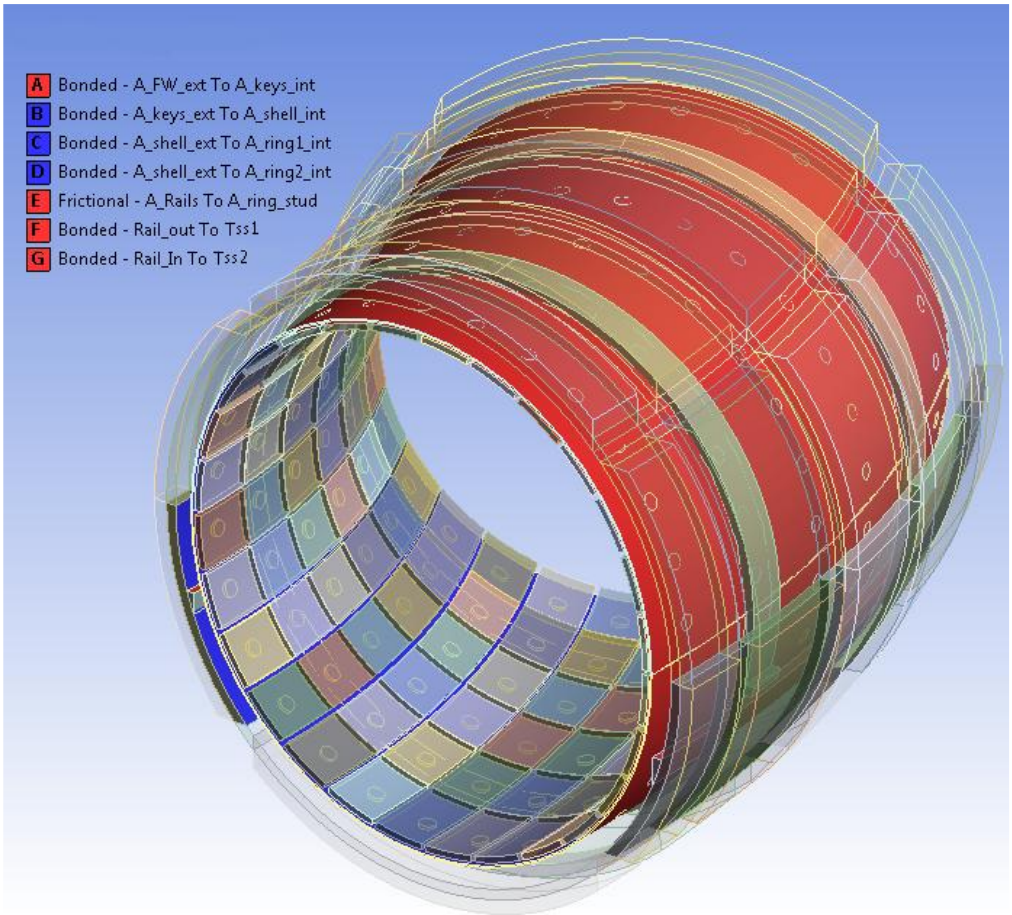

Figure 62: Contact condition between different components

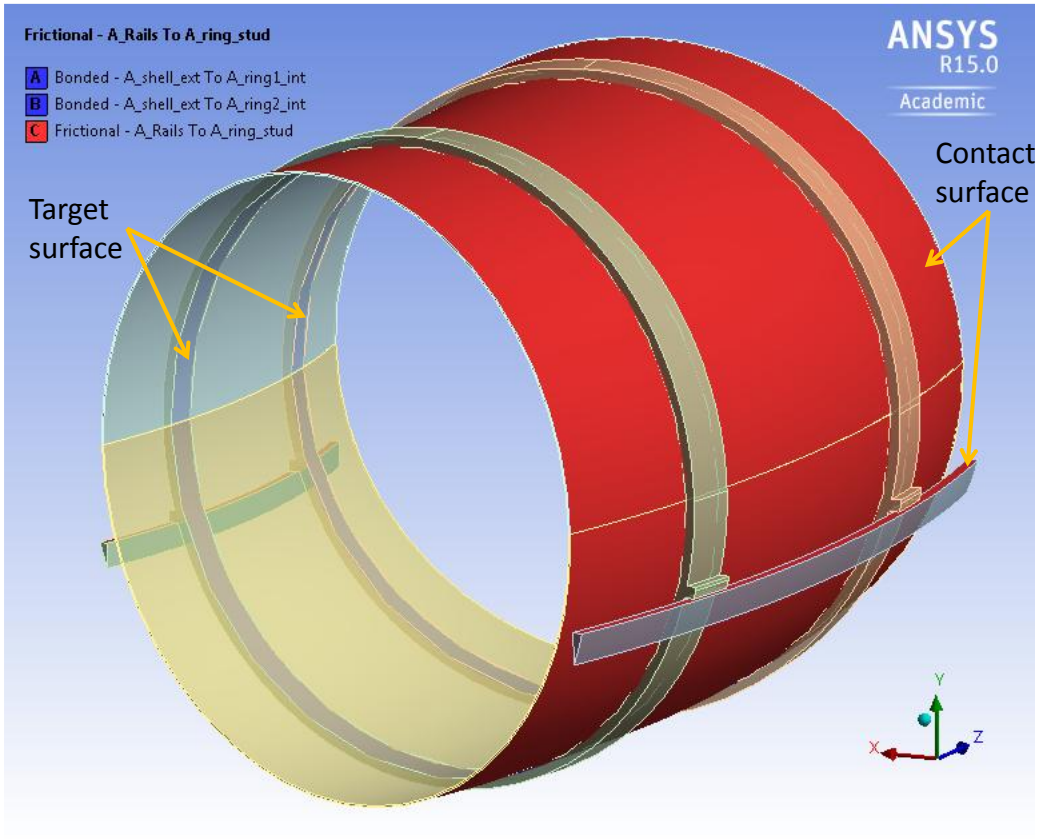

Figure 63: Contact condition between Shell to rings and rings to rails

The model is divided in solid bodies and mesh size has been adjusted to get a good quality and a good distribution of elements in the different parts of the components. With reference to ANSYS software, SOLID186 elements are generated. Total 48308 elements are generated with 290605 nodes. The Figure 64 shows details of the FE model features. Figure 65 shows the number of elements on thickness of different components.

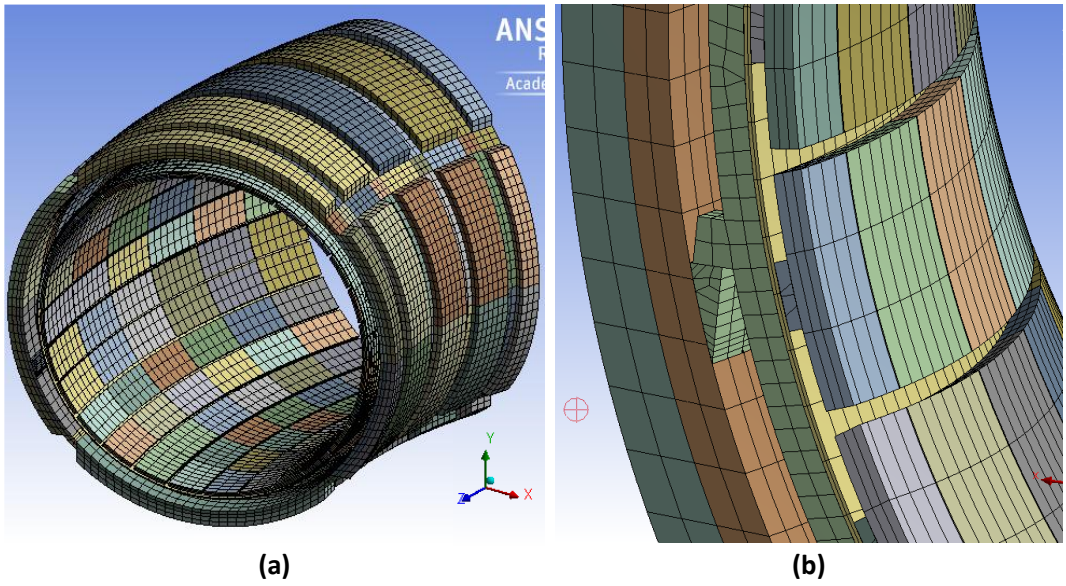

Figure 64: (a) FE model of 30 degree sector (b) Sectional view of mesh

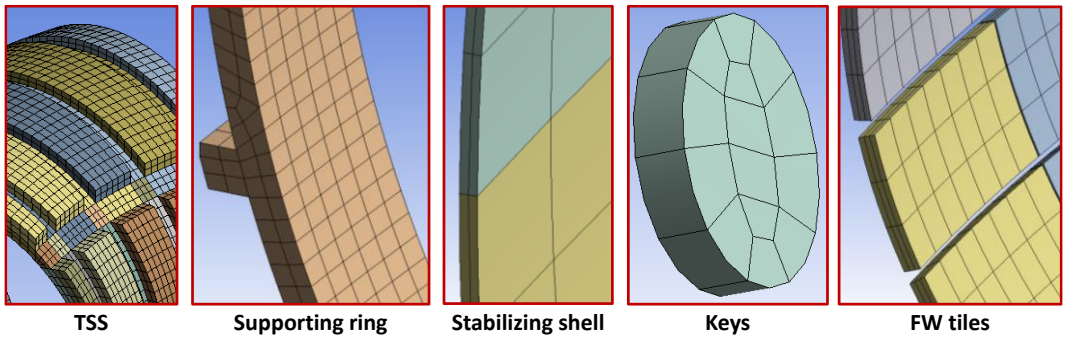

Figure 65: Mesh details of each component

5.2.2 Common Boundary conditions for analyses

There is not active cooling applied to any component of RFX-mod2 assembly, so boundary conditions applied are related to thermal conduction, radiation and natural air convection at the outer surface of TSS. Followings are the general boundary conditions applied for different thermal analyses;

1. Initial condition of 21 °C uniform temperature applied
2. Typical natural air convection coefficient 20 W/m² °C has been applied on the outer surface of TSS
3. Surface-to-surface thermal radiation is applied between stabilizing shell and TSS. Emissivity for copper material is 0.7 and for stainless steel material 0.5 considered [51]. As stabilizing shell is fully covered by TSS, viewing factor 1 is applied for radiation calculation.

Considering different operating conditions and loading scenarios, different temperature and heat flux load applied to the FW tiles plasma facing surface as described in section 4. Thermal analyses are carried out for three cases as describe below;

5.2.3 Simulation of baking and glow discharge cleaning condition

A further thermal load was added to the above boundary conditions, 170 °C temperature uniformly applied to plasma facing surface of FW tiles to simulate baking and GDC operation as describe in load specification (See section 4); Figure 66 shows applied boundary conditions to the model.

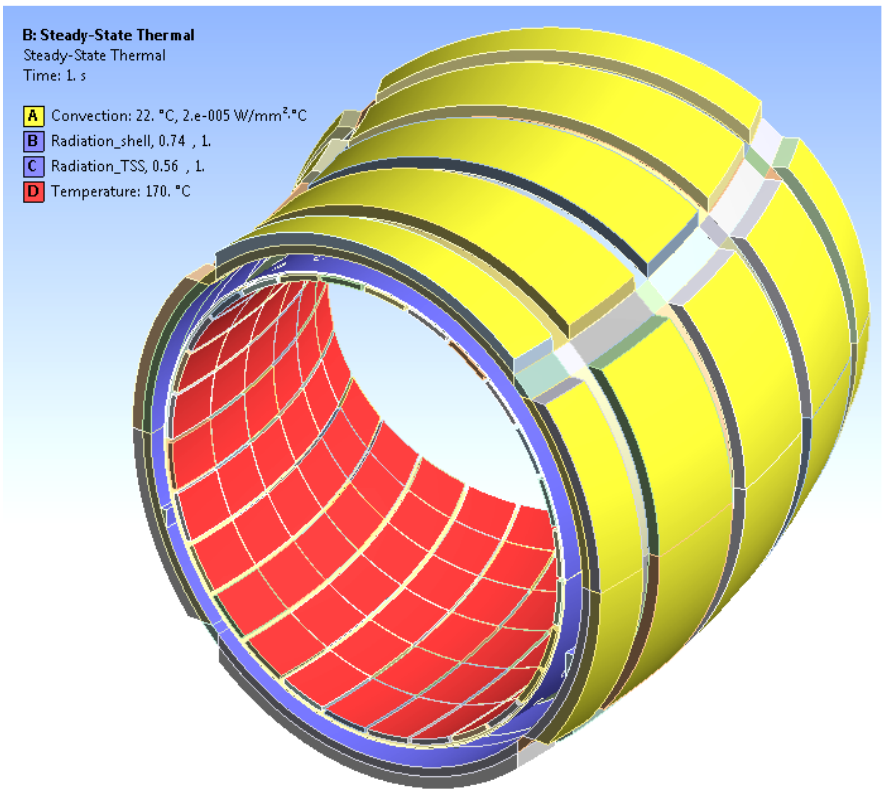

Figure 66: Boundary conditions applied for baking and GDC condition

5.2.3.1 Simulation results

A static thermal analysis was carried out for this load combination. The results achieved from simulation are shown in Figure 67, Figure 68 and Figure 69 as temperature distribution contour in different components.

The TSS attains maximum temperature of 78 °C and minimum temperature is 59 °C. Temperature distribution is higher at internal side of TSS and highest temperature is in toroidal grooves for saddle coil. Supporting rings are the only heat conductive part from shell to TSS, so it attains 169 °C uniform temperature distribution in ring section except in studs, where it shows minimum temperature of 64 °C (see Figure 68). There is high temperature difference within stud as shown in Figure 68. The temperature in the stabilizing shell varies from 164 °C to 169 °C as shown in Figure 69. The major portion of heat is transferred through radiation between shell and TSS. Net heat transferred from stabilizing shell through radiation is 2177 W.

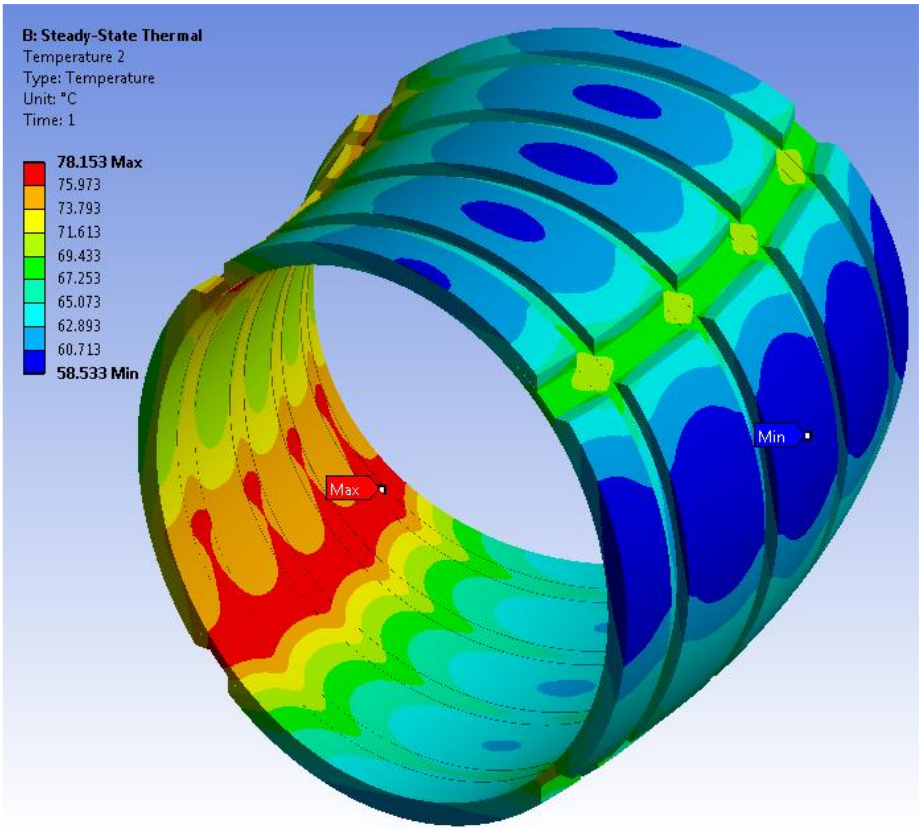

Figure 67: Temperature distribution [°C] in TSS

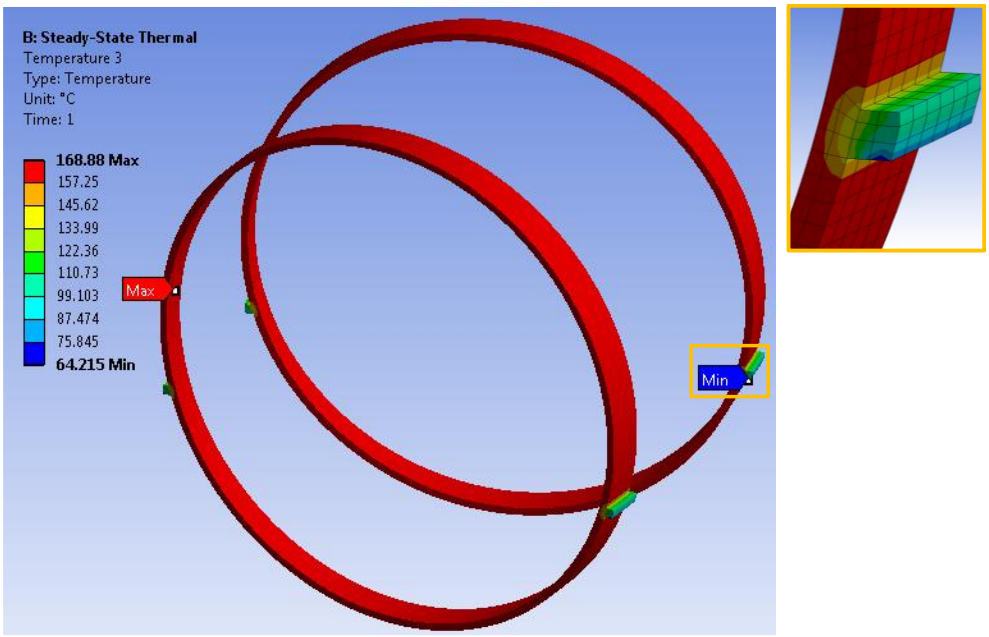

Figure 68: Temperature distribution [°C] in supporting rings

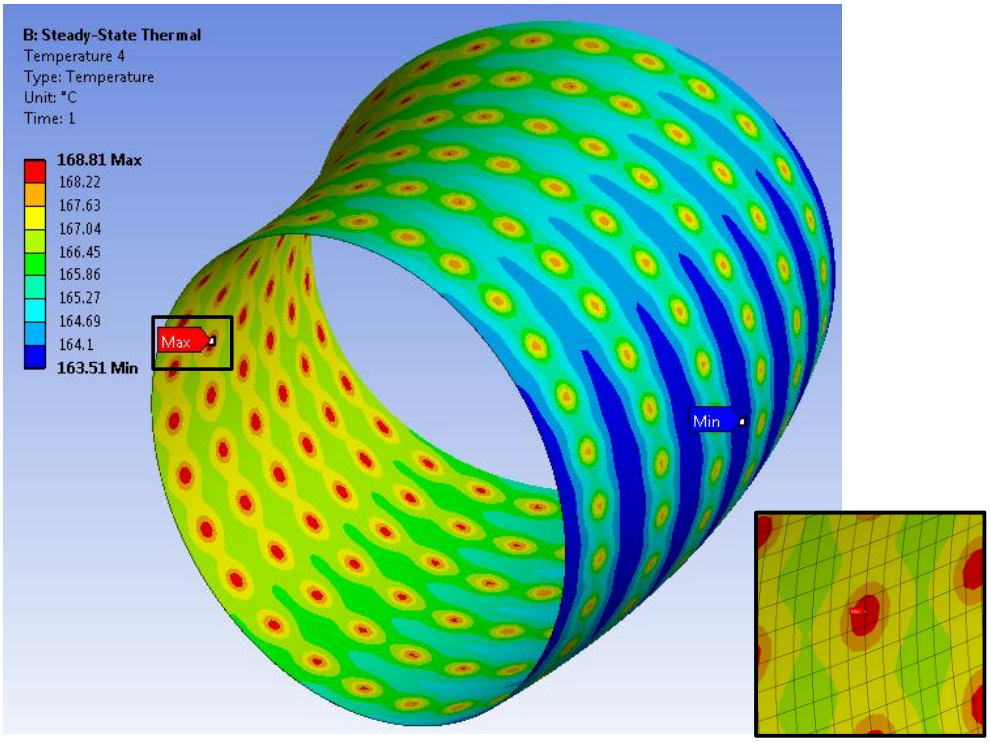

Figure 69: Temperature distribution [°C] in stabilizing shell

5.2.4 Simulation of normal RFP operation

Boundary conditions are complemented by applying heat flux to the FW tiles plasma facing surface as given in 4.1.3.3.2. Figure 70 shows applied boundary conditions to the model. The simulation of a full day experimental session has been carried out, considering one pulse every 20 min for 10 h.

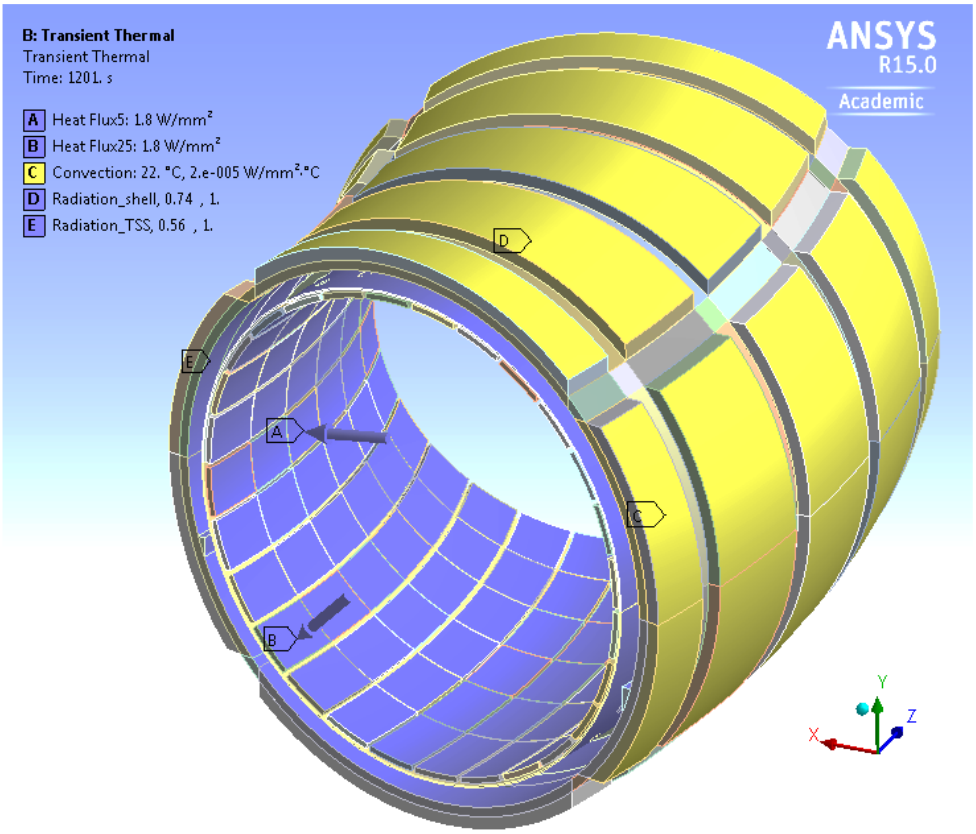

Figure 70: Boundary conditions applied for normal RFP operation

5.2.4.1 Simulation results

In order to estimate the temperature and heat transfer distribution in the assembly for an overall time of 37201 s a transient thermal analysis has been performed. Contour plot of temperature distribution in TSS, supporting rings and Stabilizing shell are shown in Figure 71, Figure 72 and Figure 73 respectively. The maximum temperature trend is plotted in Figure 74 for different components.

Temperature in TSS increases steadily with time and reach to 56 °C after a full day operation. After half day of operation the shell and supporting rings get thermal stabilization and there is not big change in temperature. The maximum temperature attained by stabilizing shell and ring assembly is 140 °C during pulse. During plasma pulse FW tiles attains maximum temperature of 223 °C and during cool down FW tiles and stabilizing shell gets thermal balance by heat transferred to shell and rings assembly.

Analysis shows that, maximum temperature attained by different components after 30 pulse (10 hrs.) operation are as follows:

- TSS, T_{TSS} = 56 °C
- Supporting rings, T_{rings} = 129 °C
- Stabilizing shell, T_{shell} = 123 °C

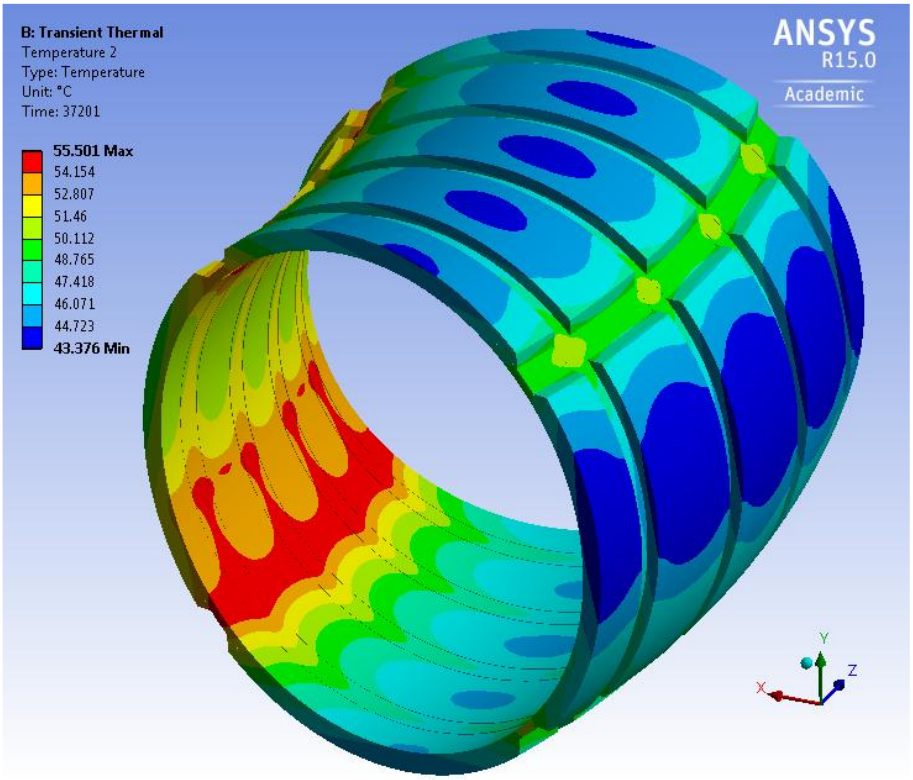

Figure 71: Temperature distribution in TSS @37201 s (Max. = 56 °C, Min. = 43 °C)

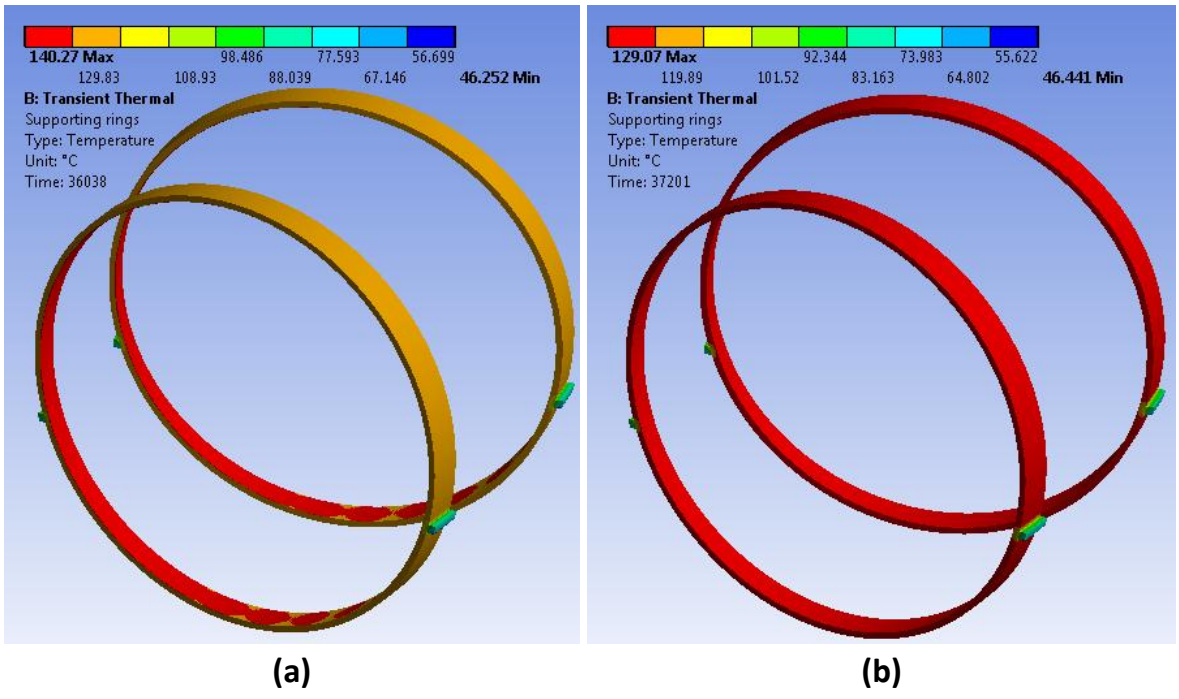

Figure 72: Temperature distribution in supporting rings (a) @ 36038 s, 140 °C; (b) @ 37201 s, 129 °C

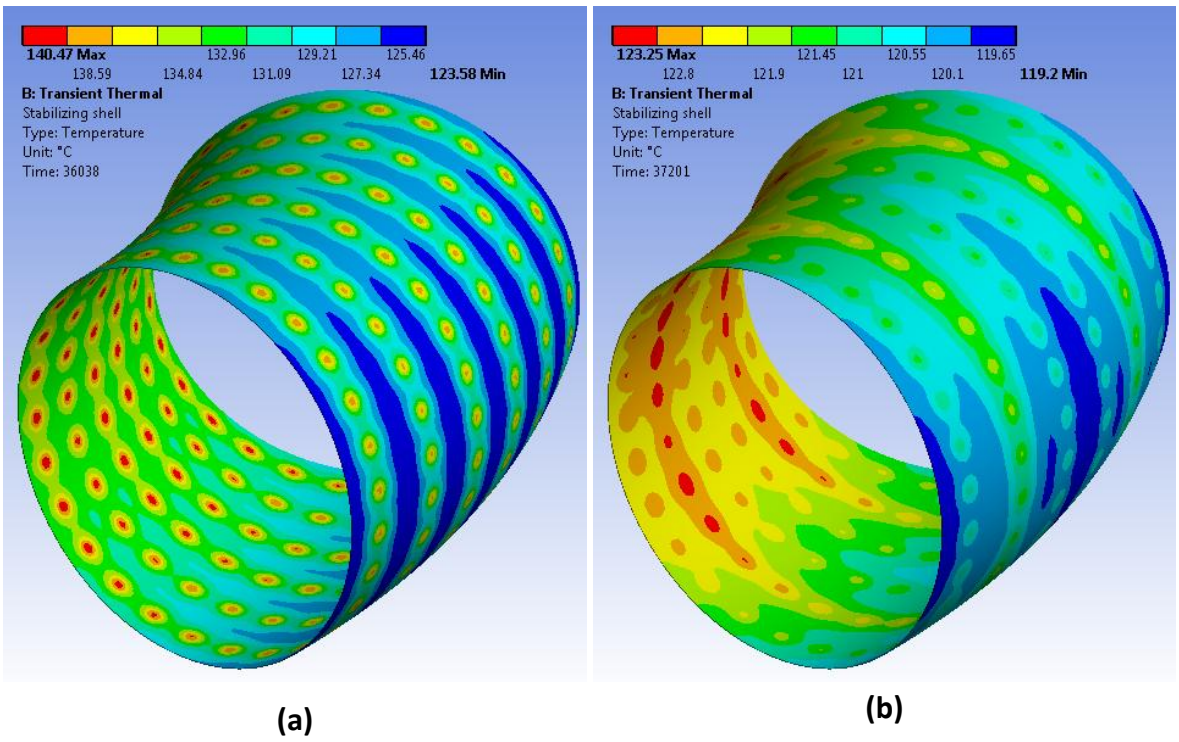

Figure 73: Temperature distribution in stabilizing shell (a) @ 36038 s, 140 °C; (b) @ 37201 s, 123 °C

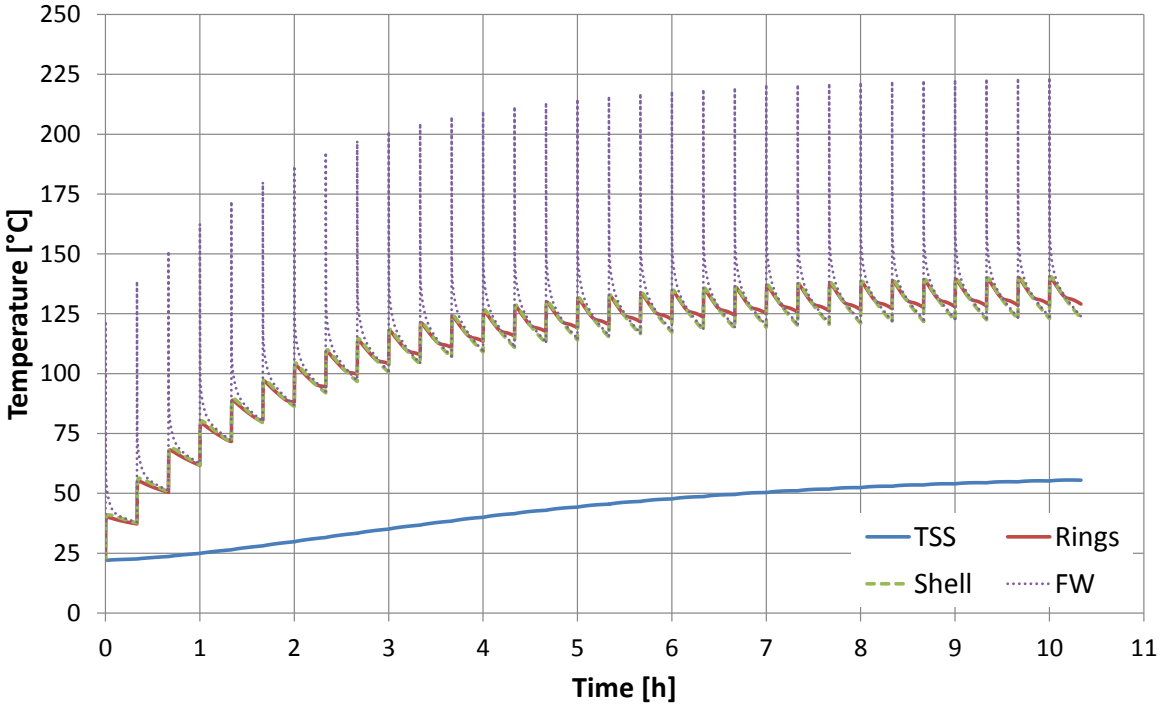

Figure 74: Graph of temperature distribution [°C] w.r.t. time [h]

5.2.5 Simulation of Wall mode locking

In addition to common boundary conditions, heat flux is applied to the FW tiles plasma facing surface. In wall mode locking scenario plasma rotation is locked to particular toroidal angle and it will receive higher heat load than rest plasma facing surface. In this model 5 °C sector is considered for wall mode locking simulation. The FW tiles in that 5 °C applied localised thermal loads and rest 25 °C is applied normal heat flux as shown in Figure 75. The simulation is carried out for 30 pulses, by applying normal pulse plasma heat load for first 29 pulses and last pulse with localised thermal loads.

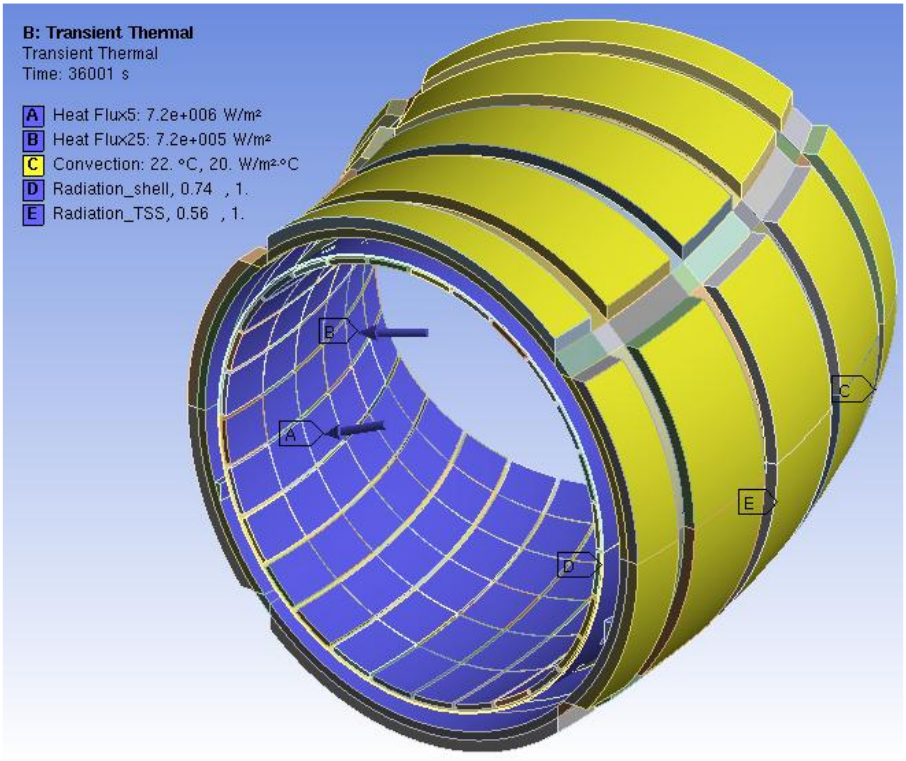

Figure 75: Thermal loads during plasma Wall-locking mode

5.2.5.1 Simulation results

A transient thermal analysis was carried out for this load combination. The results achieved from simulation are shown in Figure 76, Figure 77, Figure 78 and Figure 79 as temperature distribution contour in different components.

As shown in Figure 76, TSS attains maximum temperature of 56 °C and minimum temperature is 43 °C similar to case of normal RFP operation, highest temperature is in toroidal grooves for saddle coil at internal side. Supporting rings reaches 142 °C maximum during last pulse and gets 131 °C maximum after full day operation. Figure 78 shows temperature distribution in stabilizing shell in last pulse. The temperature is manly concentrated in shell below FW tiles receiving higher heat flux due to wall mode locking. In FW tiles temperature varies from 115 °C to 132 °C as shown in Figure 79.

Figure 80 and Figure 81 shows graph of maximum temperature w.r.t. time in all the components. The stabilizing shell receive high temperature pick in last pulse, pick

temperature is varying from 140 °C to 191 °C in last 2 pulse. The pick temperature attains by FW tiles is 523 °C in last pulse compared to 223 °C pulse before.

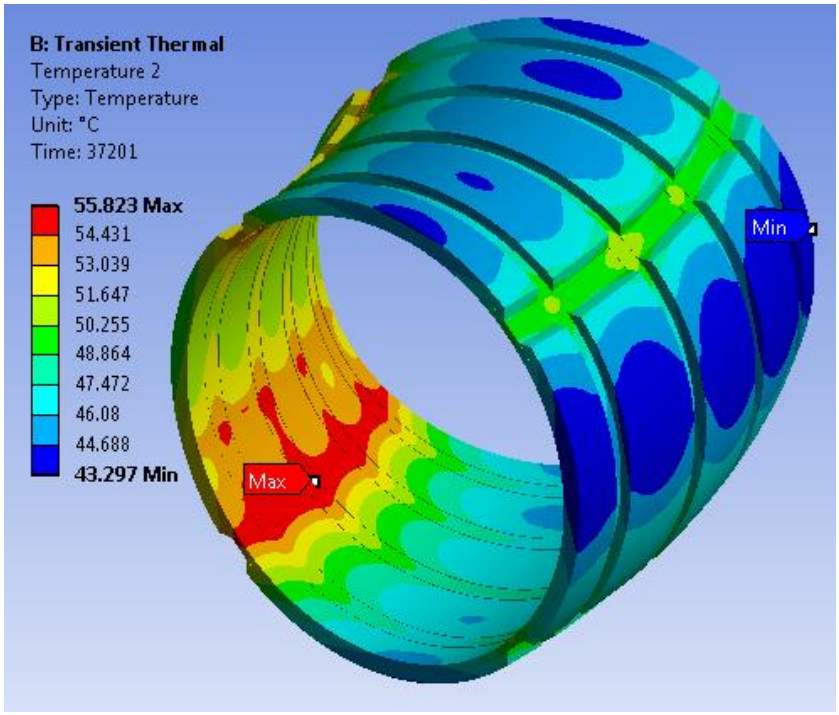

Figure 76: Temperature contour plot of TSS @37201 s (Max. = 56 °C, Min. = 43 °C)

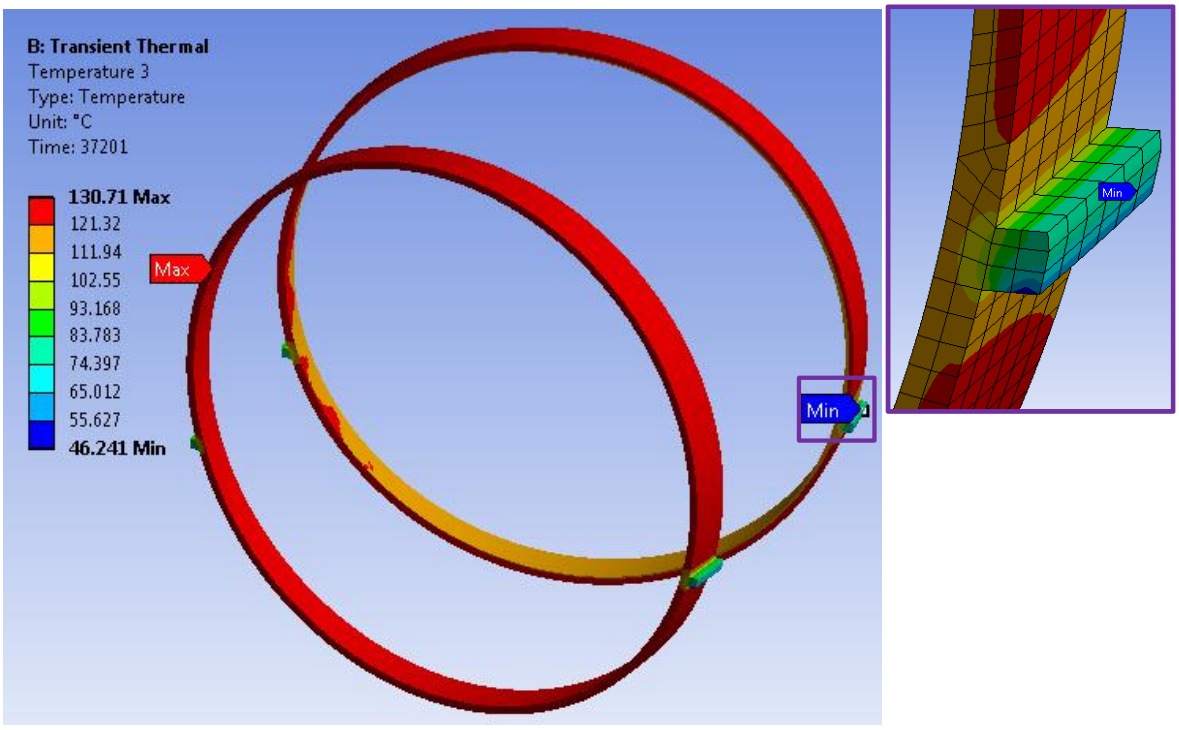

Figure 77: Temperature contour plot of supporting rings @ 37201 s (T_{max} = 131 °C, T_{min} = 46 °C)

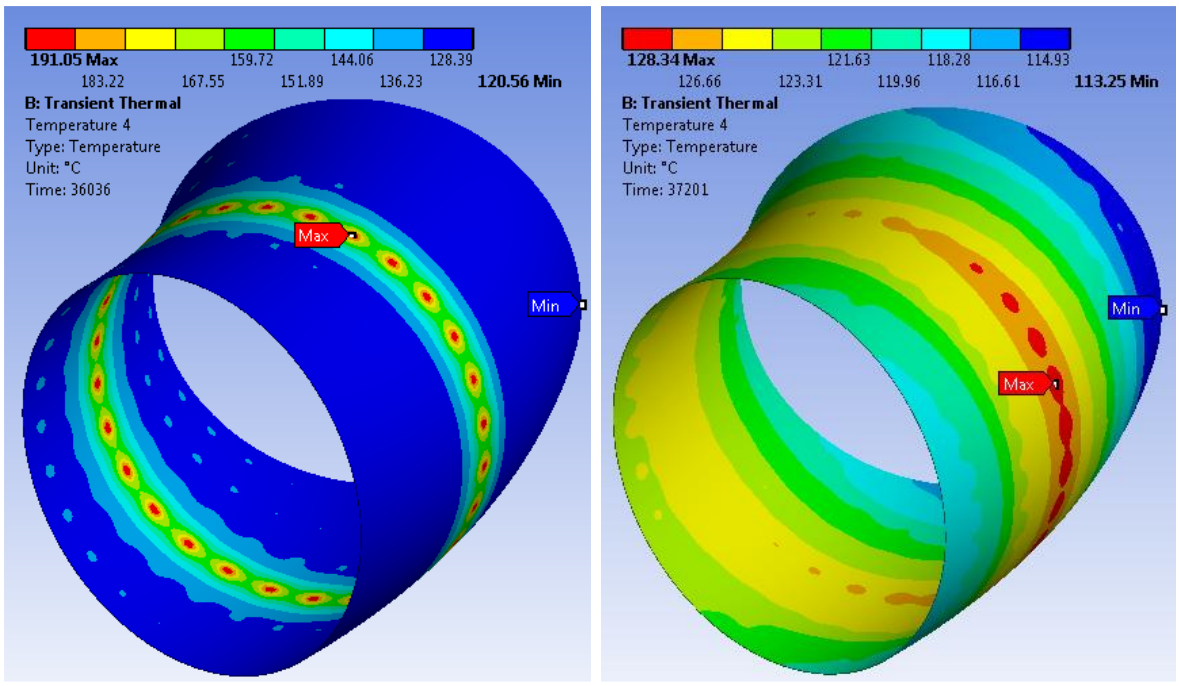

Figure 78: Temperature distribution in stabilizing shell (a) @ 36036 s 191 °C (b) @ 37201 s 128 °C

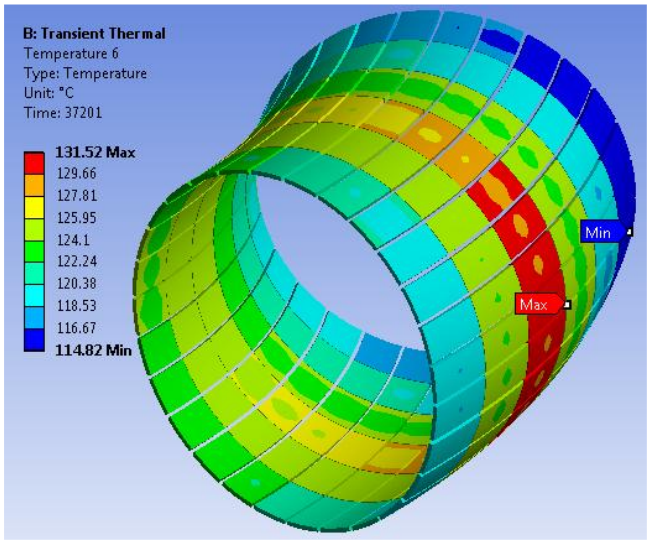

Figure 79: Temperature contour plot of FW tiles @ 37201 s (Max. = 132 °C, Min. = 115 °C)

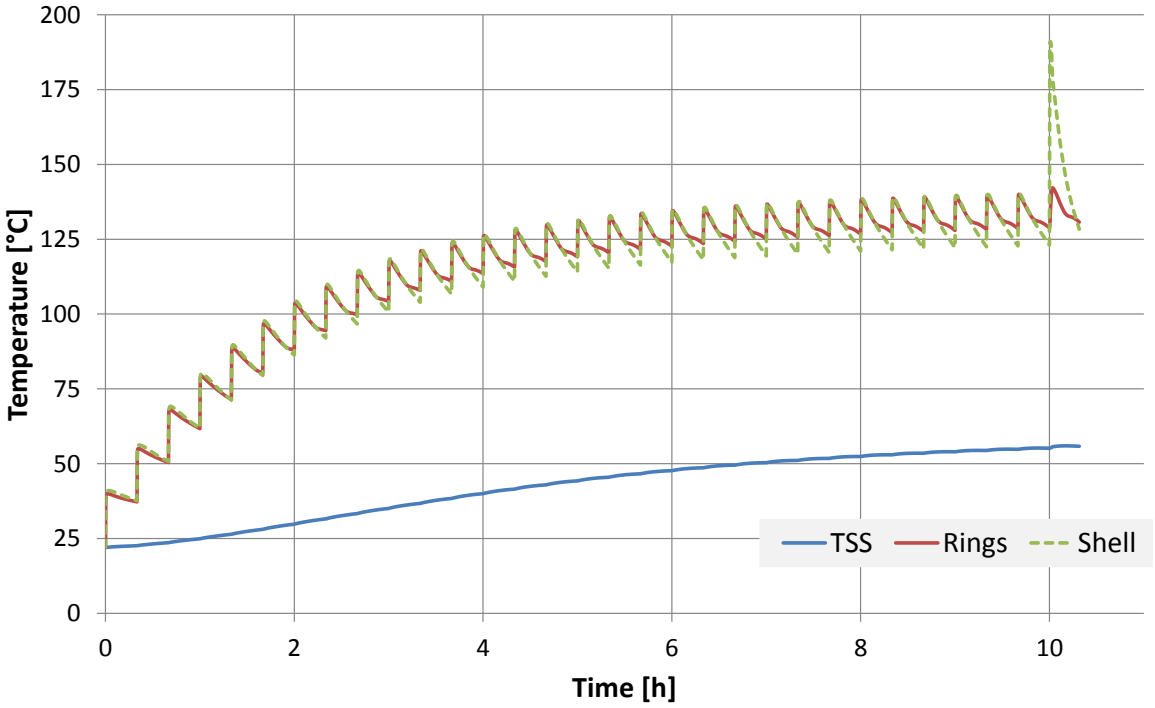

Figure 80: Graph of maximum temperature w.r.t. time in components

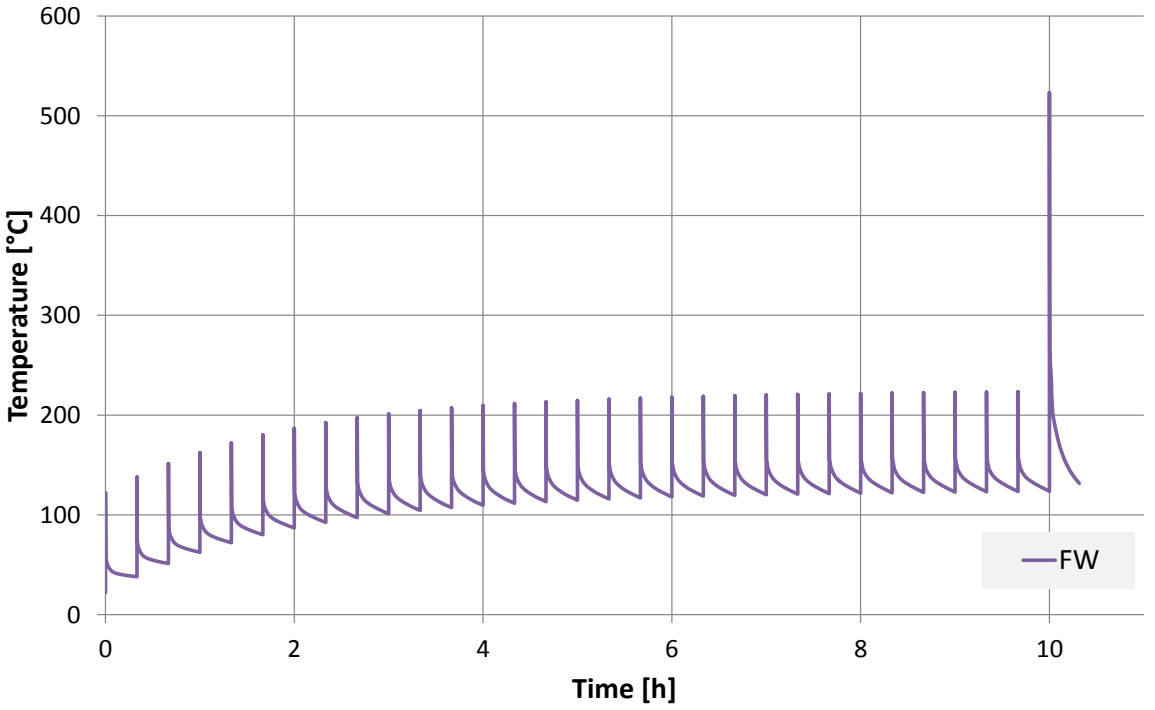

Figure 81: Graph of maximum temperature w.r.t. time in FW tiles

5.3 Conclusion

A set of analyses carried out to find thermal distribution in RFX-mod2 assembly. The results show that temperature difference between machine components for three different operating conditions. It demonstrates that the baking and GDC condition produces highest temperature in all the components. The major portion of heat is transferred through radiation between shell and TSS in all the cases.

The temperature limit for the components is from material, which are 2750 °C graphite (FW tiles), 204 °C for OFHC (stabilizing shell), 275 °C for Torlon® (Supporting rings), and 500 °C for AISI304L (TSS). The temperature values resulted for all components are within allowable values.

These results of temperature distribution in components will be used to calculate stresses and described in CHAPTER 6 and CHAPTER 7.

CHAPTER 6 THERMO-MECHANICAL ANALYSIS AND VERIFICATION OF THE PASSIVE STABILIZING SHELL ASSEMBLY

The chapter describes thermo-mechanical analyses of passive stabilizing shell assembly and the design iterations for supporting rings. Section 6.1, 6.2 and 6.3 illustrate analysis carried out for supporting rings to select proper material, number of rings and support geometry. Section 6.4 gives detail on results of thermo-mechanical analysis.

6.1 Study of the interfaces between stabilizing shell and TSS

In this section the study of the interfaces is described considering thermal loads and contact conditions at shell, rings and TSS.

6.1.1 Design conditions and parameters

The significant load combination considered for this study is baking as it produces the maximum thermal deformations and it requires proper materials supporting the maximum expected temperature. The material properties addressed the study as the Coefficient of thermal expansion (CTE) determines the stress condition at contacts and maximum stresses and strains have to be verified.

Two preliminary analyses have been carried out for the shell interfaced with rings: a first one with fully free thermal expansion of the stabilizing shell, and second analysis simulating fixed position of the rings with respect to the TSS.

The first model has been preferred as the poloidal location of sensors mounted between tiles and shell will remain constant during baking and also with any thermal load applied during pulse operation. The identification of this solution will imply a proper development of a sliding interface between shell and TSS due to relative thermal displacements as detailed in section 1.3.

The baking loading combination is considered for the selection of the better constraining condition considering the interface of the shell with TSS through the support rings. Indeed, large thermal deformations are produced by this loading condition and free thermal expansion with minimum thermal stresses is considered the parameter of the optimization to be minimized.

6.1.1.1 Boundary conditions

The baking loading condition consists of:

- Thermal condition of 180 °C is applied on shell and ring bodies.
- Equivalent force (F=1000 N) of weight of tiles and keys is applied.
- Standard earth gravity is applied to all components.
- Toroidal symmetry of shell is applied by in-plane displacement.
- Shell and Rings connected with bonded contacts

Baking condition represents the first Load combination required for the analysis and verification of the shell as detailed in the component verification Table 17.

The reference systems used to constrain the parts of the model by blocking the degrees of freedom are cylindrical coordinate systems with X as radial dimension, Y as tangential, and Z as vertical.

6.1.1.2 Material properties

Followings are the material properties considered for the material selection of supporting rings. Main material properties affect are CTE, temperature limit and stress limit of the material, which are as descried in following:

Table 19 List of material properties to select for supporting ring [52]

Property	**Investigated ring material**					**Shell**
	PEEK	**VESPEL**	**PTFE**	**TORLON 5030**	**SS304L**	**OFHC (C10200)**
Glass transition temp. (Tg) *(°C)*	**143**	-	-	275	-	
Melting temp. (Tm) *(°C)*	350	400	327		1400	
Density *(kg/m3)*	1320	1430	2160	1610	7900	8900
Youngs modulus *(GPa)*	3.6	2.4	0.5	14.5	195	117
Poisson's ratio	0.38	0.41	0.46	0.43	0.3	0.31
CTE *(µm/m/k)*	13	**54**	**112**	**16.2**	**15.3**	**16.7**
Specific heat *(J/kg * K)*	1700	1130	1200	1369	483	385
Thermal conductivity *(W/m * K)*	0.25	0.35	0.3	0.36	14.87	391

6.1.1.3 Preliminary analysis simulating free thermal expansion of shell

The free thermal expansion of shell is analysed to investigate the shell behaviour under baking condition with maximum shell displacement with respect to the TSS. Shell is considered in two halves with 20 mm gap in between and there geometrical constraint of no vertical displacement is applied on areas of gap.

A static structural analysis carried, following results show that shell is expanding on its major axis up to 7 mm and 1.5 mm on its minor axis. There is no stress generated in shell.

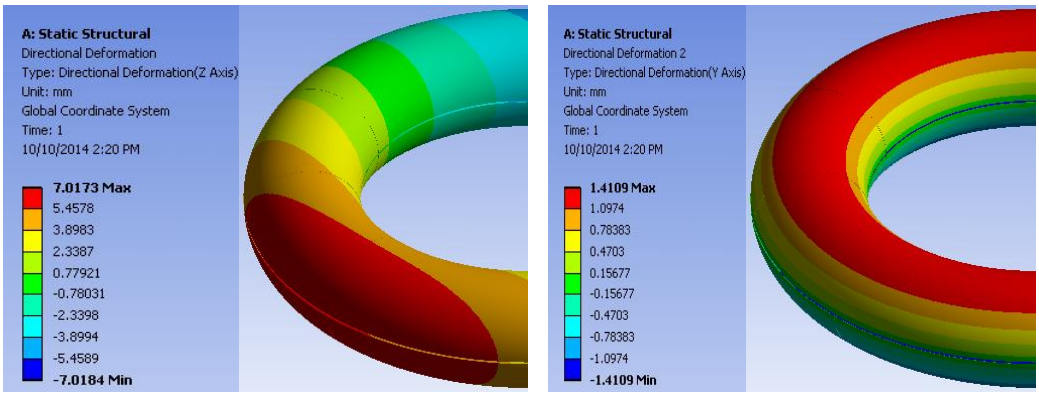

B. Horizontal displacement Max. = 7.01 mm

C. Vertical displacement Max. = 1.41 mm

Figure 82: Results of preliminary analysis of free expansion of shell

6.1.1.4 Preliminary analysis simulating rings constraining the shell shape

A simple structural analysis is carried out to check deformation of shell structure considering temperature ramp up in stabilizing shell to 180°C. Also to calculate induced stresses due to applied boundary conditions to maintain circular c/s of torus.

The model contains top and bottom toroidal shell with 20 mm gap between considering RFX-mod stabilizing shell configuration. There are 10 toroidal support ring included to maintain shape of shell. Frictionless sliding contact applied between shell and support. Also frictionless contacts applied between surfaces of shell in gap. Stainless steel material property is applied to the rings. Ring are supposed to remain at room temperature and at fixed location at the outer diameter.

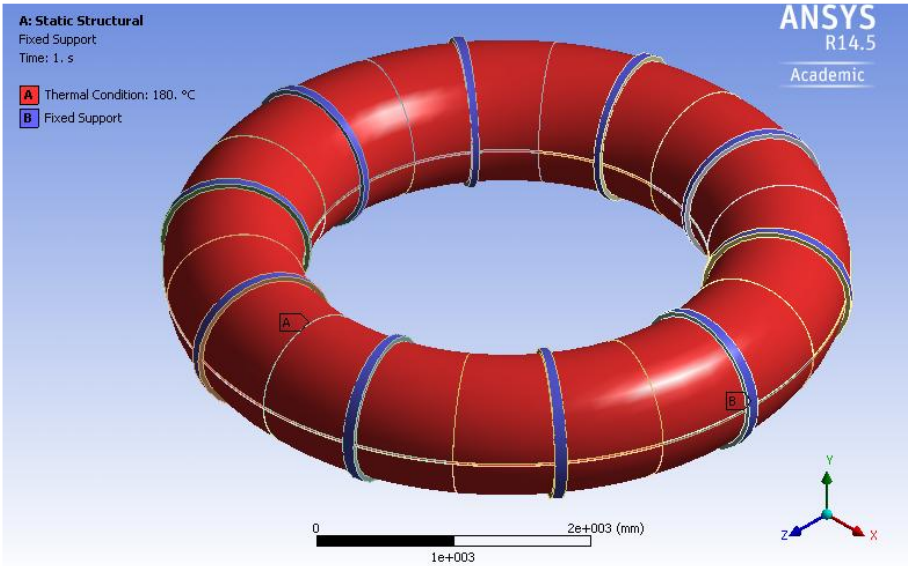

Figure 83: Boundary conditions applied

Followings are the results of FEA thermo-mechanical analysis,

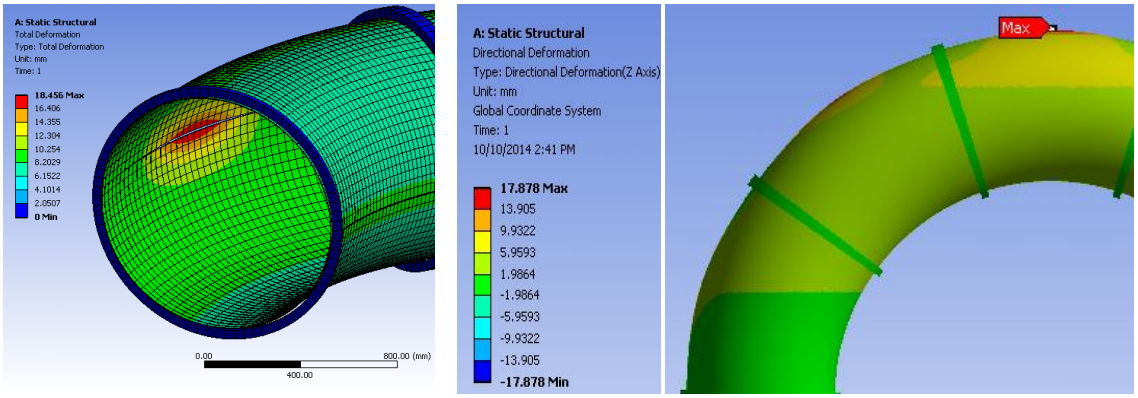

A. Total displacement Max. = 18.45

B. Radial displacement Max. = 17.87 mm

C. V

Figure 84: Displacement of shell under temperature raise

Due to increase in temperature of shell, it deforms and top and bottom shell touches each other. Results show that maximum deformation of 18.45 mm is at external equatorial location between two supports. At this location shell tries to get apart and make bulge in shape.

Following Figure 85 shows induced stresses in the stabilizing shell due to restriction on deformation. Maximum stress of 123 MPa induced in elements below supports where top and bottom shell meets. Results show that while maintaining the circular section under thermal deformation, the stabilizing shell closes the gap and touch which produce high local contact stress.

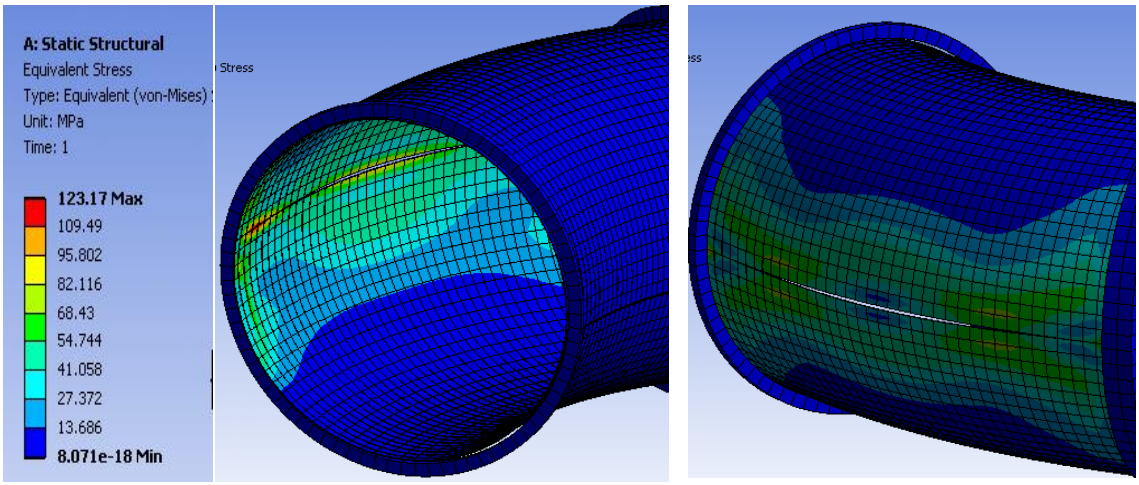

Equivalent stresses
Max. = 123.1 MPa

Figure 85: Induced stresses in shell

6.2 Selection of ring material and number

The selection of the proper material and number of rings surrounding shell are decided by series of analysis. The design has been addressed considering material limits like coefficient of thermal expansion (CTE) and stresses to follow the thermal deformation of the shell.

The model contains top and bottom stabilizing shell with 20 mm gap between considering RFX-mod stabilizing shell configuration. First 3 analyses are carried out with 24 rings surrounding to the shell and last analysis carried out with 12 rings surrounding to shell. Supporting rings have the top and bottom stud for supports as shown in Figure 86.

Frictional contact applied between shell and support and between shell gaps, with frictional coefficient of 0.2. The model contains 69866 elements and 396692 nodes.

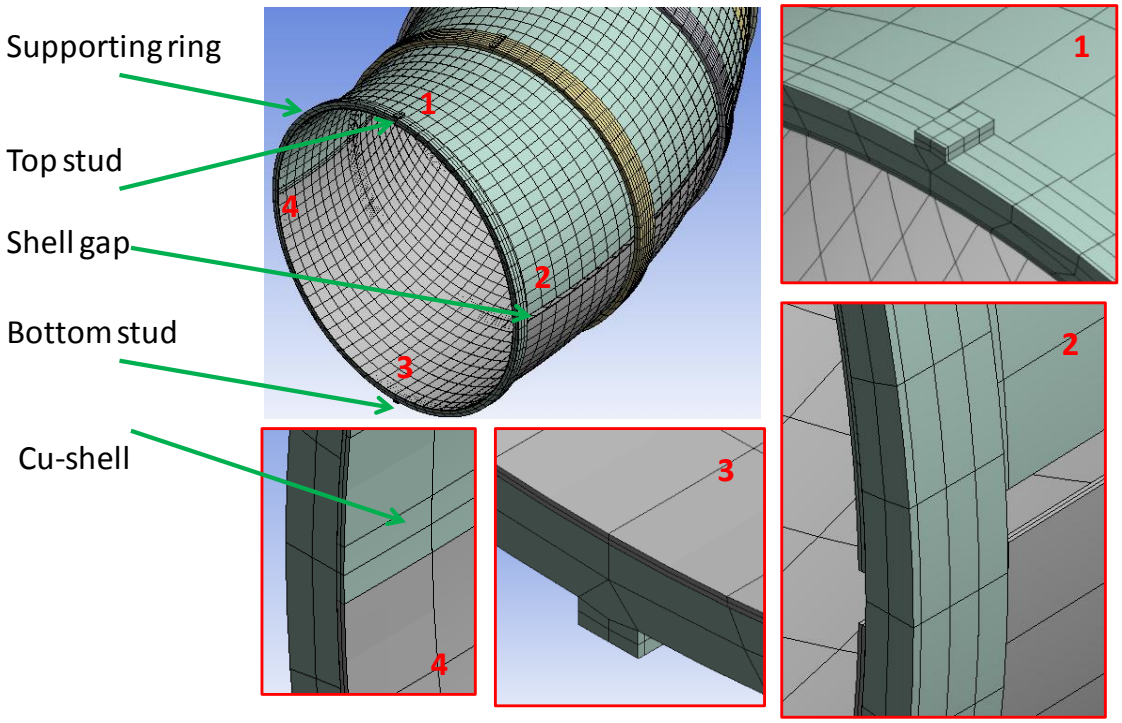

Figure 86 Model for material selection

The selection of material and number of rings is undertaken by applying the same constraints on different models. Baking load condition applied to the shell and rings. The ring is constrained by following conditions,

Ring top Stud: X=0, Y, Z=Free

Ring bottom Stud: X, Z=0, Y=Free

The reference systems used to constrain the parts of the model by blocking the degrees of freedom are cylindrical coordinate systems with X as radial dimension, Y as tangential, and Z as vertical.

Simulation are carried out for following cases,

Table 20 List of cases for material and number of rings selection

Sr. #	Problem Description	Results
1.1	shell: one 20mm gap on ext. side 2-support, 24 Rings **(SS304L)**	Ring: Dmax=3.65mm, Smax=832MPa Shell: Dmax=12.85mm, Smax=137 MPa
1.2	shell: one 20mm gap on ext. side 2-support, 24 Rings **(VESPEL)**	Ring: Dmax=7.29mm, Smax=37.9MPa Shell: Dmax=7.35mm, Smax=3.9MPa
1.3	shell: one 20mm gap on ext. side 2-support, 24 Rings **(TORLON 5030)**	Ring: Dmax=5.6mm, Smax=70.5MPa Shell: Dmax=10.5mm, Smax=52 MPa
1.4	shell: one 20mm gap on ext. side **2-support, 12 Rings** (TORLON 5030)	Ring: Dmax=4.7mm, Smax=70.2MPa Shell: Dmax=10.7mm, Smax=33.5 MPa

Results of above cases are shown in Table 21, Table 22, Table 23 and Table 24.

The results show that, in case 1.1 stresses are very high due to thermal expansion of shell is restricted by rings. In case 1.2, it shows detachment between shell and rings at inner equatorial side due to CTE of VESPEL is higher than CTE of OFHC. Considering that results, analysis does not carried out with PTFE material as it has very high CTE. The PEEK material option is strike out as it has low glass transition temperature than required condition of baking. Results of 3rd case show optimistic behavior of shell and ring assembly. The TORLON® 5030 has CTE very near and lowers than OFHC. It has higher thermal limit also and good material properties also. Hence TORLON® 5030 is selected as ring material to carry out further geometrical design of supporting rings.

The 4th analysis is carried out considering similar condition of case-3 with only 12 rings surrounding to stabilizing shell. The results show a bulging of shell between two rings. Hence 24 rings surrounding to shell shows better supporting condition for shell, which is same number as radial support used for VV in present configuration of RFX-mod.

Table 21 Results of case # 1.1

Displacement [mm]	**Shell: Dmax=12.85mm Ring: Dmax=3.65mm**

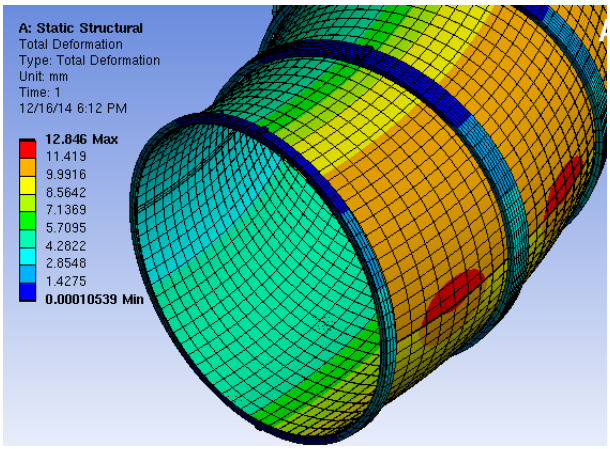

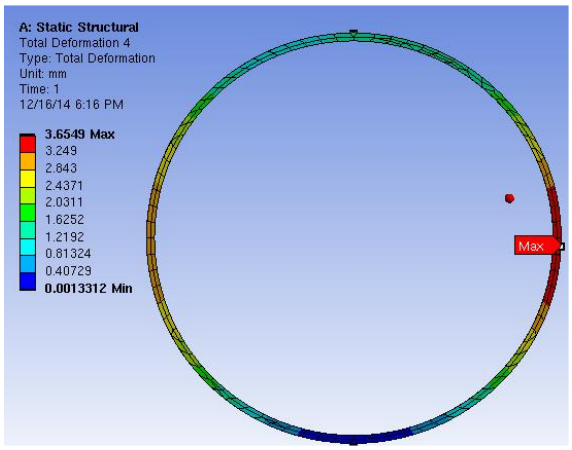

Equivalent stress [MPa]	**Shell: Smax=137 MPa Ring: Smax=832 MPa**

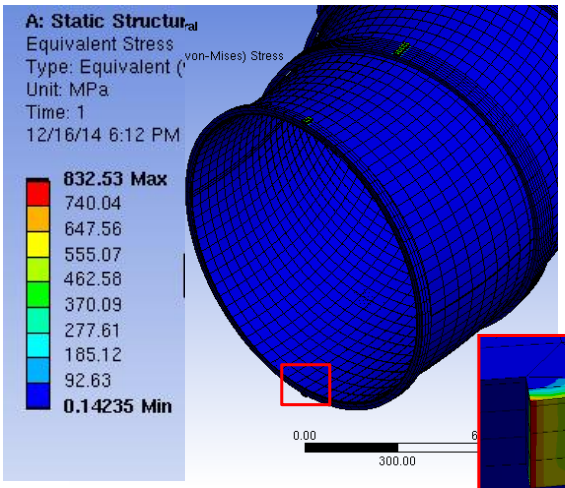

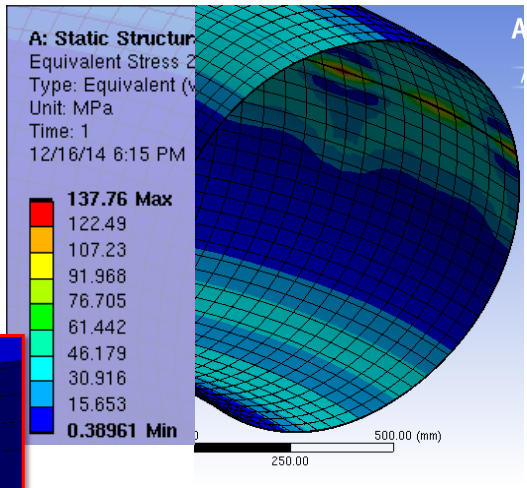

Contact status

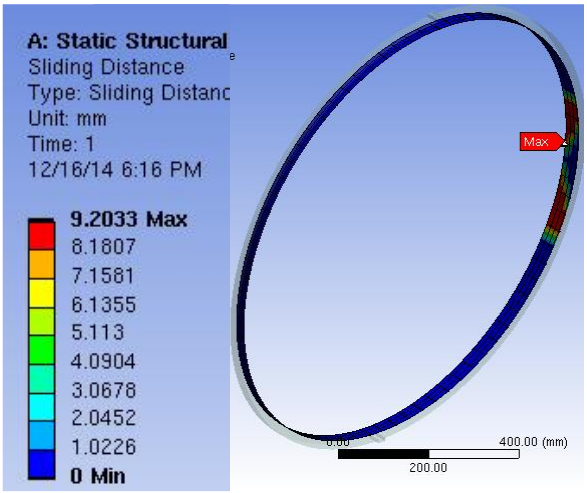

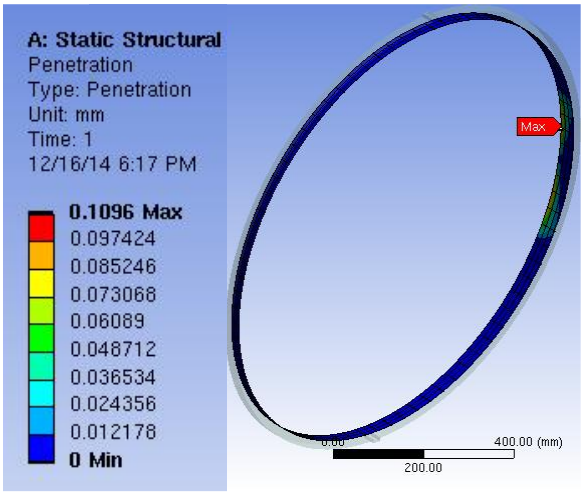

Table 22 Results of case # 1.2

Displacement [mm]	**Shell: Dmax=7.35mm Ring: Dmax=7.29mm**
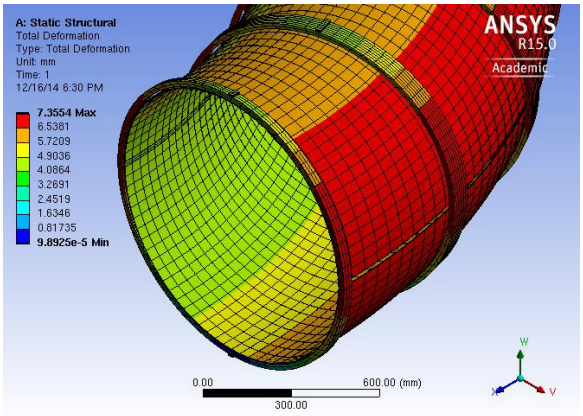	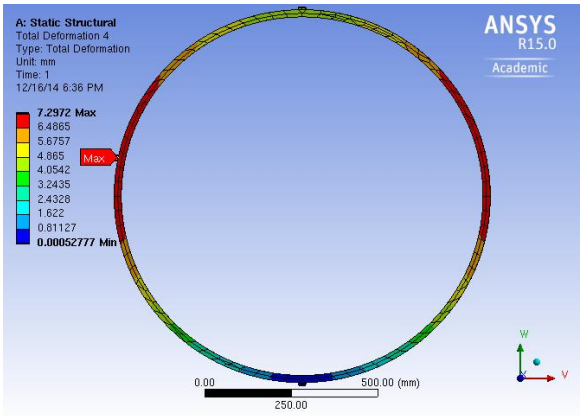
Equivalent stress [MPa]	**Shell: Smax=3.9 MPa Ring: Smax=37.9 MPa**
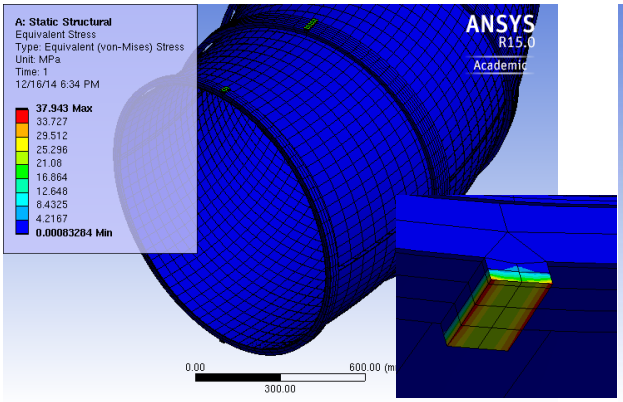	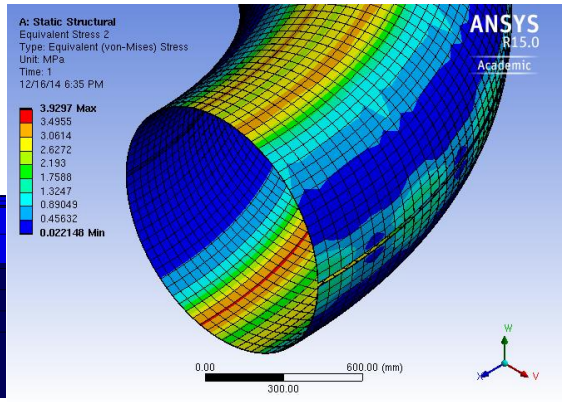
Contact status	
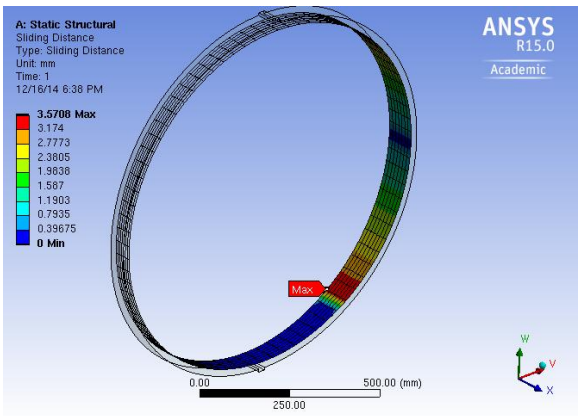	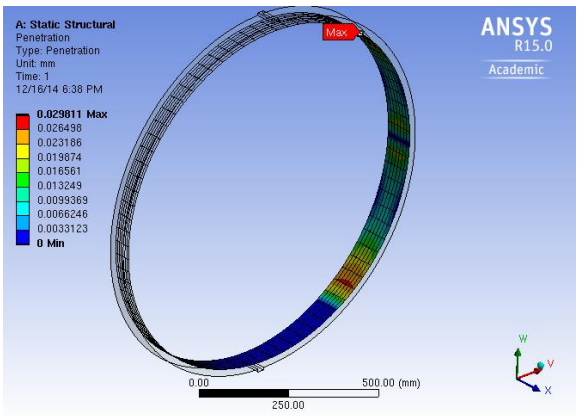

Table 23 Results of case # 1.3

Displacement [mm]	**Shell: Dmax=10.5mm Ring: Dmax=5.6mm**

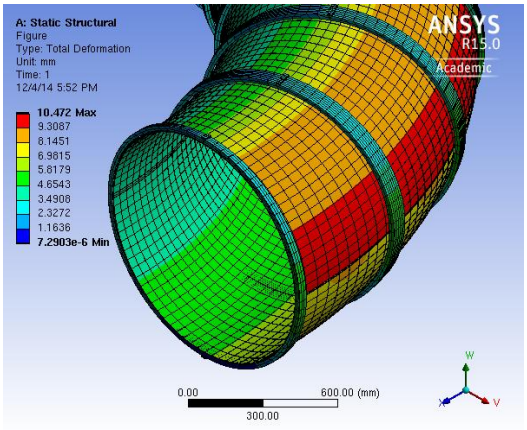

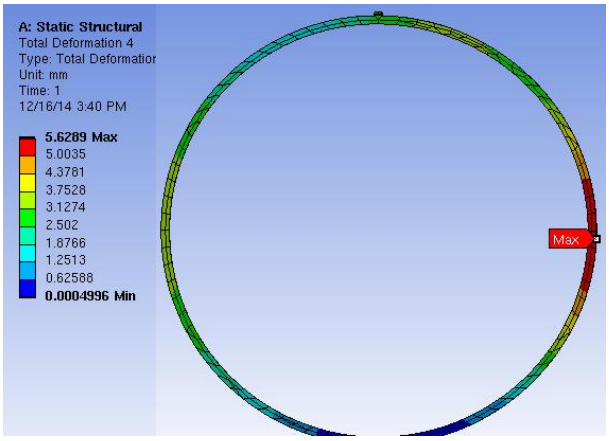

Equivalent stress [MPa]	**Shell: Smax=52 MPa Ring: Smax=70.5MPa**

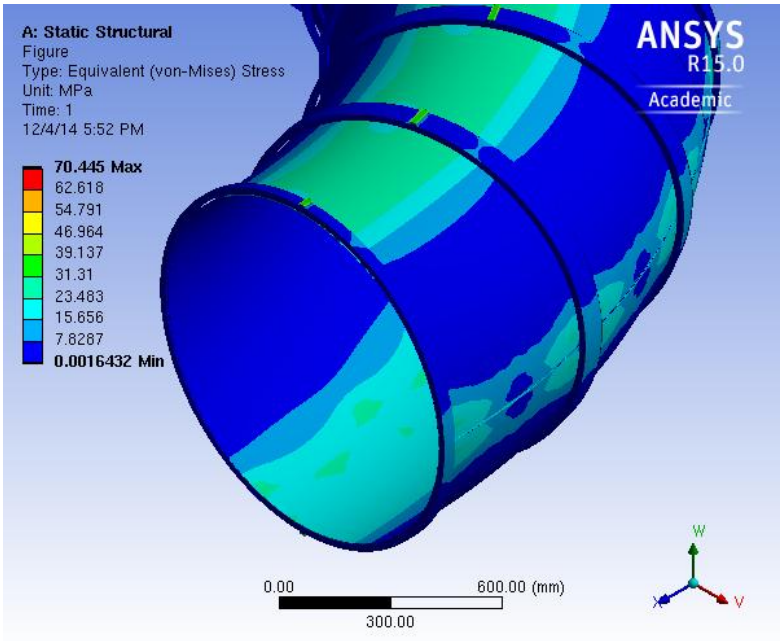

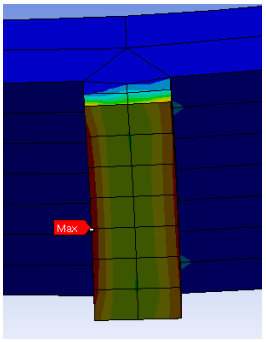

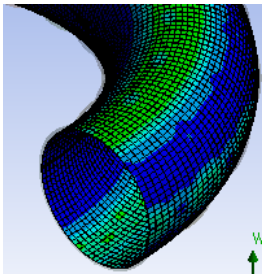

Contact status

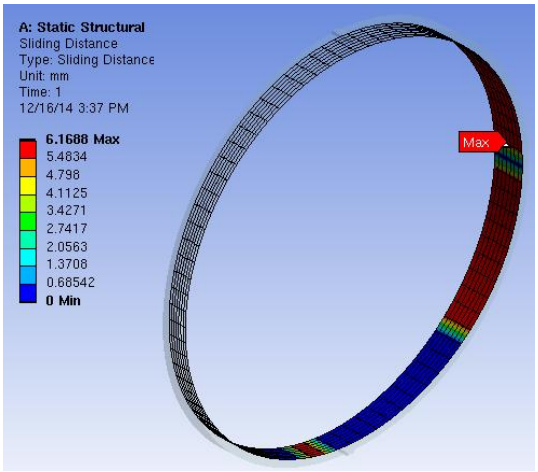

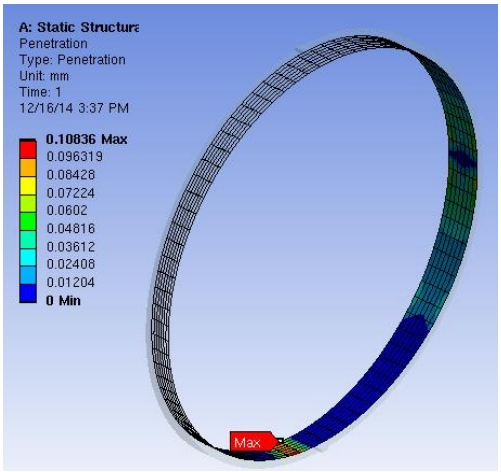

Table 24 Results of case # 1.4

Displacement [mm]	**Shell: Dmax=10.7mm Ring: Dmax=4.7mm**
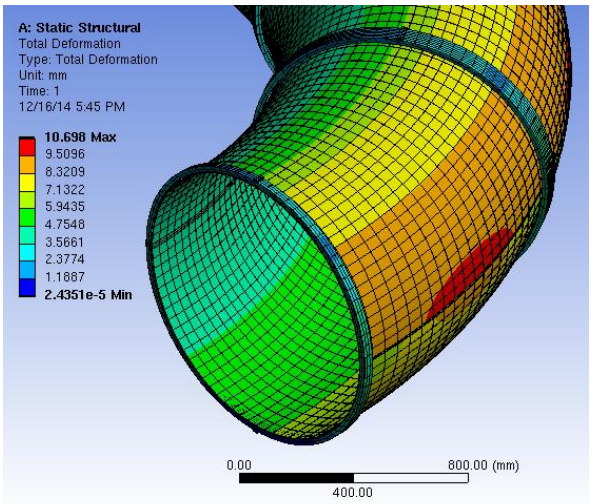	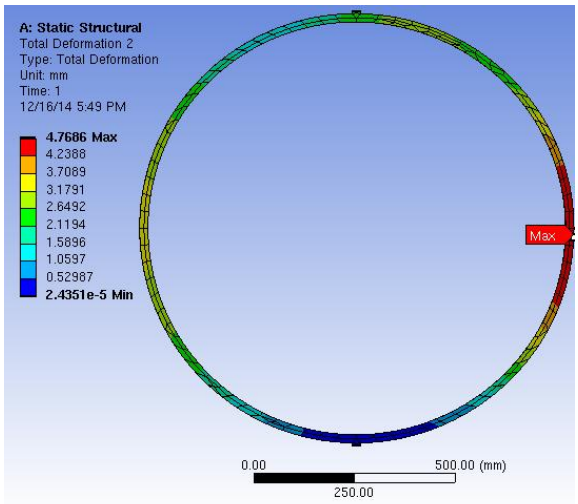
Equivalent stress [MPa]	**Shell: Smax=33.5 MPa Ring: Smax=70.2MPa**
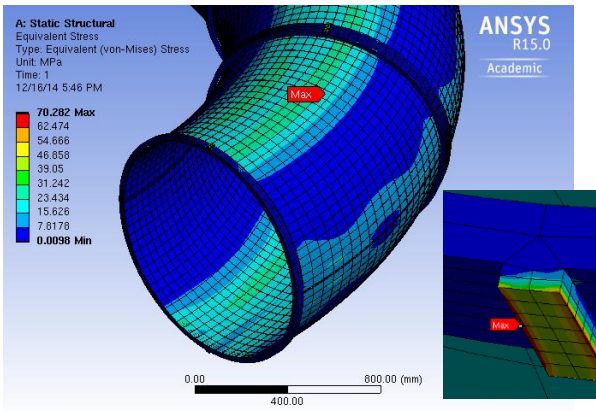	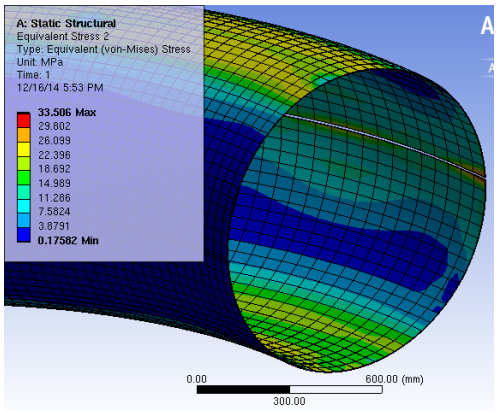
Contact status	
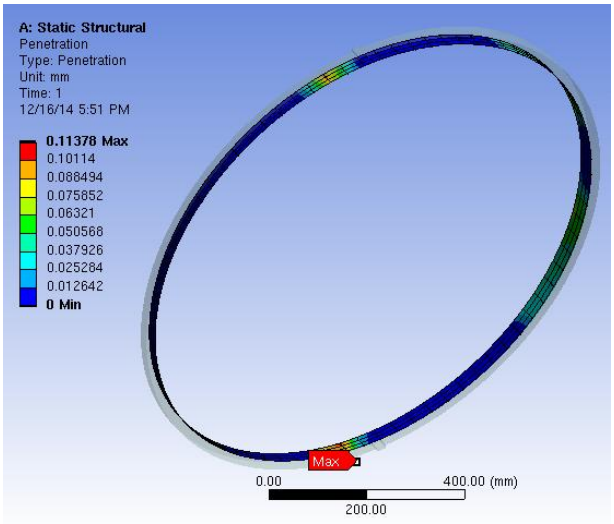	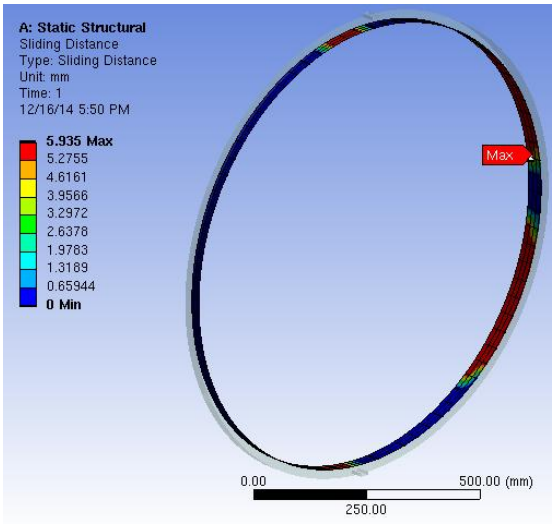

6.3 Development of the interface of rings with shell and TSS

In this section the geometrical design of supporting rings is analysed. Interface between rings and TSS is studied considering some concepts of the geometry with different number of contact points. The interface between rings and shell has been analysed considering sliding or fixed contact.

Major radius of stabilizing shell and TSS are 1995 mm and 2000 mm respectively (see Figure 87). So, gap between shell and TSS is varying from 33 mm at inner side to 43 mm at external side on poloidal section.

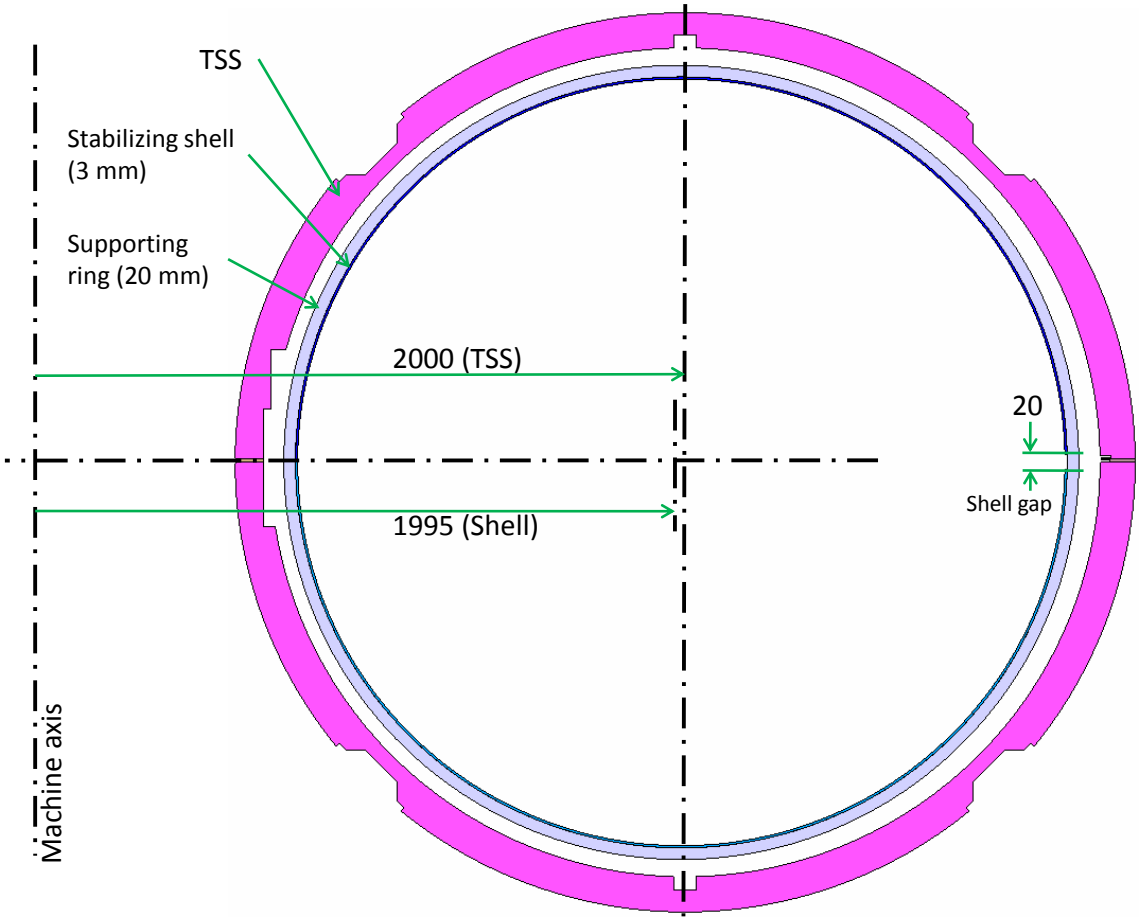

Figure 87: Sectional view of TSS, stabilizing shell and supporting ring

The analyses are carried out to evaluate concepts of supporting rings for passive stabilizing shell. The analysis carried out using 30 degree model. It consist 2 supporting rings per sector (Total 24 rings on full torus). The supporting rings are considered 20 mm thick radially and extended 1° toroidally.

Baking load condition (180° C) applied to the shell and rings. The ring is constrained by different conditions inside TSS. TSS is modelled to provide proper constraints to supporting rings, and TSS is fixed fully from outer surface. Also equivalent force of tile weight is applied at inner surface of stabilizing shell.

Table 25 shows list of four different cases studied considering shape of supporting rings and stabilizing shell interface. The table also shows maximum values of investigated parameters for all the cases.

Table 25 List of cases for geometrical design of supporting rings

Sr. #	Problem Description	Results
2.1	Shell with 20 mm gap, Sliding contacts 3-support: 1 top rail type, 2-bottom sliding in TSS	Ring: Dmax=10.4mm, Smax=2.6 MPa Shell: Dmax=8.8mm, Smax=8.8 MPa
2.2	Full shell 3-support: 1 top rail type, 2 bottom sliding in TSS	Ring: Dmax=9.83mm, Smax=253 MPa Shell: Dmax=9.83mm, Smax=221 MPa
2.3	Full shell Only 2 bottom sliding in TSS	Ring: Dmax=10.07mm, Smax=12.4 MPa Shell: Dmax=10.03mm, Smax=29 MPa
2.4	Full shell 2 radial sliding support (DY=0)	Ring: Dmax=7.07mm, Smax=3.9 MPa Shell: Dmax=7.06mm, Smax=15 MPa

6.3.1 Concept 2.1: Supporting rings with 1 top stud and 2 bottom sliding studs

This concept of supporting rings is having 3 studs poloidally. One top stud is with rail configuration and 2 bottom studs are having sliding configuration at inner surface of TSS. There is 60° symmetric angle between bottom sliding studs. All Contacts between shell, rings and TSS are considered frictional sliding contacts. For this simulation shell is considered with 20 mm gap at its external equatorial section.

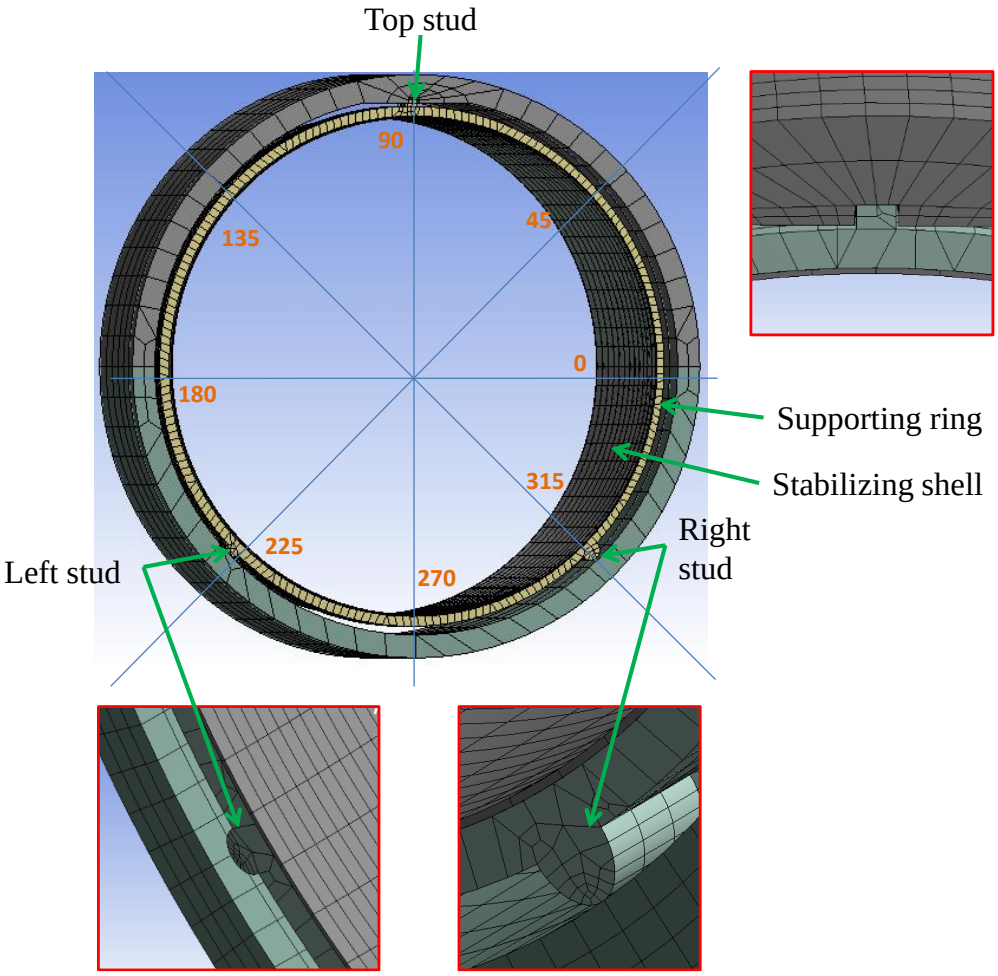

Figure 88: Model for concept 2.1

Results of simulation shows that,

- Maximum total displacement is 10.4 mm in right bottom stud of ring which slides in TSS
- Due to gap in shell it slides on rings and gap reduced to 16 mm from 20 mm
- At inner poloidal section contact between shell and ring released by 2mm
- Top stud move vertically 5 mm and touch to TSS and left stud loose contact with TSS
- This configuration is shows very less stress values, Shell shows maximum stress of 9 MPa and supporting rings shows maximum stress of 3 MPa

Table 26 Results of concept 2.1

Displacement	**Shell: Dmax=8.8 mm Ring: Dmax=10.4 mm**

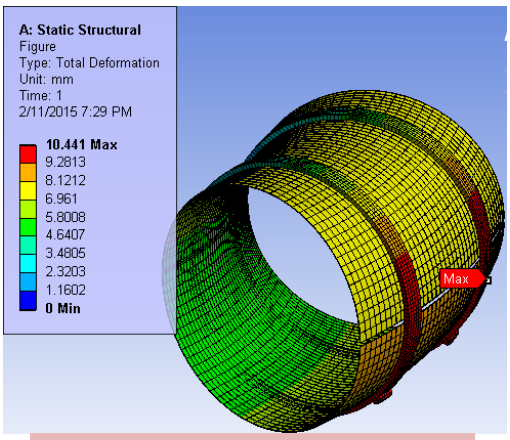

Total Displacement

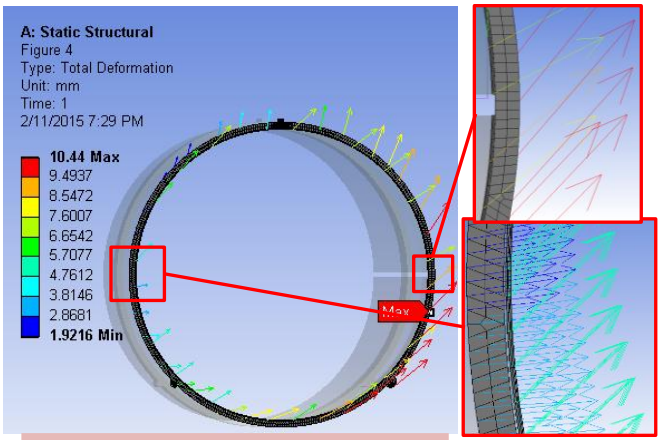

Total Displacement - directional

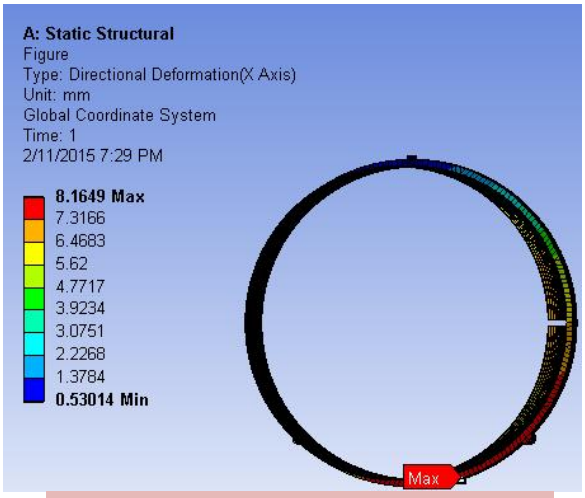

Radial Displacement

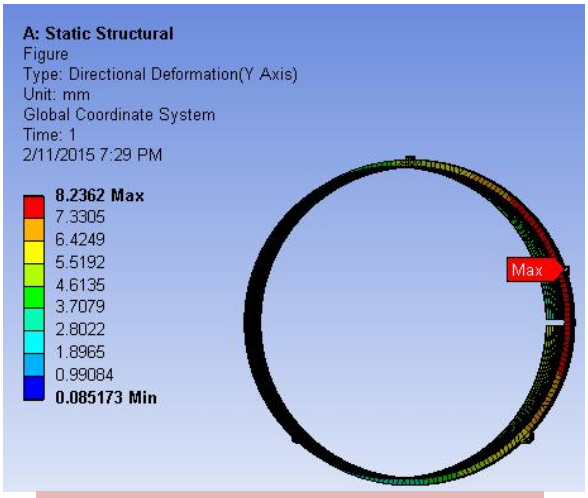

Vertical Displacement

Equivalent stress	**Shell: Smax=8.8 MPa Ring: Smax=2.6 MPa**

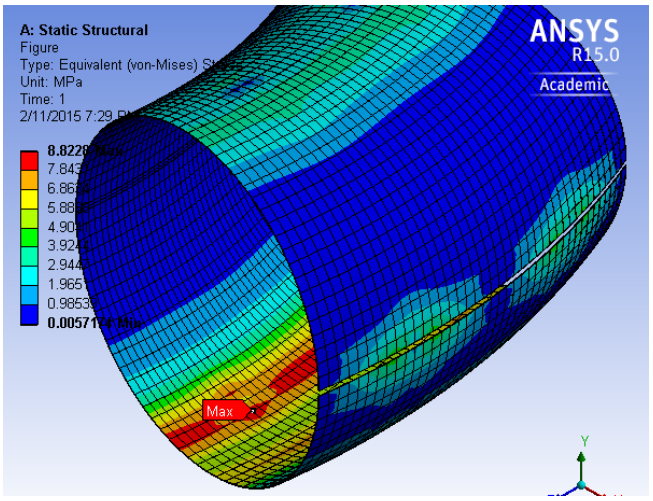

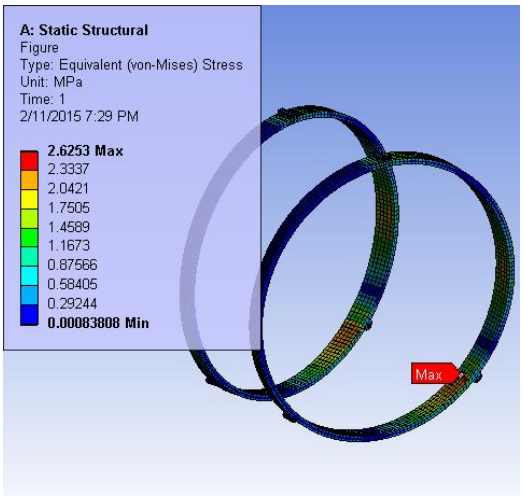

6.3.2 Concept 2.2: Supporting rings with 1 top stud and 2 bottom sliding studs with full shell

This simulation is carried out with same configuration as 2.1 but considering full stabilizing shell without any gap. Contacts between shell and rings are considered bonded. Contacts between rings and TSS are considered frictional sliding contacts.

The results show that,

- Maximum displacement is 9.8mm at 45° of poloidal angle, which is similar for shell and rings as they are in bonded condition.
- Maximum radial displacement of 7mm is near external equatorial surface and max. vertical disp. of 7mm is at 45° poloidal angle due to sliding of rings in TSS
- This configuration is producing very high stresses
- Maximum stress of 253 MPa is in top studs of rings due to it prevent radial displacement. Result shows penetration of contacts of 0.5 mm at this location. Due to this it produce stresses in top edge of stud instead middle of stud where it meets edge of TSS.
- Shell shows maximum stress of 221 MPa exactly at location below studs. Another high stress location in shell is portion in contact with left bottom stud.

Table 27 Results of concept 2.2

Displacement	**Shell: Dmax=9.83 mm Ring: Dmax=9.83 mm**

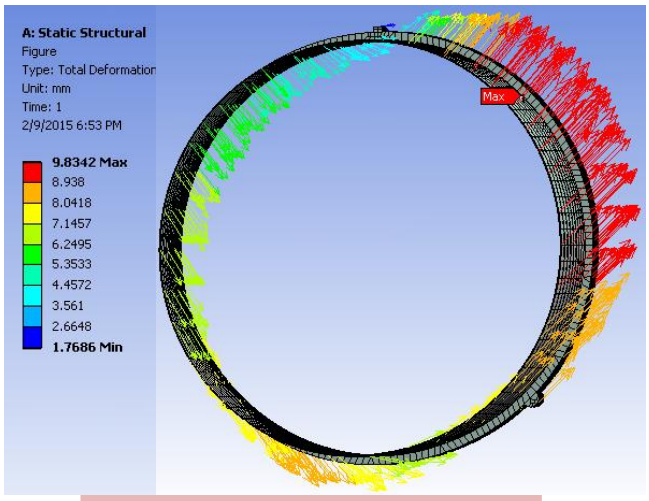

Total Displacement - directional

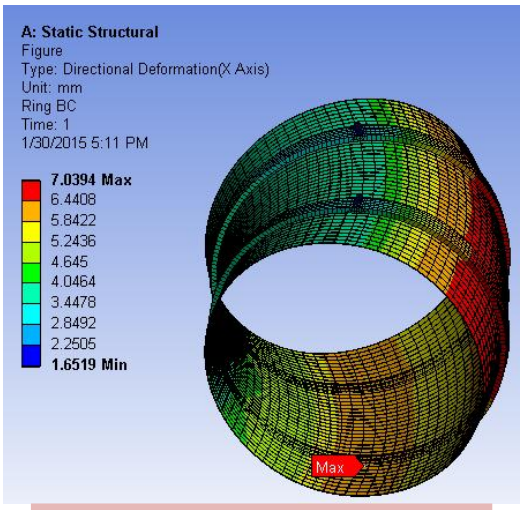

Radial Displacement

Equivalent stress	**Shell: Smax=221 MPa Ring: Smax=253 MPa**

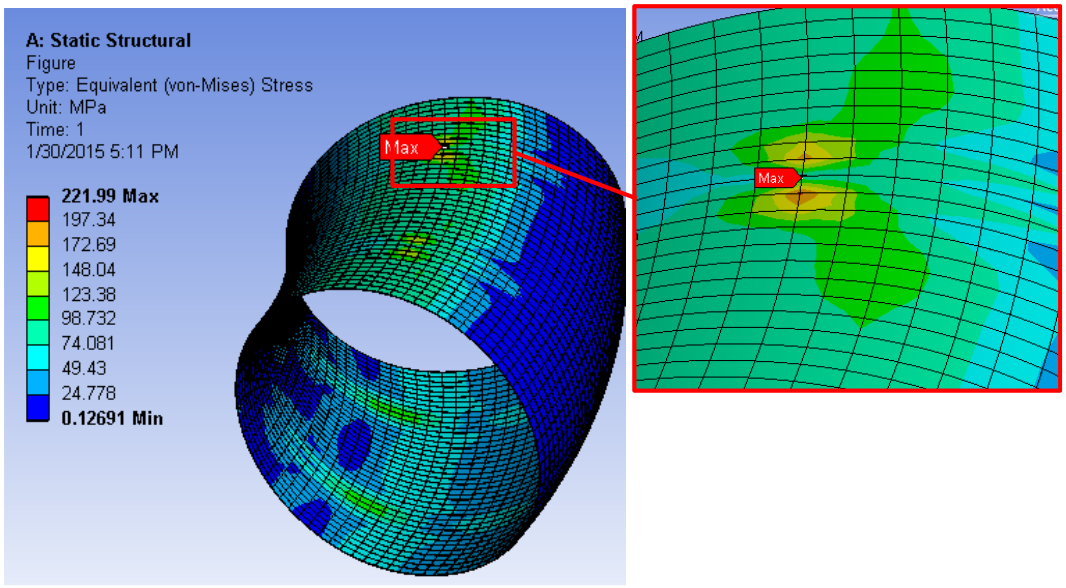

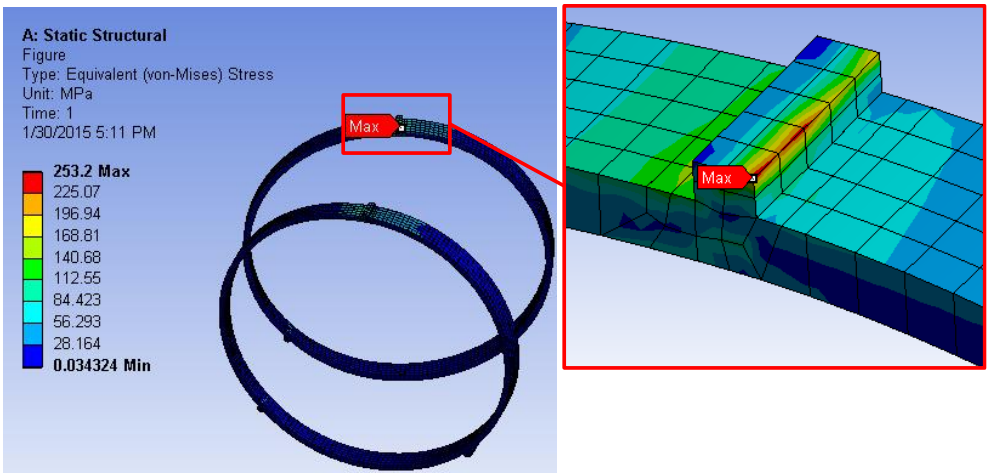

6.3.3 Concept 2.3: Supporting rings with only 2 bottom sliding studs - Full shell

This simulation is with same configuration as 2.3 but without considering top stud of supporting rings. Contacts between shell and rings are considered bonded, and between rings and TSS are considered frictional sliding contacts.

Results of analysis shows that,

- Maximum displacement is 10mm at 45° of poloidal angle, which is similar for shell and rings as they are in bonded condition.
- Maximum radial disp. of 6.8mm is near external equatorial surface and max. vertical disp. of 7.6mm is at 45° poloidal angle due to sliding of rings in TSS
- This configuration is shows less stresses as radial displacement here made free by removing top stud, Stabilizing shell shows maximum stress of 29 MPa near to locations below studs and rings shows max. stress of 12 MPa

Table 28 Results of concept 2.3

Displacement	**Shell: Dmax=10.03mm Ring: Dmax=10.07mm**

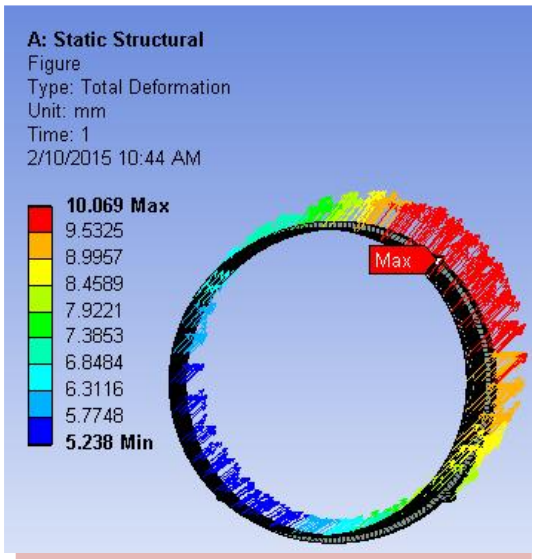

Total Displacement - directional

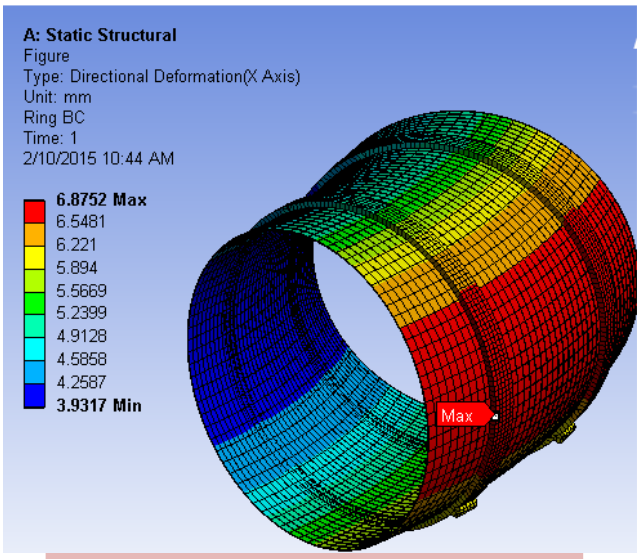

Radial Displacement

Equivalent stress	**Shell: Smax=29 MPa Ring: Smax=12.34 MPa**

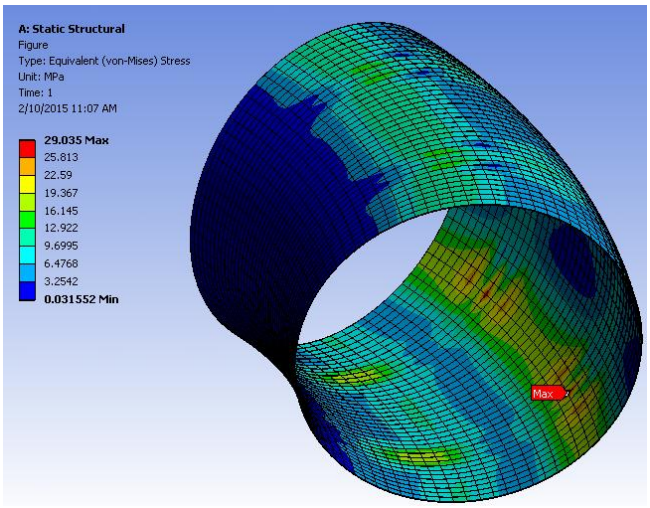

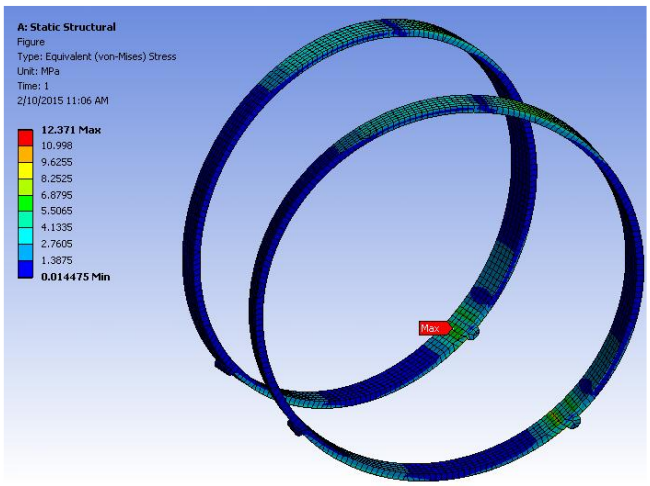

6.3.4 Concept 2.4: Supporting rings with radial sliding support and full shell

In this concept of supporting rings, it is provided with 2 radial studs at inner and external side 150 mm below equatorial plane as shown in Figure 89. Length of sliding edge of support stud is 12.5 mm. TSS geometry is not considered in this concept. Bonded contacts condition applied between shell and rings.

Bottom surface of radial studs are fixed for vertical movement and free for radial displacement.

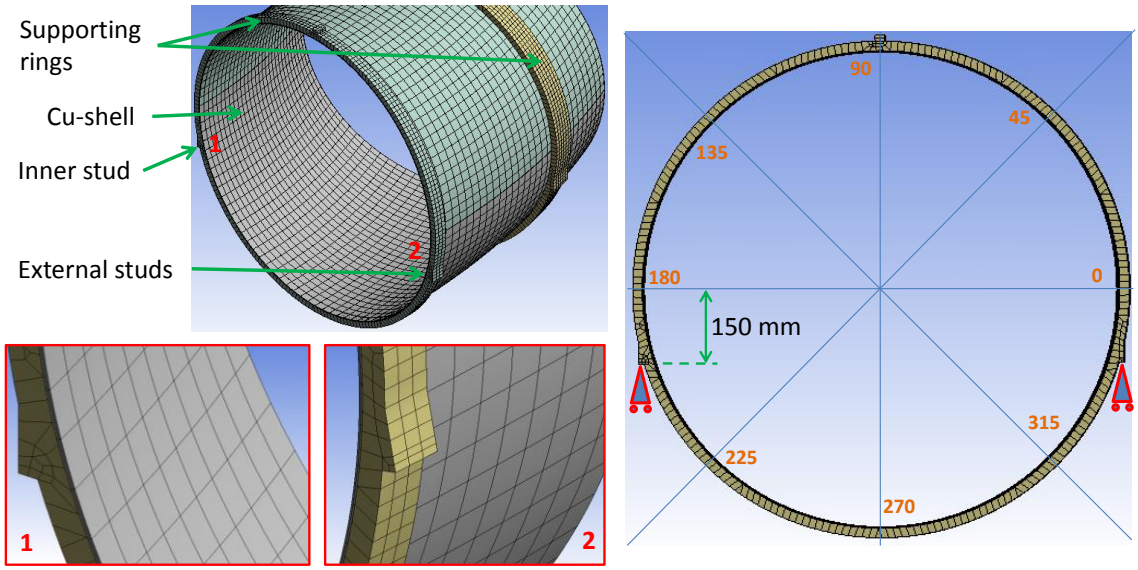

Figure 89: Details of model for concept 2.4

Results of the analysis shows that,

- Max. displacement is 7mm at 0° of poloidal angle
- Major contribution of displacement is from radial disp. with 6.7mm
- Vertical disp. of 1.8mm is at 90° poloidal angle
- Stresses are the lowest in this configuration compared to all above. This configuration is shows distributed values of results along poloidal section. There is not big variation in values from node to node.
- Shell shows maximum stress of 15 MPa and rings show 4 MPa

Table 29 Results of concept 2.4

Displacement	**Shell: Dmax=7.06 mm Ring: Dmax=7.079 mm**

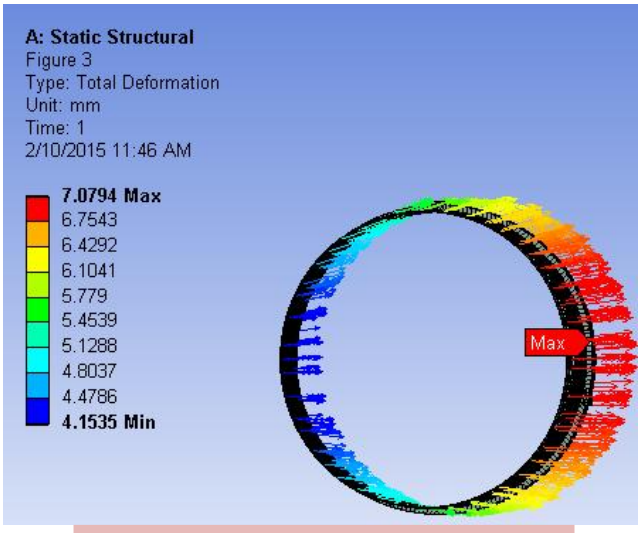

Total Displacement

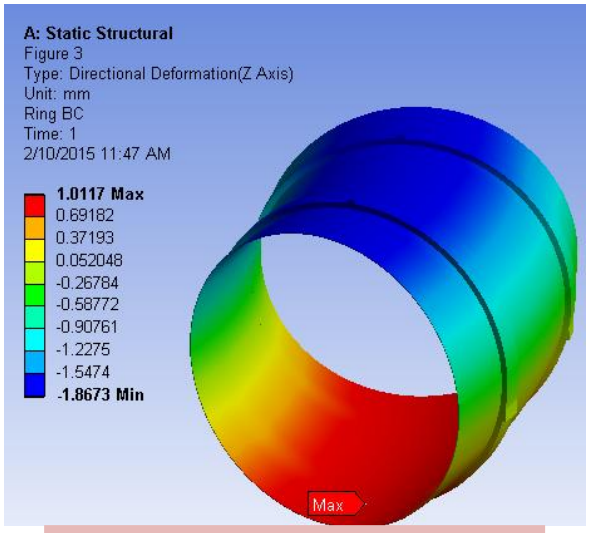

Vertical Displacement

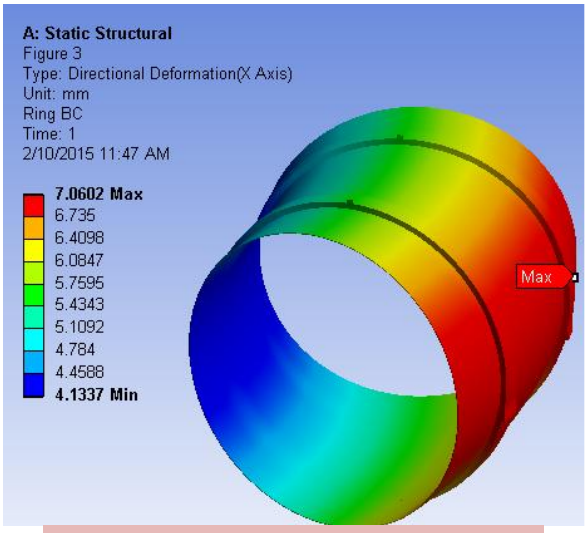

Radial Displacement

Equivalent stress	**Shell: Smax=15 MPa Ring: Smax=3.9 MPa**

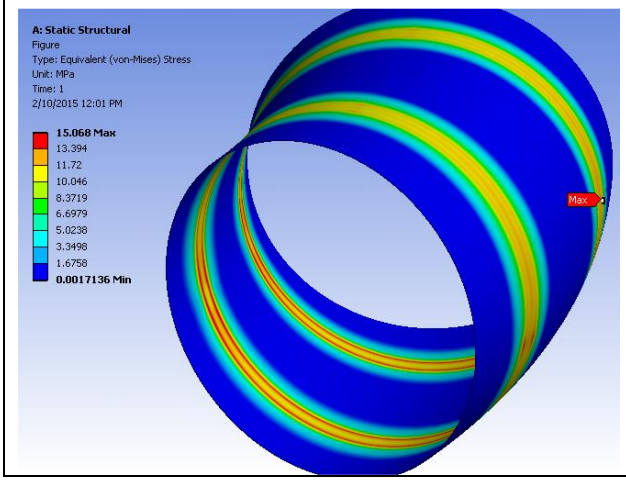

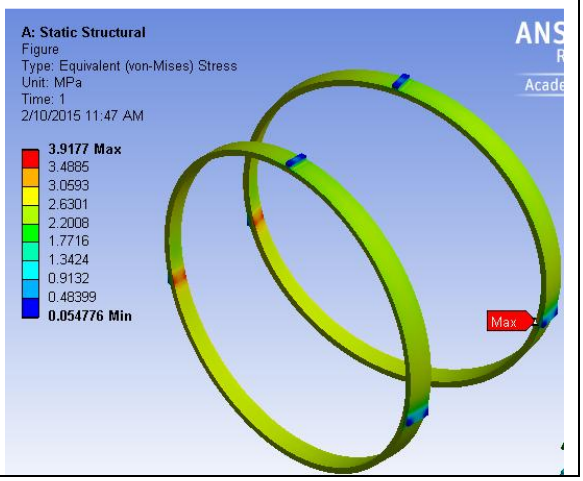

The table below summarizes the poloidal values of results from above configurations,

Table 30 Poloidal values of investigated parameters for ring geometry design

		UX		UY		Usum		Eqv. Stress	
Pol. angle	Configuration	Shell	Ring	Shell	Ring	Shell	Ring	Shell	Ring
0	Config. 2.2	6.5	6.49	6.39	6.39	9.25	9.25	2.96	0.78
45	Config. 2.2	6.17	5.99	7.35	7.37	9.71	9.61	17.8	1.98
90	Config. 2.2	3.67	3.55	0.1	-0.51	3.77	3.7	93.1	82.9
Left stud	Config. 2.2	4.92	5.65	-5.86	5.65	7.74	8.11	49.5	
Top stud	Config. 2.2		1.64		0.73		1.82		253
0	Config. 2.3	6.81	6.87	6.62	6.67	9.5	9.57	5.38	0.49
45	Config. 2.3	6.39	6.44	7.69	7.67	10	10	14.6	0.39
315	Config. 2.3	5.9	5.9	5.83	5.82	8.3	8.29	29	5.73
Right stud	Config. 2.3	5.97	6.05	5.92	5.83	8.41	8.4	24.8	3.95
0	Config. 2.4	6.74	6.74	0.42	0.43	7.01	7.02	14.99	2.3
90	Config. 2.4	5.39	5.41	1.78	1.78	5.87	5.9	13.57	3.11
Inner stud	Config. 2.4	4.12	4.03	0	0	4.28	4.19	14.93	0.28

The worst solution consists of that one with the larger number of rows (maximum values) in the table above table. In the table it can be appreciated the poloidal location where are identified the maximum values for possible criticalities.

From above results and summaries, we can see that configuration 2.4 shows minimum stresses in shell and rings. Also it shows distributed values of results over geometry.

6.4 Thermo-mechanical verifications of the stabilizing shell assembly

The design of stabilizing shell and supporting ring assembly is verified against different operating and loading conditions as described in table 7 of section 4:

1. Test / Commissioning loading: Testing conditions are not considered separately as it had same loads considered in pulsed condition.
2. Operational loadings:
   2.1. Baking and Glow Discharge Cleaning ……. (see section)
   2.2. Normal RFP operation ……. (see sections)
3. Likely loadings:
   3.1. Plasma fast termination ……. (see sections)
   3.2. Wall Mode Locking ……. (see sections)
4. Unlikely loadings
   4.1. Fault condition – Emag ……. (see sections)
   4.2. Seismic event – 1 ……. (see sections)

The baking and GDC load combination has been already analysed and discussed in above section 6.3.4.

Analyses regarding points 2.2, 3.1, 3.2, 4.1, 4.2 are described in the following.

6.4.1 Description of model

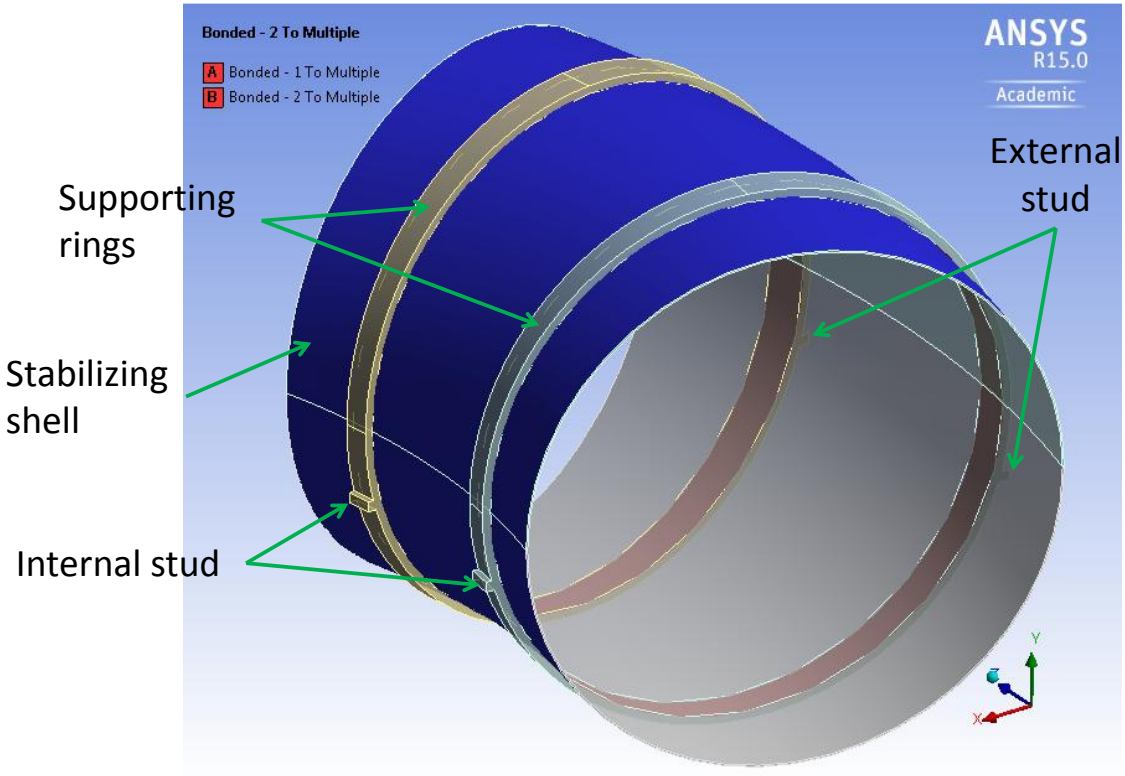

Figure 90: Model of stabilizing shell and supporting ring assembly for structural analyses

The model consists of stabilizing shell and supporting rings to estimate mechanical behaviour of modified stabilizing shell and new supporting rings. A symmetric 30° sector

of stabilizing shell and supporting rind is prepared as shown in Figure 90. The supporting rings are having 2 radial studs at internal and external equatorial side. The toroidal gap of stabilizing shell is ignored and considered full section of shell, as they are connected by series of plates by bolted joints. The length of radial stud is different in external stud from internal stud, as it is designed considering radial thermal expansion of stabilizing shell at equatorial plane. The external stud length is 22.5 mm and for internal stud it is 17.5 mm.

The FE model is shown in Figure 91. The model contains 72020 elements and 391798 elements, two elements are considered in stabilizing shell thickness and 3 elements are considered in ring thickness.

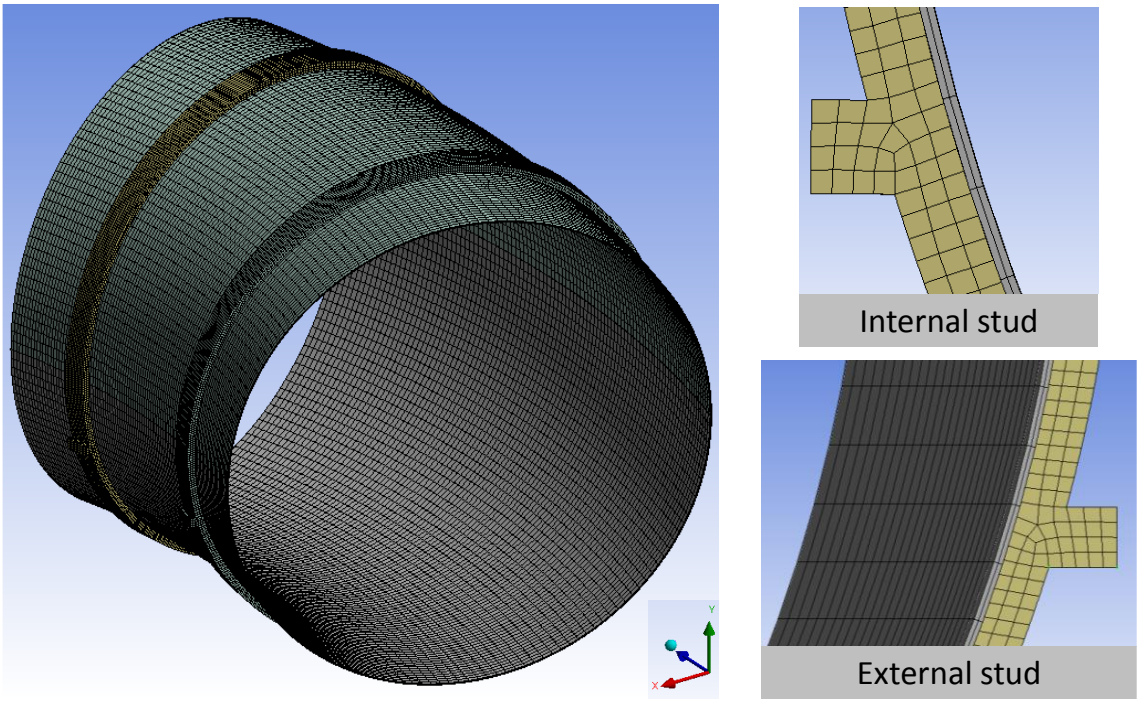

Figure 91: FE model of stabilizing shell and supporting ring assembly

6.4.2 General boundary conditions for the model

Followings are the common boundary conditions applied to the model for all analyses;

1. The stabilizing shell is bolted to the supporting rings, contacts between shell and rings are considered bonded as shown in Figure 90
2. The stabilizing shell assembly is supported on TSS rail by means of supporting rings. So, Supporting ring studs are fixed for any vertical displacement and free for radial sliding as shown in Figure 92
3. Weight of FW tiles are applied uniformly to internal surface of stabilizing shell
4. Cyclic symmetric boundary condition are applied to the shell to simulate the behaviour of the whole machine

As per different load combinations described in Table 17, further electromagnetic forces and temperature gradient are considered and applied on the particular models.

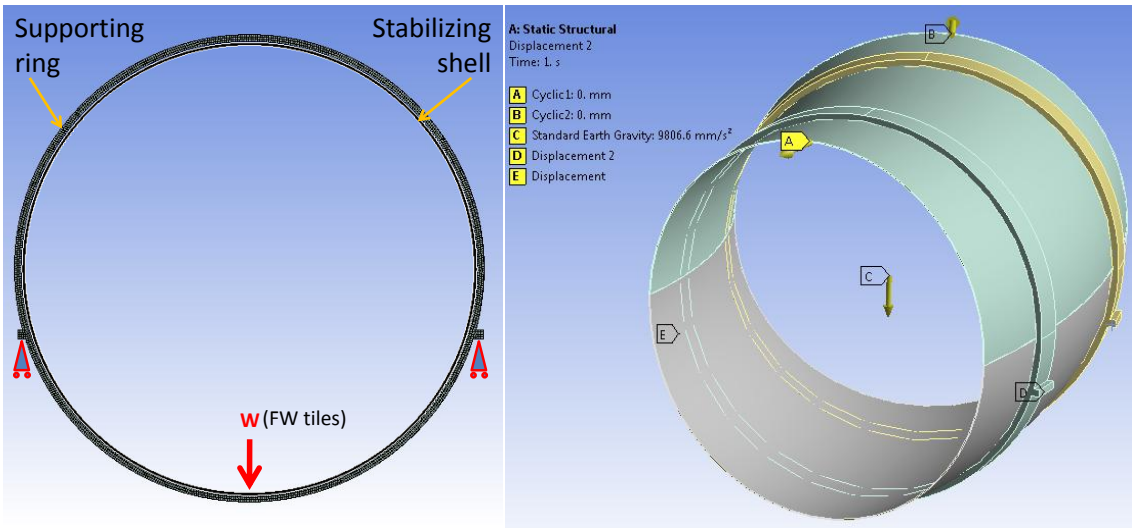

Figure 92: General boundary conditions

6.4.3 Simulation of normal RFP operation

In addition to above described boundary conditions, following loads applied to the model;

1. Temperature distribution in stabilizing shell resulted in thermal analysis for normal RFP operation case
2. Temperature distribution in supporting rings resulted in thermal analysis for normal RFP operation case
3. Electromagnetic forces for the normal RFP operation

A nonlinear static structural analysis was carried out.

The Figure 93 shows vector plot of total displacement of stabilizing shell and supporting rings under applied loads. The displacement mainly occurs due to applied thermal condition. The maximum displacement of assembly occurs at external equatorial side with displacement of 4.6 mm and minimum of 2.8 occurs at internal equatorial side, which is compatible and below to the assembly design limit.

The Figure 94 shows von-mises stress contour in stabilizing shell, maximum stress is 25.4 MPa which is well below to its allowable material limit. Figure 95 shows contour of maximum principal stress and minimum principal stress, which shows that highest stress is arise from compressive force in shell below supporting ring. Figure 96 shows von-mises stress contour in supporting rings with maximum stress value of 11.2 MPa.

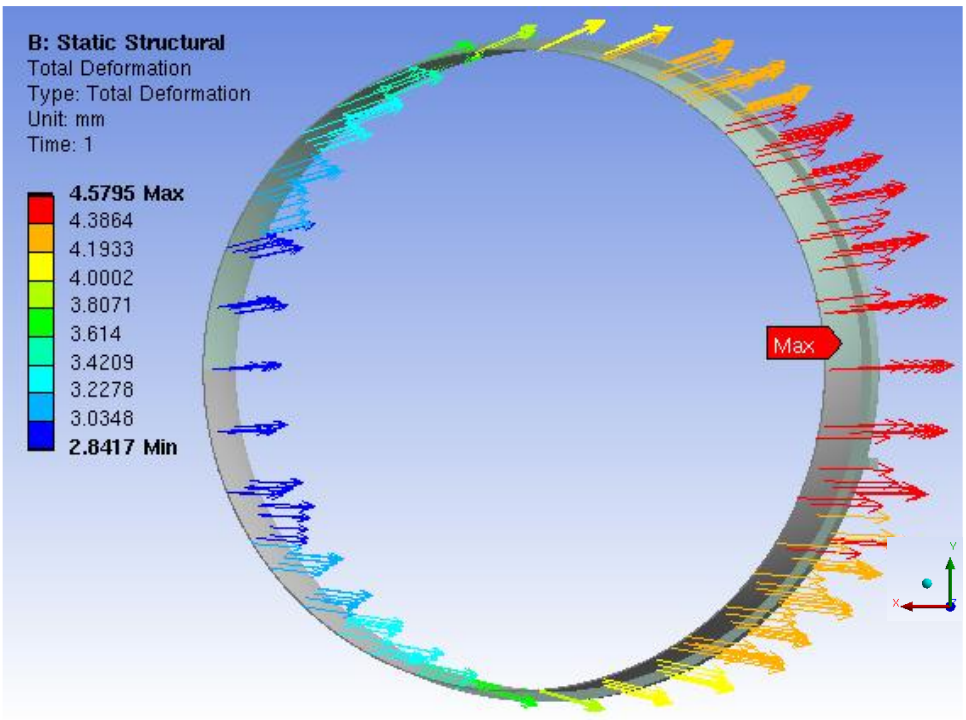

Figure 93: Case# 2.2: Total displacement vector plot (Max. = 4.6 mm, min. = 2.8 mm)

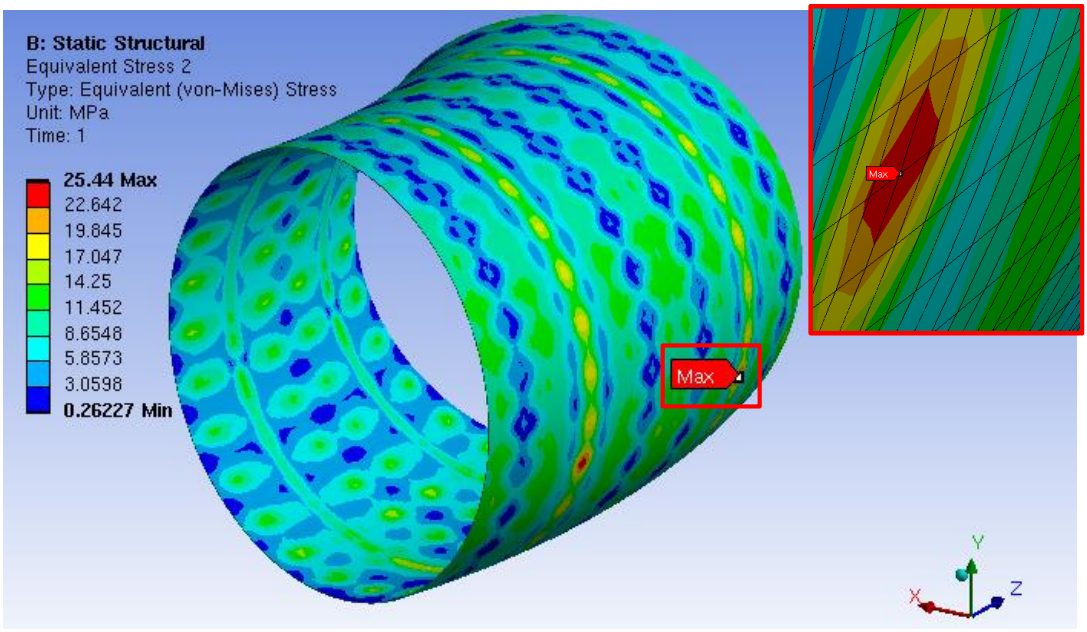

Figure 94: Case# 2.2: Equivalent stress contour in shell (Max. = 25.44 MPa)

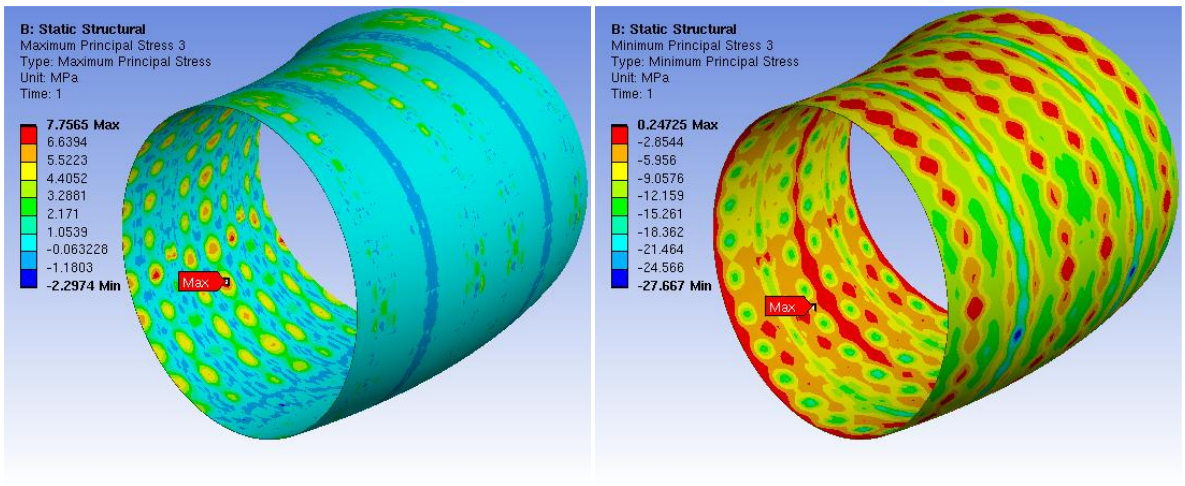

Figure 95: Case# 2.2: Maximum and minimum principal stress [MPa] contour in shell

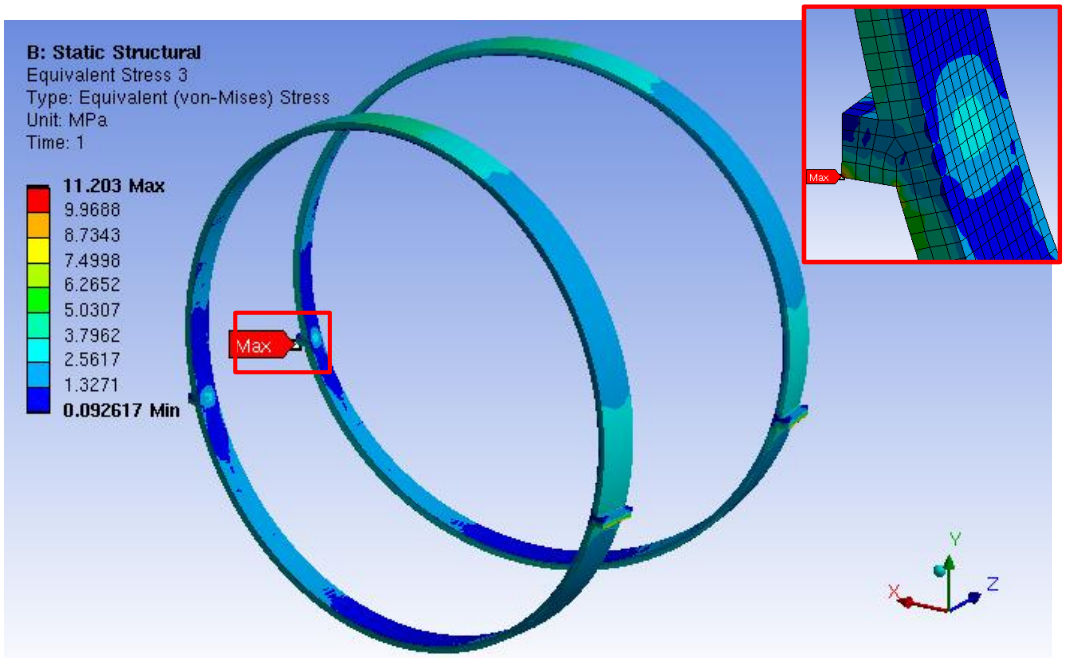

Figure 96: Case# 2.2: Equivalent stress contour in rings (Max. = 11.2 MPa)

Results are further verified by stress linearization method. Stresses are assessed by categorization at maximum stress locations through shell thickness and compared with material limits as per ASME standard. Results are found well below to the limit as shown in Table 31;

Table 31 Case# 2.2: Stress linearization and verification with allowable stress limits [MPa]

Component	**Stabilizing shell (OFHC)**			**Support rings (Torlon® 5030)**		
Stress categories	P_L	$Pm+Pb$	$Pm+Pb+Q$	P_L	$Pm+Pb$	$Pm+Pb+Q$
Allowable stress[#] [MPa]	**53**	**53**	**105**	**102**	**102**	**204**
2.2 Normal RFP operation [MPa]	19.9	25.4	25.4	4.8	9.0	11.2

Allowable stress limits are calculated at maximum applied temperature (180 °C)

6.4.4 Simulation of fast termination of plasma

In addition to described general boundary conditions, following loads applied to the model;

1. Temperature distribution in stabilizing shell for normal RFP operation case
2. Temperature distribution in supporting rings for normal RFP operation case
3. Electromagnetic forces developed due to fast termination of plasma

Results of nonlinear static structural analysis are similar to the results of normal RFP operation. The Figure 97 shows vector plot of total displacement (maximum 4.6 mm and minimum of 3). Maximum equivalent stress in stabilizing shell is 24.5 MPa as shown in Figure 98. Figure 99 shows von-mises stress contour in supporting rings with maximum stress value of 11.3 MPa.

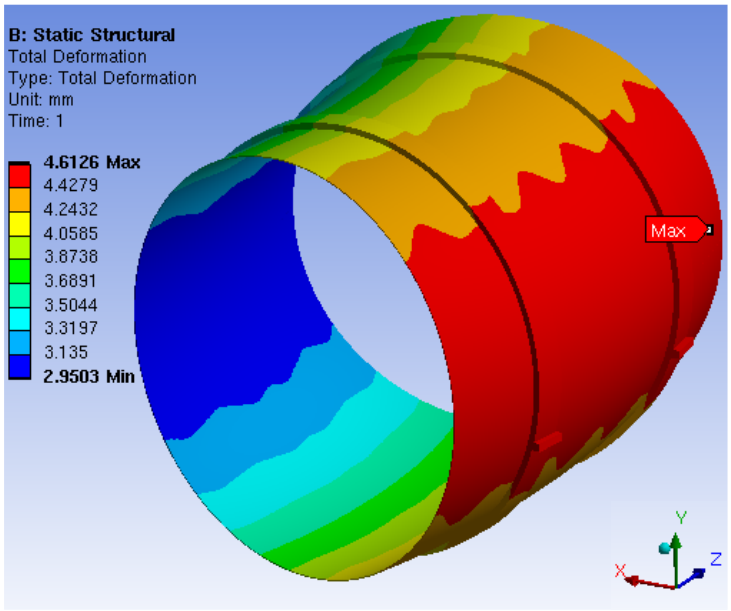

Figure 97: Case# 3.1: Total displacement vector plot (Max. = 4.6 mm, min. = 3 mm)

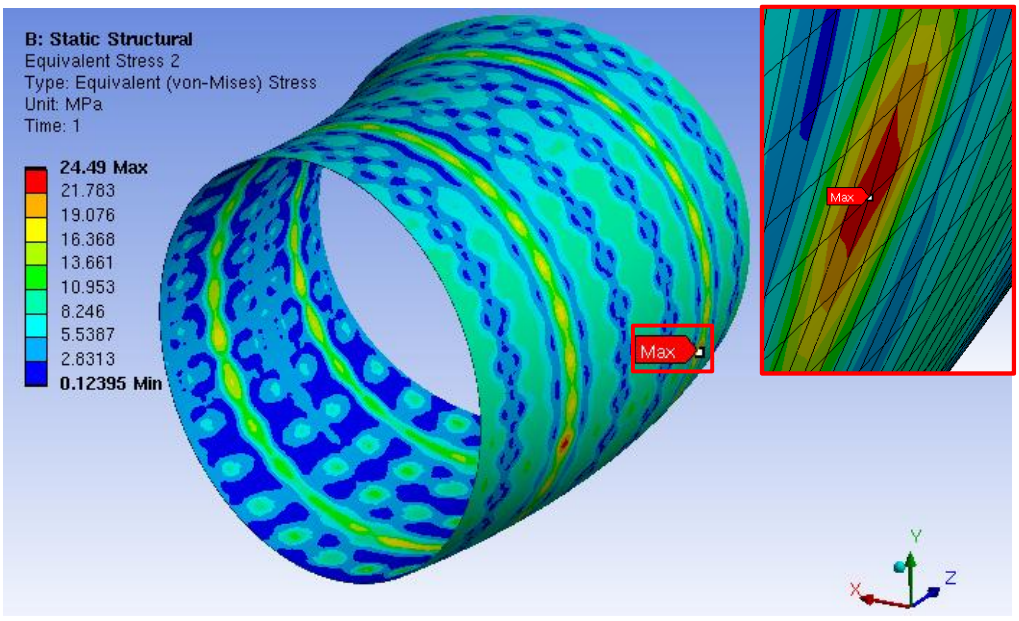

Figure 98: Case# 3.1: Equivalent stress contour in shell (Max. = 24.5 MPa)

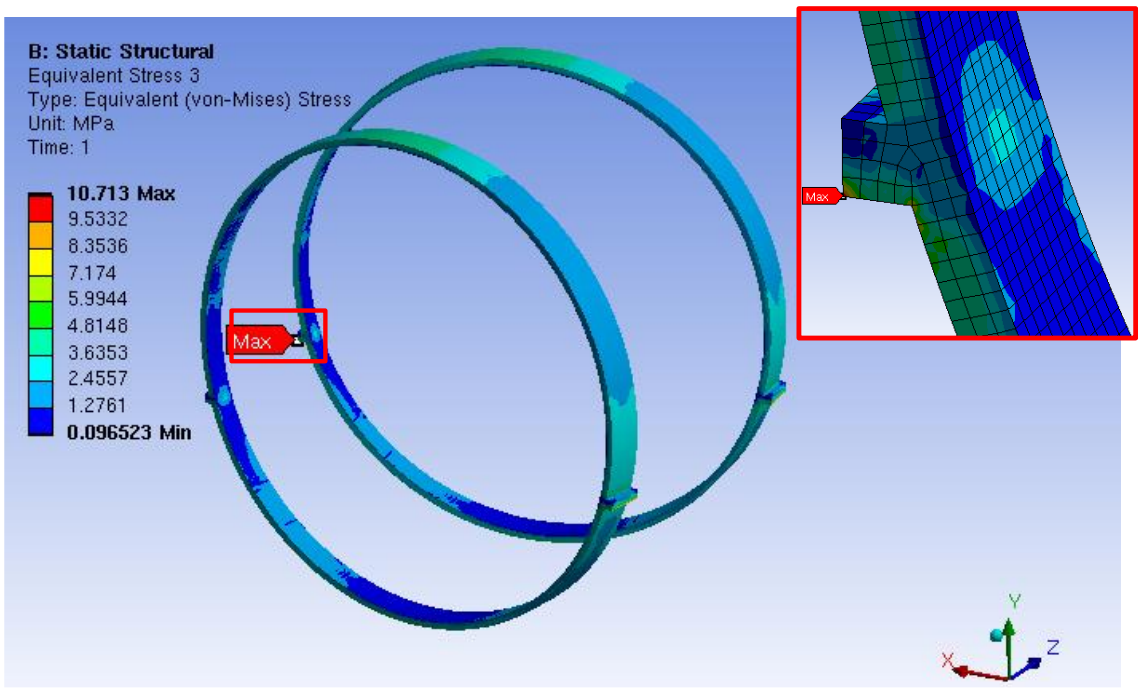

Figure 99: Case# 3.1: Equivalent stress contour in rings (Max. = 10.7 MPa)

Results are further verified by stress linearization method. Stresses are assessed by categorization at maximum stress locations through shell thickness and compared with material limits as per ASME standard. Results are found well below to the limit as shown in Table 32;

Table 32 Case# 3.1: Stress linearization and verification with allowable stress limits [MPa]

Component	**Stabilizing shell (OFHC)**			**Support rings (Torlon® 5030)**		
Stress categories	P_L	$Pm+Pb$	$Pm+Pb+Q$	P_L	$Pm+Pb$	$Pm+Pb+Q$
Allowable stress # [MPa]	**53**	**53**	**105**	**102**	**102**	**204**
3.1 Plasma fast termination [MPa]	19	24.5	24.5	4.7	8.5	10.7

Allowable stress limits are calculated at maximum applied temperature (180 °C)

6.4.5 Simulation of wall mode locking

In addition to general boundary conditions, following loads applied to the model;

1. Temperature distribution in stabilizing shell for wall mode locking case
2. Temperature distribution in supporting rings for wall mode locking case
3. Electromagnetic forces caused by normal RFP operation

Results of nonlinear static structural analysis are as below; The Figure 100 and Figure 101 shows total displacement occur in stabilizing shell and supporting rings under applied loads. The maximum displacement of assembly occurs at external equatorial side with displacement of 4.8 mm and minimum of 2.7 occurs at internal equatorial side.

Stresses are concentrated in shell below the position of FW tiles of sector where wall mode locking occurs. The Figure 102shows von-Mises stress contour in stabilizing shell, maximum stress is 52.8 MPa which is well below to its allowable material limit. Figure

103 shows contour of maximum principal stress and minimum principal stress. Figure 104 shows von-Mises stress contour in supporting rings with maximum stress value of 11.6 MPa, which is very well below to its allowable material limit.

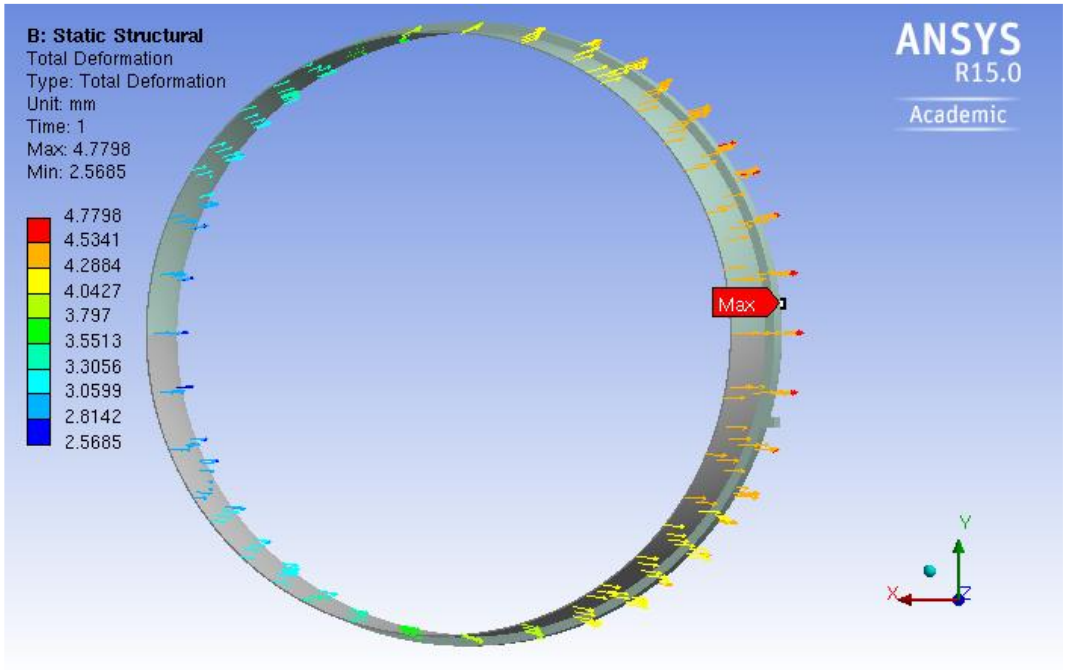

Figure 100: Case# 3.2: Total displacement vector plot (Max. = 4.8 mm, min. = 2.7 mm)

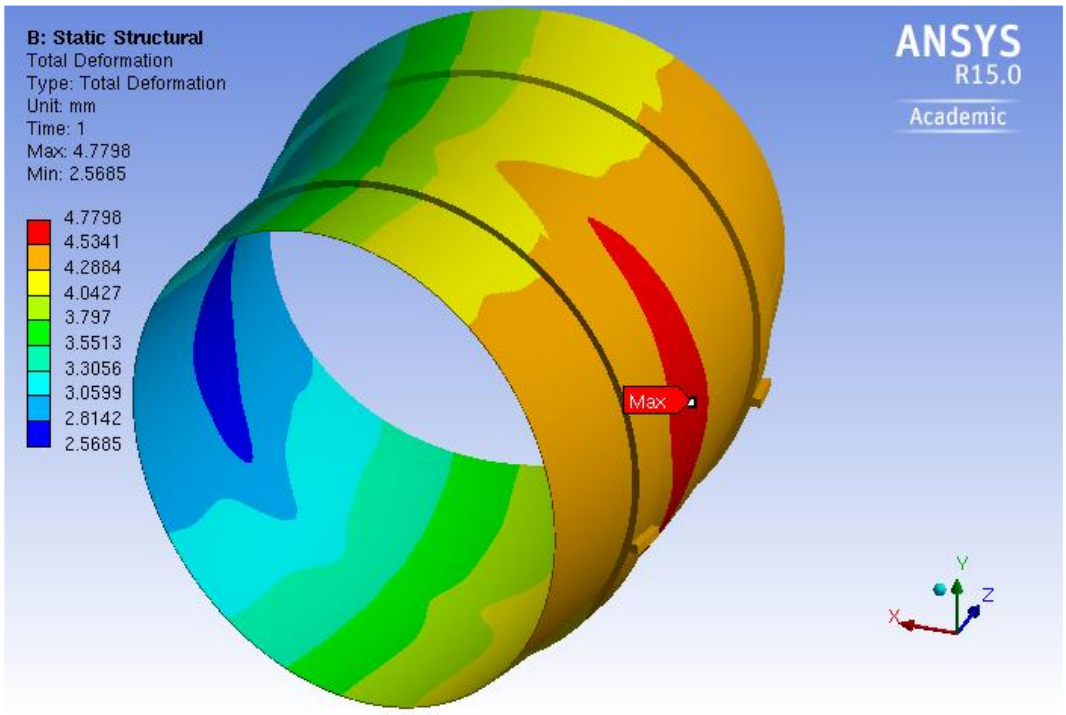

Figure 101: Case# 3.2: Total displacement contour plot [mm]

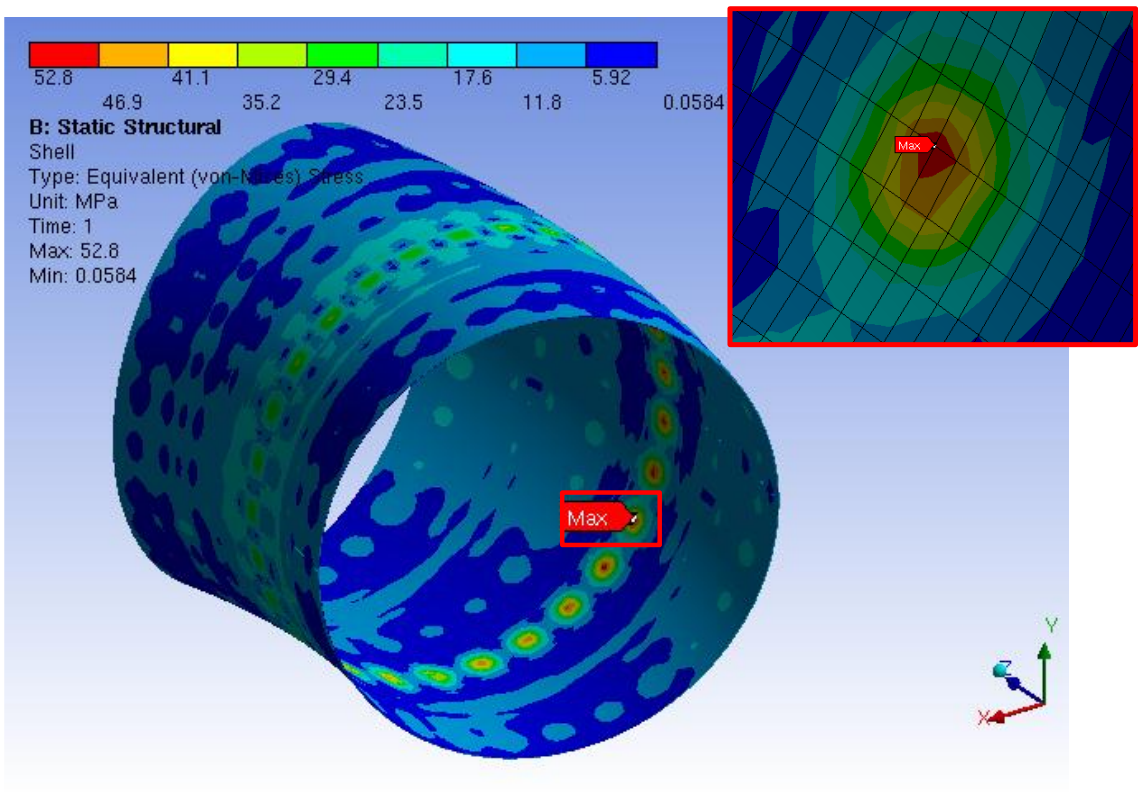

Figure 102: Case# 3.2: Equivalent stress contour in shell (Max. = 52.8 MPa)

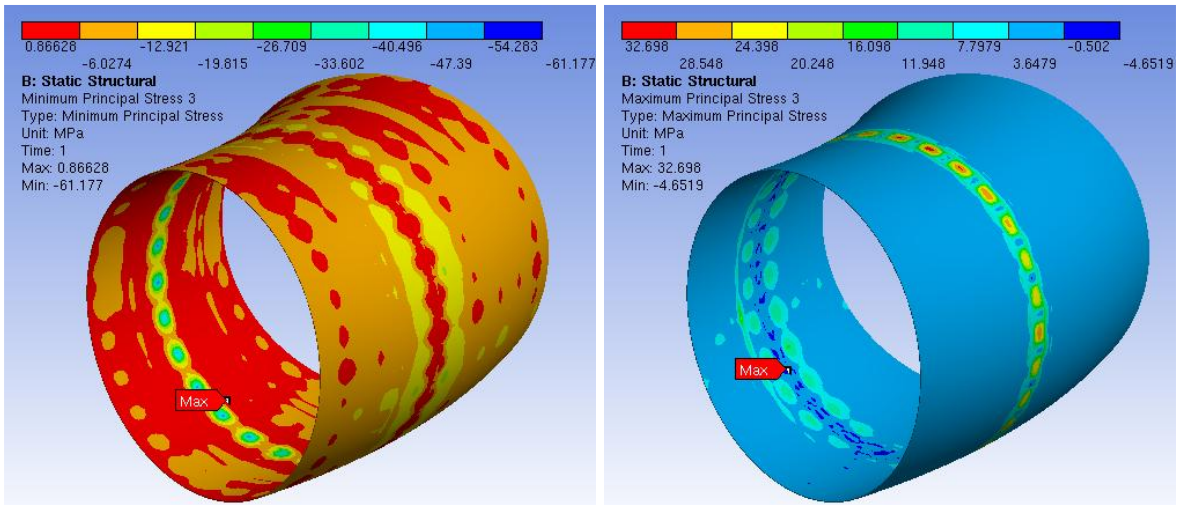

Figure 103: Case# 3.2: Maximum and minimum principal stress [MPa] contour in shell

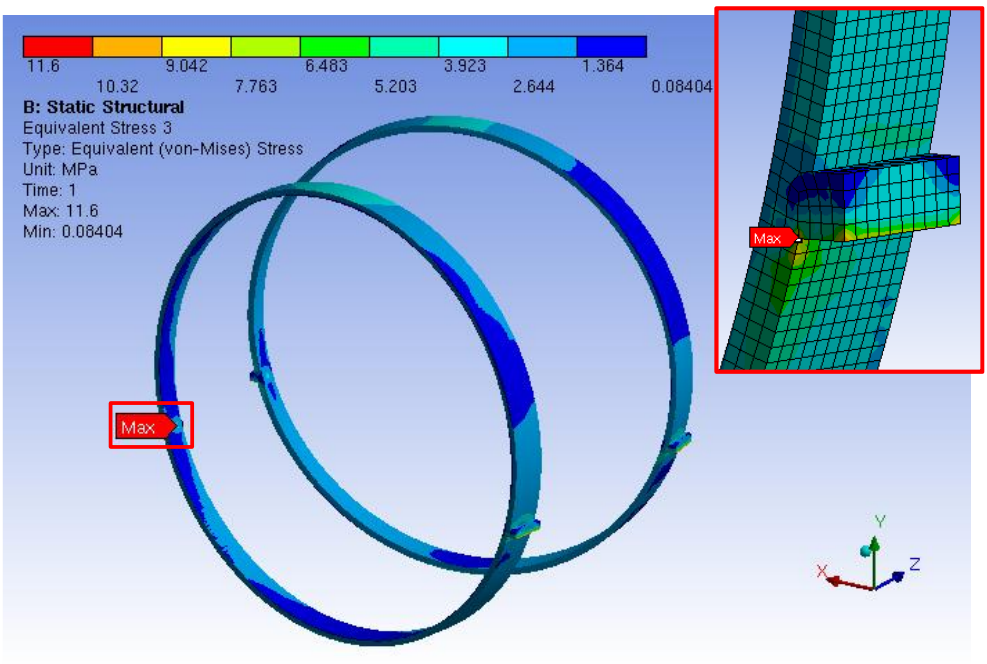

Figure 104: Case# 3.2: Equivalent stress contour in rings (Max. = 11.6 MPa)

Results are further verified by stress linearization method. Stresses are assessed by categorization at maximum stress locations through shell thickness and compared with material limits as per ASME standard. Results are found well below to the limit as shown in Table 33;

Table 33 Case# 3.2: Stress linearization and verification with allowable stress limits [MPa]

Component	**Stabilizing shell (OFHC)**			**Support rings (Torlon® 5030)**		
Stress categories	P_L	$Pm+Pb$	$Pm+Pb+Q$	P_L	$Pm+Pb$	$Pm+Pb+Q$
Allowable stress # [MPa]	**53**	**53**	**105**	**102**	**102**	**204**
3.2 Wall Mode Locking [MPa]	27.9	51.2	52.8	2.5	6.5	11.6

Allowable stress limits are calculated at maximum applied temperature (180 °C)

6.4.6 Simulation of fault case of electromagnetic event

In addition to general boundary conditions, only electromagnetic forces are applied to stabilizing shell caused by fault condition. In the fault case of electromagnetic event, there is no plasma produced inside TSS and forces produced due to eddy currents produced from magnetic field produced by coil systems. So no thermal load arises in system.

Results of nonlinear static structural analysis are as below;

The maximum displacement of 0.7 mm occurs equally at top and bottom of assembly as shown in Figure 105, which is within safe limit.

The Figure 106 shows von-mises stress contour in stabilizing shell, maximum stress is 30.5 MPa which is well below to its allowable material limit. Figure 107 shows von-mises stress contour in supporting rings with maximum stress value of 3 MPa.

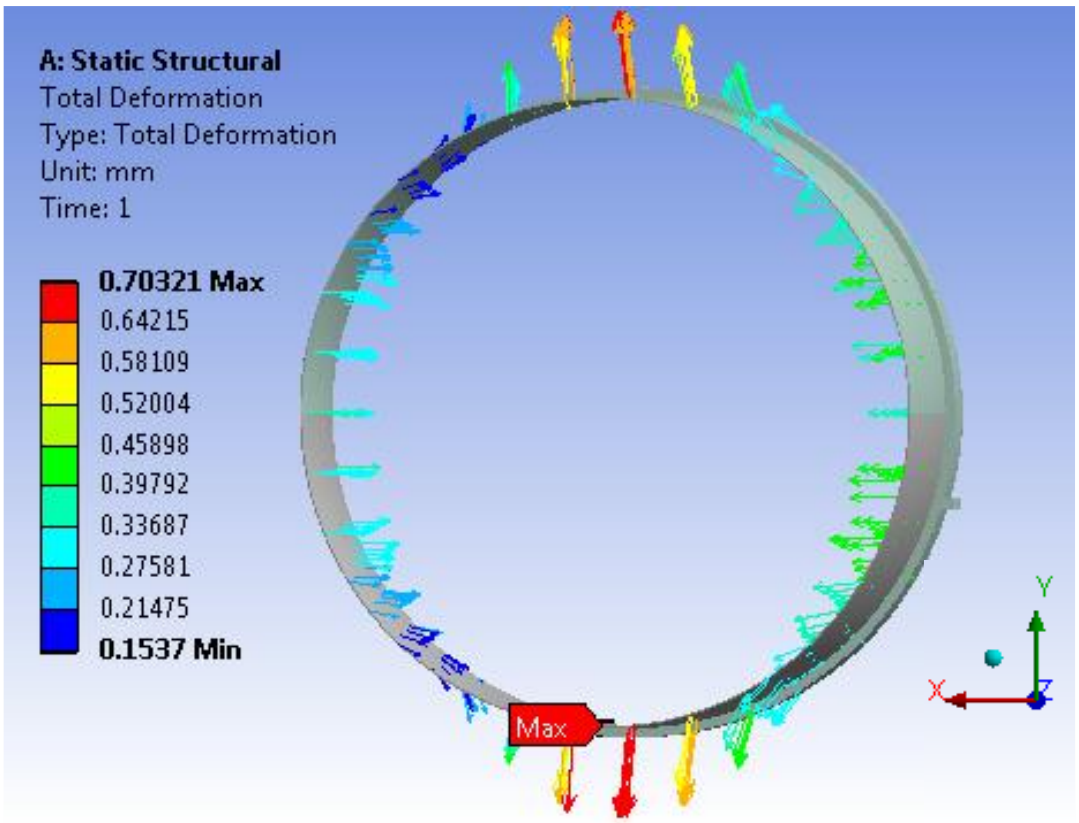

Figure 105: Case# 4.1: Total displacement vector plot (Max. = 0.7 mm, min. = 0.2 mm)

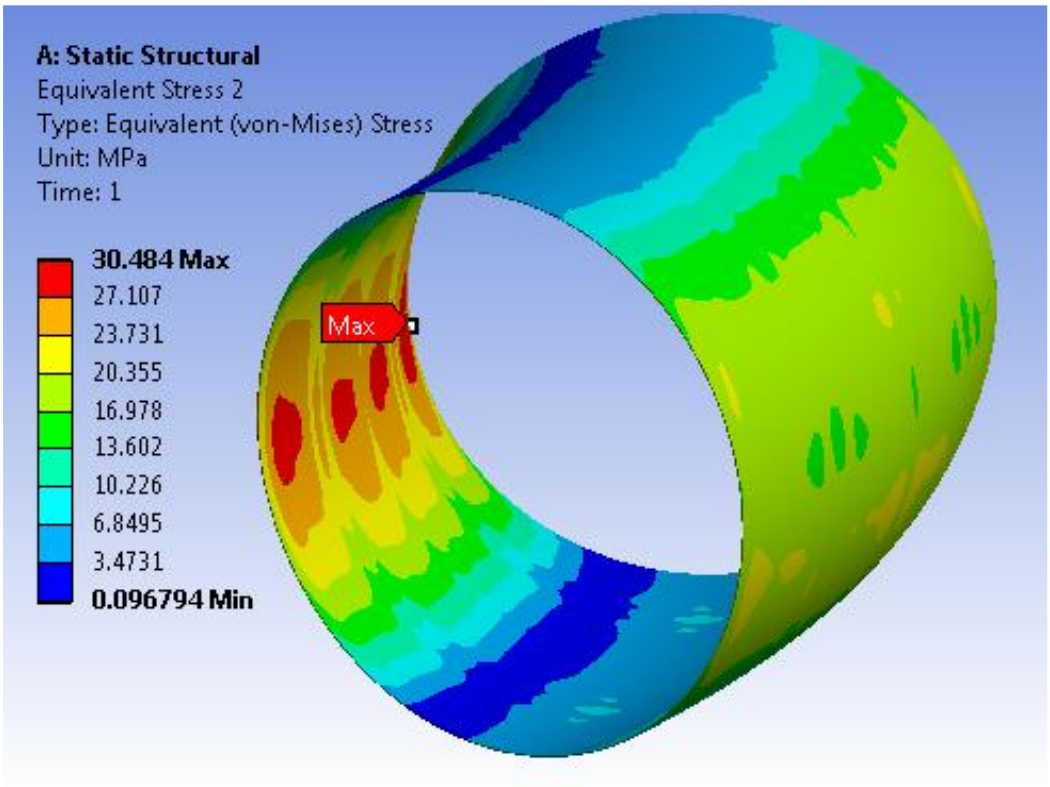

Figure 106: Case# 4.1: Equivalent stress contour in shell (Max. = 30.5 MPa)

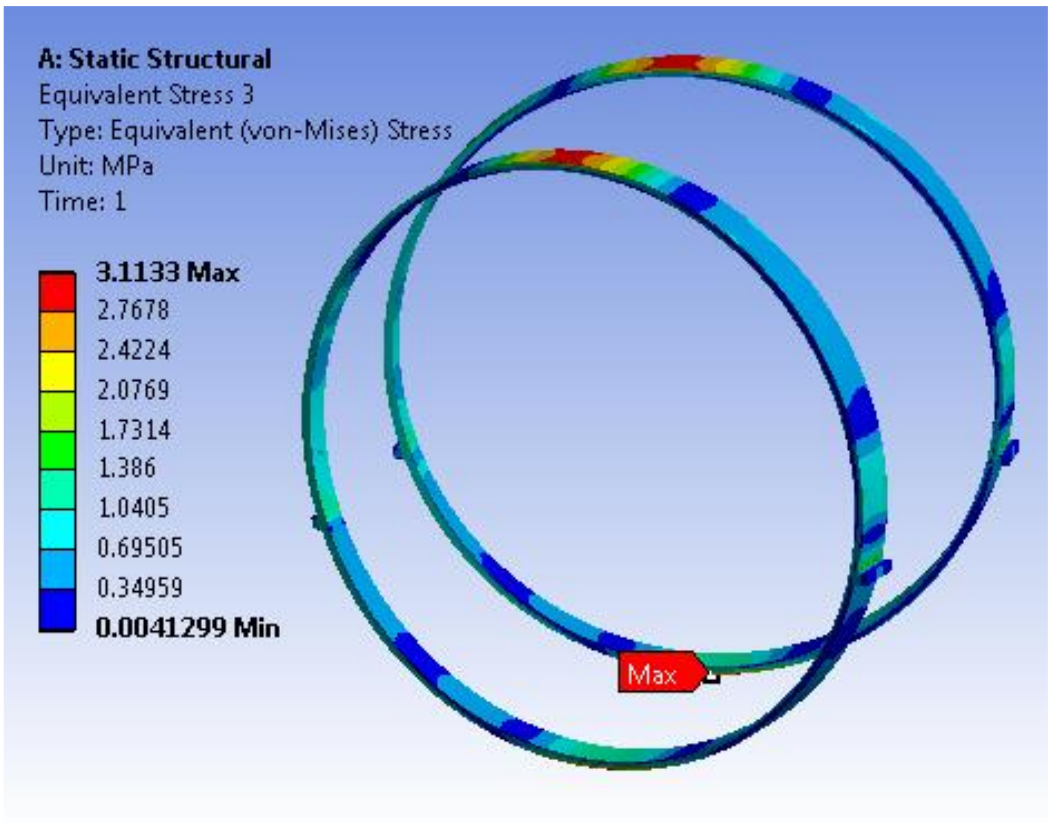

Figure 107: Case# 4.1: Equivalent stress contour in rings (Max. = 3 MPa)

Results are further verified by stress linearization method. Stresses are assessed by categorization at maximum stress locations through shell thickness and compared with material limits as per ASME standard. Results are found well below to the limit as shown in Table 34;

Table 34 Case# 4.1: Stress linearization and verification with allowable stress limits [MPa]

Component	**Stabilizing shell (OFHC)**			**Support rings (Torlon® 5030)**		
Stress categories	P_L	$Pm+Pb$	$Pm+Pb+Q$	Pm	$Pm+Pb$	$Pm+Pb+Q$
Allowable stress # [MPa]	**64**	**64**	**126**	**122**	**122**	**245**
4.1 Fault condition – Emag [MPa]	25.7	29.8	29.9	0.8	2.8	2.8

Allowable stress limits are calculated at maximum applied temperature (180 °C)

6.4.7 Modal analysis for Seismic event

This subsection presents the details of modal analysis of a 180° sector of the stabilizing shell assembly of RFX-mod2 machine. The analysis is carried out to find natural frequency of the assembly which is supported on TSS rail through supporting rings.

The 180° sector model consists of FW tiles attached to stabilizing shell by cylindrical keys and 12 supporting rings to support the shell. Figure 108 show model details.

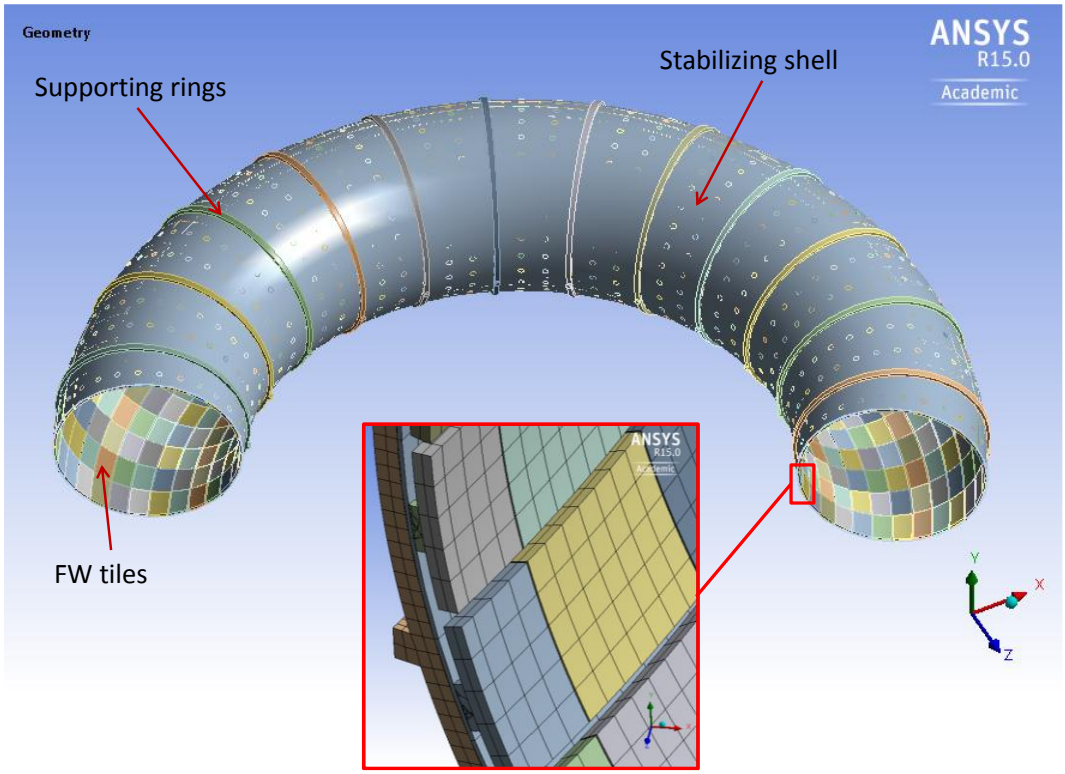

Figure 108: Case# 4.2: Model details for Modal analysis

The analysis aims at evaluate the modal behaviour of 180° sector of stabilizing shell assembly. Calculated eigenvalues are shown in Table 35 and the corresponding modal shapes for first 3 modes are illustrated in Figure 109, Figure 110 and Figure 111.

The first deformation mode on the natural frequency of the stabilizing shell assembly is shown in Figure 109, which depicts that the assembly is swayed horizontally toward a same direction.

From the results, it is found that natural frequency of the assembly is reasonably high in the view of a seismic response compared with accelerations given in section 4.2.2.3.

Table 35: Case# 4.2: Calculated natural frequency of the model

Mode	1	2	3	4	5	6
Frequency [Hz]	35	75	84	93	101	104

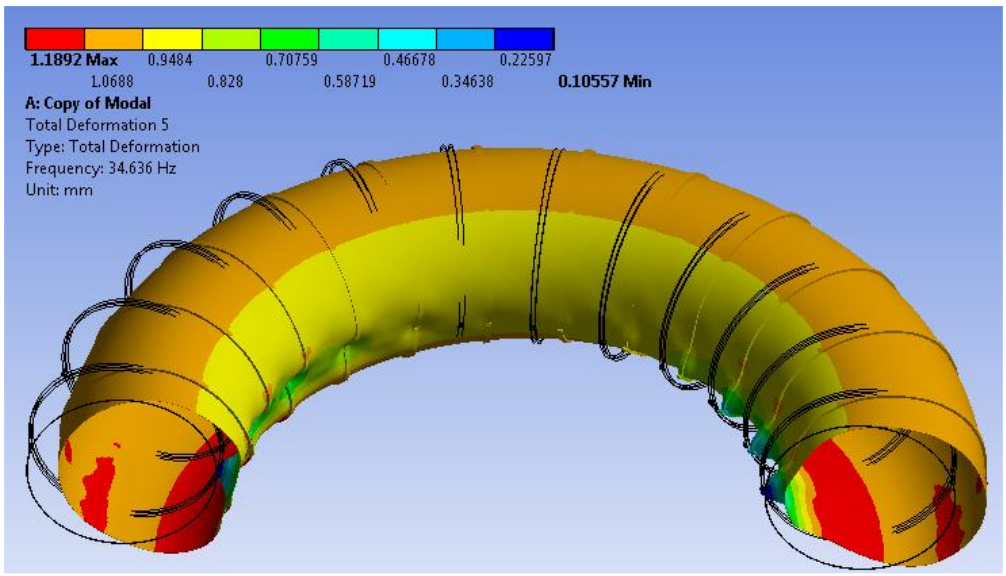

Figure 109: Case# 4.2: Total deformation for mode 1 (scaled to 160X)

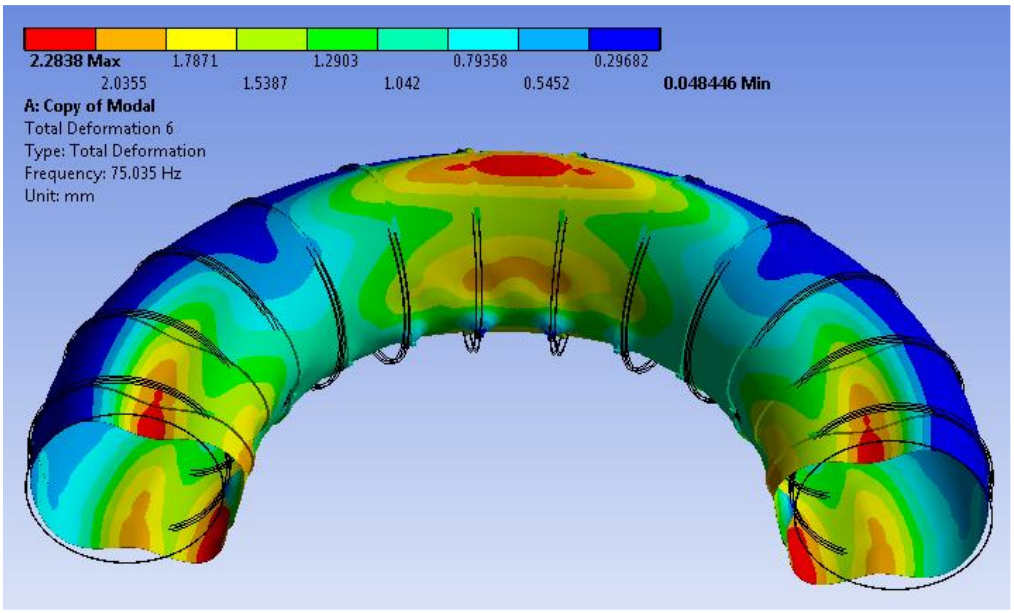

Figure 110: Case# 4.2: Total deformation for mode 2 (scaled to 160X)

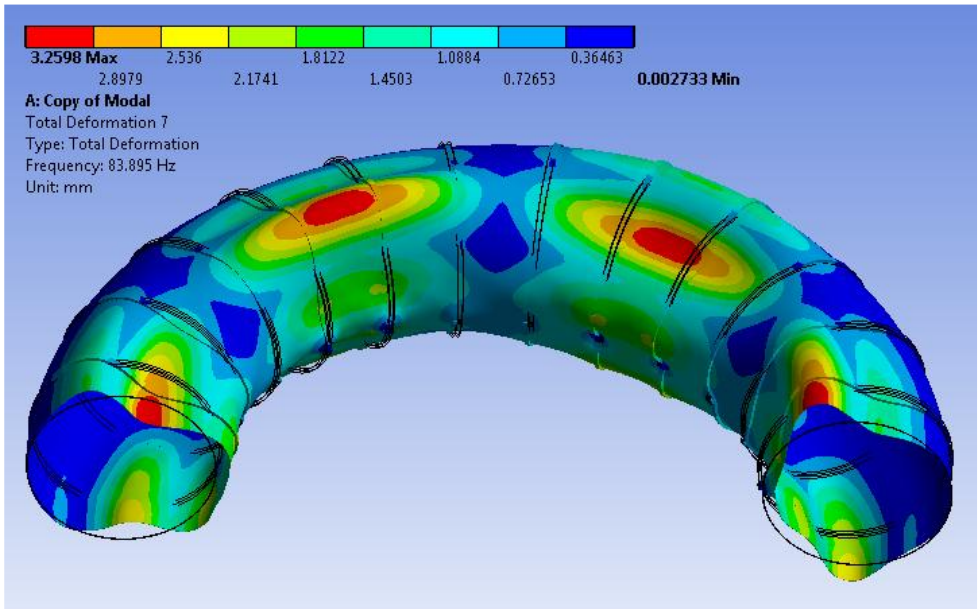

Figure 111: Case# 4.2: Total deformation for mode 3 (scaled to 160X)

6.5 Conclusion

Results of thermo-mechanical simulations of stabilizing shell and supporting rings assembly are shown above. Total displacement is comparable in scenario 1 and 2, in scenario-3 displacement at internal side is little higher and displacement at external side little lower comparing to other 2 scenarios.

The wall mode locking simulation shows highest stress in stabilizing shell. The stresses in stabilizing shell are mainly concentrated on portion below FW tile sector getting highest heat load due to plasma wall locking. Results of normal RFP and plasma fast termination condition show comparable stresses. While baking condition shows lowest stresses as temperature distribution in shell and rings are uniform. Primary bending stresses are higher in stabilizing shell in all the cases compared to primary membrane stress. The stresses in supporting rings are always below 12 MPa in all the scenarios, which is well below to TORLON material limit of 150 MPa at 200 °C temperature.

Categorized stresses of all the cases are compiled in below Table 36. Results in stabilizing shell and supporting rings are found well below to the material limit.

Table 36 Summary of stress [MPa] verification for Stabilizing shell and supporting rings

Component	**Stabilizing shell (OFHC)**			**Supporting rings (Torlon® 5030)**		
Stress categories	P_L	$Pm+Pb$	P_L+Pb+Q	P_L	$Pm+Pb$	P_L+Pb+Q
Allowable stress[#] [MPa] (Service level A)	**53**	**53**	**105**	**102**	**102**	**204**
2.1 Baking and GDC [MPa]	6.6	8.9	8.8	1.2	3.6	4.4
2.2 Normal RFP operation [MPa]	19.9	25.4	25.4	4.8	9.0	11.2
3.1 Plasma fast termination [MPa]	19	24.5	24.5	4.7	8.5	10.7
3.2 Wall Mode Locking [MPa]	27.9	51.2	52.8	2.5	6.5	11.6
Allowable stress [MPa] (Service level C)	**64**	**64**	**126**	**122**	**122**	**245**
4.1 Fault condition – Emag [MPa]	25.7	29.8	29.9	0.8	2.8	2.8

Allowable stress limits are calculated at maximum applied temperature (180 °C)

CHAPTER 7 THERMO-MECHANICAL ANALYSIS AND VERIFICATION OF THE TOROIDAL SUPPORT STRUCTURE

This chapter gives details on different analysis carried out for Toroidal Support Structure (TSS) and Thin Resistive Plate (TRP), including seals and bolted joints. For these components, two different models are prepared applying proper load combinations defined in CHAPTER 4.

The first model prepared simulates TSS and clamping rings assembly. The mechanical strength of the modified TSS needs to be verified considering added pressure difference due to internal vacuum condition along with other loads. The thermo-mechanical verifications for design modification of TSS are carried out using this model for different operating and loading conditions as described in Table 17:

1. Test / Commissioning loading: testing conditions are not analysed separately as corresponding loads are already applied in pulsed condition.
2. Operational loadings:
   2.1. Baking and Glow Discharge Cleaning ……. (see section 7.1.3)
   2.2. Normal RFP operation ……. (see sections 7.1.4)
3. Likely loadings:
   3.1. Plasma fast termination …… (see sections 7.1.5)
   3.2. Wall Mode Locking ……. (see sections 7.1.6)
4. Unlikely loadings
   4.1. Fault condition – Emag …… (see sections 7.1.7)

Furthermore buckling analysis are carried out for the highest stress produced by load combination from above list and results are discussed in the section 7.1.8.

Second model is prepared for TRP seal, which includes closing plate and local reinforcements to preserve the radial width of the TRP. A structural analysis is performed to verify the behaviour of TRP under external pressure as explained in 7.2.

7.1 Thermo-mechanical verifications of Toroidal support structure

The modified TSS of RFX-mod2 is foreseen to realise the vacuum seal as additional requirement to the other mechanical ones. Also it has to resist the electrodynamic loads imparted by each component during the pulse. The upper and the lower halves are preloaded together by 24 clamping rings.

The load combinations described in section 4 are applied on the following non-linear static structural analyses to verify the TSS design against rules of codes.

7.1.1 Model description

The geometry of the TSS is obtained from the CAD model as shown below; the model is basically produced for manufacturing purpose and contains all manufacturing details as shown in Figure 112.

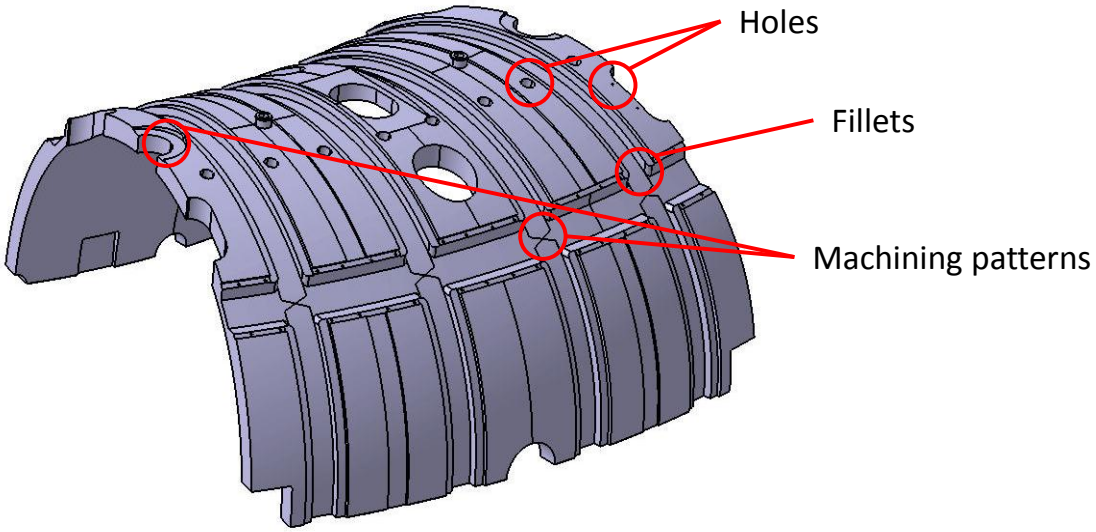

Figure 112: CAD model of TSS

The model is simplified since not all the details are significant for the simulation purpose. Simplification of geometry is done as follows:

1. Removed all the fillets and chamfer which will not affect the strength of structure. This may produce stress concentration on corners which may be studied later as sub-modelling in the finite element environment if required.
2. Removed small holes
3. Removed small machining patterns
4. Insulation gaps of 5 mm between sectors are considered as inherent part of TSS and the same material as TSS is assigned.

A 30 degree model of TSS is used for the analysis. Geometry of TSS is made of upper and lower half. The upper TSS and lower TSS geometries are symmetric. The upper and lower TSS are clamped together by total 24 clamping rings toroidally located with 15° step, where TSS is supported from TSS bush on mechanical structure [8] through 12 clamping

rings positions out of total 24 clamping rings as shown in Figure 113. The load combination applied on the finite element model is detailed in section 4.1.3.2. The simplified CAD model is imported in ANSYS workbench.

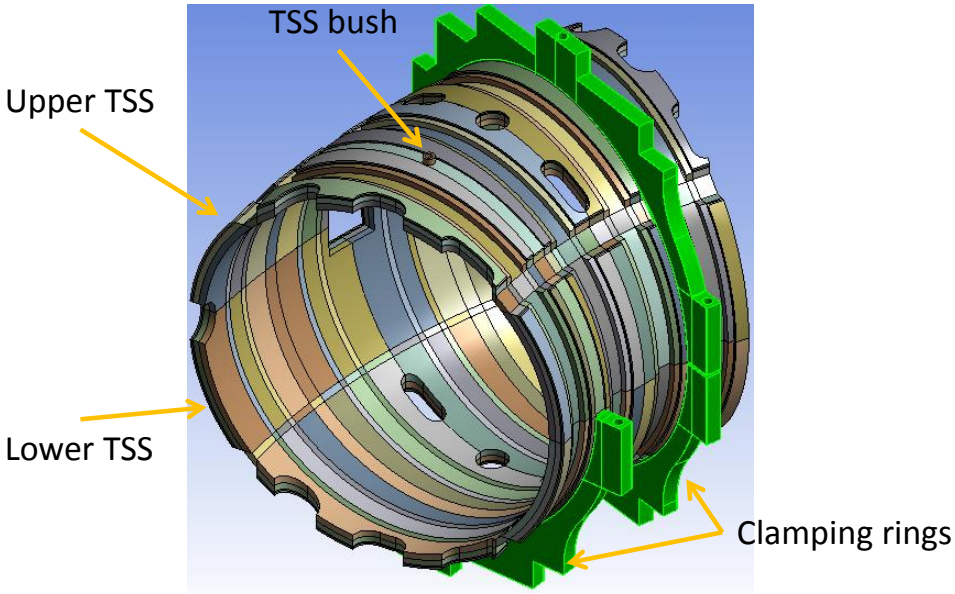

Figure 113: Simplified 30° model of TSS with 2 clamping ring to be used for analysis

The model is divided into many solid bodies to generate good distributed mesh elements as shown in Figure 113 and Figure 114. Total 441812 elements (1711571 nodes) generated are SOLID186 and SOLID187 elements with reference to ANSYS software. The mesh for the TSS has been adjusted to get a good quality. The Figure 114 below shows some details of the mesh.

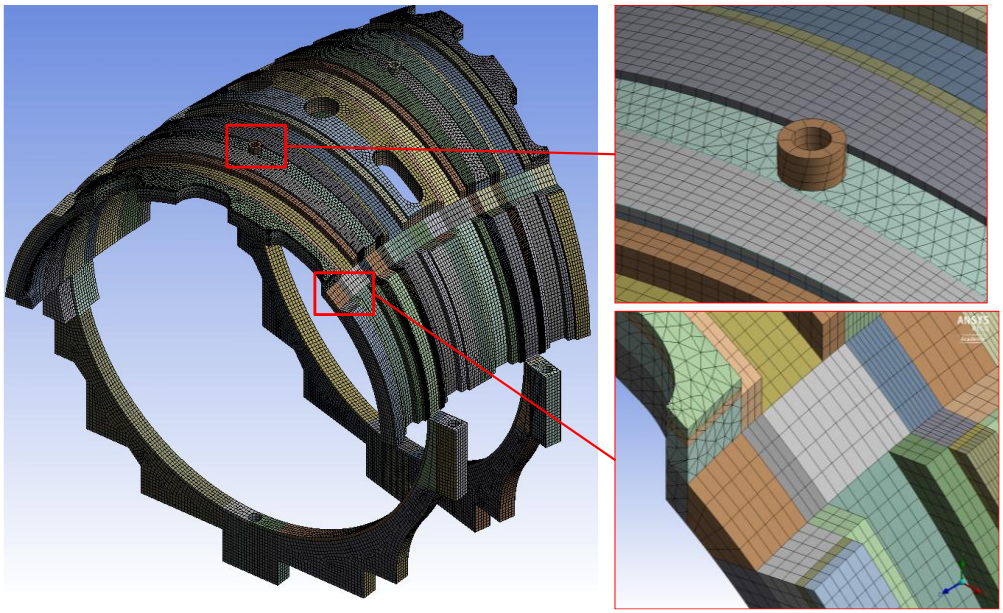

Figure 114: Finite element model of TSS and clamping ring

7.1.2 Common Boundary conditions

7.1.2.1 Constraints

The top and bottom TSS bush is provided with spring load of 11600 N/mm at one of the clamping ring location. Toroidal continuity of the model is replaced by establishing frictionless supports on both side faces of 30 degree TSS sector as shown in Figure 115.

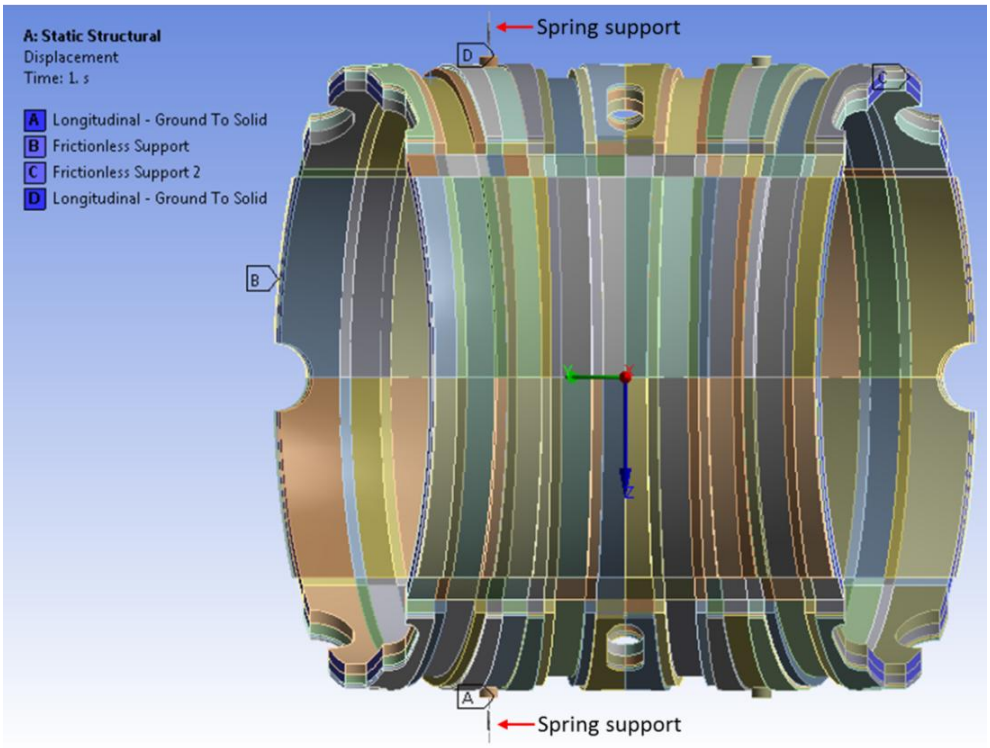

Figure 115 Shows applied displacement boundary condition on TSS

7.1.2.2 Contacts

The TSS model is divided into upper TSS and lower TSS and these two halves are clamed together by clamping rings. The internal equatorial cut between upper and lower TSS is provided with insulation in between and at external cut a spacer is welded in between TSS. Frictional contacts are defined between all these components as shown below in Figure 116, except external cut where bonded contact is realized. Frictional coefficient 0.2 is applied between contacts. Below Table 37 shows list of all contacts.

Table 37 Contact conditions applied for TSS model

Sr. #	Contacts between components	Contact type
1	Upper and Lower TSS - Internal	Frictional
2	Upper and Lower TSS - External	Bonded
3	Ring 1 and Upper TSS	Frictional
4	Ring 1 and Lower TSS	Frictional
5	Ring 2 and Upper TSS	Frictional
6	Ring 2 and Lower TSS	Frictional

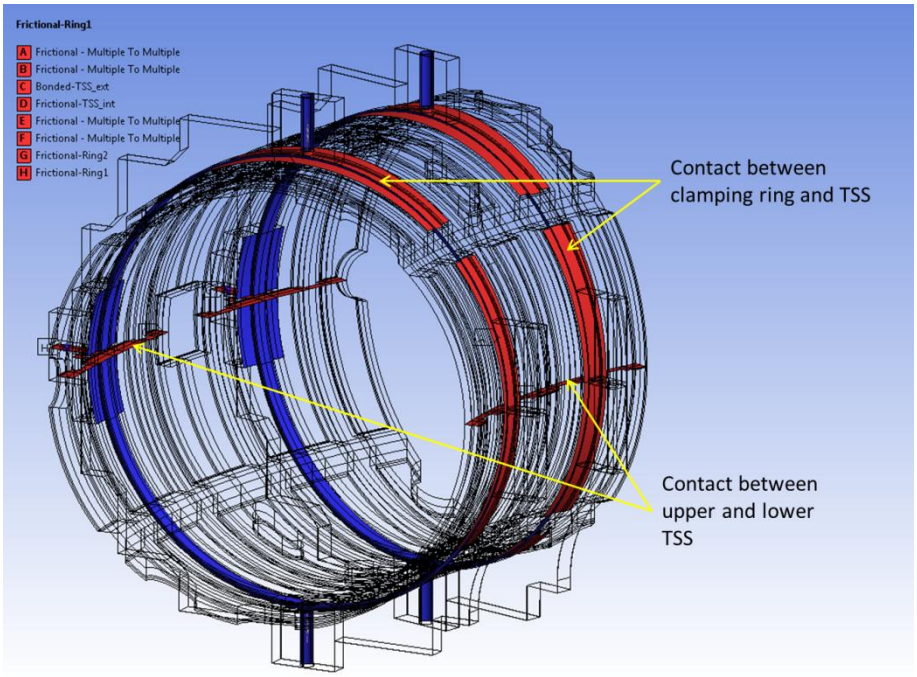

Figure 116 Shows contact between different parts of TSS and clamping rings

7.1.2.3 Structural Loads

Several loads are applied on TSS directly and some are through clamping rings as required by all the load combination in Table 17 and detailed as below:

1. External pressure of 0.1 MPa is applied on outer surfaces of TSS due to vacuum inside, as shown in Figure 117(a).

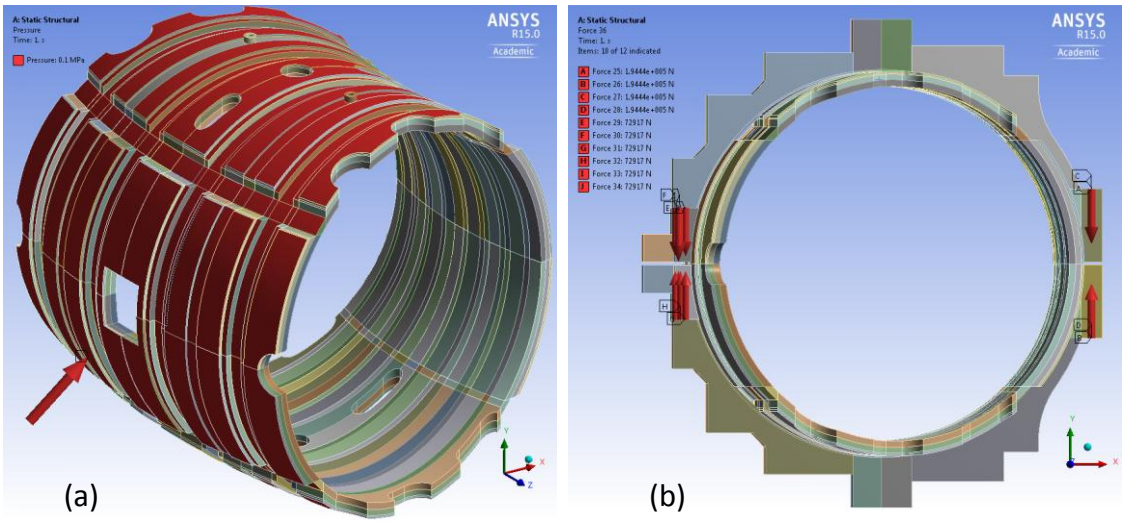

Figure 117: (a) Applied external pressure on TSS (b) Shows pre-load on clamping ring

2. Two halves of TSS is preloaded together by means of clamping rings. There is M27 single bolt connection at internal side and two M24 bolt connections at external side of each clamping ring. This preload is applied on each bolt connection calculated from its actual applied torque, which is 1050 N*mm and 350 N*mm for M27 bolt and M24 bolt respectively. Above Figure 117(b) shows applied preload on clamping rings.

3. Field shaping coils numbers 3 to 8 are supported on clamping rings. So, the weight of these coils is transfer to TSS through clamping rings. Field shaping coils at bottom part of clamping rings are supported thought clamps. Below Figure 118(a) shows forces on a clamping ring due to PF coils weight.
4. In-TSS components like FW and Cu-shell are supported through TSS rails. The weights of In-TSS components are applied on four positions in 30 degree sector as shown in Figure 118(b).
5. The coil systems like saddle coils and TF coils are also supported through TSS accommodated in their external grooves. Respective weights of systems are applied on TSS as force vertically downward. Saddle coils exerts weight of 15000 N on TSS and TF coil exerts weight of 147150 N on TSS.
6. TF coils are pressed on surface of TSS by means of belts, which exert pressure of 3MPa on surfaces which support TF coils as shown in Figure 119.
7. Uniform temperature is applied to clamping ring assumed from average temperature applied to TSS body

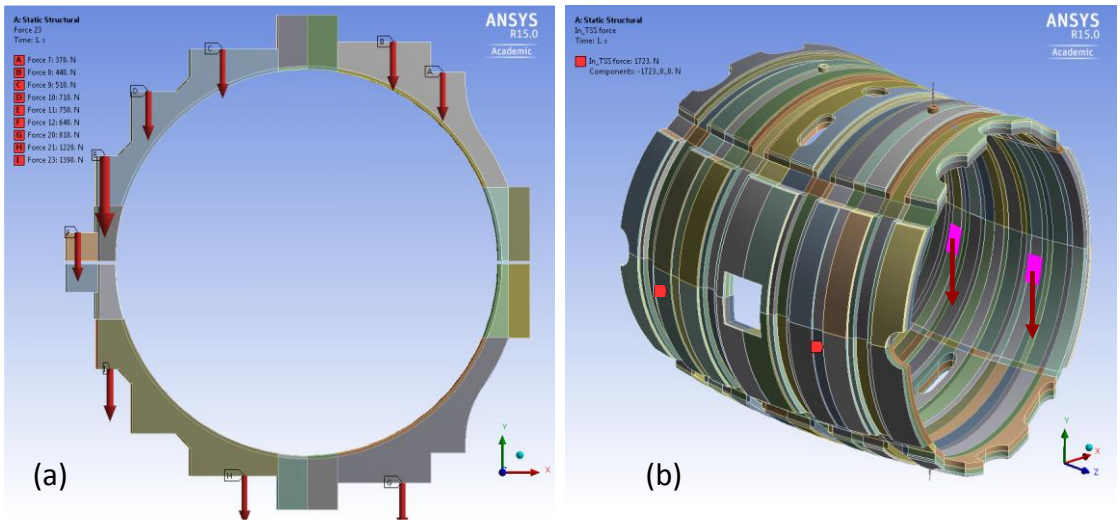

Figure 118 (a) Forces due to PF coil weight (b) Forces due to In-TSS components weight

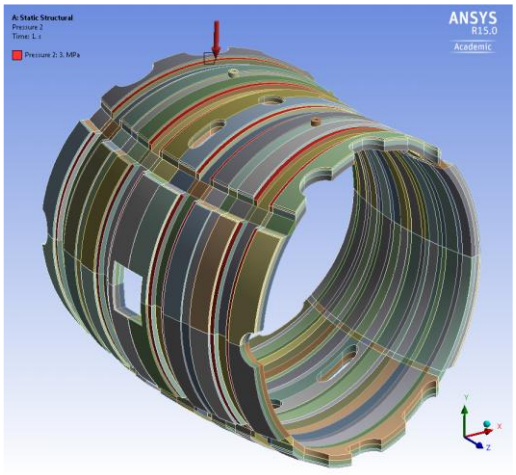

Figure 119 Pressure on TSS surfaces due to TF belts

Additional loads of electromagnetic forces and temperature gradient are considered and applied on the model as per different load combinations. Radial and tangential electromagnetic loads are applied on TSS and vertical electromagnetic forces are applied on clamping rings.

The Figure 120 and Figure 121 show the proper locations considered for the result post-processing and verifications explained in following subsections.

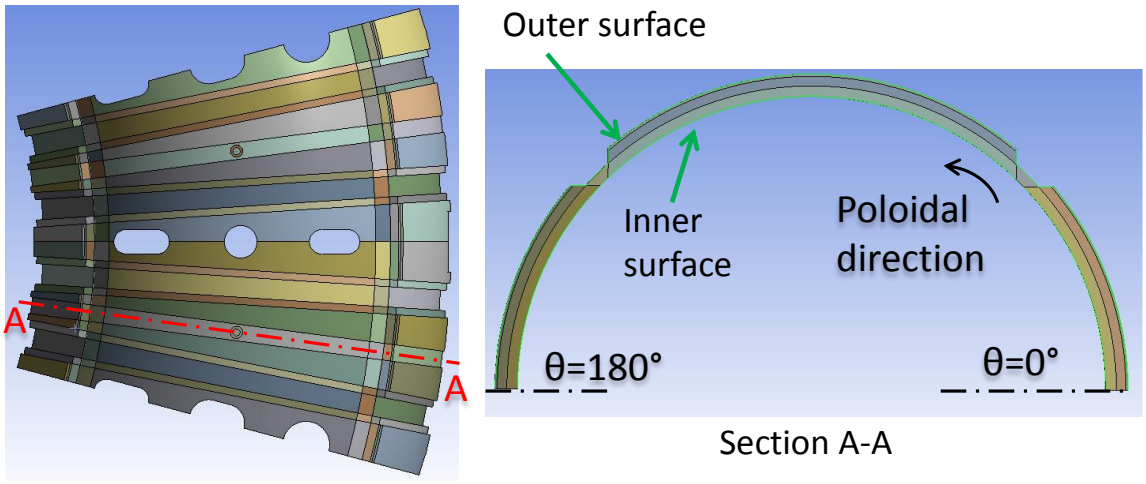

Figure 120 Location of inner and outer edges for results of poloidal stresses graph

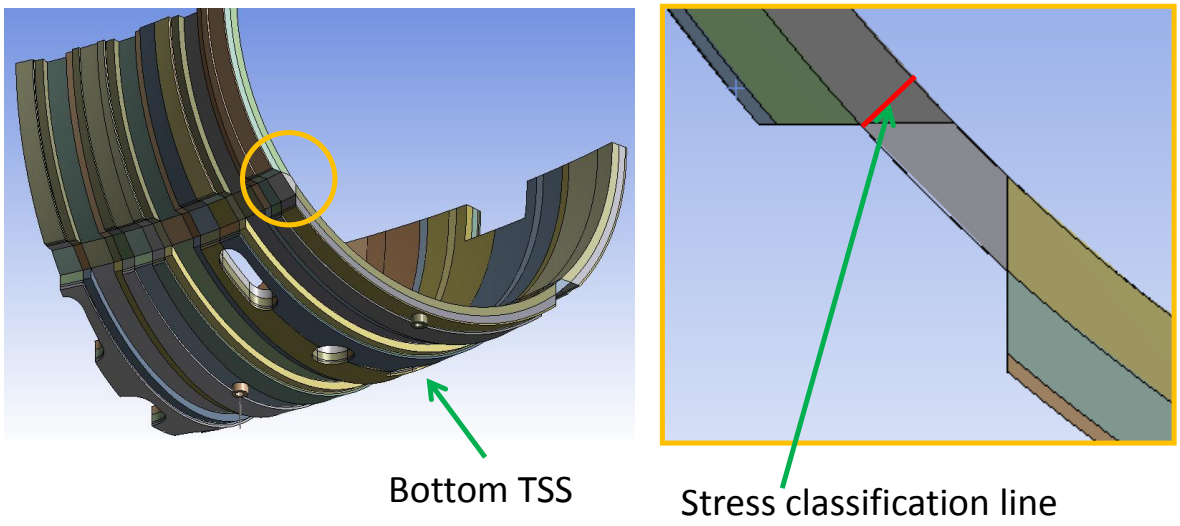

Figure 121: Location of stress classification line for stress linearization

7.1.3 Simulation of baking and GDC operation

In addition to above described common structural loads, temperature distribution in TSS resulted from thermal analysis for Baking and GDC condition is applied to the TSS geometry. There are no electromagnetic forces produced during baking condition as explained in Table 17 (component verification table).

A nonlinear static structural analysis was carried out.

The Figure 122 shows vector plot of total displacement of TSS under applied loads. The displacement occurs due to applied thermal condition and component weight. The maximum displacement of assembly occurs at the external equatorial side with maximum displacement value of 2.5 mm and minimum of 1.5 occurring at internal equatorial side. Figure 123 shows directional displacement of TSS.

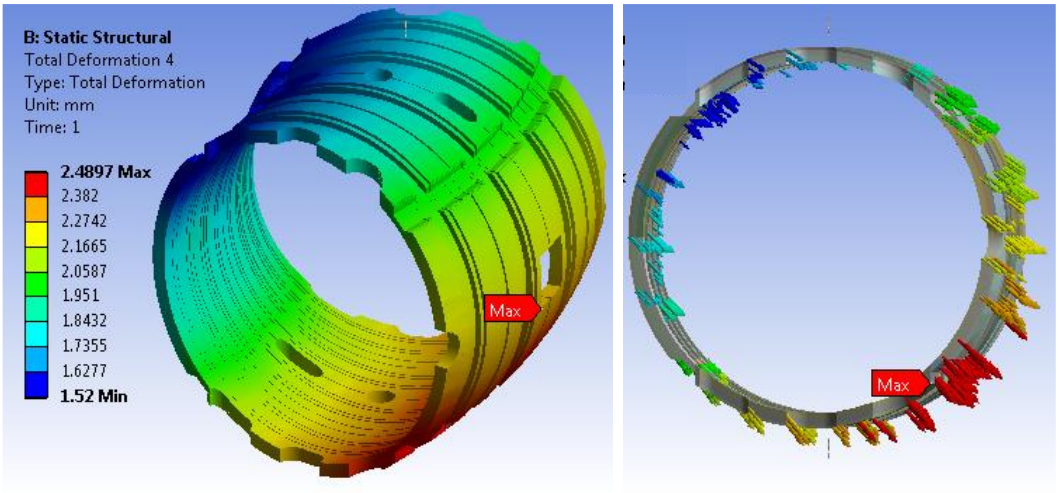

Figure 122 Case# 2.1: Total displacement contour of TSS [mm]

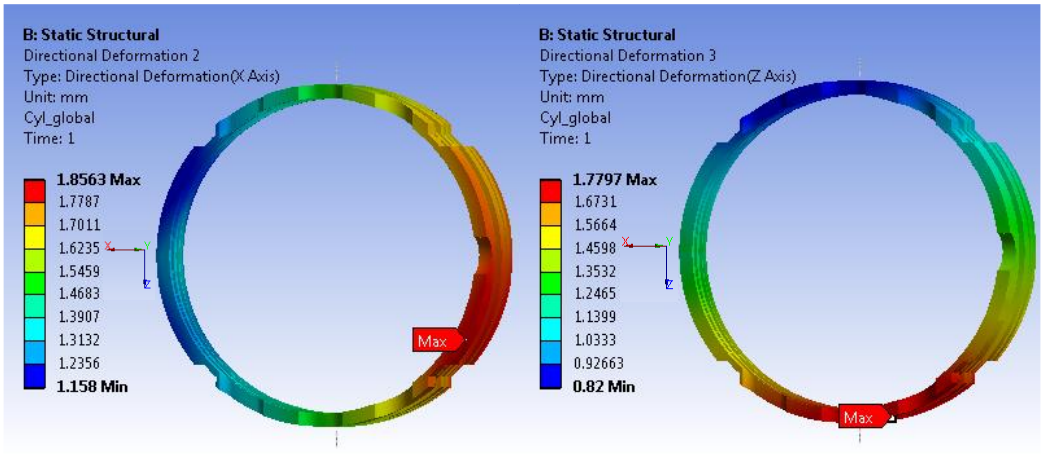

Figure 123 Case# 2.1: Directional displacement contour of TSS [mm]

The Figure 124 shows von-Mises stress contour in TSS; result shows stress concentration on one of the corner due to geometry simplification by removing the fillet. The region of minimum wall thickness of TSS shows higher stress concentration compared to others, especially at the location below the clamping ring. Figure 125 shows contour of maximum principal stress and minimum principal stress, which shows that the highest stress arises

from compressive forces from clamping the ring. Figure 126 (a.) shows that maximum 16 MPa of pressure applied on TSS from clamping rings and Figure 126 (b.) shows the contact condition at internal equatorial cut of TSS, which is very less and so negligible.

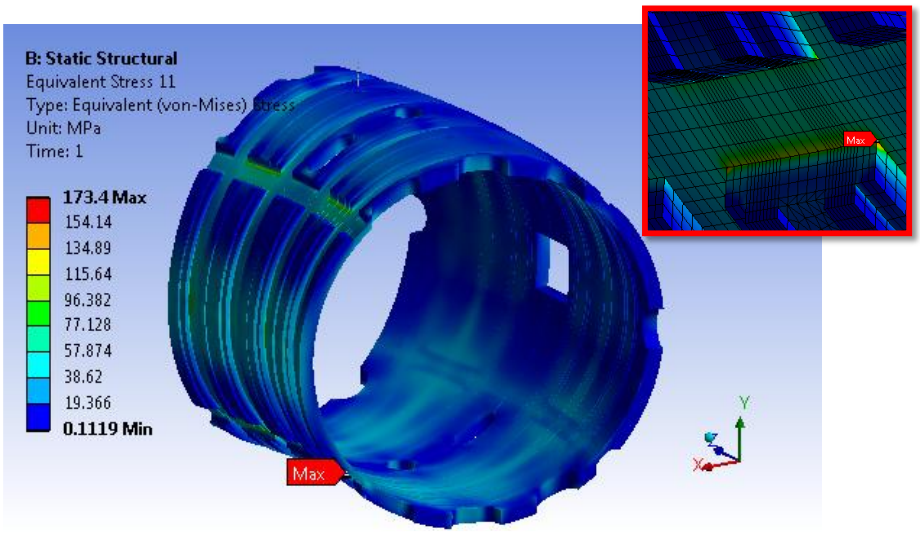

Figure 124 Case# 2.1: Stress contour for von-mises stress in TSS [MPa]

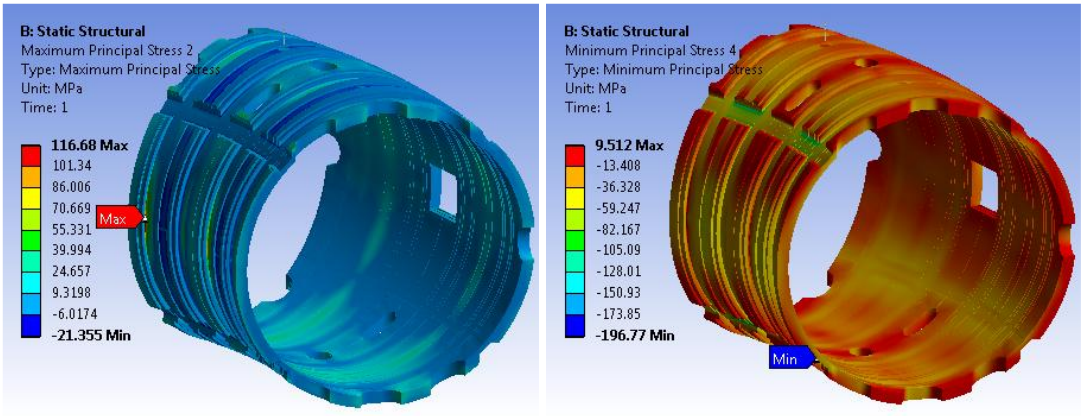

Figure 125 Case# 2.1: Stress contour for maximum and minimum principal stresses in TSS [MPa]

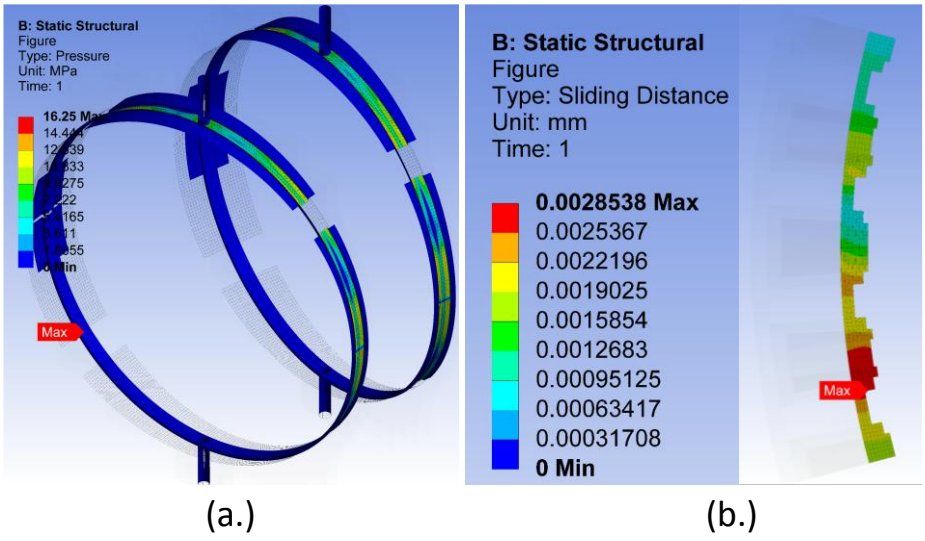

Figure 126: Case# 2.1: Contact status (a.) pressure from clamping rings to (TSS max. 16 MPa) (b.) sliding at inner equatorial joint of TSS

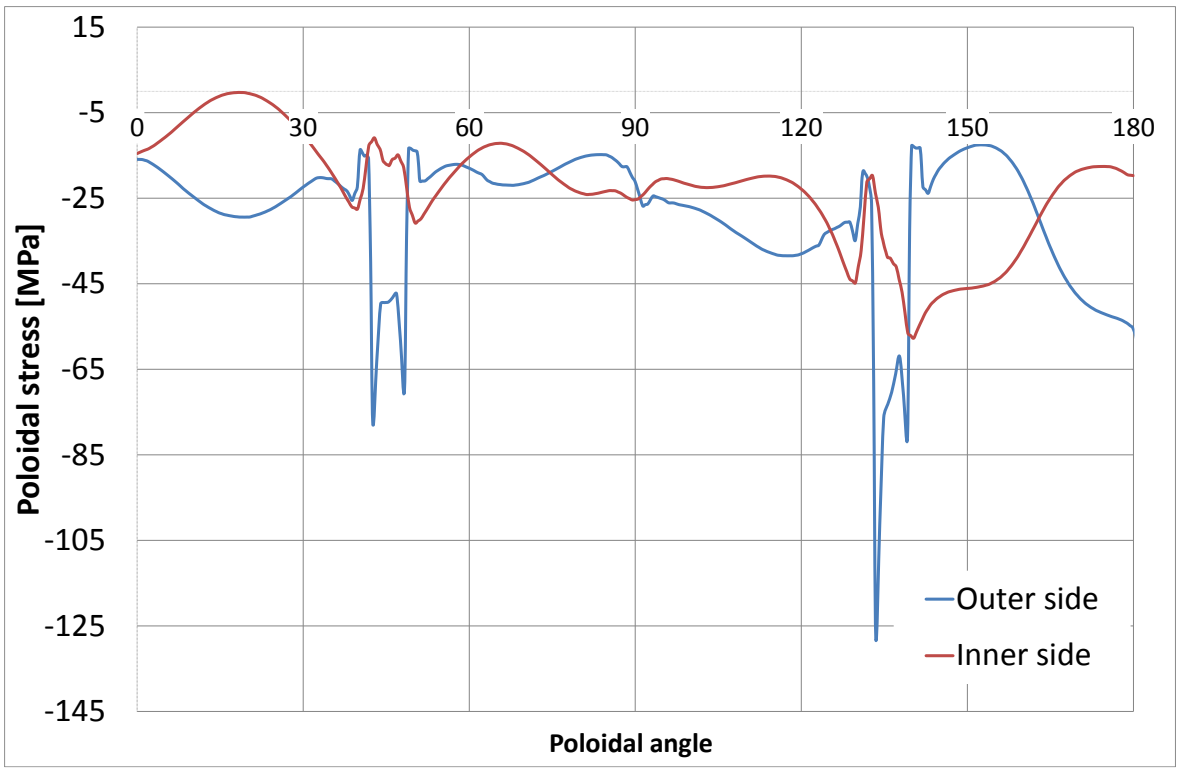

Figure 127: Case# 2.1: Poloidal stresses in [MPa] TSS corresponding to clamping ring location

Above Figure 127 shows graph of poloidal stress (minimum principal) vs. poloidal angle, the poloidal stress is plotted for inner TSS and outer TSS surfaces. It shows that compressive stresses are higher on toroidal grooves of coil at outer TSS surface.

Results are further verified by stress linearization method. Stresses are assessed by categorization at maximum stress locations through wall thickness and compared with material limits as per ITER SDC-IC standards as shown in section 4.2.5. Results are found well below to the limits as shown in Table 38;

Table 38 Case# 2.1: Stress linearization and verification with allowable stress limits [MPa]

Component	**TSS (AISI 304L)**		
Stress categories	P_L	$Pm+Pb$	$Pm+Pb+Q$
Allowable stress # [MPa]	**153**	**153**	**303**
2.1 Baking and GDC [MPa]	54	89	112

Allowable stress limits are calculated at maximum applied temperature (80 °C)

7.1.4 Simulation of normal RFP operation

In addition to the above described general loading conditions, the following loads are applied to the model:

1. Temperature distribution in TSS resulted from thermal analysis for normal RFP operation
2. Radial and tangential electromagnetic forces on TSS due to normal RFP operation
3. Vertical electromagnetic forces on clamping rings due to normal RFP operation

Results of nonlinear static structural analysis are shown below; the Figure 128 shows total displacement occur in TSS under applied thermal structural and electromagnetic loads. The maximum displacements of assembly occurring at external equatorial side with value of 1.9 mm and minimum of 1.3 mm occurs at upper internal equatorial side. Figure 129 shows radial and vertical displacements of TSS.

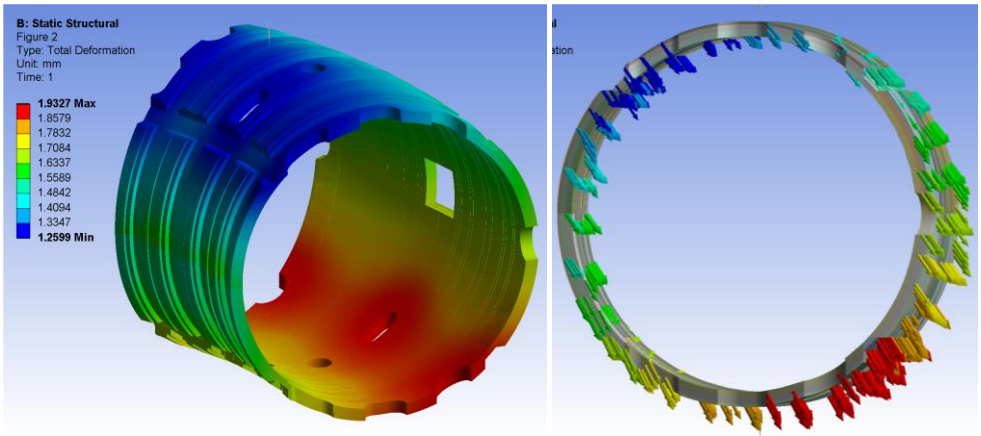

Figure 128 Case# 2.2: Total displacement contour of TSS [mm]

The Figure 130 shows von-Mises stress contour in TSS. Stresses are concentrated in saddle coil grooves, where TSS has minimum wall thickness. Figure 131 shows contour of maximum principal stress and minimum principal stress, which shows that major part of stresses are generated by compressive forces applied on TSS. Figure 132 (a.) shows sliding contact between upper and lower TSS parts at internal equatorial cut and Figure 132 (a.) shows pressure from clamping rings on TSS which is 14.5 MPa maximum.

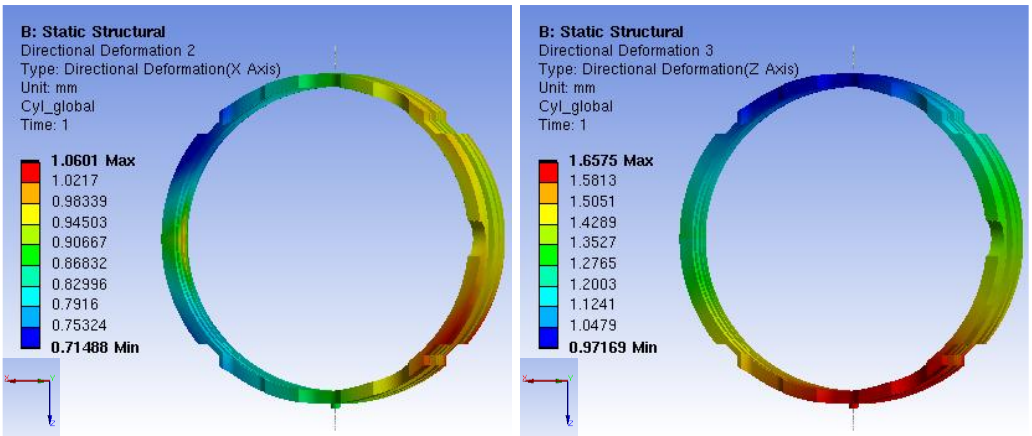

Figure 129 Case# 2.2: Directional displacement contour of TSS [mm]

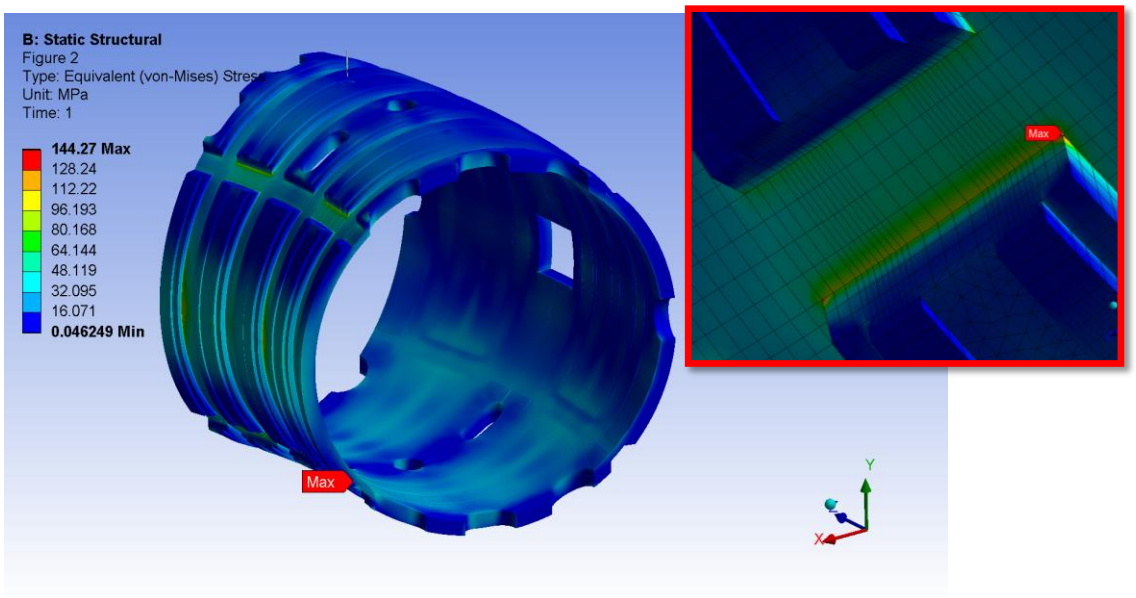

Figure 130 Case# 2.2: Stress contour of von-Mises stress in TSS [MPa]

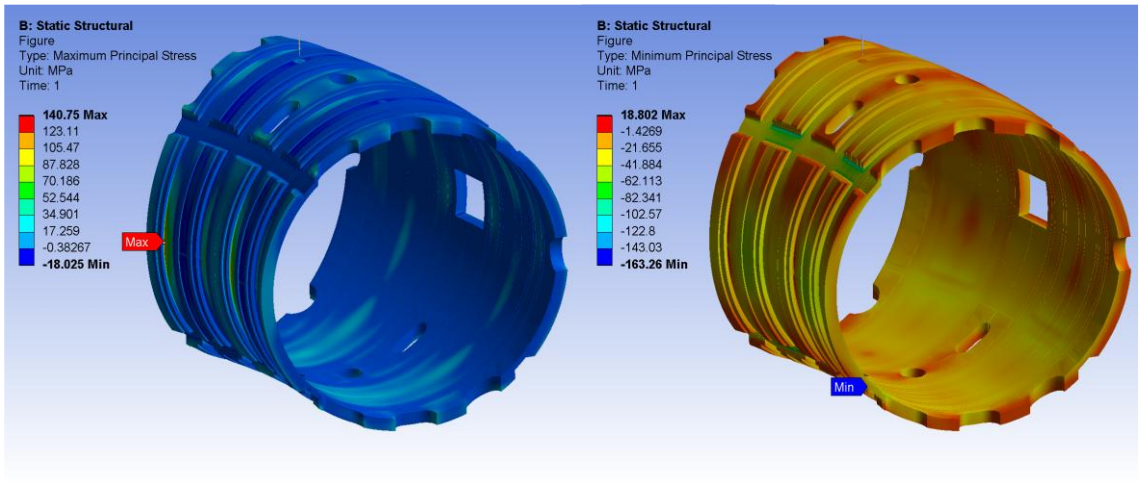

Figure 131 Case# 2.2: Stress contours of maximum and minimum principal stresses in TSS [MPa]

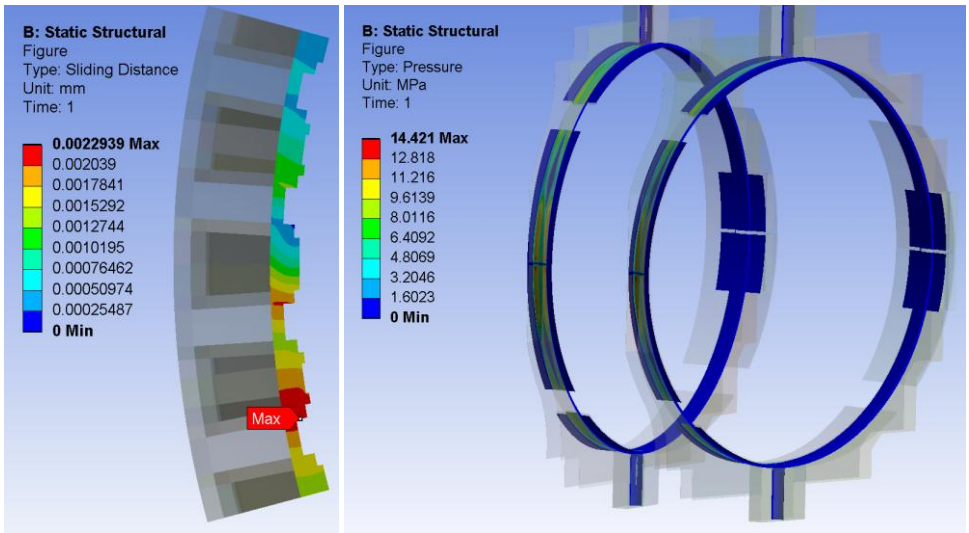

Figure 132 Case# 2.2: Contact status (a.) sliding at inner equatorial joint of TSS (b.) pressure from clamping rings to (TSS max. 14.5 MPa)

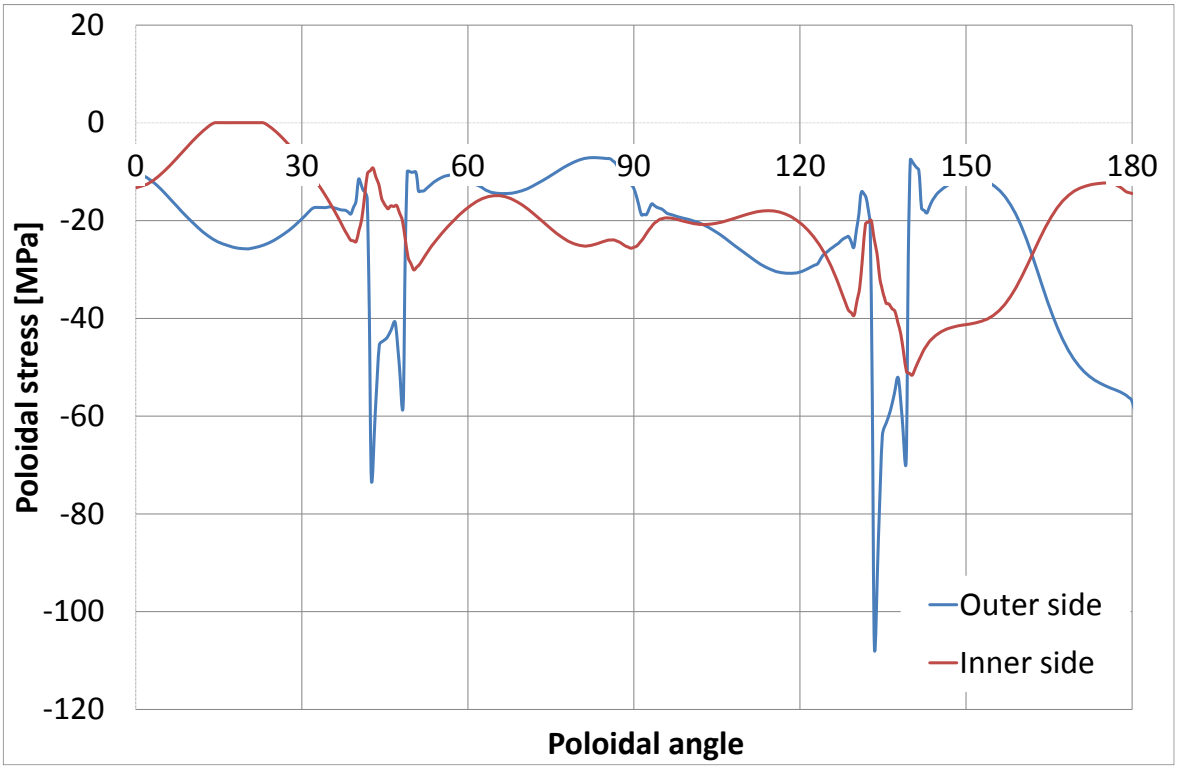

Figure 133: Case# 2.2: Poloidal stresses [MPa] in TSS corresponding to clamping ring location

Above Figure 133 shows graph of poloidal stress (minimum principal) vs. poloidal angle, the poloidal stress are plotted for inner TSS and outer TSS surfaces. It shows that compressive stresses are higher on toroidal grooves of coil at outer TSS surface.

Results are further verified by stress linearization method. Stresses are assessed by categorization at maximum stress locations through wall thickness and compared with material limits as per ITER SDC-IC standard as shown in section 4.2.5. Results are found well below to the limits as shown in Table 39;

Table 39 Case# 2.2: Stress linearization and verification with allowable stress limits [MPa]

Component	**TSS (AISI 304L)**		
Stress categories	P_L	$Pm+Pb$	$Pm+Pb+Q$
Allowable stress # [MPa]	**153**	**153**	**303**
2.2 Normal RFP operation [MPa]	48	75	95

Allowable stress limits are calculated at maximum applied temperature (80 °C)

7.1.5 Simulation of fast termination of plasma

In addition to general loading conditions described above, following loads are applied to the model:

1. Temperature distribution in TSS resulted from thermal analysis of fast termination of plasma condition
2. Radial and tangential electromagnetic forces on TSS due to fast termination of plasma
3. Vertical electromagnetic forces on clamping rings due to fast termination of plasma

Results of nonlinear static structural analysis are much similar to the results of normal RFP operation. The Figure 134 shows vector plot of total displacements with maximum 1.9 mm and minimum of 1.3. Figure 135 shows maximum displacement of 1 mm and 1.7 mm in radial and vertical directions respectively. Maximum equivalent stress in TSS is 144 MPa as shown in Figure 136.

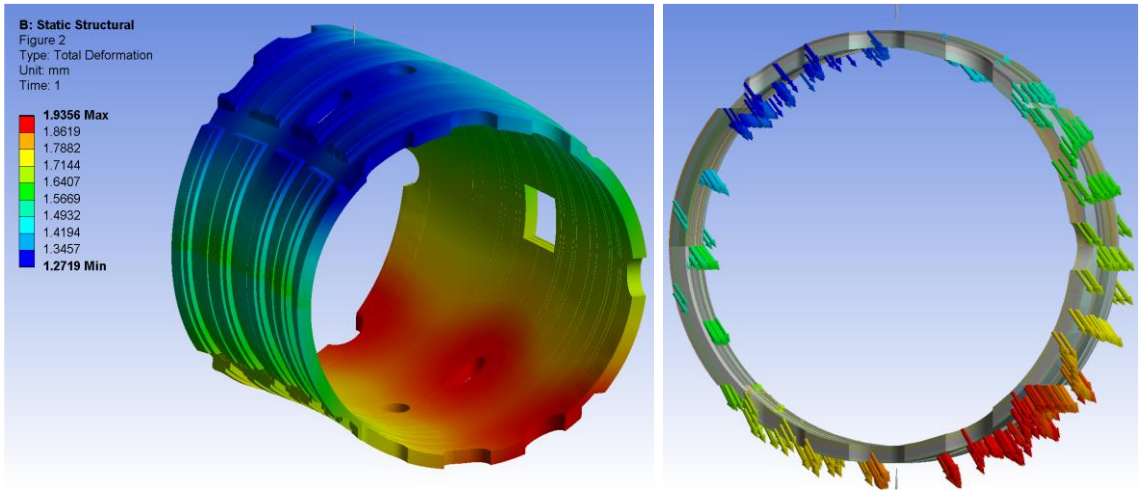

Figure 134 Case# 3.1: Total displacement contour of TSS ($D_{max.}$ = 1.9 mm, $D_{min.}$ = 1.3 mm)

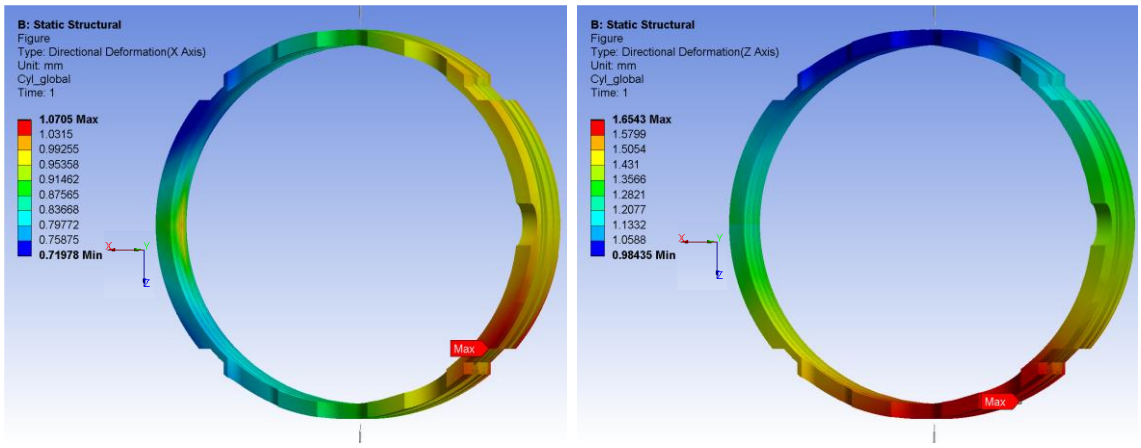

Figure 135 Case# 3.1: Directional displacement contour of TSS [mm]

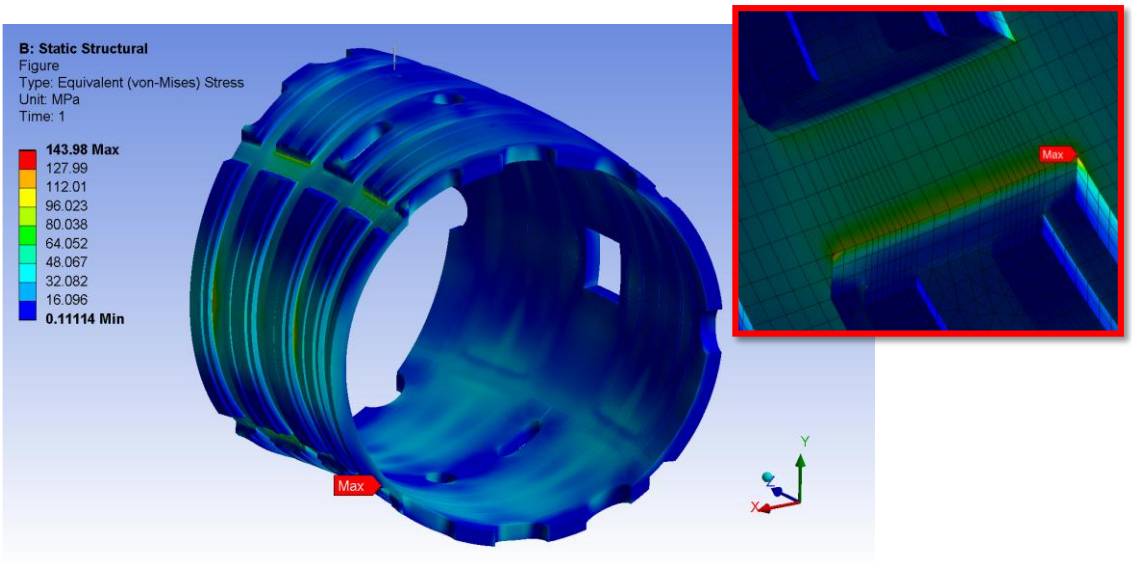

Figure 136 Case# 3.1: Stress contour for von-mises stress in TSS [MPa]

Results are further verified by stress linearization method. Stresses are assessed by categorization at maximum stress locations through wall thickness and compared with material limits as per ITER SDC-IC standard as shown in section 4.2.5. Results are found well below to the limits as shown in Table 40;

Table 40 Case# 3.1: Stress linearization and verification with allowable stress limits [MPa]

Component	**TSS (AISI 304L)**		
Stress categories	P_L	$Pm+Pb$	$Pm+Pb+Q$
Allowable stress # [MPa]	**153**	**153**	**303**
3.1 Plasma fast termination [MPa]	48	76	95

Allowable stress limits are calculated at maximum applied temperature (80 °C)

7.1.6 Simulation of wall mode locking

For this load combination, as shown in Table 17, structural load and temperature distribution to be applied resulted from thermal analysis for normal RFP operation on TSS. As described in section 5.2.5.1, thermal distribution in TSS is same as thermal distribution of normal RFP operation condition. So, for TSS this load combination will produce same results of case # 2.2 as described in section 7.1.4.

7.1.7 Simulation of fault case of electromagnetic event

In addition to general boundary conditions described above, only electromagnetic forces are applied to TSS and clamping rings caused by fault condition. In the fault case of electromagnetic event, there is no plasma produced inside TSS and forces produced by eddy currents. So no thermal loads arise in system (see load combination 4.1 in Table 17, component verification table). This load combination has the service level C as defined in Table 16

Results of nonlinear static structural analysis are described below.

The maximum displacement of 1.5 mm occurs in TSS where shown in Figure 137, which depicts that only vertical displacements take place in absence of thermal loads.

The Figure 138 shows von-Mises stress contour in TSS. The stress distribution in TSS is similar to above cases of load combinations but the value of stress is higher in comparison. Stresses are verified by linearization and details are given in following. Figure 139 shows contour of maximum principal stress and minimum principal stress. Figure 140 (a.) shows sliding between contact of upper and lower TSS at internal equatorial cut and Figure 132 (a.) shows pressure from clamping rings on TSS which is 14.5 MPa maximum.

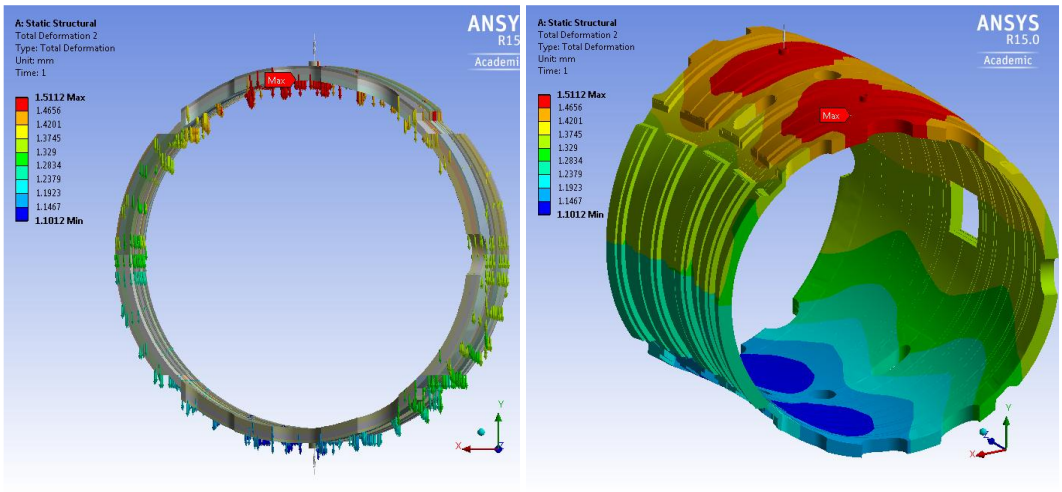

Figure 137 Case# 4.1: Total displacement contour of TSS [mm]

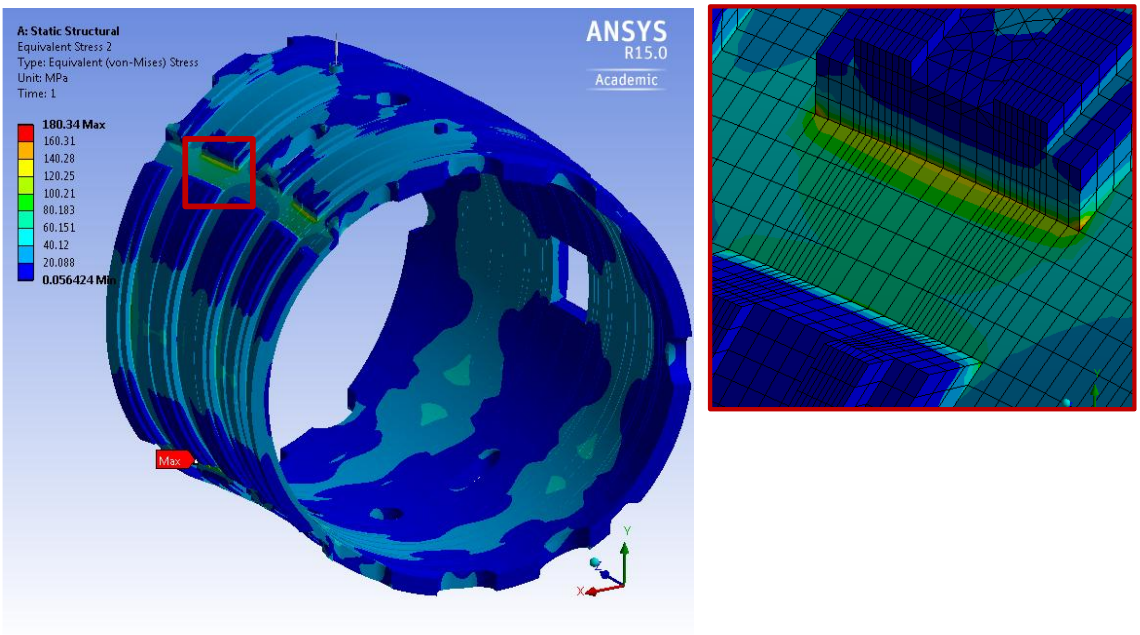

Figure 138 Case# 4.1: Stress contour for von-mises stress in TSS [MPa]

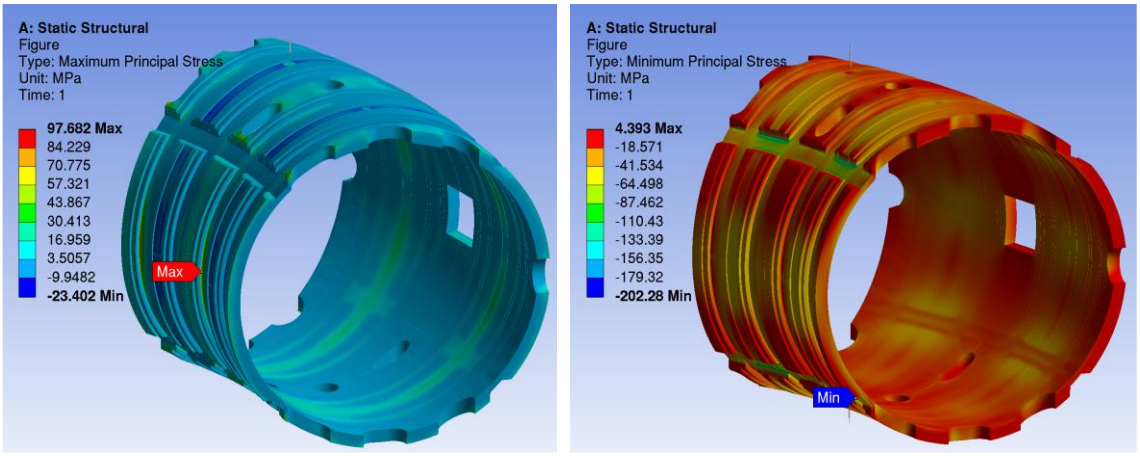

Figure 139: Case# 4.1: Stress contour for maximum and minimum principal stresses in TSS [MPa]

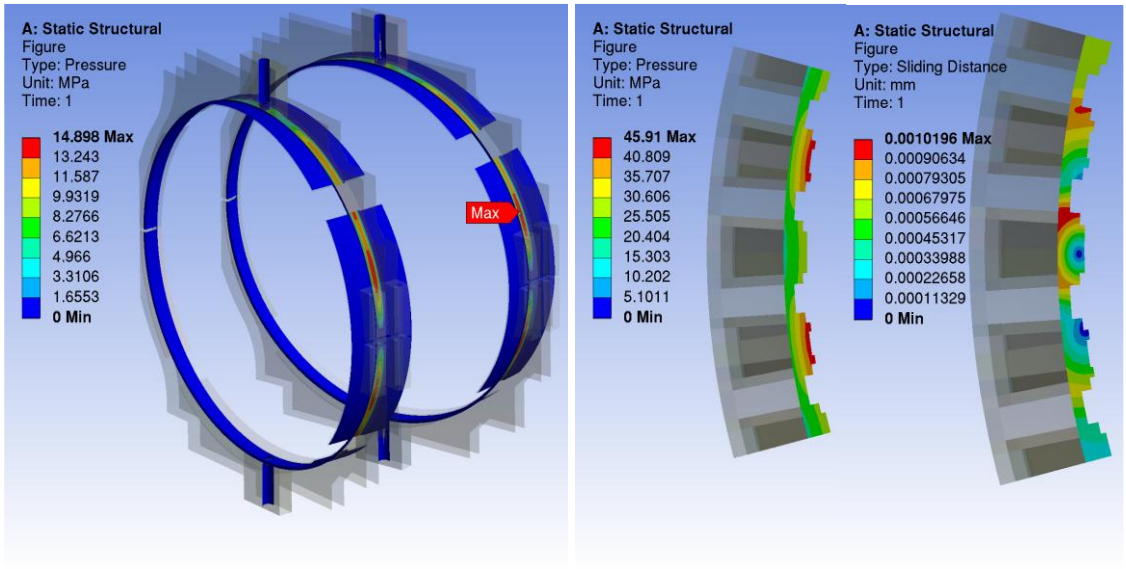

(a.) (b.)

Figure 140: Case# 4.1: Contact status (a.) pressure from clamping rings to TSS (max. 15 MPa) (b.) sliding and pressure at inner equatorial contacts of TSS

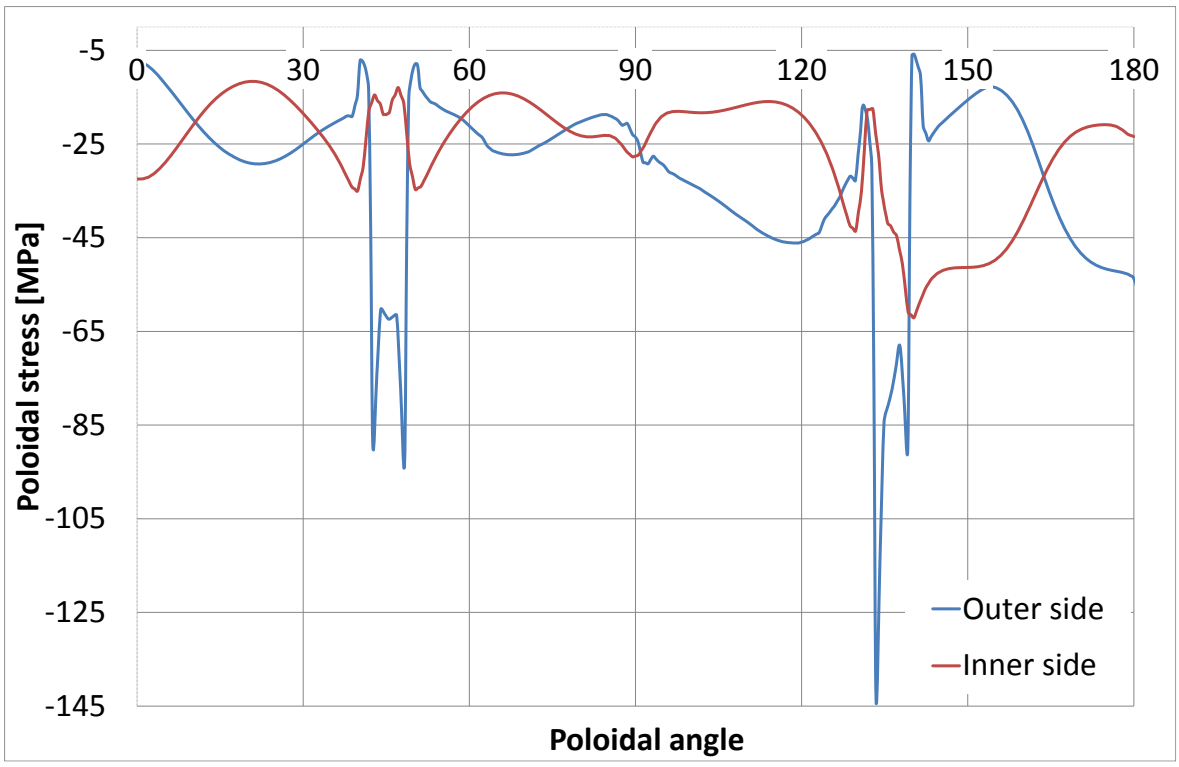

Figure 141: Case# 4.1: Poloidal stresses [MPa] in TSS corresponding to clamping ring location

Above Figure 141 shows graph of poloidal stress (minimum principal) vs. poloidal angle, the poloidal stress is plotted for inner TSS and outer TSS surfaces.

Results are further verified by stress linearization method. Stresses are assessed by categorization at maximum stress locations through TSS thickness and compared with material limits as per ITER SDC-IC standard for service level C as shown in section 4.2.4. Results are found well below to the limits as shown in Table 41;

Table 41 Case# 4.1: Stress linearization and verification with allowable stress limits [MPa]

Component	**TSS (AISI 304L)**		
Stress categories	P_L	$Pm+Pb$	$Pm+Pb+Q$
Allowable stress [MPa]	**200**	**200**	**400**
4.1 Fault condition – Emag [MPa]	66	103	129

7.1.8 Buckling analysis of TSS

Above results show that in all load combinations the major part of stresses is coming from compressive loads. A linear buckling analysis is carried out to study the instability of the structure subjected to compressive stresses due to applied loads. The load combination (see load combination 4.1 in Table 17, component verification table) corresponding to fault case of electromagnetic event is considered for the simulation, including structural loads. The linear buckling analysis shows the buckling instabilities and the related buckling load factors. Table 42 shows the list of buckling load factors for the first five buckling modes. Load factor corresponding to first buckling mode is 51, which is significantly higher than required minimum buckling load factor 3 as defined in ASME III NH [53]. Figure 142 shows deformation (scaled = 120X) of the TSS for first and second buckling mode.

Table 42 List of load multiplier for buckling modes

Mode	1	2	3	4	5
Load factor	51	72	79	98	104

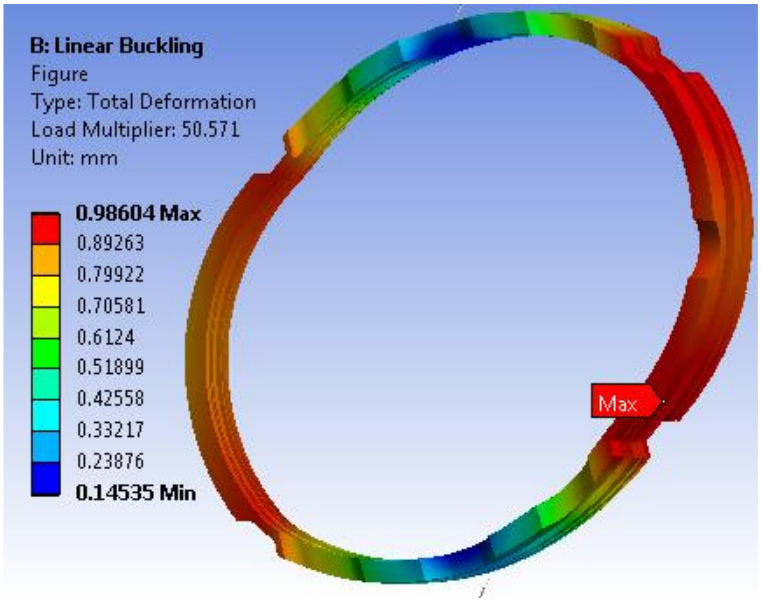

Figure 142: TSS deformation under first buckling mode (Scaled = 120X)

7.2 Mechanical verification of Thin Resistive Plate

As explained in section 2.3.2.5, Thin Resistive Plate (TRP) is designed for the vacuum sealing of internal toroidal cut of TSS. The TRP has to withstand a pressure of 10^5 N/m^2 applied at its external surfaces which are exposed to air side. Local reinforcing studs are investigated between plates of TRP to preserve the radial width of the TRP under external pressure.

A 90° model is prepared to simulate the condition as shown in Figure 143. The model consists of TRP, reinforcing studs and closing plate. TRP is 1 mm thick plate with total poloidal length of 200 mm and radial width of 12 mm. There is 5 mm gap between two plates of TRP. Reinforcing studs are solid cylinders of 20 mm diameters and 5 mm thickness. Reinforcing studs are distributed in 4 rows (X = 37 mm) along poloidal direction and distributed (θ = 5°) toroidally to get uniform supporting condition as shown in Figure 143. Closing plate is placed to close the end of TRP.

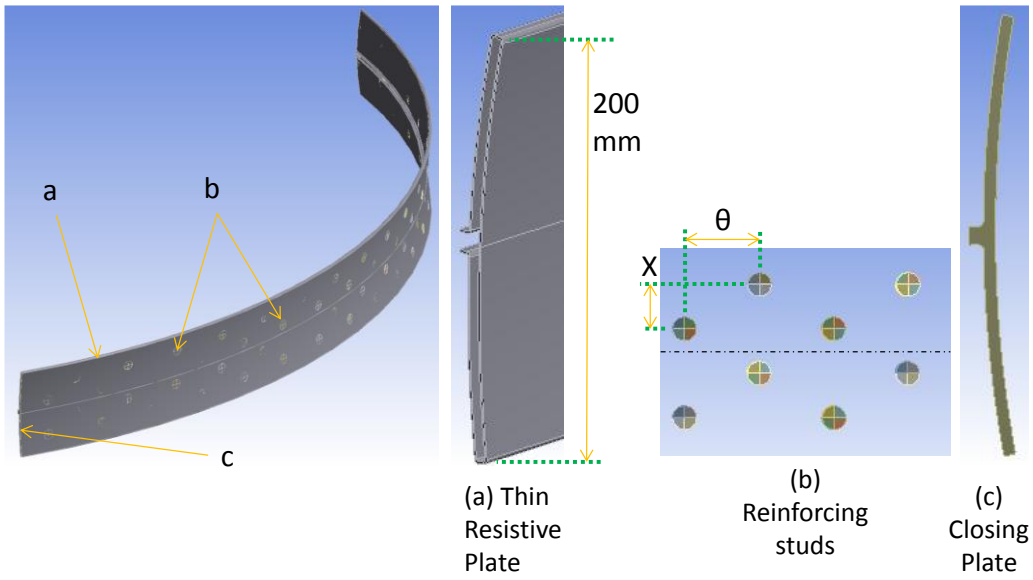

Figure 143: Finite element model of TRP with geometrical details

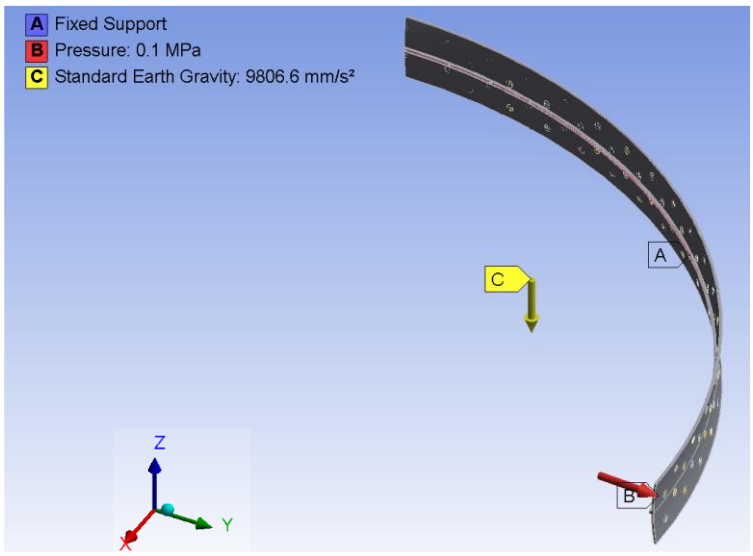

Figure 144: Boundary conditions applied to the finite element model

Applied boundary conditions are shown in Figure 144. A 105 N/m2 pressure is applied on all the external surfaces of TRP which are exposed to air side. Fixed supporting conditions are applied on the both faces which are going to be welded with top and bottom TSS. Bonded contacts are defined between reinforcing studs and TRP. Symmetric condition is applied on plane X-Z. Incone625 material is selected for TRP and closing plate and TORLON 5030 is selected for reinforcing studs.

A static structural analysis is carried out and results are shown below figures. Figure 145 shows contour plot of the total deformation that is well distributed over the geometry with maximum value of 0.3 mm. Figure 146 shows stress distribution in TRP, maximum stress of 276 MPa arises in the vicinity of reinforcing stud. Stress singularity appeared in the closing plate as shown in Figure 147. Stresses are well below of material limits of TRP and closing plate. Stresses are further verified with design rules as explained below.

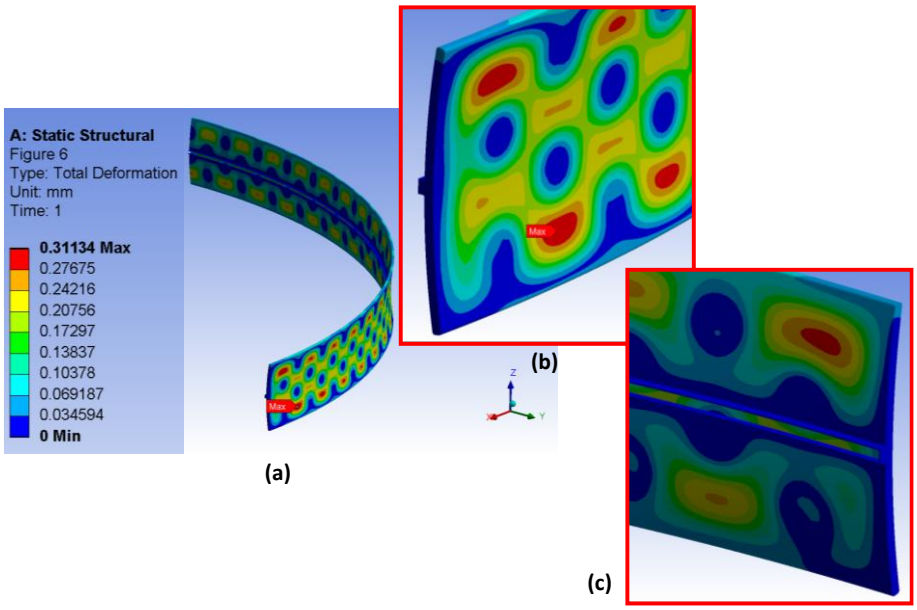

Figure 145 Total displacements [mm] resulting for TRP

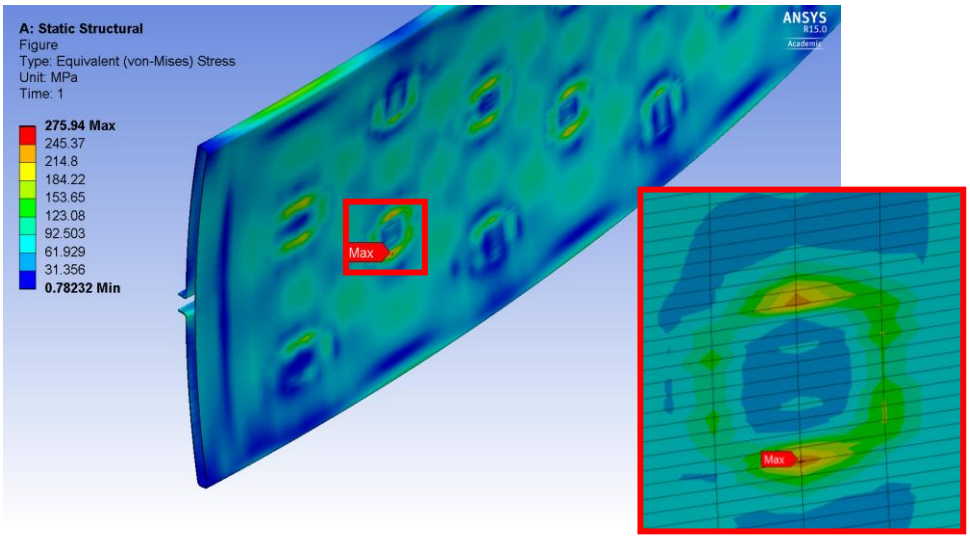

Figure 146 Von-Mises stress contour of TRP (Max. = 276 MPa)

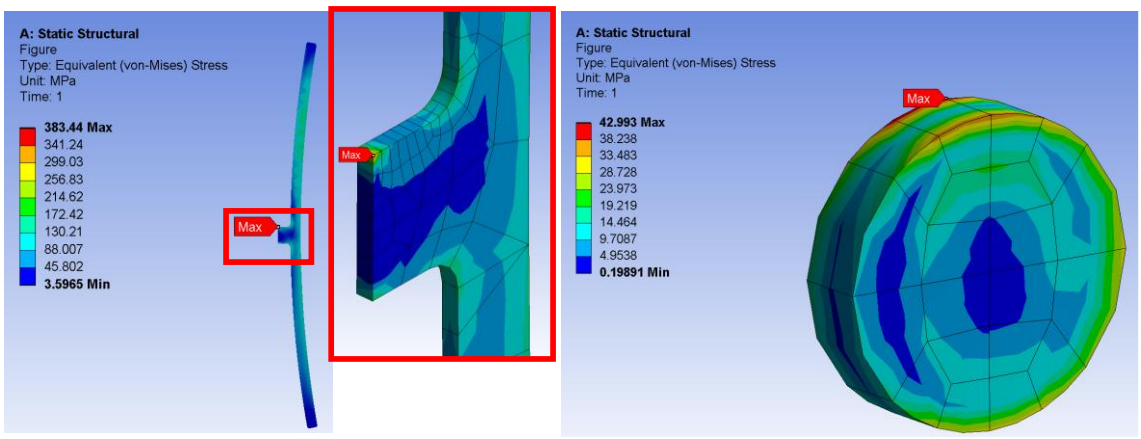

(a) (b)

Figure 147 Von-Mises stress [MPa] contour of (a) closing plate, and (b) reinforcing stud

Results are further verified by stress linearization method. Three different stress classification lines (SCL) are considered for different components at highest stress occurring section. Stresses are assessed by categorization at maximum stress locations through wall thickness and compared with material limits as per ITER SDC-IC standard for service level C as shown in section 4.2.5. Results are found well below to the limits as shown in Table 43;

Table 43 Stress linearization and verification with allowable stress limits [MPa]

Component	**TSS (AISI 304L)**		
Stress categories	P_L	$Pm+Pb$	$Pm+Pb+Q$
Allowable stress [MPa]	**439**	**439**	**876**
SCL-1 (TRP) [MPa]	23	253	253
SCL-2 (Closing plate) [MPa]	152	195	195
Allowable stress [MPa]	**102**	**102**	**204**
SCL-3 (Reinforcing stud) [MPa]	9	32	43

7.3 Conclusion

Non-linear structural analyses with elastic material properties are performed to verify the mechanical behaviour of TSS using a 30° model with clamping rings. The simulations are carried out for different load combinations and obtained results are summarized as follows:

- Maximum displacement of the TSS is found to be 2.5 mm under the baking and GDC load combination
- Maximum stresses are found in the TSS for the load combination of fault case of electromagnetic event
- The major stress contributions are coming from clamping ring preloads and TF belt pressure
- Maximum stress is produced in TSS location below clamping rings and toroidal grooves of coil
- Figure 19 and Figure 133 shows that pattern of stress is comparable between present TSS and modified design with little higher values of stress in later case.
- No sliding occur between internal equatorial contacts of TSS
- Buckling load factor is much higher than critical buckling load
- Stresses are categorised and verified against ITER SDC-IC design rules, and found well below to the allowable material limits

Analysis results for the respective load combinations for normal and off-normal operations are summarized in Table 44.

Table 44 Summary of stress [MPa] verification for TSS

Component	**TSS (AISI 304L)**		
Stress categories	P_L	*Pm+Pb*	*Pm+Pb+Q*
Allowable stress # [MPa] (Service level A)	**153**	**153**	**303**
2.1 Baking and GDC [MPa]	53.5	88.7	111.7
2.2 Normal RFP operation [MPa]	48	75	95
3.1 Plasma fast termination [MPa]	48	76	95
3.2 Wall Mode Locking [MPa]	48	75	95
Allowable stress [MPa] (Service level C)	**200**	**200**	**400**
4.1 Fault condition – Emag [MPa]	66	103	129

Allowable stress limits are calculated at maximum applied temperature (80 °C)

Also, mechanical behaviour of the TRP is verified by static structural analysis under external pressure loading. The investigated local reinforcing studs are maintaining radial width of TRP. Simulated stresses are well below the material limits.

CHAPTER 8 CONCLUSION AND FUTURE WORK

New concepts of the RFX-mod components were developed for the design of the upgraded machine named RFX-mod2. The mechanical modifications are proposed to enhance passive MHD control by bringing passive stabilising shell as near as possible to the plasma (reduced plasma-shell distance) and to improve plasma wall lock mode scenario by minimizing braking torque on plasma through the elimination of vacuum vessel. The improvements are realized by major changes on the present components including first wall (FW), vacuum vessel, passive stabilizing shell and Toroidal Support Structure (TSS). Load specifications are prepared with appropriate assumptions made from available experimental data and published articles on RFX-mod. Combinations of loads acting on the machine during operation including fault condition are recognised and applied onto components for the thermo-mechanical simulation by finite element analysis and for the verification against international design rules.

As a major impact of these modifications, the vacuum barrier is shifted to TSS which is composed by four parts mechanically joined and electrically insulated. Most of the effort focused on the design of vacuum seal for the TSS. Commercially available vacuum seals and solutions implemented in other machines were investigated with iterations and combinations of designs for different TSS cuts. Due to stringent sealing requirements and geometrical constraints, custom-designed joints and seals are developed and proposed: fully welded solution at the external equatorial joint to integrate vessel openings, thin resistive plate at the internal equatorial joint to realise the required inductive-resistive condition, and ceramic-metal brazed rings at the two poloidal joints to realise the electrical insulation.

The ceramic-metal brazed rings at two poloidal joints are designed with metal sheets to be lip welded on the TSS to realise the vacuum tight; the technological feasibility is verified considering accesses for subsequent lip sealing with welding torch. The poloidal gap at the TSS is increased to accommodate the ceramic-metal brazed ring. Mechanical continuity of poloidal joints will be realised by changing the present bolted junctions that is verified by calculations considering the gap increment.

The internal toroidal joint is mechanically closed on an insulating plate and a resistive sheet seals the vacuum boundary. The sheet behaviour under load combinations is verified and local reinforcing studs grid are proposed to reduce the deformation under external pressure; furthermore, the path length of the resistive sheet was designed to obtain an electrical resistance compatible with resistive-inductive circuit requirements.

Joining of openings interfaced with vacuum pumping and diagnostics at the external toroidal joint is designed for lip welding at the vacuum side and structural welding at the air side to avoid trapped volumes and virtual leaks.

Technical specifications are prepared for the procurement of a mock-up replicating all the developed joints to be qualified by testing.

The present overlapping of 20° sector of the stabilizing shell will be removed as not compatible with the poloidal joining being the last cut to be joined as foreseen by the new assembly procedure. The upper and lower shells will be bolted together by series of plates and the electrical insulation conditions at inner and outer equatorial joint are reversed with respect to TSS joint configuration considering magnetic field penetration. The passive stabilizing shell is supported on the TSS through supporting rings. Among different materials and supporting conditions analysed by finite element thermal-mechanical simulations, Torlon® is selected as material of the rigid rings to match ring-shell thermal deformations and supports are positioned at the equator to accommodate free thermal expansions also during baking.

Thermal analyses are carried out on 3D models of modified torus assembly for different loading conditions to evaluate temperature distributions in different components. The designed components reach the highest temperature in baking and GDC loading condition, in which TSS attains 78 °C, stabilizing shell and supporting ring attain 169 °C. As all FW tiles are directly attached on stabilizing shell, the thermal conductance is high and heat transfer from FW tiles to shell occurs very quickly, so thermal picks are seen in temperature profile of shell during pulse operation. The shell is supported on TSS only by 48 supports at the 24 support rings, so the thermal conductance is small and heat transfer from shell to TSS occurs very slowly during the experimental day. The major portion of heat is transferred through radiation between stabilizing shell and TSS. The temperature values resulted for all components within allowable values and these results of temperature distribution in components were used to calculate thermal stresses.

The assessment of different load combinations is performed for the passive stabilizing shell with supporting rings. Stresses in stabilizing shell are mainly localised on portion below FW tile. Primary bending stresses are higher in stabilizing shell in all the cases compared to primary membrane stress. The newly designed supporting rings allow thermal expansion of stabilizing shell, which limits the stresses at low values. Stresses in supporting rings are very low compared to material limits given by design rules of international standards. Based on the results, the thermo-mechanical verifications resulted satisfied so demonstrating the soundness and the feasibility of the proposed modification and of developed solutions for the tile and shell support concept.

The design modifications of TSS are analysed by carrying out finite element simulations applying combinations of loads expected during operations and results are post-processed according to design rules of international standards. The major stress contributions are coming from clamping ring preloads and pressure of toroidal field coil belts. Maximum stress is produced in TSS location below clamping rings and toroidal grooves of coils. No sliding is seen between internal equatorial contact surfaces of TSS where the resistive sheet

sealing is proposed. As many of the loads are compressive in nature, buckling analysis is carried out and applied loads result much lower than critical buckling load. Design of TSS modifications shows strong structural integrity with enough margins.

Preliminary engineering design of RFX-mod2 components has been carried out and resulted satisfied so demonstrating the soundness of the design as explained in this thesis. Final engineering design will be undertaken in next step. Also proposed experimental mock-up for the sealing joints will be executed to prove the validity of the implemented solutions.

Technical specifications for the procurement of the machine modifications will be prepared detailing tests required at the factory and for the acceptance of construction on site. Follow-up of the procurement will be done assisting the supplier during manufacturing and assembling.

Appendix A: Material properties

The material properties used for FE calculations and stress verification are listed here.

1. Stainless steel AISI 304L --------(Toroidal Support Structure)
2. Oxygen-free copper C10200 ----(Stabilizing shell)
3. TORLON® 5030 ----------(Supporting rings)
4. Polycrystalline Graphite ---------(First Wall tiles)
5. Molybdenum ----------(First Wall keys)
6. Inconel 625 ----------(Thin Resistive Plate seal)
7. Austenitic cast steel ----------(Clamping rings)

A.1 Stainless steel AISI 304L (EN grades 1.4306)

The operating temperature for this steel is 20 - 500 °C for an unirradiated component.

Temperature [°C]	Density [kg/m^3]	Coefficient of thermal expansion [µm/m/K]
20	7900	15.3
50	7900	15.6
100	7900	16.0
150	7900	16.6
200	7900	17.0
250	7900	17.4

Temperature [°C]	Young's Modulus [MPa]	Poisson's Ratio	Bulk Modulus [MPa]	Shear Modulus [MPa]
21	1.95e+005	0.3	1.625e+005	75000
93	1.9e+005	0.3	1.5833e+005	73077
149	1.86e+005	0.3	1.55e+005	71538
204	1.83e+005	0.3	1.525e+005	70385
260	1.78e+005	0.3	1.4833e+005	68462

Temperature [°C]	Thermal Conductivity [W/m * K]	Specific Heat [J/kg * K]
21	14.87	483
121	16.6	518

Temperature [°C]	Tensile Yield Strength (Sy) [MPa]	Tensile Ultimate Strength (Su) [MPa]	Allowable stress intensity (Sm) [MPa]
20	180	460	120
100	145	410	120

A.2 Oxygen-free copper C10200

The operating temperature for this material is specified as 20-204 °C.

Temperature [°C]	Density [kg/m^3]	Coefficient of thermal expansion [µm/m/K]
21	8900	16.7
200	8900	17.6

Temperature [°C]	Young's Modulus [MPa]	Poisson's Ratio	Bulk Modulus [MPa]	Shear Modulus [MPa]
21	1.17e+005	0.31	1.03e+005	44656
260	1.07e+005	0.31	93860	40840

Temperature [°C]	Thermal Conductivity [W/m * K]	Specific Heat [J/kg * K]
20	401	388
250	388	406

Temperature [°C]	Tensile Yield Strength (Sy) [MPa]	Tensile Ultimate Strength (Su) [MPa]	allowable stress intensity (Sm) [MPa]
20	69	200	46
200	51	152	34

A.3 TORLON® 5030

The operating temperature for this material is specified as 20-275 °C

Density [kg/m^3]	Coefficient of thermal expansion [µm/m/K]	Thermal Conductivity [W/m * K]	Specific Heat [J/kg * K]
1610	16.2	0.36	1369

Young's Modulus [MPa]	Poisson's Ratio	Bulk Modulus [MPa]	Shear Modulus [MPa]
14500	0.43	34524	5070

Temperature [°C]	Tensile Yield Strength (Sy) [MPa]	allowable stress intensity (Sm) [MPa]
20	205	68

A.4 Polycrystalline Graphite

The operating temperature for this material is specified as 20 - 2750 °C

Density [kg/m^3]	Thermal Conductivity [W/m * K]	Specific Heat [J/kg * K]
1820	108	710

A.5 Molybdenum

The operating temperature for this material is specified as 20 - 600 °C

Density [kg/m^3]	Thermal Conductivity [W/m * K]	Specific Heat [J/kg * K]
10200	138	217

A.6 Inconel 625

The operating temperature for this material is from cryogenic to 980 °C

Temperature [°C]	Density [kg/m^3]	Thermal Conductivity [W/m * K]
21	8440	9.5
204	8440	11

Temperature [°C]	Young's Modulus [MPa]	Poisson's Ratio	Bulk Modulus [MPa]	Shear Modulus [MPa]
21	2.075e+005	0.278	1.5578e+005	81182
93	2.04e+005	0.279	1.5385e+005	79750
204	1.98e+005	0.28	1.5e+005	77344

Tensile Yield Strength (Sy) [MPa]	Tensile Ultimate Strength (Su) [MPa]	allowable stress intensity (Sm) [MPa]
517	930	292

A.7 Austenitic cast steel

Density [kg/m^3]	Coefficient of thermal expansion [µm/m/K]
7750	16

Young's Modulus [MPa]	Poisson's Ratio	Bulk Modulus [MPa]	Shear Modulus [MPa]
1.95e+005	0.3	1.625e+005	75000

Bibliography

[1]. D F Escande, "What is a reversed field pinch?" Aix-Marseille University, Marseille, France.

[2]. P Piovesan, et al., "RFX-mod: A multi-configuration fusion facility for three-dimensional physics studies" Physics of Plasmas, vol. 20, no. 5, 2013.

[3]. G Rostagni, et al., "RFX: an expected step in RFX research" Fusion Engineering and Design, vol. 25, pp. 301-303, 1995.

[4]. P.Sonato, et al., "Machine modification for active MHD control in RFX" Fusion Engineering and Design, Vols. 66-68, pp. 161-168, 2003.

[5]. S Martini, et al., "Active MHD control at high currents in RFX-mod" Nuclear Fusion, vol. 47, p. 783–791, 2007.

[6]. G Chitarin, et al., "The design of 192 saddle coils for RFX" Fusion Engineering and Design, vol. 66–68, p. 1055–1059, September 2003.

[7]. P Zaccaria, et al., "Tests and analyses for the mechanical and thermal qualification of the new RFX first wall tiles" in 22nd SOFT, Helsinki, 2002.

[8]. F Gnesotto, et al., "The plasma system of RFX" Fusion Engineering and Design, vol. 25, p. 335 372, 1995.

[9]. P Zaccaria, "First Wall, Blanket and divertor, Basic Engineering course" 27-29 May 2013, Consorzio RFX, Padova.

[10]. P Sonato, et al., "Investigation of plasma facing components and vacuum vessel in RFX," Journal of Nuclear Materials, Vols. 241-243, pp. 982-987, 1997.

[11]. W baker, et al., "Design of a new toroidal shell and support structure for RFX" Fusion Engineering and Design, vol. 63–64, p. 461–466, December 2002.

[12]. D Marcuzzi, et al., "Non-axisymmetric structural analyses of the new components for the modified RFX machine," in IEEE/NPSS, 20th Symposium on Fusion Engineering, San Diego, CA, USA, 14-17 Oct. 2003.

[13]. Internal Report, "Physics motivation and engineering concepts for RFX-mod improvements" Consorzio RFX, 2015.

[14]. P Zanca, "Avoidance of tearing modes wall-locking in a reversed field pinch with active feedback coils" Plasma Physics and Controlled Fusion, vol. 51, p. 38, 2009.

[15]. R.Fitzpatrick, "Effect of a resistive vacuum vessel on dynamo mode rotation in reversed field pinches," Physics of Plasmas, vol. 6, no. 10, October 1999.

[16]. R.Cavazzana, et al., "PRELIMINARY ELECTROMAGNETIC ANALYSES ON THE SHORT CIRCUIT OF THE MECHANICAL SUPPORT STRUCTURE," 2013.

[17]. P.Zanca, "ESTIMATE OF THE COILS' SIDEBANDS IMPACT IN CONFIGURATIONS WITH A VACUUM TIGHT MECHANICAL STRUCTURE FOLLOWING SONATO'S PROPOSAL" Consorzio RFX, FC/85, 2013.

[18]. Ring design "Parker O-Ring Handbook".

[19]. M G Nicholas, Joining of Ceramics; Advanced Ceramic Reviews-Institute of Ceramics, Chapman and hall, New York, USA

[20]. R N Dexter, et al., "The Madison Symmetric Torus," Fusion Technology, vol. 19, pp. 131-139, Jan. 1991.
[21]. R N Dexter, et al., "MST technical design considerations," University of Wisconsin, Dec. 1985.
[22]. Material Data Sheet: Inconel 625, Special Metals Corporation, 2013.
[23]. Coefficient Thermal Expansion of materials, BRIGHAM YOUNG UNIVERSITY
[24]. Micro-Tig welding, http://www.aviationpros.com
[25]. ASME B1.1-2003, Unified Inch Screw Threads.
[26]. Thread engagement calculations, Roy Beardmore, RoyMech.
[27]. TORLON design guide: www.solvayplastics.com.
[28]. P Zaccaria, et al., "Thermo-mechanical analyses of large ceramic rings during brazing process," Fusion Engineering and Design, vol. 82, p. 2588–2594, 2007.
[29]. Pertti Auekari, "Mechanical and physical properties of engineering alumina ceramics," VTT manufacturing technology.
[30]. Technical data sheet, "Kovar alloy UNS K94610" Carpenter Technology Corporation.
[31]. C R Ader, et al., "MECHANICAL DESIGN OF CERAMIC BEAM TUBE BRAZE JOINTS FOR NOVA KICKER MAGNETS" Fermi National Accelerator Laboratory, USA.
[32]. C R Ader, et al., "RECENT EXPERIENCE IN THE FABRICATION AND BRAZING OF CERAMIC BEAM TUBES FOR KICKER MAGNETS AT FNAL" Fermi National Accelerator Laboratory, USA.
[33]. G J Qiao, "Thermal cyclic test of alumina/kovar joint brazed by Ni-Ti active filler" ceramic international, vol. 29, pp. 7-11, 2003.
[34]. M.E. Puiatti, et al., “Overview of the RFX-mod contribution to the International Fusion Science Program”, Consorzio RFX, Padova, Italy
[35]. Load specification for ITER vacuum vessel.
[36]. S Munaretto, "Wall-conditioning techniques in RFX-mod: status and perspectives" Consorzio RFX, 2008.
[37]. G Chitarin, et al., "Evaluation of electrodynamic forces on the passive components of the new RFX load assembly" Fusion Engineering and Design, vol. 63–64, p. 467–473, December 2002.
[38]. A Canton,et al., "Density control in RFX-mod Reversed Field Pinch device," in 35th EPS Conference on Plasma Physics, ECA Vol.32D, D-1.002 (2008), Hersonissos, 9-13 June 2008.
[39]. S Dal Bello, et at., “Wall conditioning techniques: status and perspectives”, RFX-mod workshop 2011
[40]. G Chitarin, et al., "An integral formulation for eddy current analyses in axisymmetric configurations" IEEE Transactions on Magnetics, vol. 25, no. 5, pp. 4330 - 4342, Sep 1989.

[41]. Luca Grando, "2D electrodynamics forces acting on passive structures of RFX-mod2" Consorzio RFX, 2015.
[42]. Internal Note, "Seismic analysis of the MITICA bio-shielding," RFX_PRIMA_TN_034_r0, Consorzio RFX.
[43]. Standards "Nuove Norme Tecniche per le Costruzioni (NTC) D.M. 14/01/2008".
[44]. Standards "Istruzioni per l'applicazione delle Nuove Norme Tecniche per le Costruzioni. Circolare 02/02/2009 N.617".
[45]. Standards "Eurocode 8: Design of structures for earthquake resistance".
[46]. "Classificazione sismica al 2010" Dipartimento della protezione civile
[47]. CATIA CAD model of RFX-mod.
[48]. "ASME Boiler and Pressure Vessel Code, Section VIII div.2".
[49]. "Structural Design Criteria for ITER In-vessel Components (SDC-IC)".
[50]. "Emissivity of different materials" OMEGA Engineering inc.
[51]. "On line materials data": http://www.matweb.com.
[52]. Disc spring standards, UNI 8737
[53]. "ASME Boiler and Pressure Vessel Code, Section III, Subsection NH".